PEPTIDE SIGNALING IN PLANTS

EDITED BY: Qingyu Wu, Fuminori Takahashi, Cao Xu, Wolfgang Schmidt and Reidunn Birgitta Aalen

PUBLISHED IN: Frontiers in Plant Science

frontiers Research Topics

ISSN 1664-8714
ISBN 978-2-88974-646-0
DOI 10.3389/978-2-88974-646-0

About Frontiers

Frontiers is more than just an open-access publisher of scholarly articles: it is a pioneering approach to the world of academia, radically improving the way scholarly research is managed. The grand vision of Frontiers is a world where all people have an equal opportunity to seek, share and generate knowledge. Frontiers provides immediate and permanent online open access to all its publications, but this alone is not enough to realize our grand goals.

Frontiers Journal Series

The Frontiers Journal Series is a multi-tier and interdisciplinary set of open-access, online journals, promising a paradigm shift from the current review, selection and dissemination processes in academic publishing. All Frontiers journals are driven by researchers for researchers; therefore, they constitute a service to the scholarly community. At the same time, the Frontiers Journal Series operates on a revolutionary invention, the tiered publishing system, initially addressing specific communities of scholars, and gradually climbing up to broader public understanding, thus serving the interests of the lay society, too.

Dedication to Quality

Each Frontiers article is a landmark of the highest quality, thanks to genuinely collaborative interactions between authors and review editors, who include some of the world's best academicians. Research must be certified by peers before entering a stream of knowledge that may eventually reach the public - and shape society; therefore, Frontiers only applies the most rigorous and unbiased reviews.
Frontiers revolutionizes research publishing by freely delivering the most outstanding research, evaluated with no bias from both the academic and social point of view. By applying the most advanced information technologies, Frontiers is catapulting scholarly publishing into a new generation.

What are Frontiers Research Topics?

Frontiers Research Topics are very popular trademarks of the Frontiers Journals Series: they are collections of at least ten articles, all centered on a particular subject. With their unique mix of varied contributions from Original Research to Review Articles, Frontiers Research Topics unify the most influential researchers, the latest key findings and historical advances in a hot research area! Find out more on how to host your own Frontiers Research Topic or contribute to one as an author by contacting the Frontiers Editorial Office: frontiersin.org/about/contact

PEPTIDE SIGNALING IN PLANTS

Topic Editors:
Qingyu Wu, Chinese Academy of Agricultural Sciences (CAAS), China
Fuminori Takahashi, Tokyo University of Science, Japan
Cao Xu, Chinese Academy of Sciences (CAS), China
Wolfgang Schmidt, Academia Sinica, Taiwan
Reidunn Birgitta Aalen, University of Oslo, Norway

Citation: Wu, Q., Takahashi, F., Xu, C., Schmidt, W., Aalen, R. B., eds. (2022). Peptide Signaling in Plants. Lausanne: Frontiers Media SA. doi: 10.3389/978-2-88974-646-0

Table of Contents

frontiers in Plant Science

EDITORIAL
published: 15 February 2022
doi: 10.3389/fpls.2022.843918

Editorial: Peptide Signaling in Plants

Qingyu Wu[1], Wolfgang Schmidt[2]*, Reidunn Birgitta Aalen[3]*, Cao Xu[4]* and Fuminori Takahashi[5]**

[1] Institute of Agricultural Resources and Regional Planning, Chinese Academy of Agricultural Sciences, Beijing, China, [2] Institute of Plant and Microbial Biology, Academia Sinica, Taipei, Taiwan, [3] Department of Biosciences, University of Oslo, Oslo, Norway, [4] State Key Laboratory of Plant Genomics, CAS-JIC Centre of Excellence for Plant and Microbial Science (CEPAMS), Institute of Genetics and Developmental Biology, Chinese Academy of Sciences, Beijing, China, [5] Faculty of Advanced Engineering, Tokyo University of Science, Tokyo, Japan

Keywords: peptide, plant development, CLE, TDIF, abiotic stress

Editorial on the Research Topic

Peptide Signaling in Plants

OPEN ACCESS

Edited and reviewed by:
Anna N. Stepanova,
North Carolina State University,
United States

****Correspondence:***
Qingyu Wu
wuqingyu@caas.cn
Wolfgang Schmidt
wosh@gate.sinica.edu.tw
Reidunn Birgitta Aalen
reidunn.aalen@ibv.uio.no
Cao Xu
aoxu@genetics.ac.cn
Fuminori Takahashi
f.takahashi@rs.tus.ac.jp

Specialty section:
This article was submitted to Plant Physiology, a section of the journal Frontiers in Plant Science

Received: *27 December 2021*
Accepted: *20 January 2022*
Published: *15 February 2022*

Citation:
Wu Q, Schmidt W, Aalen RB, Xu C and Takahashi F (2022) Editorial: Peptide Signaling in Plants. Front. Plant Sci. 13:843918. doi: 10.3389/fpls.2022.843918

Small peptides, molecules that consist of <100 amino acids, control a plethora of important biological processes in plants, including development, nutrient signaling, and stress responses. Although significant progress has been made over the past two decades in deciphering plant peptide signaling pathways, many facets of the biogenesis, function, and molecular mechanisms by which peptides act in plants remain to be clarified.

The articles in this Research Topic encompass an evolutionary comparison of different peptide families from a wide range of species, large-scale identification of novel peptides using a combination of multi-omics techniques, an analysis of peptide and receptor interactions using biochemical and molecular genetic approaches, and reviews summarizing recent findings in the field of plant peptides. Through the efforts of the contributors to this Research Topic, we have achieved a wider and deeper understanding of peptides in plants.

Despite significant progress, identifying small peptides remains challenging. Although bioinformatics approaches already in 2006 postulated the presence hundreds of Arabidopsis genes encoding small secreted peptides (Lease and Walker, 2006), relatively small number of peptide genes have been identified and functionally characterized. Thus, the number of peptides available for use in training sets for identifying new peptides is limited. As reviewed by Ren et al. many unconventional small peptides are derived from undocumented regions of the genome, such as intergenic regions, untranslated regions, introns, reading frames differing from those of annotated genes, and non-coding RNAs, rather than from well-annotated coding sequences, further hampering the identification of small peptides. New approaches are therefore needed to identify peptides at scale. Liang et al. identified 2,695 peptides by integrating a large-scale dataset that includes mRNA-seq, Ribo-seq, and mass spectrometry data from six tissues of maize (*Zea mays*). This study expands the inventory of known plant peptides. Unfortunately, many small peptides seem to function at extremely low concentrations in plants, and are difficult to detect due to technical limitations. Thus, a key goal in the field is developing highly sensitive technologies capable of cataloging these low-abundance peptides.

Examples of peptides that perform critical biological functions but are maintained at very low concentrations are members of the CLAVATA3/EMBRYO SURROUNDING REGION-RELATED (CLE) family. CLAVATA3 (CLV3), a peptide consisting of 12 or 13 amino acids in its mature form, regulates shoot meristem maintenance in the classical CLAVATA–WUSCHEL pathway

(Clark et al., 1995) and was the first characterized member of this family. This pathway includes a secreted peptide, CLV3; a leucine-rich repeat receptor-like kinase, CLV1; and a homeodomain transcription factor, WUSCHEL (WUS). Binding of the CLV3 peptide by CLV1 leads to repression of WUS, which in turn promotes *CLV3* expression, thereby forming a negative feedback pathway [reviewed by (Li et al., 2021)]. This pathway is functionally conserved among a subset of flowering plants, including *Arabidopsis*, rice (*Oryza sativa*), tomato (*Solanum lycopersicum*), maize, and *Brassica juncea*. Works by Zhu et al. and Takahashi et al. expand our knowledge of the CLV–WUS pathway to a larger group of species. Zhu et al. show that ablation of *Setaria viridis* FLORAL ORGAN NUMBER 2 (SvFON2), the homolog of *Arabidopsis* CLV3 and rice FON2 peptides, results in a larger inflorescence meristem, suggesting that SvFON2 functions in inflorescence meristem development. Results reported by Takahashi et al. revealed that, similar to the *Arabidopsis* model, the receptor MpCLV1 and co-receptor MpCLAVATA3 INSENSITIVE RECEPTOR KINASE (MpCIK) form a complex that perceives signals from the *Marchantia polymorpha* CLV3 ortholog MpCLE2, suggesting that the function of CLV3-like peptides and their receptors is conserved beyond flowering plants.

Members of the CLE family, such as DODECAPETIDE TRACHEARY ELEMENT DIFFERENTIATION INHIBITORY FACTOR (TDIF)/CLE41, are also important regulators of vascular development, as reviewed by Yuan and Wang. TDIF/CLE41 binds to its receptor PHLOEM INTERCALATED WITH XYLEM/TDIF RECEPTOR (PXY/TDR) and signals through two WUSCHEL-related HOMEOBOX transcription factors, WOX4 and WOX14 (Hirakawa et al., 2010; Etchells et al., 2013). Xu et al. identified a new regulator in the CLE41/TDIF-TDR/PXY signaling pathway: PXY-CORRELATED 3 (PXC3). The width of the hypocotyl stele and the number of vascular cells are reduced in *pxc3* loss-of-function mutants, indicating that PXC3 functions in vascular development in *Arabidopsis*. Tian et al. demonstrate that ectopic expression of the switchgrass *CLE* family member *DODECAPETIDE TRACHEARY ELEMENT DIFFERENTIATION INHIBITORY FACTOR-LIKE 1* (*PvTDIFL1*) in *Arabidopsis* strongly inhibits plant growth, increases cell division in vascular tissue, and disrupts the cellular organization of the hypocotyl, suggesting that TDIFL proteins are functionally conserved between switchgrass and *Arabidopsis*.

Our knowledge of the evolutionary processes that gave rise to small peptides is limited. To address this shortcoming, Furumizu and Sawa searched for members of the ROOT GROWTH FACTOR (RGF)/GOLVEN (GLV)/CLE-LIKE (CLEL) family of peptides in a wide range of species, including liverworts, mosses, hornworts, lycophytes, and ferns. All major extant land plant lineages, except hornworts, harbored subsets from a total of more than 400 identified RGF-like peptides. The authors demonstrate that MpRGF from *Marchantia polymorpha* possesses known RGF-like activities and can affect plant growth when constitutively expressed in *Arabidopsis* or *Marchantia polymorpha*. This study advances our understanding of how peptide signaling pathways evolved.

In addition to their developmental functions, plant peptides are involved in abiotic stress responses via cell-to-cell communication networks (Kim et al.). In their review, the authors summarize the roles of different peptide families in orchestrating plant responses to drought, salt, heat, nutrient deficiency, and reactive oxygen species (ROS). Remarkably, the ability of plants to modulate ROS production allows small peptides to regulate pollen tube growth. Kou et al. show that adding purified phytosulfokine PSK2 to pollen promotes pear pollen tube elongation in a dose-dependent manner by increasing ROS production, indicating a potential application of peptides in improving pollination efficiency.

Collectively, this Research Topic provides fascinating and topical information on plant peptide signaling. The articles cover important aspects of plant peptides, such as their involvement in plant development and abiotic stress, and the mining of peptides from multi-omics data. However, several questions remain to be addressed. How can low-abundance peptides be detected efficiently? How do receptors recognize and distinguish different peptides that share high sequence similarity? Can external application of small peptides improve crop yield and tolerance to biotic and abiotic stresses? Can small peptides be tweaked to improve agronomic traits and increase agricultural sustainability? Given the potential benefits that answers to these questions may hold, we would like to invite more scientists to join us in studying these impressive and intriguing small molecules.

AUTHOR CONTRIBUTIONS

All authors wrote and approved the editorial.

ACKNOWLEDGMENTS

We thank the all authors, reviewers, and Frontiers editorial staff for contributing to this Research Topic. QW acknowledge the financial support provide by the National Key Research and Development Program of China (2021YFF1000400) and National Natural Science Foundation of China (32171925).

REFERENCES

Clark, S. E., Running, M. P., and Meyerowitz, E. M. (1995). CLAVATA3 is a specific regulator of shoot and floral meristem development affecting the same processes as CLAVATA1. *Development* 121, 2057–2067. doi: 10.1242/dev.121.7.2057

Etchells, J. P., Provost, C. M., Mishra, L., and Turner, S. R. (2013). WOX4 and WOX14 act downstream of the PXY receptor kinase to regulate plant vascular proliferation independently of any role in vascular organisation. *Development* 140, 2224–2234. doi: 10.1242/dev.091314

Hirakawa, Y., Kondo, Y., and Fukuda, H. (2010). TDIF peptide signaling regulates vascular stem cell proliferation via the WOX4 homeobox gene in Arabidopsis. *Plant Cell* 22, 2618–2629. doi: 10.1105/tpc.110.076083

Lease, K. A., and Walker, J. C. (2006). The arabidopsis unannotated secreted peptide database, a resource for plant peptidomics. *Plant Physiol.* 142, 831–838. doi: 10.1104/pp.106.086041

Li, S., Meng, S., Weng, J., and Wu, Q. (2021). Fine-tuning shoot meristem size to feed the world. *Trends Plant Sci.* doi: 10.1016/j.tplants.2021.10.004. [Epub ahead of print].

Conflict of Interest: The authors declare that the research was conducted in the absence of any commercial or financial relationships that could be construed as a potential conflict of interest.

Publisher's Note: All claims expressed in this article are solely those of the authors and do not necessarily represent those of their affiliated organizations, or those of the publisher, the editors and the reviewers. Any product that may be evaluated in this article, or claim that may be made by its manufacturer, is not guaranteed or endorsed by the publisher.

frontiers in Plant Science

ORIGINAL RESEARCH
published: 30 November 2020
doi: 10.3389/fpls.2020.601993

The Peptide PbrPSK2 From Phytosulfokine Family Induces Reactive Oxygen Species (ROS) Production to Regulate Pear Pollen Tube Growth

Xiaobing Kou†, Qian Liu†, Yangyang Sun, Peng Wang, Shaoling Zhang and Juyou Wu**

State Key Laboratory of Crop Genetics and Germplasm Enhancement, Centre of Pear Engineering Technology Research, College of Horticulture, Nanjing Agricultural University, Nanjing, China

OPEN ACCESS

Edited by:
Qingyu Wu, Chinese Academy of Agricultural Sciences (CAAS), China

Reviewed by:
Xu Fang, Shandong University, China
Guodong Wang, Shaanxi Normal University, China

***Correspondence:**
Shaoling Zhang
slzhang@njau.edu.cn
Juyou Wu
juyouwu@njau.edu.cn

† These authors have contributed equally to this work

Specialty section:
This article was submitted to Plant Physiology, a section of the journal Frontiers in Plant Science

Received: *02 September 2020*
Accepted: *27 October 2020*
Published: *30 November 2020*

Citation:
Kou X, Liu Q, Sun Y, Wang P, Zhang S and Wu J (2020) The Peptide PbrPSK2 From Phytosulfokine Family Induces Reactive Oxygen Species (ROS) Production to Regulate Pear Pollen Tube Growth. Front. Plant Sci. 11:601993. doi: 10.3389/fpls.2020.601993

Phytosulfokines (PSKs) are plant peptide growth factors that participate in multiple biological processes, including cell elongation and immune signaling. However, little is known about PSKs in Rosaceae species. Here, we identified 10 *PSK* genes in pear (*Pyrus bretschneideri*), 11 in apple (*Malus* × *domestica*), four in peach (*Prunus persica*), six in strawberry (*Fragaria vesca*), and five in Chinese plum (*Prunus mume*). In addition, we undertook comparative analysis of the *PSK* gene family in pear and the four other species. Evolutionary analysis indicated that whole genome duplication events (WGD) may have contributed to the expansion of the *PSK* gene family in Rosaceae. Transcriptomes, reverse transcription-PCR and quantitative real-time-PCR analyses were undertaken to demonstrate that *PbrPSK2* is highly expressed in pear pollen. In addition, by adding purified *E. coli*-expressed PbrPSK2 to pollen and using an antisense oligonucleotide approach, we showed that PbrPSK2 can promote pear pollen tube elongation in a dose-dependent manner. Furthermore, PbrPSK2 was found to mediate the production of reactive oxygen species to regulate pear pollen tube growth.

Keywords: phytosulfokine, pear, WGD events, pollen tube growth, ROS

INTRODUCTION

Polypeptide signals play essential roles in many aspects of plant life including growth, development, reproduction and immunity (Story, 1991; Pearce et al., 2001; Peng et al., 2002; Ryan et al., 2002). For example, CLE (CLV3/ESR-related) peptides, identified as intercellular signaling molecules, could regulate cell differentiation and division in plant development (Fiers et al., 2007; Araya et al., 2014). RGF (root meristem growth factor) is a secreted peptide involved in the maintenance of root stem cell niche (Mari et al., 2010; Matsubayashi, 2013). Classified as secreted peptides, IDA (INFLORESCENCE DEFICIENT IN ABSCISSION) are characterized to play important roles in petal abscission (Melinka, 2003; Estornell et al., 2015). PLS (POLARIS) peptide family is identified to be involved in longitudinal cell expansion and increased radial expansion (Topping and Lindsey, 1997). SP11/SCR (S-locus protein 11 or S-locus Cys-rich) is a male determinant, involved in process of *Brassica* self-incompatibility (Shiba et al., 2001; Sato et al., 2004; Fujimoto et al., 2006). Similarly, AtLURE1 is a defensin-like peptide that functions in attracting pollen tubes into the embryo sac in *arabidopsis*

(Okuda et al., 2009). SCA (Stigma/stylar cysteine-rich adhesion) belongs to lipid transfer proteins and is involved in adhesion of pollen tube to the extracellular matrix of female tissues (Mollet et al., 2000). RALFs (Rapid alkalization factors) are a group of cysteine-rich peptides (CRPs) regulating pollen tube growth and burst in plant reproduction (Wu et al., 2000; Ge et al., 2017). In addition, phytosulfokine (PSK) is a plant peptide family, plays a role in plant cell growth, and thus employed as the research objective in our study.

Synthesized from 80 to 120 amino acid prepropeptides, PSK is a small peptide containing an N-terminal signal peptide sequence and a C-terminal PSK sequence (Yang et al., 2001). PSK was firstly identified as a key regulator for inducing division in cell cultures at low density (Stuart and Street, 1969). Since the first *PSK* gene was characterized, more members of the *PSK* gene family have been identified in various plant species. For example, *PSK* genes are ubiquitously expressed in *Arabidopsis*, where the peptides are encoded by a small gene family containing six members (Lorbiecke and Sauter, 2002). Moreover, seven *PSK* genes are predicted to exist in the rice (*Oryza sativa*) genome (Yang et al., 1999). Nevertheless, PSKs those in Rosaceae have yet to be characterized and remain unstudied.

Since identified as a signaling molecule, PSKs have been verified functions in plant growth and development (Yamakawa et al., 1998; Yang et al., 1999; Kim et al., 2006). For example, PSK can induce the proliferation of asparagus and rice cells in low-density cell cultures (Matsubayashi et al., 1996). PSKs also act as signaling molecules of root elongation involving in growth regulation. For instance, AtPSK1 affects root elongation primarily via control of mature cell size in *Arabidopsis* (Kutschmar et al., 2009). PSK promotes root growth by repressing expression of pectin methylesterase inhibitor (PMEI) genes in *Medicago truncatula* (Yu et al., 2020). In *Cunninghamia lanceolate*, PSK had been shown to promote primary root growth and adventitious root formation (Wu et al., 2019). Additionally, PSK acts as a growth factor to stimulate somatic embryogenesis in *carrot* (Hanai et al., 2000). PSK interacts with phytosulfokine receptor 1 (PSKR1) to participate in the regulation of hypocotyl length and cell expansion in *Arabidopsis* (Stührwohldt et al., 2011). Known as a significant process that limits crop yield, the drought-induced premature abscission of flowers and fruits is identified to be regulated by PSKs (Reichardt et al., 2020). Furthermore, PSK acts as a signal molecule in the fertilization of female tissues. In tobacco (*Nicotiana tabacum* L.), PSK could promote pollen germination in a dose–dependent manner (Chen et al., 2000). In maize (*Zea mays* L.), two *PSK* precursor genes were shown to be specifically expressed in male and female gametophytes (Lorbiecke et al., 2005). In *Arabidopsis*, PSK peptide signaling (*AtPSK2*) participates in the processes of pollen tube growth and funicular pollen tube guidance (Stührwohldt et al., 2015), indicating that PSK plays important roles in plant reproduction. In addition, crucial regulatory roles for PSK in plant immunity have been confirmed in some *Arabidopsis* cultivars with enhanced plant immunity and resistance (Yamakawa et al., 1999; Igarashi et al., 2012). In Tomato (*Solanum lycopersicum*), PSK peptide Initiates auxin-dependent immunity through cytosolic Ca^{2+} signaling (Zhang et al., 2018). Nevertheless, functional investigations of PSKs have been limited in model plants and the roles of these molecules are poorly understood in the Rosaceae.

Pear is one of the most economically important fruit crops world-wide. The pear genome has recently been reported (Wu et al., 2013), which enables the comprehensive analysis of the *PSK* gene family in pear. In the present study, we conducted a comprehensive analysis of the *PSK* gene family in pear and four other Rosaceae species. In addition, we identified a *PSK* gene in pear, *PbrPSK2*, which can regulate pollen tube growth. These results provide valuable information for future functional studies of PSK in pear.

MATERIALS AND METHODS

Identification of *PSK* Genes in Rosaceae

To identify potential members of the *PSK* gene family in Rosaceae, we performed multiple database searches. The PSK domain PF06404, downloaded from Pfam[1], was used as a query to perform BLAST searches in HMMER3 software against pear and other Rosaceae genome databases. Apple, peach and strawberry PSK protein sequences were downloaded from the GDR[2] and Phytozome v.9.1[3] (Goodstein et al., 2012). Pear PSK protein sequences were downloaded from the pear genome project database[4] (Wu et al., 2013). Chinese plum PSK protein sequences were downloaded from the *Prunus mume* Genome Project[5] (Zhang et al., 2012). All *PSK* genes with expected *E*-values of < 0.001 were collected. Candidate sequences were then examined, and SMART[6] was used to confirm the candidate *PSK* genes.

In addition, EXPASY[7] was used to compute the theoretical isoelectric point and molecular weight values from the amino acid sequences of the *PSK* genes.

Rosaceae PSK Domain Sequence Analysis

To determine the level of sequence conservation and functional homology of PSK in pear, apple, peach, strawberry and Chinese plum, multiple sequence alignment of partial selected candidate PSK domains was carried out using ClustalX[8] in SMS[9]. The PSK domain was acquired from Pfam[10].

Phylogenetic Analysis

The complete PSK protein sequence was used to perform multiple sequence alignments using ClustalX (see footnote)

[1]http://pfam.xfam.org/family/PF06404
[2]http://www.rosaceae.org/
[3]http://www.phytozome.net/search.php
[4]http://peargenome.njau.edu.cn/
[5]http://prunusmumegenome.bjfu.edu.cn/index.jsp
[6]http://smart.embl-heidelberg.de/
[7]http://web.expasy.org/compute_pi/
[8]http://www.clustal.org/
[9]http://www.bioinformatics.org/sms2/
[10]http://pfam.xfam.org/family/PF06404

with default parameters (Larkin et al., 2007). The neighbor-joining method was used to construct a phylogenetic tree with MEGA 7.0 from the full-length protein sequences of PSK in five Rosaceae species. The phylogenetic trees were presented using EVOLVIEW[11] (He et al., 2016) and the reliability was tested using the bootstrap method with 1,000 replicates.

Conserved Motif and Gene Structure Analysis

In order to examine the relationships involved in the structural evolution of *PSK* genes, we compared the gene structures and motifs of individual *PSK* genes in pear, apple, peach,strawberry and Chinese plum. The motifs were constructed online in Multiple Expectation Maximization for Motif Elicitation (MEME)[12] using the full-length amino acid sequences of all Rosaceae PSK proteins (Bailey et al., 2006). Exon-intron structural information for the *PSK* genes was obtained from the pear, apple, peach, strawberry, and Chinese plum genome project. The motifs and gene structures of the *PSK* genes were redrawn using TBtools (Chen et al., 2018).

Synteny Analysis of *PSK* Genes

Information on the synteny relationships among pear, apple, peach, strawberry and Chinese plum were obtained from the pear, apple, peach, strawberry, and Chinese plum genome project, respectively (Velasco et al., 2010; Shulaev et al., 2011; Zhang et al., 2012; Verde et al., 2013; Wu et al., 2013), and the orthologous and paralogous relationships among the five species were plotted using the circos project[13] (Krzywinski et al., 2009). MCScanX was further used to identify whole-genome duplication/segmental, tandem, proximal and dispersed duplications in the PSK gene family (Wang et al., 2012).

Calculating the Ka and Ks Values for the *PSK* Gene Family

The Ka and Ks substitution rates of the syntenic gene pairs were annotated using MCScanX downstream analysis tools. KaKs_Calculator 2.0 was used to determine Ka and Ks (Wang et al., 2012).

Gene Inhibition by Antisense Oligodeoxynucleotides (ODN)

The construction of *PbrPSK2* mRNA was predicted using the RNA fold Web Server[14]. The candidate as-ODN sequence was evaluated in DNAMAN and SnapGene. The as-ODN sequence was synthesized from phosphorothioate and purified by high-performance liquid chromatography. Pollen was pre-cultured in liquid medium for 45 min at 25°C, 120 rpm. The culture contained: 0.03% Ca $(NO_3)_2{\cdot}4H_2O$, 0.01% H_3BO_3, 10% sucrose and 0.58% 2-(N-morpholino) ethanesulfonic acid hydrate (MES) at pH 6.2 (adjusted with Tris). The PbrPSK2-asODN primers were mixed with Lipofectamine™ 2000 Transfection Reagent (11668027, Thermo Fisher Scientific, Shanghai) and incubated for 15 min before being added into the pre-cultured pollen. The pollen tubes were kept in the culture for 1.5 h and visualized with a Nikon Eclipse E100 microscope. The lengths of the pollen tubes were measured with IPWin32 software. Finally, pollen samples were centrifuged, the supernatant removed and the precipitate kept. Then, samples were preserved by freezing in liquid nitrogen and stored at −80°C. All materials were harvested for the extraction of total RNA. Quantitative real-time (qRT) PCR was used to detect the expression of *PbrPSK2*. The primers used for this assay are listed in **Supplementary Table S4.**

Expression and Purification of PbrPSK2 Protein From *E. coli*

A DNA fragment encoding PbrPSK2 was cloned into the pCold TF vector and expressed in *E. coli* strain BL21. A single positive clone was cultured in medium containing 100 μg/mL ampicillin at 25°C and 220 rpm for 16 h and then transferred to fresh medium at a dilution of 1/100. When the OD600 of the culture reached 0.6–1.2, IPTG was added to induce recombinant protein expression at 15°C and 220 rpm for 24 h. The expression of the recombinant protein was identified by SDS-PAGE. Finally, the purified protein was dialyzed (Spectra/por® membrane, molecular cutoff 2,000–3,000) against 1 L of pollen medium at 4°C for 24 h and stored at -80°C. The primers used for this assay are listed in **Supplementary Table S4.**

Nitroblue Tetrazolium (NBT) Assay for the Detection of Reactive Oxygen Species

To detect a change of reactive oxygen species (ROS) in pollen tube tips after PbrPSK2 treatment, pear pollen was pre-cultured in liquid medium at 25°C and 120 rpm for 45 min and then treated with recombinant PbrPSK2 protein. As a negative control, DPI (diphenylene iodonium) and Mn-TMPP [Manganese (III) 5,10,15,20-tetra (4-pyridyl)-21H,23H-porphine] were used to treat the pre-cultured pollen tubes. The pollen was cultured for another 1.5 h. Finally, the pollen tubes were stained with NBT (1 mg/mL) for 5 min. The change in ROS content at pollen tube tips was visualized with a Nikon Eclipse E100 microscope. More than 50 pollen tubes were detected in each treatment, with three repeats.

Expression Analyses of *PSKs* in Five Pear Tissues

RT-PCR analysis was used to study the expression of PSK genes in five types of tissue, including young root, leave, stem, pollen and pistil from the pear "Dangshansuli." Total RNA was extracted using a Plant Total RNA Isolation Kit (FOREGENE, Chengdu, China) and genomic DNA contamination was removed by Dnase I. RT-PCR was carried out according to the manufacturer's instructions. The PCR temperature scheme was regulated according to the oligonucleotide primers employed for the experiments. The RT-PCR process was as follows: 3 min at 94°C, 30 cycles of 30 s at 94°C, 30 s at 60°C, 1 min at 72°C and 10 min

[11] http://www.evolgenius.info/evolview/

[12] http://meme.nbcr.net/meme/cgibin/meme.cgi

[13] http://circos.ca/

[14] http://rna.tbi.univie.ac.at/cgi-bin/RNAWebSuite/RNAfold.cgi

of extension at 72°C. All PCR experiments were repeated three times to confirm the reproducibility of the results.

Analyses of *PbrPSKs* Expression During Pollen Tube Growth

Quantitative RT-PCR was used to analyze the expression of *PbrPSK* genes in pollen during the developmental stages of the pear "Dangshansuli." Primer 5.0 was used to design the unique primers according to the *PbrPSK* gene sequences. Neither primer dimers nor unexpected products were found and primers were diluted sixfold. qRT-PCR was performed on LightCycler-480 Detection System (Roche, Penzberg, Germany) using AceQ® qPCR SYBR® Green Master Mix (Vazyme, Nanjing, China), according to the manufacturer's protocol. Reactions were prepared in a total volume of 20 μL containing: 10 μL of AceQ® qPCR SYBR® Green Master Mix, 5 μL of nuclease-free water, 2.5 μL of each diluted primer and 0.1 μL of cDNA. The qRT-PCR began with 5 min at 95°C, followed by 45 cycles at 95°C for 3 s, 60°C for 10 s and 30 s of extension at 72°C. *PbrTUB* was used as reference gene and the relative expression levels were calculated using the 2-ΔΔCt method. All RNA extraction and cDNA synthesis experiments for all samples were performed with three biological and technical replicates.

RESULTS

Identification and Bioinformation of *PSK* Genes in the Rosaceae

A Hidden Markov Model search (HMM search) using "Phytosulfokine precursor protein" domain (Pfam: PF06404) was carried out in five Rosaceae genome databases and

TABLE 1 | Characteristics of the PSK proteins.

Gene name	Gene ID	Chr locous	Genomic position	CDS length (bp)	Protein length (aa)	PI	MW (kDa)	
PbrPSK1	Pbr033759.1	15	30125362–30126069	249	82	5.05	9	WGD
PbrPSK2	Pbr019776.1	15	7007426–7007908	255	84	5.2	9.3	WGD
PbrPSK3	Pbr001074.1	2	12193941–12194510	255	84	4.85	9.3	WGD
PbrPSK4	Pbr029236.1	1	2370098–2370610	258	85	6.9	9.6	WGD
PbrPSK5	Pbr017982.1	17	19789236–19789748	258	85	6.9	9.6	WGD
PbrPSK6	Pbr030039.1	13	4052766–4053325	306	101	4.64	10.8	WGD
PbrPSK7	Pbr025638.1	10	16763000–16763383	258	85	5.61	9.4	dispersed
PbrPSK8	Pbr005499.1	12	20880364–20881482	249	82	6.05	9.6	WGD
PbrPSK9	Pbr004808.1	3	13115592–13116225	285	94	5.06	10.5	WGD
PbrPSK10	Pbr016802.1	14	3257529–3257919	240	79	4.92	9	WGD
MdPSK1	MD02G1189200	14	17279050–17279779	303	100	4.90	11.1	WGD
MdPSK2	MD15G1066300	15	4612903–4613689	255	84	5.82	9.6	WGD
MdPSK3	MD15G1300000	15	28529252–28529832	249	82	4.85	8.9	WGD
MdPSK4	MD05G1105500	5	21872939–21873522	261	86	4.97	9.3	WGD
MdPSK5	MD13G1053700	13	3785657–3786239	306	101	4.48	10.8	
MdPSK6	MD10G1110000	10	18087718–18088297	258	85	4.68	9.3	WGD
MdPSK7	MD08G1079100	8	6590799–6591412	258	85	7.84	95	WGD
MdPSK8	MD11G1157500	11	15199717–15200525	285	94	5.87	10.6	WGD
MdPSK9	MD14G1016200	14	1461086–1462014	249	82	5.19	9.4	WGD
MdPSK10	MD12G1018200	12	1740431–1741485	249	82	6.71	9.6	WGD
MdPSK11	MD03G1134700	3	13446978–13448023	285	94	4.61	10.4	WGD
PpPSK1	Prupe.6G217500.1	6	22440310–22441230	246	81	4.85	8.9	WGD
PpPSK2	Prupe.8G150200.1	8	16361784–16362457	255	84	4.7	9.3	WGD
PpPSK3	Prupe.7G116900.1	7	14189550–14190256	237	78	5.09	9.1	
PpPSK4	Prupe.1G420000.1	1	36347487–36348242	255	84	5.21	9.3	WGD
FvPSK1	FvH4_1g18100.1	1	10519153–10520025	192	63	10.18	6.8	
FvPSK2	FvH4_6g17920.1	6	11755315–11755987	240	79	5.36	9.2	Dispersed
FvPSK3	FvH4_2g32750.1	2	17924199–17924836	324	107	6.63	12	Dispersed
FvPSK4	FvH4_2g03340.1	2	24747841–24748458	261	86	4.88	9.6	Proximal
FvPSK5	FvH4_2g03370.1	2	2656597–2657767	354	117	4.66	13	Proximal
FvPSK6	FvH4_3g29900.1	3	23002017–23003111	285	94	4.9	10.5	Dispersed
PmPSK1	Pm021096	6	6679335–6679722	255	84	5.05	9.2	WGD
PmPSK2	Pm002355	1	18913407–18913747	234	77	4.83	8.5	WGD
PmPSK3	Pm005428	2	10969139–10969477	252	83	5.21	9.2	WGD
PmPSK4	Pm001229	1	8232164–8232742	291	96	4.58	10.6	WGD
PmPSK5	Pm026233	8	8630210–8630575	237	78	5.69	9.1	WGD

SMART was used to confirm the candidate *PSK* genes (Eddy, 2011). Protein sequences lacking the PSK domain or with *E*-values > 1e-15 were removed. As a result, 36 candidate *PSK* genes were surveyed in our study. A total of 10 *PSK* genes were identified in pear (*PbrPSKs*), 11 in apple (*MdPSK*s), four in peach (*PpPSKs*), six in strawberry (*FvPSKs*), and five in Chinese plum (*PmPSKs*). The *PbrPSK* genes were distributed unevenly through the genome, with two of the genes located on chromosome 15. Similar to the *PbrPSK* genes, the distribution of *PSK* genes in the other four Rosaceae genomes was also random. We determined that *PbrPSK4* (Chr1:2370098-2370610) and *PbrPSK5* (Chr17: 19789236-19789748) have the same CDS length, isoelectric point and molecular weight (**Supplementary Figure S3** and **Table 1**), and further studies have found that these two genes are, in fact, the same gene located on different chromosomes.

The physical and chemical characteristics of the *PSK* gene family are shown in **Table 1**. The protein sequence lengths varied from 63 to 117 amino acids, but most were between 80 and 90 amino acids long. The values of the isoelectric point were between 4.48 and 10.18 and the molecular weights of the proteins were between 6.8 and 13 kDa.

Phylogenetic Analysis and Structural Characterization of the *PSK* Family

In order to examine the evolutionary relationships of *PSK* genes between pear and the other Rosaceae species (apple, peach, strawberry, and Chinese plum), we constructed a neighbor-joining phylogenetic tree in MAGA 7.0 using the full-length protein sequences of 10 PbrPSKs from pear, 11 MdPSKs from apple, four PpPSKs from peach, six FvPSKs from strawberry and five PmPSKs from Chinese plum. According to the phylogenetic tree (**Figure 1A**), the PSK family members were divided into three major groups (Groups I-III). Interestingly, GroupIIconstituted the smallest branch, with only three members. In addition, GroupIpossessed the largest number of PSK members, with six *PSK* genes in pear (**Figure 1B**).

To investigate the protein structures of PSK in the five Rosaceae species studied, 10 conserved motifs were constructed using the MEME website. From Group I, only PmPSK3 is missing motif 4 and FvPSK5 contains two copies of motif 5, whereas motif 10 only exists in MdPSK5 and PbrPSK6. We also found that, bar FvPSK1, motifs 1 and 2 (containing YIYTQ motif) are present throughout the PSK family in the Rosaceae indicating that they may be conserved among this gene family (**Figure 2** and **Supplementary Figure S4**).

The introns and exons of *PSK* genes were established using GSDS 2.0 (Hu et al., 2015), giving similar results for the motif and gene structures, which were conserved within the same branch. According to the predicted structures, all *PSK* genes have two to three exons with relatively conserved arrangements and similar size.

Evolutionary Pattern Analysis of *PSK*s

Gene duplications play important roles in the expansion of gene families and the generation of new functionalities. To explain the origin of the *PSK* gene family expansion, the MCScanX package was used to analyze the different duplication modes of the *PSK* genes. Three duplication patterns were shown to drive the expansion of the *PSK* gene family: whole-genome, dispersed and proximal duplication. As shown in **Supplementary Table S1** and **Figure 3B**, whole-genome duplication is the main driver of the expansion of the PSK family, as it accounts for 90% (9 for 10), 90% (10 for 11), 75% (3 for 4), and 100% (5 for 5) of gene expansion events studied in pear, apple, peach and Chinese plum, respectively. It is worth noting that two *FvPSKs* (33.3%) were assigned to the proximal duplication block, while the other three (50%) were assigned to the dispersed duplication block. These results showed that a whole-genome duplication event played a critical role in the expansion of the *PSK* gene family in the Rosaceae.

The identification of orthologous genes is required for the accurate understanding of the *PSK* gene family. Therefore, synteny analyses were performed among pear and the other four Rosaceae species. A total of 41 collinear gene pairs were identified among pear and the other Rosaceae species (**Figure 3A** and **Supplementary Table S2**). Collinear pairs within the same species were also identified (**Supplementary Figure S1**) including six pairs in pear, 12 in apple, two in peach and four in Chinese plum. The Ka/Ks ratio for the collinear gene pairs was calculated to identify which selection process drove the evolution of the *PSK* gene family in pear. A ratio of <1 indicates purification selection, a ratio >1 implies positive selection and a ratio = 1 indicates neutral selection. As shown in **Supplementary Table S3**, all Ka/Ks values were <1 indicating that the PSK gene family was conserved, which is consistent with results seen in *Arabidopsis* (Lorbiecke and Sauter, 2002). The Ks value is usually used to estimate the evolutionary dates of WGD events. Previous studies have shown that the pear genome has undergone two WGD events: a recent WGD (30–45 MYA) and an ancient WGD (∼ 140 MYA) (Wu et al., 2013). According to the Ks value of the *PbrPSK* family in our study, we found that the duplicated gene pairs were distributed at the two Ks value peaks (**Figure 3C**). Thus, the recent (30–45 MYA) and ancient (∼140 MYA) WGDs might led to the expansion of the *PbrPSK* gene family.

Expression Profile Analysis of *PSK* Genes in Pear

To study the tissue-specific expression pattern of *PbrPSK* genes in pear, the expression levels of PSK genes in different tissues were determined using transcriptome data (RPKM values) (**Figure 4A**) and RT-PCR (**Figure 4B**), however, we focused more on the genes highly expressed in pollen. The results showed that *PbrPSK2* and *PbrPSK4/5* were highly expressed in pear pollen, and *PbrPSK2* shown a highest expression. *PbrPSK2* is highly expressed in pollen, and lowly expressed in multiple tissues (**Figures 4A,B**). Furthermore, qRT-PCR was used to analyze the expression of *PbrPSK* genes during pollen development in the pear "Dangshansuli." The following stages were investigated: mature pollen, hydrated pollen, pollen tubes that had been growing for 6 h and pollen tubes that had

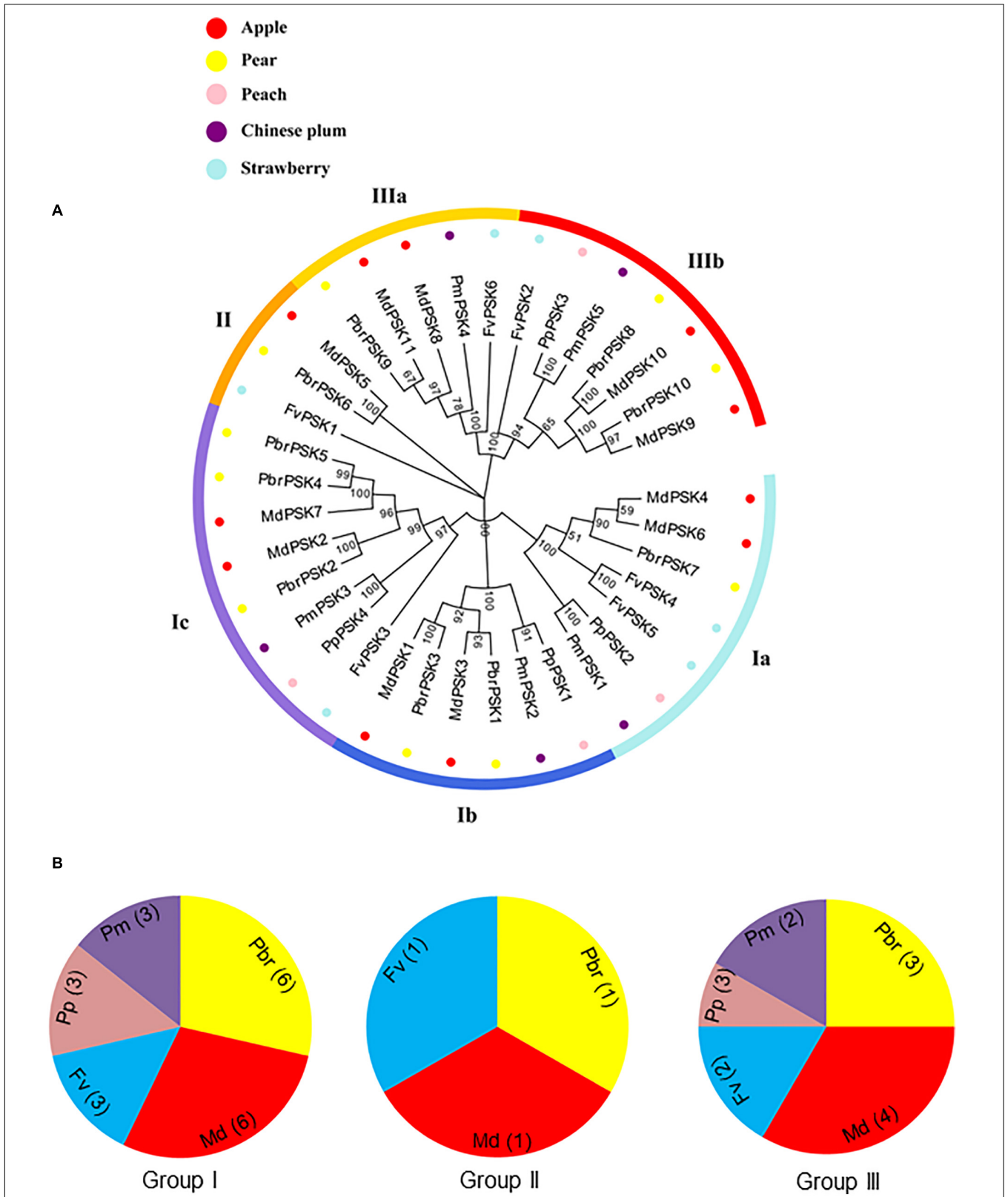

FIGURE 1 | Phylogenetic tree of PSK genes in five Rosaceae species. **(A)** Complete amino acid sequences of PSK proteins identified in five Rosaceae species (pear, apple, peach, strawberry, and Chinese plum) were aligned using Clustal X. The phylogenetic tree was constructed using MEGA7.0 program by the neighbor-joining (NJ) method. A bootstrap test was set as 1,000 replications to test the confidence of the tree. **(B)** The numbers of PSK genes from Rosaceae in group I, II, and III.

FIGURE 2 | Gene structure and the conserved protein motifs in 36 *PSK* genes from five Rosaceae species. Analysis with MEME to investigate 10 conserved motifs in PSK proteins. Ten motifs (1–10) were identified and are indicated by different colors. Introns and exons are represented by black lines and yellow boxes, respectively. The number indicates the phases of the corresponding introns. Each section of bar represents 0.2 kb.

stopped growing. As shown in **Figure 4C**, we found that *PbrPSK2* and *PbrPSK4/5* were highly expressed throughout pollen development. Based on the RT-PCR and qRT-PCR results, *PbrPSK2* was selected for the study of its function in pear pollen tube growth.

PbrPSK2 Regulates Pollen Tube Growth

To examine the roles of *PbrPSK2* in the growth of pear pollen tubes, we expressed and purified PbrPSK2 in *E. coli* (**Supplementary Figure S2**) and dialyzed the proteins in pollen medium for 24 h. When we used these purified PbrPSK2 proteins to treat pear pollen, we found that pollen tube growth was significantly promoted (**Figures 5A,B**). Moreover, pollen germination was significantly promoted by PbrPSK2 (**Figure 5C**). To check the dose effect of PbrPSK2 on pear pollen tube growth, we used different concentrations of the protein to treat pear pollen. The results showed that when the concentration of PbrPSK2 was 0.3 μmol, the promotion of pollen tube growth was at its strongest, but when the concentration of PbrPSK2 exceeded 0.3 μmol, the promotion of pollen tube growth showed a downward trend, but compared with the control, still had a promoting effect (**Figure 5D**). These results showed that *PbrPSK2* can promote pear pollen tube growth in a dose-dependent manner.

In addition, to further study the functions of PbrPSK2 on pear pollen tube growth, we used the as-ODN approach to knock down the expression of *PbrPSK2* in pear pollen and used qRT-PCR to detect the subsequent expression level. As shown in **Figure 5E**, when the expression of *PbrPSK2* was significantly knocked down by ODN treatment (**Figure 5F**), we observed that the elongation of pollen tubes was significantly inhibited (**Figure 5G**), indicating PbrPSK2 could promote pear pollen tube growth.

PbrPSK2 Increases the Production of ROS in Pear Pollen Tube

Reactive oxygen species play important roles in pollen tube growth (Potocký et al., 2007; Speranza et al., 2012; Duan et al., 2014). To further study the effect of PbrPSK2, we detected ROS production in pollen tubes using an NBT assay (Wang et al., 2010). NBT can be reduced to blue formazan precipitates by superoxide radicals, so the position of ROS can be detected. Typical images of pollen tubes with NBT staining under different treatments are shown in **Figure 6**. The control pollen tubes displayed the tip-localized pattern of NBT staining, indicating that pollen tube tips were rich with ROS. Compared with the control and pCold-TF treatment, the gray value at the pollen tube tips increased significantly after PbrPSK2 treatment. ROS at the tips of pollen tubes treated with DPI (a NOX inhibitor) and Mn-TMPP (a ROS scavenger) were removed, and TMPP obviously inhibited pollen tube growth (**Supplementary Figure S5**), which indicated that ROS are necessary for pear pollen tube growth and these ROS may be produced by an RBOH. When we used PbrPSK2 with TMPP to treat pear pollen, the promotion growth pollen tube was less sensitive to PbrPSK2 (**Supplementary Figure S5**). These results showed that PbrPSK2 increased the production of ROS and promoted pear pollen tube growth.

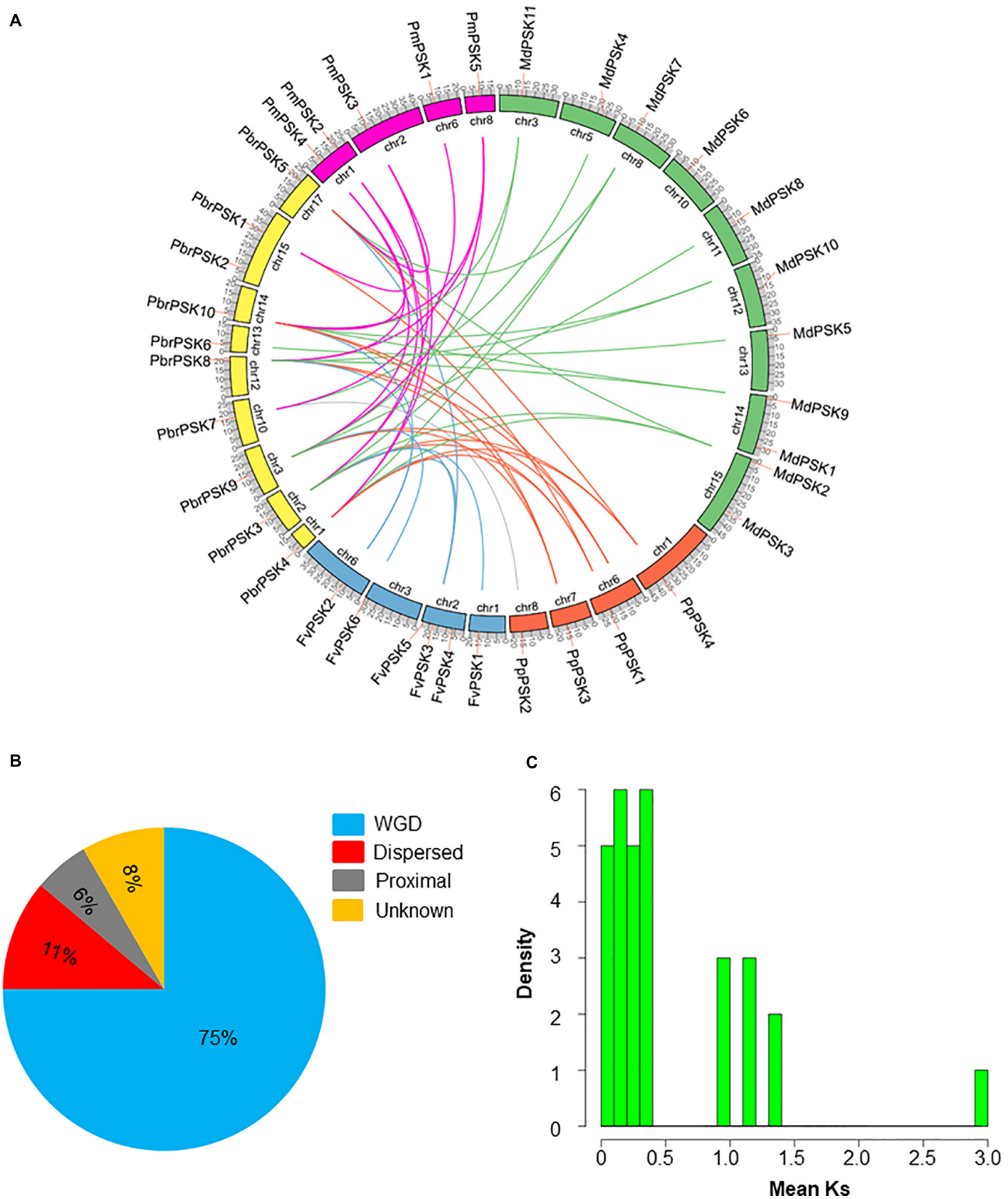

FIGURE 3 | Evolution pattern of PSK genes in pear and other Rosaceae species. **(A)** Synteny analyses of *PbrPSK* genes and other four Rosaceae species. Colorized lines indicate all synteny blocks between pear and other Rosaceae species. Chromosome numbers are indicated on the inner side; gene pairs with syntenic relationships are joined by lines. **(B)** The proportion of duplication model of PSK genes in pear and other Rosaceae. The duplication model includes WGD duplication event, dispersed duplication and proximal duplication. **(C)** Distribution of mean Ks values of *PbrPSK* genes. The *x*-axis represents the mean Ks value; *y*-axis represents the density of the distribution.

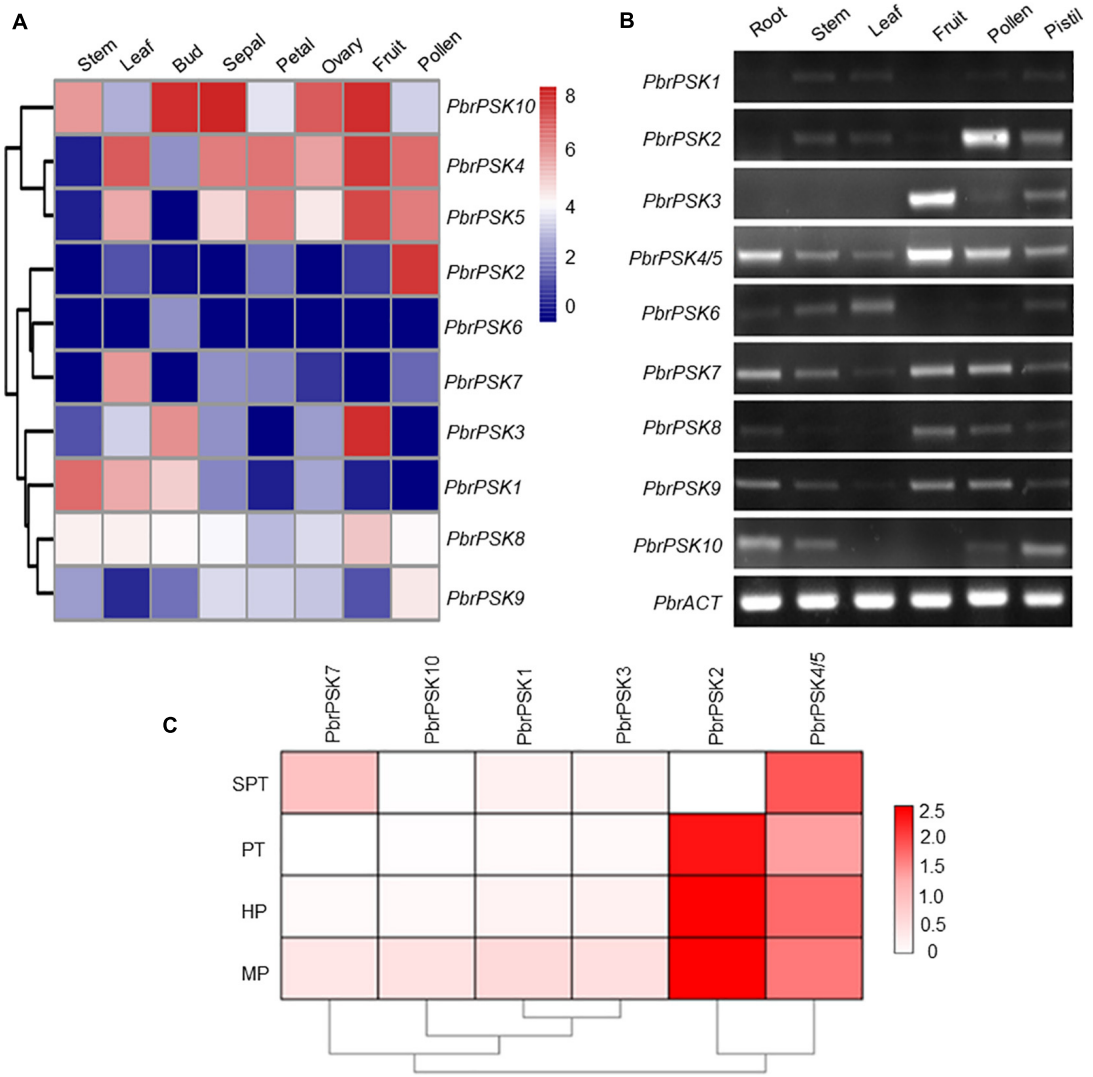

FIGURE 4 | Expression pattern of pear *PSK* genes. **(A)** Expression heatmap of pear *PSK* genes in eight tissues. The expression levels of pear *PSK* genes were measured using RPKM value. Blue indicates a low expression level, white indicates a medium level, and red indicates a high level. **(B)** Expression pattern of *PbrPSK* genes in six tissues using RT-PCR. RT-PCR was performed using root, stem, leaf, fruit, pollen and pistil in pear. An amplified *PbrACT* gene was used as a loading control. Reactions were performed with 30 cycles and experiments were repeated at least three times. **(C)** Heatmap of the expression levels of *PbrPSK* genes during pollen development using qRT-PCR. MP, HP, PT, and SPT correspond to four different developmental stages: mature pollen grains, hydrated pollen, growing pollen tubes 3 h post-hydration and stopped growing pollen tubes, respectively. *PbrTUB* was used as a reference gene.

DISCUSSION

Phytosulfokines are plant peptides that play essential roles in many aspects of plant development such as root growth, pollen tube growth, pollen tube guidance and immune responses (Yamakawa et al., 1999; Kutschmar et al., 2009; Stührwohldt et al., 2015). *PSK* gene families have been identified in many plants (Lorbiecke and Sauter, 2002; Stührwohldt et al., 2015). However, the ensuing biological and genetic roles of these peptides in pear and other Rosaceae species remain uncharacterized. In the present work, we performed a comprehensive investigation of the *PSK* gene family in pear and four other Rosaceae species (apple, peach, strawberry and Chinese plum). A total of 10 *PSK* genes were identified in pear, 11 in apple, four in peach, six in strawberry and five in Chinese plum (**Table 1**). It is interesting that the number of *PSK* genes in pear and apple are almost double the number of in peach, strawberry and Chinese plum. Pear and apple belong to the Maloideae, while strawberry belongs to the Rosoideae, peach and Chinese plum belong to the Prunoideae; a recent whole-genome duplication event occurred in the Maloideae, but not in the Rosoideae or Prunoideae. Therefore, the results indicated that the recent whole-genome duplication may have led to the expansion of the PSK gene family in the Maloideae.

Phylogenetic relationship can provide novel insights into the evolution of diverse gene family members and gene multiplicity

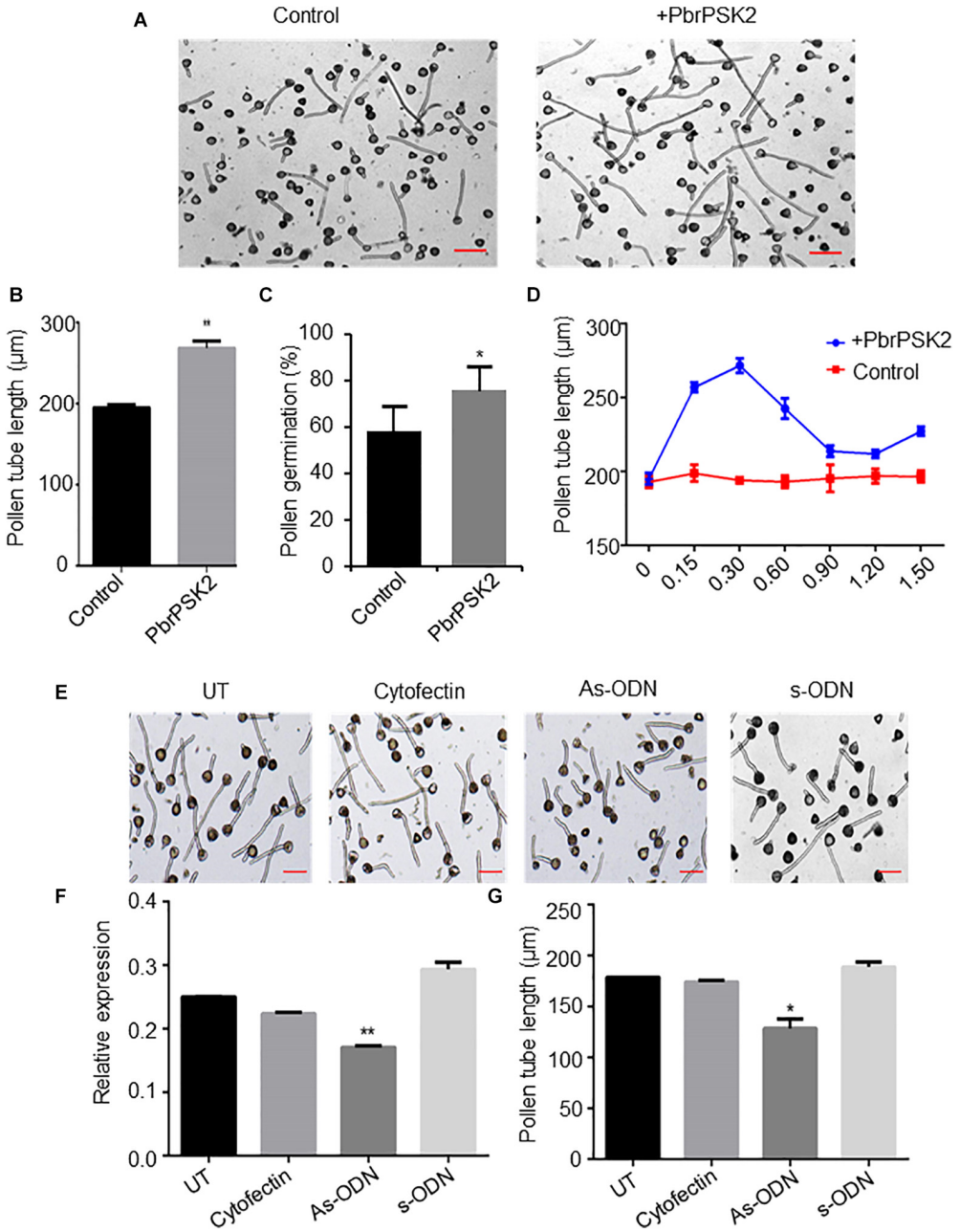

FIGURE 5 | PbrPSK2 promote pear pollen tube growth. **(A)** PbrPSK2 promotes pear pollen tube growth. Images shown were acquired 2 h after treatment without or with purified recombinant PbrPSK2. The experiments were repeated at least three times. Bar = 40 μm. **(B)** The statistical analysis of pollen tube length. Differences were identified using Student's *t*-test and were considered significant when $p < 0.01$, indicating **. More than one hundred pollen tubes were measured. **(C)** The statistical analysis of pollen germination rate. Differences were identified using Student's *t*-test and were considered significant when $p < 0.05$, indicating *. More than one hundred pollen tubes were measured. **(D)** PbrPSK2 promotes pear pollen tube growth in a dose-dependent manner. The statistical analysis of pollen tube length was measured. More than one hundred pollen tubes were measured. **(E)** Knock-down *PbrPSK2* inhibited pollen tube growth using antisense oligonucleotides. UT suggests no treatment controls, cytofectin and s-ODN are used as negative controls. The experiments were repeated at least three times. Bar = 40 μm. **(F)** The expression level of PbrPSK2 is decreased after as-ODN treatment. Cytofection and s-ODN are used as controls. Differences were identified using Student's *t*-test and were considered significant when $p < 0.05$, indicating *. **(G)** The statistical analysis of pollen tube length after as-ODN treatment. Differences were identified using Student's *t*-test and were considered significant when $p < 0.05$, indicating *. More than one hundred pollen tubes were measured.

(Smith et al., 2008). The comparative phylogenetic analysis in this study showed that *PSK* genes in pear and other Rosaceae species can be categorized into three distinct subclasses, which is similar to the classification of PSK genes in *Arabidopsis* (**Figure 1**). Gene structural diversity can offer important information on the evolutionary history of gene families, providing additional

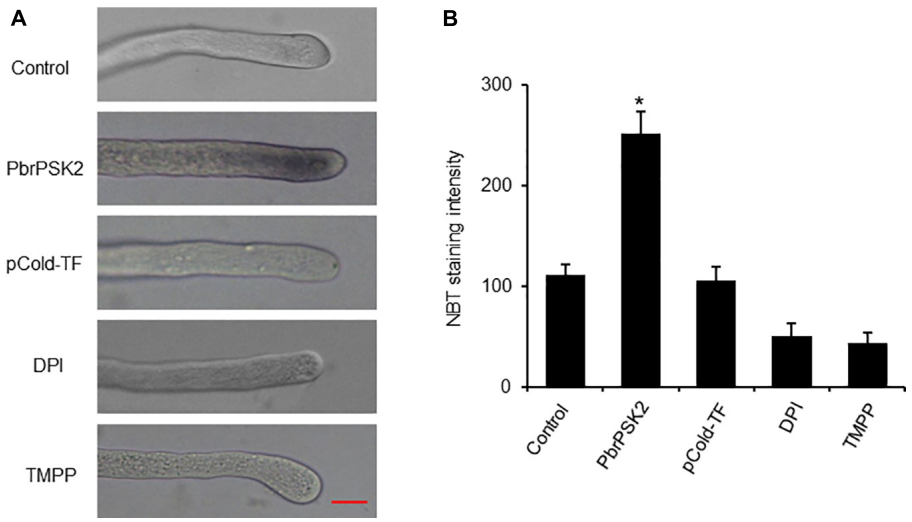

FIGURE 6 | PbrPSK2 induces reactive oxygen species (ROS) production in pollen tubes. **(A)** Typical images of pollen tubes stained with NBT under different treatment conditions for 30 min. At least three independent experiments were repeated with similar results. Mean pixel intensity at the tips of pollen tubes stained with NBT only, NBT with PbrPSK2 (100 nM), NBT with DPI (300 μM), or with Mn-TMPP (300 μM) but without NBT. Bar = 20 μm. **(B)** Statistical analysis of NBT staining intensity in pear pollen tube. Differences were identified using Student's *t*-test and were considered significant when $p < 0.05$, indicating *. More than one hundred pollen tubes were measured.

help to phylogenetic classification (Ames et al., 2012). Based on the phylogenetic analysis, PSKs with similar motif compositions and gene structures were clustered, which were similar to results described for *Arabidopsis*. These findings suggest that PSK genes are highly conserved.

Gene duplication, which may occur through chromosomal segmental duplication or tandem duplication, is thought to be an important means of expanding and gaining functional diversity during evolution (Schacherer et al., 2005; Suhre, 2005). Whole-genome, tandem and segmental duplication are the three main duplication models for gene family expansion (Freeling, 2009). In this study, analysis of duplication models showed that most *PSK* genes in pear and other Rosaceae species were duplicated in WGD duplication events (**Figure 3B** and **Supplementary Table S1**). The number of homologous genes between pear and apple considerably exceeds the number of homologous genes between pear and the other Rosaceae species studied. This result may be due to the recent whole-genome duplication event in pear, which is consistent with the two Ks value peaks in *PbrPSK* duplicated gene pairs, which indicated that the recent (30–45 MYA) and ancient (∼140 MYA) WGDs led to the expansion of *PSK* genes in pear. The Ka/Ks ratios were used to represent the selection constraint for evolutionary selection (Hu and Banzhaf, 2008). Our result showed that all the ratios of duplicated pairs in *PSK* genes were <1 (**Supplementary Table S3**), indicating that the *PSK* genes were conserved.

Gene expression patterns provide important information on gene function. In *Arabidopsis*, many members of the PSK family have been reported to be involved in cell development (Yamakawa et al., 1998; Yang et al., 1999; Kim et al., 2006). To dissect the expression patterns of *PSK* genes in pear, Transcriptome data (RPKM values) and RT-PCR were used to map the expression level in different tissues of pear. For the *PSK* genes in pear, we were most interested in those which play important roles during pear reproductive processes. The results showed that five *PSK* genes were expressed in pear pollen (*PbrPSK2*, *PbrPSK4/5*, *PbrPSK7*, *PbrPSK8,* and *PbrPSK9*), with *PbrPSK2* showing the largest expression level (**Figures 4A,B**). *PbrPSK2* was expressed at a low level in multiple tissues, but highly expressed in pollen, indicating that *PbrPSK2* may play important roles in pear pollen development. Furthermore, we examined the expression level in pear pollen tube development using qRT-PCR and generated a heatmap (**Figure 4C**). Based on the heatmap, *PbrPSK4/5* was expressed in all four stages of pollen tube growth. *PbrPSK2* was highly expressed at all stages of pollen tube development except in those that had stopped growth. The expression level of *PbrPSK2* in pollen tube growth was significantly higher than that for other *PbrPSK* genes. These results further demonstrated that *PbrPSK2* is likely to play important roles in pear pollen tube growth.

Many proteins have been identified as regulators in pollen tube growth. For example, pollen tube growth in *Arabidopsis* and tomato is respectively inhibited by AtRALF4/19 and SlRALF (Covey et al., 2010; Mecchia et al., 2017). Transmitting-tract-specific protein (TTS), as positive regulator, plays important roles in pollen tube growth (Wu et al., 2000). In this study, several pieces of evidence suggested a promoting effect of PbrPSK2 on pear pollen tube growth. In pear pollen treated with purified *E. coli*-expressed PbrPSK2, pollen tube elongation was promoted in a dose-dependent manner (**Figures 5A–D**). When the expression level of *PbrPSK2* was knocked down in pear pollen using ODN, the pollen tube grew slower (**Figures 5E–G**). These results provide more evidence that pollen peptides, which pollen itself produces, regulate pollen tube growth.

Reactive oxygen species production is essential for cell signaling and regulation, but excess ROS accumulation is injurious to cell survival (Thannickal and Fanburg, 2000). Excessive ROS in cells can serve as a second messenger to mediate multiple signaling pathways (Bae et al., 2011). In our study, we examined the ROS production of pollen tubes after PbrPSK2 treatment using NBT. We observed that PbrPSK2 could increase the production of ROS in pear pollen tubes (**Figure 6**). Its possible mechanism is that PbrPSK2 activates downstream receptors that transduce signals into the cytosol, leading to the production of ROS and elongation of pollen tubes. In summary, based on our results, PbrPSK2 may promote pollen tube growth, but its mechanism for regulating pollen tube growth requires further study.

DATA AVAILABILITY STATEMENT

The raw data supporting the conclusions of this article will be made available by the authors, without undue reservation, to any qualified researcher.

AUTHOR CONTRIBUTIONS

XK and QL conceived the experimental design. XK performed experiments and data analyses. QL and YS contributed synteny analyses and the Perl script, and configured some of the figures. PW revised the final manuscript. JW and SZ managed the experiments. All authors read and approved the final manuscript.

FUNDING

This work was financially supported through grants from the National Natural Science Foundation of China (31772256 and 31772276), the Fundamental Research Funds for the Central Universities (KYTZ202002, KYZ201836 and JCQY201903), and the project funded by the Priority Academic Program Development of Jiangsu Higher Education Institutions.

SUPPLEMENTARY MATERIAL

The Supplementary Material for this article can be found online at: https://www.frontiersin.org/articles/10.3389/fpls.2020.601993/full#supplementary-material

Supplementary Figure 1 | Synteny analyses of PSK genes in the same species and chromosome location. Chromosome numbers are indicated on the inner side; gene pairs with syntenic relationships are joined by lines.

Supplementary Figure 2 | PbrPSK2 protein expression and purification *in vitro*. Recombinant proteins for the PbrPSK2 and purified using the *E. coli* system.

Supplementary Figure 3 | Alignment of PbrPSK4 and PbrPSK5 amino acid sequences. PbrPSK4 and PbrPSK5 shared 100% identity at the amino acid level.

Supplementary Figure 4 | The multiple sequence alignments from all identified PSK homologs and some functionally characterized PSKs.

Supplementary Figure 5 | ROS are necessary for pear pollen tube growth. **(A)** The ROS effect on pollen tube growth. The ROS scavenger TMPP arrests pollen tube elongation. Images shown were acquired 2 h after treatment PbrPSK2, TMPP or PbrPSK2 with TMPP. The experiments were repeated at least three times. Bar = 40 μm. **(B)** The statistical analysis of pollen tube length was measured. More than one hundred pollen tubes were measured.

Supplementary Table 1 | Numbers of PSK genes from different origins in five Rosaceae genomes.

Supplementary Table 2 | The orthology of PSK genes in five Rosaceae species.

Supplementary Table 3 | Ka and Ks substitution rates between gene pairs in pear.

Supplementary Table 4 | Primers of PbrPSK genes for this work (*represents the modification).

REFERENCES

Ames, R. M., Money, D., Ghatge, V. P., Whelan, S., and Lovell, S. C. (2012). Determining the evolutionary history of gene families. *Bioinformatics* 28, 48–55. doi: 10.1093/bioinformatics/btr592

Araya, T., Miyamoto, M., Wibowo, J., Suzuki, A., Kojima, S., Tsuchiya, Y. N., et al. (2014). CLE-CLAVATA1 peptide-receptor signaling module regulates the expansion of plant root systems in a nitrogen-dependent manner. *Proc. Natl. Acad. Sci. U.S.A.* 111, 2029–2034. doi: 10.1073/pnas.1319953111

Bae, Y. S., Oh, H., Rhee, S. G., and Do Yoo, Y. (2011). Regulation of reactive oxygen species generation in cell signaling. *Mol. Cells* 32, 491–509. doi: 10.1007/s10059-011-0276-3

Bailey, T. L., Williams, N., Misleh, C., and Li, W. W. (2006). MEME: discovering and analyzing DNA and protein sequence motifs. *Nucleic Acids Res.* 34, W369–W373.

Chen, C., Chen, H., He, Y., and Xia, R. (2018). TBtools, a toolkit for biologists integrating various biological data handling tools with a user-friendly interface. *bioRxiv* [Preprint]. doi: 10.1101/289660 bioRxiv: 289660,

Chen, Y.-F., Matsubayashi, Y., and Sakagami, Y. (2000). Peptide growth factor phytosulfokine-α contributes to the pollen population effect. *Planta* 211, 752–755. doi: 10.1007/s004250000370

Covey, P. A., Subbaiah, C. C., Parsons, R. L., Pearce, G., Lay, F. T., Anderson, M. A., et al. (2010). A pollen-specific RALF from tomato that regulates pollen tube elongation. *Plant Physiol.* 153, 703–715. doi: 10.1104/pp.110.155457

Duan, Q., Kita, D., Johnson, E. A., Aggarwal, M., Gates, L., Wu, H.-M., et al. (2014). Reactive oxygen species mediate pollen tube rupture to release sperm for fertilization in *Arabidopsis*. *Nat. Commun.* 5:3129.

Eddy, S. R. (2011). Accelerated profile HMM searches. *PLoS Comput. Biol.* 7:e1002195. doi: 10.1371/journal.pcbi.1002195

Estornell, L. H., Mari, W., Pérez-Amador, M. A., Manuel, T., Tadeo, F. R., and Butenko, M. A. (2015). The IDA peptide controls abscission in *Arabidopsis* and *Citrus*. *Front. Plant Sci.* 6:1003. doi: 10.3389/fpls.2015.01003

Fiers, M., Ku, K. L., and Liu, C.-M. (2007). CLE peptide ligands and their roles in establishing meristems. *Curr. Opin. Plant Biol.* 10, 39–43. doi: 10.1016/j.pbi.2006.11.003

Freeling, M. (2009). Bias in plant gene content following different sorts of duplication: tandem, whole-genome, segmental, or by transposition. *Annu. Rev. Plant Biol.* 60, 433–453. doi: 10.1146/annurev.arplant.043008.092122

Fujimoto, R., Sugimura, T., Fukai, E., and Nishio, T. (2006). Suppression of gene expression of a recessive SP11/SCR allele by an untranscribed SP11/SCR allele in *Brassica* self-incompatibility. *Plant Mol. Biol.* 61, 577–587. doi: 10.1007/s11103-006-0032-9

Ge, Z., Bergonci, T., Zhao, Y., Zou, Y., Du, S., Liu, M.-C., et al. (2017). *Arabidopsis* pollen tube integrity and sperm release are regulated by RALF-mediated signaling. *Science* 358, 1596–1600. doi: 10.1126/science.aao3642

Goodstein, D. M., Shu, S., Howson, R., Neupane, R., Hayes, R. D., Fazo, J., et al. (2012). Phytozome: a comparative platform for green plant genomics. *Nucleic Acids Res.* 40, D1178–D1186.

Hanai, H., Matsuno, T., Yamamoto, M., Matsubayashi, Y., Kobayashi, T., Kamada, H., et al. (2000). A secreted peptide growth factor, phytosulfokine, acting as a stimulatory factor of carrot somatic embryo formation. *Plant Cell Physiol.* 41, 27–32. doi: 10.1093/pcp/41.1.27

He, Z., Zhang, H., Gao, S., Lercher, M. J., Chen, W.-H., and Hu, S. (2016). Evolview v2: an online visualization and management tool for customized and annotated phylogenetic trees. *Nucleic Acids Res.* 44, W236–W241.

Hu, B., Jin, J., Guo, A.-Y., Zhang, H., Luo, J., and Gao, G. (2015). GSDS 2.0: an upgraded gene feature visualization server. *Bioinformatics* 31, 1296–1297. doi: 10.1093/bioinformatics/btu817

Hu, T., and Banzhaf, W. (2008). "Nonsynonymous to synonymous substitution ratio ka/ks: measurement for rate of evolution in evolutionary computation," in *Proceedings of the 10th International Conference Parallel Problem Solving from Nature-ppsn X, September 13–17*, Dortmund.

Igarashi, D., Tsuda, K., and Katagiri, F. (2012). The peptide growth factor, phytosulfokine, attenuates pattern−triggered immunity. *Plant J.* 71, 194–204. doi: 10.1111/j.1365-313x.2012.04950.x

Kim, B. J., Gibson, D. M., and Shuler, M. L. (2006). Effect of the plant peptide regulator, phytosulfokine−α, on the growth and Taxol production from *Taxus* sp. suspension cultures. *Biotechnol. Bioeng.* 95, 8–14. doi: 10.1002/bit.20934

Krzywinski, M., Schein, J., Birol, I., Connors, J., Gascoyne, R., Horsman, D., et al. (2009). Circos: an information aesthetic for comparative genomics. *Genome Res.* 19, 1639–1645. doi: 10.1101/gr.092759.109

Kutschmar, A., Rzewuski, G., Stührwohldt, N., Beemster, G. T., Inzé, D., and Sauter, M. (2009). PSK−α promotes root growth in *Arabidopsis*. *New Phytol.* 181, 820–831. doi: 10.1111/j.1469-8137.2008.02710.x

Larkin, M. A., Blackshields, G., Brown, N. P., Chenna, R., McGettigan, P. A., McWilliam, H., et al. (2007). Clustal W and Clustal X version 2.0. *Bioinformatics* 23, 2947–2948. doi: 10.1093/bioinformatics/btm404

Lorbiecke, R., and Sauter, M. (2002). Comparative analysis of PSK peptide growth factor precursor homologs. *Plant Sci.* 163, 321–332. doi: 10.1016/s0168-9452(02)00101-2

Lorbiecke, R., Steffens, M., Tomm, J. M., Scholten, S., Von Wiegen, P., Kranz, E., et al. (2005). Phytosulphokine gene regulation during maize (*Zea mays L.*) reproduction. *J. Exp. Bot.* 56, 1805–1819. doi: 10.1093/jxb/eri169

Mari, O. O., Matsuzaki, Y., Mori, A., and Matsubayashi, Y. (2010). Secreted peptide signals required for maintenance of root stem cell niche in *Arabidopsis*. *Science* 329, 1065–1067. doi: 10.1126/science.1191132

Matsubayashi, Y. (2013). Root meristem growth factor, an secreted peptide signal involved in root meristem development(Plant Peptide Signals). *Regul. Plant Growth Dev.* 48, 54–59.

Matsubayashi, Y., Hanai, H., Hara, O., and Sakagami, Y. (1996). Active fragments and analogs of the plant growth factor, phytosulfokine: structure–activity relationships. *Biochem. Biophys. Res. Commun.* 225, 209–214. doi: 10.1006/bbrc.1996.1155

Mecchia, M. A., Santos-Fernandez, G., Duss, N. N., Somoza, S. C., Boisson-Dernier, A., Gagliardini, V., et al. (2017). RALF4/19 peptides interact with LRX proteins to control pollen tube growth in *Arabidopsis*. *Science* 358, 1600–1603. doi: 10.1126/science.aao5467

Melinka, A. B. (2003). Inflorescence deficient in abscission controls floral organ abscission in *Arabidopsis* and identifies a novel family of putative ligands in plants. *Plant Cell* 15, 2296–2307. doi: 10.1105/tpc.014365

Mollet, J. C., Park, S. Y., Nothnagel, E. A., and Lord, E. M. (2000). A lily stylar pectin is necessary for pollen tube adhesion to an in vitro stylar matrix. *Plant Cell* 12, 1737–1750. doi: 10.2307/3871186

Okuda, S., Tsutsui, H., Shiina, K., Sprunck, S., Takeuchi, H., Yui, R., et al. (2009). Defensin-like polypeptide LUREs are pollen tube attractants secreted from synergid cells. *Nature* 458, 357–361. doi: 10.1038/nature07882

Pearce, G., Moura, D. S., Stratmann, J., and Ryan, C. A. (2001). RALF, a 5-kDa ubiquitous polypeptide in plants, arrests root growth and development. *Proc. Natl. Acad. Sci. U.S.A.* 98, 12843–12847. doi: 10.1073/pnas.201416998

Peng, L., Jiang, Y., and Yang, S. (2002). Plant polypeptide signals: properties and functions. *Sheng Wu Hua Xue Yu Sheng Wu Wu Li Jin Zhan* 29, 877–880.

Potocký, M., Jones, M. A., Bezvoda, R., Smirnoff, N., and Žárský, V. (2007). Reactive oxygen species produced by NADPH oxidase are involved in pollen tube growth. *New Phytol.* 174, 742–751. doi: 10.1111/j.1469-8137.2007.02042.x

Reichardt, S., Piepho, H., Stintzi, A., and Schaller, A. (2020). Peptide signaling for drought-induced tomato flower drop. *Science* 367, 1482–1485. doi: 10.1126/science.aaz5641

Ryan, C. A., Pearce, G., Scheer, J., and Moura, D. S. (2002). Polypeptide hormones. *Plant Cell* 14, S251–S264.

Sato, Y., Okamoto, S., and Nishio, T. (2004). Diversification and alteration of recognition specificity of the pollen ligand SP11/SCR in self-incompatibility of *Brassica* and *Raphanus*. *Plant Cell* 16, 3230–3241. doi: 10.1105/tpc.104.027029

Schacherer, J., De Montigny, J., Welcker, A., Souciet, J.-L., and Potier, S. (2005). Duplication processes in *Saccharomyces cerevisiae* haploid strains. *Nucleic Acids Res.* 33, 6319–6326. doi: 10.1093/nar/gki941

Shiba, H., Takayama, S., Iwano, M., Shimosato, H., Funato, M., Nakagawa, T., et al. (2001). A pollen coat protein, SP11/SCR, Determines the pollens-specificity in the self-incompatibility of *Brassica* species. *Plant Physiol.* 125, 2095–2103. doi: 10.1104/pp.125.4.2095

Shulaev, V., Sargent, D. J., Crowhurst, R. N., Mockler, T. C., Folkerts, O., Delcher, A. L., et al. (2011). The genome of woodland strawberry (*Fragaria vesca*). *Nat. Genet.* 43:109.

Smith, L. L., Fessler, J. L., Alfaro, M. E., Streelman, J. T., and Westneat, M. W. (2008). Phylogenetic relationships and the evolution of regulatory gene sequences in the parrotfishes. *Mol. Phylogenet. Evol.* 49, 136–152. doi: 10.1016/j.ympev.2008.06.008

Speranza, A., Crinelli, R., Scoccianti, V., and Geitmann, A. (2012). Reactive oxygen species are involved in pollen tube initiation in kiwifruit. *Plant Biol.* 14, 64–76.

Story, M. (1991). Polypeptide modulators of prostatic growth and development. *Cancer Surveys* 11, 123–146.

Stuart, R., and Street, H. (1969). Studies on the growth in culture of plant cells: IV. The initition of division in suspensions of stationary-phase cells of *Acer pseudoplatanus* L. *J. Exp. Bot.* 20, 556–571. doi: 10.1093/jxb/20.3.556

Stührwohldt, N., Dahlke, R. I., Kutschmar, A., Peng, X., Sun, M. X., and Sauter, M. (2015). Phytosulfokine peptide signaling controls pollen tube growth and funicular pollen tube guidance in *Arabidopsis thaliana*. *Physiol. Planta.* 153, 643–653. doi: 10.1111/ppl.12270

Stührwohldt, N., Dahlke, R. I., Steffens, B., Johnson, A., and Sauter, M. (2011). Phytosulfokine-α controls hypocotyl length and cell expansion in *Arabidopsis thaliana* through phytosulfokine receptor 1. *PLoS One* 6:e21054. doi: 10.1371/journal.pone.0021054

Suhre, K. (2005). Gene and genome duplication in *Acanthamoeba polyphaga* Mimivirus. *J. Virol.* 79, 14095–14101. doi: 10.1128/jvi.79.22.14095-14101.2005

Thannickal, V. J., and Fanburg, B. L. (2000). Reactive oxygen species in cell signaling. *Am. J. Physiol. Lung Cell. Mol. Physiol.* 279, L1005–L1028.

Topping, J. F., and Lindsey, K. (1997). Promoter trap markers differentiate structural and positional components of polar development in *Arabidopsis*. *Plant Cell* 9, 1713–1725. doi: 10.2307/3870519

Velasco, R., Zharkikh, A., Affourtit, J., Dhingra, A., Cestaro, A., Kalyanaraman, A., et al. (2010). The genome of the domesticated apple (*Malus*× *domestica* Borkh.). *Nat. Genet.* 42, 833–839.

Verde, I., Abbott, A. G., Scalabrin, S., Jung, S., Shu, S., Marroni, F., et al. (2013). The high-quality draft genome of peach (*Prunus persica*) identifies unique patterns of genetic diversity, domestication and genome evolution. *Nat. Genet.* 45, 487. doi: 10.1038/ng.2586

Wang, C.-L., Wu, J., Xu, G.-H., Gao, Y.-b, Chen, G., Wu, J.-Y., et al. (2010). S-RNase disrupts tip-localized reactive oxygen species and induces nuclear DNA degradation in incompatible pollen tubes of *Pyrus pyrifolia*. *J. Cell Sci.* 123, 4301–4309. doi: 10.1242/jcs.075077

Wang, Y., Tang, H., DeBarry, J. D., Tan, X., Li, J., Wang, X., et al. (2012). MCScanX: a toolkit for detection and evolutionary analysis of gene synteny and collinearity. *Nucleic Acids Res.* 40:e49. doi: 10.1093/nar/gkr1293

Wu, H., Zheng, R., Hao, Z., Meng, Y., Weng, Y., Zhou, X., et al. (2019). Cunninghamia lanceolata PSK peptide hormone genes promote primary root growth and adventitious root formation. *Plants* 8:520. doi: 10.3390/plants8110520

Wu, H.m, Wong, E., Ogdahl, J., and Cheung, A. Y. (2000). A pollen tube growth−promoting arabinogalactan protein from *Nicotiana alata* is similar to the tobacco TTS protein. *Plant J.* 22, 165–176. doi: 10.1046/j.1365-313x.2000.00731.x

Wu, J., Wang, Z., Shi, Z., Zhang, S., Ming, R., Zhu, S., et al. (2013). The genome of the pear (*Pyrus bretschneideri* Rehd.). *Genome Res.* 23, 396–408.

Yamakawa, S., Matsubayashi, Y., Sakagami, Y., Kamada, H., and Satoh, S. (1999). Promotive effects of the peptidyl plant growth factor, phytosulfokine-α, on the growth and chlorophyll content of *Arabidopsis* seedlings under high night-time temperature conditions. *Biosci. Biotechnol. Biochem.* 63, 2240–2243. doi: 10.1271/bbb.63.2240

Yamakawa, S., Sakuta, C., Matsubayashi, Y., Sakagami, Y., Kamada, H., and Satoh, S. (1998). The promotive effects of a peptidyl plant growth factor, phytosulfokine-α, on the formation of adventitious roots and expression of a gene for a root-specific cystatin in cucumber hypocotyls. *J. Plant Res.* 111, 453–458. doi: 10.1007/bf02507810

Yang, H., Matsubayashi, Y., Nakamura, K., and Sakagami, Y. (1999). Oryza sativa PSK gene encodes a precursor of phytosulfokine-α, a sulfated peptide growth factor found in plants. *Proc. Natl. Acad. Sci.* 96, 13560–13565. doi: 10.1073/pnas.96.23.13560

Yang, H., Matsubayashi, Y., Nakamura, K., and Sakagami, Y. (2001). Diversity of *Arabidopsis* genes encoding precursors for phytosulfokine, a peptide growth factor. *Plant Physiol.* 127, 842–851. doi: 10.1104/pp.010452

Yu, L., Zhou, W., Zhang, D., Yan, J., and Luo, L. (2020). Phytosulfokine-α promotes root growth by repressing expression of pectin methylesterase inhibitor (PMEI) genes in *Medicago truncatula*. *Phyton* 89, 1–9. doi: 10.32604/phyton.2020.011882

Zhang, H., Hu, Z., Lei, C., Zheng, C., Wang, J., Shao, S., et al. (2018). A plant phytosulfokine peptide initiates auxin-dependent immunity through cytosolic Ca^{2+} signaling in tomato. *Plant Cell* 30, 625–667.

Zhang, Q., Chen, W., Sun, L., Zhao, F., Huang, B., Yang, W., et al. (2012). The genome of *Prunus mume*. *Nat. Commun.* 3:1318.

Conflict of Interest: The authors declare that the research was conducted in the absence of any commercial or financial relationships that could be construed as a potential conflict of interest.

frontiers in Plant Science

ORIGINAL RESEARCH
published: 15 February 2021
doi: 10.3389/fpls.2021.636749

The *CLV3* Homolog in *Setaria viridis* Selectively Controls Inflorescence Meristem Size

Chuanmei Zhu[1], *Lei Liu*[2], *Olivia Crowell*[1], *Hui Zhao*[1,3], *Thomas P. Brutnell*[1,4], *David Jackson*[2] *and Elizabeth A. Kellogg*[1]*

[1] Donald Danforth Plant Science Center, St. Louis, MO, United States, [2] Cold Spring Harbor Laboratory, Cold Spring Harbor, NY, United States, [3] Institute of Tropical Bioscience and Biotechnology and Hainan Key Laboratory for Biosafety Monitoring and Molecular Breeding in Off-Season Reproduction Regions, Chinese Academy of Tropical Agricultural Sciences, Haikou, China, [4] Joint Laboratory for Photosynthesis Enhancement and C_4 Rice Development, Biotechnology Research Institute, Chinese Academy of Agricultural Sciences, Beijing, China

The CLAVATA pathway controls meristem size during inflorescence development in both eudicots and grasses, and is initiated by peptide ligands encoded by *CLV3*/*ESR*-related (*CLE*) genes. While CLV3 controls all shoot meristems in *Arabidopsis*, evidence from cereal grasses indicates that different meristem types are regulated by different CLE peptides. The rice peptide FON2 primarily controls the size of the floral meristem, whereas the orthologous peptides CLE7 and CLE14 in maize have their most dramatic effects on inflorescence and branch meristems, hinting at diversification among CLE responses in the grasses. *Setaria viridis* is more closely related to maize than to rice, so can be used to test whether the maize CLE network can be generalized to all members of subfamily Panicoideae. We used CRISPR-Cas9 in *S. viridis* to knock out the *SvFON2* gene, the closest homolog to *CLV3* and *FON2*. *Svfon2* mutants developed larger inflorescence meristems, as in maize, but had normal floral meristems, unlike *Osfon2*, suggesting a panicoid-specific CLE network. Vegetative traits such as plant height, tiller number and leaf number were not significantly different between mutant and wild type plants, but time to heading was shorter in the mutants. *In situ* hybridization showed strong expression of *Svfon2* in the inflorescence and branch meristems, consistent with the mutant phenotype. Using bioinformatic analysis, we predicted the co-expression network of *SvFON2* and its signaling components, which included genes known to control inflorescence architecture in maize as well as genes of unknown function. The similarity between SvFON2 function in Setaria and maize suggests that its developmental specialization in inflorescence meristem control may be shared among panicoid grasses.

Keywords: inflorescence development, Setaria, FON2, CLE, CLV3/ESR-related, grass, meristem maintenance, spikelet

OPEN ACCESS

Edited by:
Reidunn Birgitta Aalen, University of Oslo, Norway

Reviewed by:
Jennifer C. Fletcher, Plant Gene Expression Center (PGEC), United States
Shinichiro Sawa, Kumamoto University, Japan

***Correspondence:**
Elizabeth A. Kellogg
ekellogg@danforthcenter.org

Specialty section:
This article was submitted to Plant Physiology, a section of the journal Frontiers in Plant Science

Received: *02 December 2020*
Accepted: *21 January 2021*
Published: *15 February 2021*

Citation:
Zhu C, Liu L, Crowell O, Zhao H, Brutnell TP, Jackson D and Kellogg EA (2021) The CLV3 Homolog in Setaria viridis Selectively Controls Inflorescence Meristem Size. Front. Plant Sci. 12:636749. doi: 10.3389/fpls.2021.636749

INTRODUCTION

The grass family (Poaceae) contains many agronomically important cereal crops, such as maize and rice, which have fed the world since the dawn of civilization. Their inflorescences, the flower- and seed-bearing structures, have been under constant selection for enhanced productivity during crop domestication. All inflorescence structures ultimately come from the inflorescence meristem,

a group of pluripotent cells that is responsible for replenishing the stem cell pool as well as initiating lateral primordia. Therefore, understanding how the inflorescence meristem maintains a proper size is key to improving crop yields.

In *Arabidopsis*, meristem size is controlled by the CLAVATA pathway (Miyawaki et al., 2013; Somssich et al., 2016; Bommert and Whipple, 2018; Kitagawa and Jackson, 2019). This pathway is activated by peptide ligands of 12 amino acids processed from the CLE domains of prepropeptides encoded by *CLAVATA3*(*CLV3*)/*Embryo Surrounding Region* (*ESR*)-related genes (i.e., *CLE*) (Djordjevic et al., 2011; Ni et al., 2011). The CLE signal is transmitted by leucine rich repeat (LRR) receptor kinases and acts to restrict the expression domain of transcription factors such as *WUSCHEL* (*WUS*) and *WUSCHEL-related homeobox* (*WOX*) genes (**Figure 1A**). *Arabidopsis* CLV3 controls the size of all shoot meristems, including the vegetative shoot apical meristem (SAM, for producing leaves), inflorescence meristem (IM, for producing inflorescence branches and flowers) and floral meristem (FM, formed from IM for producing floral organs). CLV3 functions through a signaling pathway that involves LRR receptors including CLAVATA1 (CLV1) and BARELY ANY MERISTEM1-3 (BAM1-3) and others (Nimchuk et al., 2015; Somssich et al., 2016), and the WUS transcription factor, among others (Dodueva et al., 2011; Miyawaki et al., 2013; Kitagawa and Jackson, 2019; and references therein; **Figure 1A**).

Pathways similar to the Arabidopsis CLAVATA pathway have been found in all plants investigated to date, but details differ. Specifically, the type of meristem (vegetative shoot, inflorescence, branch, flower) regulated by each CLE/CLV/WOX combination varies, as do patterns of redundancy and co-regulation. Recently, Rodríguez-Leal et al. (2019) have analyzed comparisons of Arabidopsis, tomato, and maize CLE knockouts, and shown that compensation mechanisms differ considerably among the three species, depending in part on how paralogous genes are regulated in each species. Because of this unexpected diversity, it is hard to generalize what the specific developmental role of any particular CLE protein might be, and to what extent its function is partially or wholly redundant to that of other CLEs.

Previous work using both phylogenetic analysis and cluster analysis in species of Poaceae has identified CLE proteins in rice, maize and Setaria that are similar to Arabidopsis CLV3 (Je et al., 2016; Goad et al., 2017) (**Figure 1B**). These include FLORAL ORGAN NUMBER 2/4 in rice (OsFON2/4) and CLE7

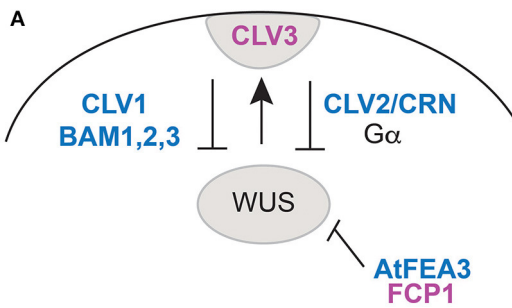

B

Arabidopsis	Rice	Maize
CLV3	FON2	CLE7/14
CLV1	FON1	TD1
CLV2	?	FEA2
Gα	?	CT2
?	FCP1	ZmFCP1
AtFEA3	?	FEA3

FIGURE 1 | (A) Diagram of the proteins involved in maintenance of meristem size in Arabidopsis, focusing on those discussed in this paper (modified from Figure 2 in Kitagawa and Jackson, 2019). CLV3 is expressed at the apex of the meristem, where it interacts with CLV1 and BAM1-3, or with CLV2 and CRN, via Gα, to trigger a signaling process that ultimately restricts the expression domain of WUS. FCP1 interacts with FEA3 to repress WUS from below. Magenta lettering, CLE peptides; blue lettering, receptors, and receptor-like proteins. **(B)** Names of orthologous proteins in Arabidopsis, rice, and maize.

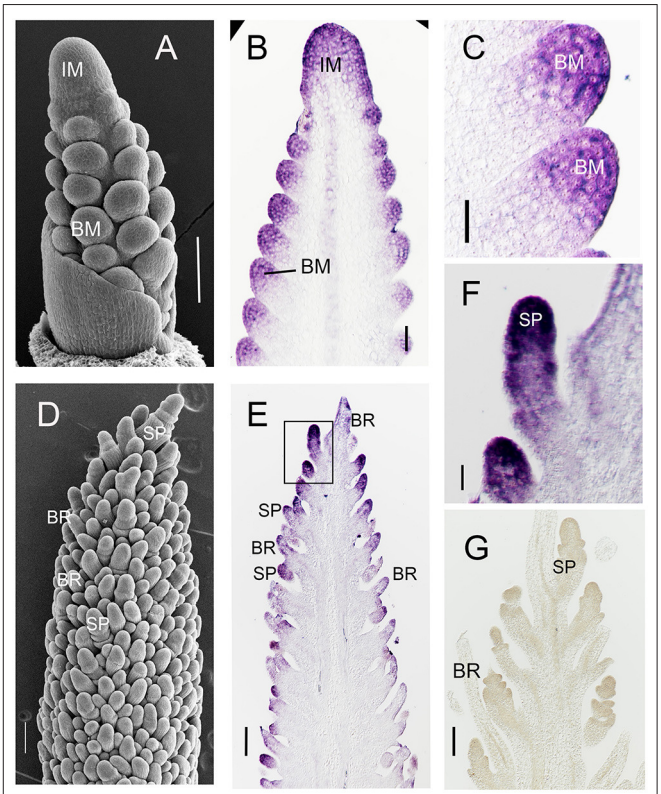

FIGURE 2 | SvFON2 is expressed in early inflorescence, branch, and spikelet meristems. SEM, showing structure of the inflorescence. Sectioned inflorescences from comparable stages showing *SvFON2* expression in the inflorescence meristem, branch meristems, spikelet meristems. **(A,D)** SEM images from early development of A10; images by Matt Box. **(B,C,E–G)** Expression of *SvFON2*, *in situ* hybridization, ME034. **(B)** inflorescence with branch meristems, slightly more mature than that in **(A)**. **(C)** branch meristems. **(D–F)** inflorescence with differentiated spikelets and bristles; ridges visible on spikelets are glumes. **(F)** close-up of area inside box in **(E)**. **(G)** sense control. Scale bars: **(A–E,G)**, 100 μm; **(F)**, 30 μm. IM, inflorescence meristem, BM, branch meristem, SP, spikelet, BR, bristle.

(GRMZM2G372364) and CLE14 (AC191109.3_FG001) in maize (Je et al., 2016; Goad et al., 2017). The grass genes form a clade/cluster (called group 1D3 by Goad et al., 2017), indicating that all are more closely related to each other than any is to CLV3 and predicting that their function should be similar to each other. At the same time, the grass genes in cluster 1D3 are more closely related to CLV3 than to any other CLEs (Je et al., 2016).

Unlike in Arabidopsis, the function of CLV3 orthologs in grasses appears restricted to a subset of shoot meristems, although whether this is due to tissue specificity or gene redundancy in some organs is less clear. Mutations in the rice gene Os*FON2* affect only the FM, which becomes larger and produces more floral organs (Suzaki et al., 2006), whereas the IM and BM are apparently not affected. In contrast, *Zmcle7* mutants produce an enlarged IM (Rodríguez-Leal et al., 2019), suggesting that the particular meristems controlled by OsFON2 and ZmCLE7 are different. This apparent functional differentiation is also seen in the receptor proteins. OsFON1, which is similar to CLV1, interacts with OsFON2 in the FM in rice (Chu et al., 2006; Suzaki et al., 2006). Conversely, the maize LRR receptor THICK TASSEL DWARF (TD1, similar to CLV1) functions only in the IM and FM, without significantly affecting the vegetative SAM, although the developmental role of the gene might differ in a different genetic background (Bommert et al., 2005; Kitagawa and Jackson, 2019).

Because the presumed CLV3 orthologs in rice and maize appear to control only particular meristems, other CLE proteins must be involved in specifying meristem size in the inflorescence, branches and flowers. One attractive candidate is FON2 CLE PEPTIDE-RELATED1 (FCP1), which is similar to FON2 in sequence and appears closely related (Je et al., 2016; Goad et al., 2017). In maize, *ZmCLE7* and *ZmFCP1* are the only CLE genes to be significantly upregulated in *cle7* mutants in the ear (female inflorescence), and when mutated, produce an enlarged inflorescence meristem (Rodríguez-Leal et al., 2019). However, FCP1 functions in a pathway parallel to CLE7/FON2 rather than being fully redundant (Je et al., 2018; Kitagawa and Jackson, 2019) (**Figure 1A**); the effects of mutations are additive in double mutants. ZmCLE7 interacts genetically with TD1 (similar to CLV1; **Figure 1B**) and ZmFCP1 with FEA3 receptors; both peptides also likely signal through FASCIATED EAR 2 (FEA2, similar to CLV2), but then signals are transmitted by different downstream effectors, CORYNE or CT2 (Je et al., 2016, 2018).

Having data only from rice and maize makes it difficult to generalize results to other grasses and cereal crops. Other species could have developmental networks and functions similar to those in rice, or in maize, or may use some novel combination of ligands and receptors. One possibility is that rice and maize are each characteristic of their own subfamilies (Oryzoideae and Panicoideae, respectively). If this is true, then the results for maize should also apply to other panicoid crops such as sorghum, foxtail millet, pearl millet, barnyard millet, and proso millet. We have investigated this possibility by studying green millet, *Setaria viridis*, the wild progenitor of foxtail millet (*S. italica*) (Le Thierry d'Ennequin et al., 2000; Benabdelmouna et al., 2001; Fukunaga et al., 2006; Hunt et al., 2008) and a tractable model system (Brutnell et al., 2010; Yang et al., 2018; Zhu et al., 2018; Mamidi et al., 2020). In their comprehensive survey of CLE genes in seed plants, Goad et al. (2017) searched the genome of *S. viridis* using a model-based search tool (HMMER3; http://hmmer.org) and identified 41 CLE proteins based on sequence similarity and presence of an identifiable CLE domain. These proteins were then clustered into groups with similar sequences. Only one *S. viridis* gene clustered with (i.e., appeared similar to) *OsFON2*; here we call this locus *SvFON2*.

In the current study we have disrupted *SvFON2* and discovered a strong effect on the inflorescence meristem, similar to mutants of the co-orthologs in maize, but little or no effect on floral meristems, contrasting with *Osfon2* (Suzaki et al., 2006) and suggesting a panicoid genetic network. We then investigated the *SvFON2* co-expression network to predict possible signaling components. Our work identifies a *CLE* gene whose most obvious function is to control the inflorescence and branch meristems in panicoid grasses; we also provide new evidence for *CLE* gene diversification among grass subfamilies, and highlight possible targets of this peptide ligand.

MATERIALS AND METHODS

Plant Material

All data presented here are from *Setaria viridis*, using either accession A10.1 or ME034v (hereafter A10 and ME034 for simplicity). Published data on inflorescence development and gene expression are based on the accession A10, which is a line that has been used for years for *S. viridis* genetics studies. A full genome sequence was released in 2012 (v1.1; Bennetzen et al., 2012) and updated and substantially improved in 2020 (v2.1; Mamidi et al., 2020). The line ME034, originally collected by Matt Estep (now at Appalachian State Univ.) in Manitoba, has come into common use recently because it is easier to transform. It was used here for CRISPR-Cas9 modification of the target gene, *SvFON2*. A genome sequence has recently been released for this accession (Thielen et al., 2020), although it was not available when most of the work reported here was conducted. The two accessions of *S. viridis* are morphologically similar, although development of ME034 is generally more rapid than that of A10 (Kellogg, pers. obs.).

Histology, Scanning Electron Microscopy (SEM), and *in situ* Hybridization

Scanning electron microscopy was performed as described in Zhu et al. (2018) for A10 plants. For ME034 wildtype and mutant plants, inflorescences were hand-dissected from *S. viridis* seedlings at 12, 14, and 17 days after sowing (DAS). Samples were then dehydrated, critical point dried using a Tousimis Samdri-780a, mounted on stubs and sputter coated using a Tousimis Samsputter-2a. Images were taken with a Zeiss Evo 10 scanning electron microscope at 20 kV at the biology department of Washington University in St. Louis.

For histology, tissues surrounding the shoot apical meristem or inflorescence primordia from 6, 9, and 12 DAS ME034 seedlings were fixed, dehydrated, paraffinized, embedded, and sectioned as described in Hodge and Kellogg (2016). Sections were then deparaffinized in 100% Histoclear twice, 10 min each,

rehydrated through an ethanol series (100, 100, 90, 70, 50, 0%, 2 min each step), and stained with 0.05% (w/v) toluidine blue for 1 min. After staining, slides were rinsed and dehydrated by dipping into water, 95 and 100% ethanol three times, 10 dippings each, followed by two xylene washes, 5 min each. Samples were then mounted in Permount with a coverslip and imaged using a Lecia DM 750 microscope at 10–40X.

mRNA *in situ* hybridization was conducted to characterize the expression pattern of *SvFON2* using fixed and embedded developing inflorescences. The primers CTTGCGTTGCTGGTTCATC and AAGGTGTGATCGGCTGCT were used to prepare the probes and *in situ* hybridization followed a previously-described protocol (Jackson et al., 1994).

Expression and Genomic Region of *SvFON2*

A complete list of *S. viridis CLE* genes was retrieved from Goad et al. (2017), which used the *S. viridis* A10 genome v1.1. We verified that all gene locus names but one were unchanged in version 2.1 of the genome (Mamidi et al., 2020); we updated the one old name (Sevir.J013000) to its new name (Sevir.3G041960) for this paper. Also *SvFCP1* was not annotated in *S. viridis* v1.1 but was annotated in v2.1 (Sevir.7G142950) so we have included that name as well and retrieved the relevant expression data from the raw reads provided by Zhu et al. (2018). Expression, quantified in Transcripts per Million (TPM), of all 42 *CLE* genes in early inflorescence development [10, 12, 14, 15, 16, 18 days after sowing (DAS)] was extracted from the comprehensive RNA-seq data reported for A10 in Zhu et al. (2018) and is reported in **Supplementary Table 1**. *CLEs* with zero TPM throughout inflorescence development in all six developmental stages are defined as non-expressed genes. For data display and ease of visualization, we considered genes for which at least one sample had TPM $>$ 6. We did not display data for Sevir.3G184200 in which all values were zero except for replicate 4 at 15DAS, which had 6.72 TPM.

Grass *FON2* genomic regions were compared using the GEvo function of CoGe (Lyons and Freeling, 2008; Lyons et al., 2008; Tang et al., 2011) (https://genomevolution.org/coge/). Sequences from *Brachypodium distachyon* (Bd21; JGI v2.0), *Oryza sativa japonica* (Phytozome 11 v323), *Setaria viridis* (A10, Phytozome v2.1), and *Zea mays* [B73, Phytozome 10 (via Gramene) vRef_Gen_v3 and MaizeSequence.org v1] were used for comparison. All genome sequences were unmasked. The *BdFCP1* gene is present but not annotated in the genome of *Brachypodium distachyon* line Bd21 (v2.0); therefore, its closest neighboring genes were used to infer the genomic context for CoGe analysis.

CRISPR-Cas9 Cloning and Tissue Culture Transformation

To generate mutants in *SvFON2*, CRISPR-Cas9 gene editing technology was used. Constructs were assembled as described (Cermák et al., 2017). Guide RNAs (gRNAs) were designed near protospacer adjacent motif (PAM, required for gRNA targeting) sites using websites http://crispor.tefor.net and http://crispr.hzau.edu.cn/CRISPR2/ (Liu H. et al., 2017). The two gRNAs, ACCACCACGGCAGCCCGTGG (gRNA1) and ACCGCCAAATGATCCACCGC (gRNA2), targeted the exonic region flanking the CLE domain and were predicted to have high specificity. The two guide RNAs were assembled into the module 2 vector pMOD_B2518 via the Esp3I/BsmBI cloning site and module 3 vector pMOD_C2616 via the BsaI cloning site, respectively. Then, the module 1 vector pMOD_A1110 containing Cas9 and hygromycin phosphotransferase genes, module 2 and module 3 vectors were assembled into a destination vector pTRANS_250d via the AarI cloning site. Constructs were sequenced to verify they were error-free and the assembled destination vector was transformed into the Agrobacterium strain AGL1.

Tissue culture transformation was performed as described in Brutnell et al. (2010). Callus was initiated from embryos of sterilized *S. viridis* ME034 seeds, incubated with Agrobacterium suspension, and selected with 40 mg/l hygromycin. Callus was subsequently transferred to plant regenerative medium to grow shoots for transgenic lines and then to rooting medium to recover roots under constant selection of 20 mg/l hygromycin. Transgenic plants were then transferred to soil for genotyping, phenotyping and seed harvest.

Plant Growth, Transgenic Plant Screening, and Phenotyping

Setaria viridis ME034 plants were grown in a greenhouse with conditions described in Acharya et al. (2017); previous work had found that the line ME034 was much healthier and produced more seeds when grown in the greenhouse compared to our controlled environment growth chamber. For root phenotypes, *S. viridis* plants were grown in germination pouches as described in Acharya et al. (2017).

DNA was extracted from leaves using methods described in Edwards et al. (1991). T0 plants were screened by PCR targeting Sevir.2G209800, a gene encoding a C2H2-type zinc finger protein in the *S. viridis* genome as a positive control (primers CAGCAAGCCGCCTATATGGAG and TCGTCTCAGGAGTGGCCAAGT), and the hygromycin phosphotransferase gene on the transgene fragment (primers AGGCTCTCGATGAGCTGATGCTTT and AGCTGCATCATCGAAATTGCCGTC). Editing rate was calculated by edited gene copies divided by total available gene copies. In the T1 generation, the same PCR primers were used to screen for stable lines in which the transgene (Cas9 and the hygromycin selectable marker) was segregated out to prevent any further undesired editing. The *SvFON2* gene region was amplified using primers GCTGGTTCATCCAGTGCAGG and TCAAGGTGTGATCGGCTGCTC and the PCR product was sequenced to screen for edited lines in T0 and then confirmed again in T1 stable lines. Stable and homozygous T2 or T3 lines were used for phenotyping.

Head out date was recorded around 16–21 days when at least half of the panicle emerged from the leaf sheath. Other phenotypes were measured when the plants were 4

weeks old unless otherwise indicated. Plant height and panicle length were measured using a ruler. The third and sixth leaves were cut at the tip to aid leaf number counting. The number of primary inflorescence branches/cm and the number of spikelets per primary branch were counted from a 1 cm region that was 1 cm above the lowermost branch of the main panicle. Experiments were repeated at least three times with at least five plants (and generally more) for each genotype in each replicate. Statistical significance was examined by Welch's two sample *t*-test as implemented in R, testing whether the difference in means between genotypes was significantly different from zero.

Co-expression Network Analysis for *SvFON2*

To plot the *SvFON2* co-expression network, the "skyblue module" containing *SvFON2* from the Weighted Gene Co-expression Network Analysis (WGCNA) data in Zhu et al. (2018) was used. In these WGCNA data, a weight value was assigned to the connection (edge) between two genes (node). After filtering by weight > 0.185, connections between known genes for inflorescence development and the genes that they directly connected with were selected to construct a co-expression network in Cytoscape v3.4.10.

LRR Receptors and *WUS/WOX* Homologs

LRR receptors and *WUS/WOX* genes in *S. viridis* were identified using blastp, (https://blast.ncbi.nlm.nih.gov/) with genes reported in Lian et al. (2014) and Liu P. L. et al. (2017), respectively, as bait. Genes were further curated by domain search and annotation from Biomart of EnsemblPlants (http://plants.ensembl.org, accessed on July 1st, 2017). Expression of these genes during early inflorescence development was also extracted from data reported in Zhu et al. (2018).

RESULTS

SvFON2 Is Expressed in Early Inflorescence Development

As a first step to understand the function of *SvFON2* in inflorescence development, we used *in situ* hybridization with a gene-specific probe for *SvFON2*, and considered the stage at which the inflorescence and branch meristems were specified (ca. 11 days after sowing, DAS, **Figure 2A**) and a slightly later stage when spikelets were clearly formed and floral meristems initiated (**Figure 2D**). Species of *Setaria* also produce sterile branches known as bristles in their inflorescences; the bristles lose their meristems during the course of development (Doust and Kellogg, 2002). Each spikelet is associated with one or more bristles. *SvFON2* was clearly expressed in inflorescence meristem and branch meristems at 11 DAS (**Figures 2B,C**). Expression was not confined to particular layers or zones of the meristem but rather extended through the apex of the inflorescence and branch. *SvFON2* was also expressed in spikelet meristems (**Figures 2E,F**). *SvFON2* expression appeared lower in developing bristles, and expression was not detected in the sense control (**Figure 2G**).

To capture the dynamics of *SvFON2* expression throughout inflorescence development, we retrieved data for all CLE genes from an available gene expression resource that summarizes gene expression from IM initiation to floral organ development (Zhu et al., 2018). Expression of *SvFON2* (Sevir.8G183800) was low at 10 DAS, increased as branch meristems initiated (12 DAS) and transitioned to spikelet meristems (14 DAS), with values mostly between 5 and 10 TPM through 16 DAS and then dropping to near its original levels as floral meristems differentiated (18 DAS; **Supplementary Figure 1** and **Supplementary Table 1**). In contrast, *SvFCP1* expression was generally zero to 1 TPM until 15 DAS, when it briefly exceeded 5 or 6 TPM, and then dropped back to near zero. This is consistent with previous findings that *ZmFCP1* is expressed in leaf primordia and may control SAM maintenance non-cell-autonomously (Je et al., 2016), so its expression in studies such as ours might be expected to be low. Sequence comparisons indicate that FCP1 gene sequences are conserved among grasses (**Supplementary Figure 2B**), consistent with the hypothesis that the function of SvFCP1 is similar to that of ZmFCP1 and are likely not central to grass inflorescence development.

In addition to *SvFON2* and *SvFCP1*, 21 other Setaria CLE genes were expressed in early inflorescence development, with TPM > 5 for at least one individual value (**Supplementary Table 1**). Of this set of 23 CLE genes, we display the 18 most highly expressed (**Supplementary Figure 1**; raw data, means and standard deviations in **Supplementary Table 1**). Other than *SvFON2* and *SvFCP1*, only a couple have well-characterized functions in any angiosperm. Goad et al. (2017) assigned all *CLE* genes in plants to one of 12 groups (1A−1J, 2, and 3) based on sequence similarity, with *FON2/CLV3*-like and *FCP1* genes falling into Group 1D. The other genes expressed in Setaria inflorescences were mainly assigned to groups 1B, 1C, 1E, and 1J, all of unknown function despite representation throughout the angiosperms. In particular, three genes from subgroup 1E1 had higher expression than *SvFON2* (Sevir.3G191400, Sevir.9G131200, Sevir.9G048500), especially at early developmental stages (**Supplementary Figure 1**).

The most highly expressed *CLE* (Sevir.1G367300) is a member of group 2 (**Supplementary Figure 1**) that functions in vascular development (Goad et al., 2017). Arabidopsis proteins in this group inhibit differentiation of tracheary elements thereby regulating xylem formation (Hirakawa and Bowman, 2015); they also appear to function in axillary bud formation (Yaginuma et al., 2011). Related CLE genes appear to be highly conserved among seed plants and thus Sevir.1G367300 may also be involved in vascular differentiation in *S. viridis* inflorescence development.

SvFON2 Regulates the Inflorescence Meristem

To further test the function of *SvFON2* during inflorescence development, we knocked it out using CRISPR-Cas9 gene editing (Cermák et al., 2017). Preliminary screening of seven T0 transgenic plants showed editing only at the gRNA2 target sites, and four plants contained editing in at least one of the two

copies of *SvFON2*, for an editing rate of 29%. Further genotyping in T1 of these four transgenic lines retrieved two differently edited *fon2* alleles. Stable homozygous lines were obtained for these two alleles, designated as *Svfon2-1* and *Svfon2-2*, and were used for analysis. *Svfon2-1* and *Svfon2-2* each had a one base pair (T and A, respectively) insertion just after the G nucleotide at CDS position 103 (**Figure 3A**). This insertion disrupts the reading frame after residue 34 (position 47 in the alignment in **Supplementary Figure 2A**), upstream of the CLE domain. Since the active product from a CLE gene is the processed CLE domain

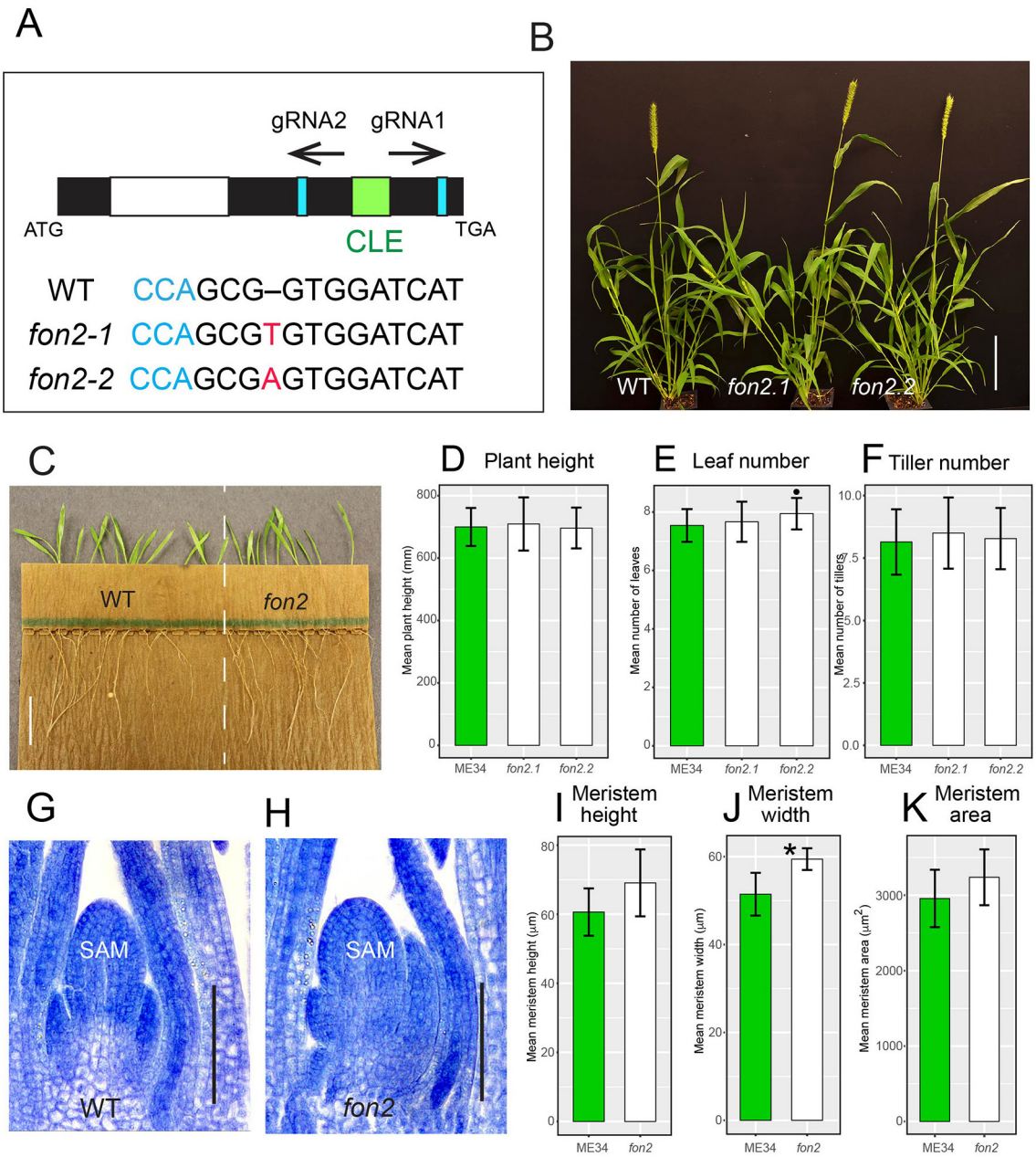

FIGURE 3 | *S. viridis fon2* mutants and phenotypic characterization during vegetative development. **(A)** Gene structure of *SvFON2* and gene editing in the mutants. Black, white, and green colored boxes represent exon, intron, and CLE domain, respectively, of the *SvFON2* gene. Blue boxes and text show PAM sites. Black arrows indicate target sites for the two guide RNAs (gRNA1 and gRNA2). ATG and TGA indicate the start and stop codons of the gene. Sequence below the gene model shows sequence comparison among wildtype (WT) and two independently edited mutants (*fon2-1* and *fon2-2*). Red highlighted bases indicate the 1 bp insertion in the gRNA2 target region. Representative set of 4-week old plants **(B)**. Roots from 5 DAS WT and *fon2* showing no significant growth defects **(C)**. Plant height **(D)**, leaf number **(E)**, and tiller number **(F)** of WT (green bars) and *fon2* mutants (*fon2-1* and *fon2-2*; white bars). Toluidine blue stained median sections of shoot apical meristems (SAM) at 6 DAS for WT **(G)** and *Svfon2* mutant **(H)**. SAM height **(I)**, width **(J)**, and area **(K)** of WT and *fon2* vegetative meristems at six DAS. Significance values by Welch's *t*-test: $^*p < 0.01$. Numbers of replicates for each statistical comparison listed in **Table 1**. Error bars are ± one standard deviation. SAM, shoot apical meristem. Scale bar: **(B)**, 10 cm; **(C)**, 2 cm; **(G,H)**, 50 μm.

TABLE 1A | Mean ± one standard deviation for plant traits comparing wild type (WT, ME034v), *Svfon2.1* and *Svfon2.2*.

	WT mean value	*Svfon2.1* mean value	*Svfon2.2* mean value	p, WT vs. *Svfon2.1*	p, WT vs. *Svfon2.2*	p, *Svfon2.1* vs. *Svfon2.2*
Plant height (mm)	700.00 ± 65.55 (34)	709.28 ± 85.26 (18)	696.5 ± 65.27 (18)	0.6845	0.8512	0.6171
Leaf number	7.54 ± 0.55 (35)	7.67 ± 0.69 (18)	7.94 ± 0.54 (18)	0.5141	**0.01586**	0.1862
Tiller number	8.14 ± 1.31 (35)	8.5 ± 1.42 (18)	8.28 ± 1.23 (18)	0.3811	0.7132	0.6194
Days to heading	19.03 ± 0.71 (35)	17.78 ± 0.94 (18)	18.22 ± 0.43 (18)	**3.376e-05**	**4.381e-06**	0.0812
Panicle length (mm)	78.46 ± 12.05 (34)	86.17 ± 9.81 (18)	84.89 ± 16.15 (18)	**0.01554**	0.1461	0.7763
Branches per cm	10.91 ± 3.67 (17)	19.12 ± 6.62 (13)	15.13 ± 4.49 (12)	**0.000834**	**0.01413**	0.09007
Spikelets per primary branch	11.40 ± 2.67 (10)	9.00 ± 1.35 (5)	9.87 ± 1.44 (5)	**0.03825**	0.174	0.3567

p-values of Welch's two-sample t-tests test whether the difference in means is significantly different from 0.
*Values significant at $p < 0.05$ marked in boldface. Sample sizes in parentheses. See also **Figures 3**, **4**.*

TABLE 1B | Mean ± one standard deviation for plant traits comparing wild type (WT, ME034v) to *Svfon2* mutants.

	WT mean value	*Svfon2* mean value	p, WT vs. *Svfon2*
6 DAS meristem height (μm)	60.631 ± 6.85 (8)	69.078 ± 9.71 (9)	0.05492
6 DAS meristem width (μm)	51.458 ± 4.86 (8)	59.430 ± 2.47 (9)	**0.00183**
6 DAS meristem area (μm^2)	2,957.42 ± 340.52 (5)	3,238.22 ± 331.09 (5)	0.271
12 DAS meristem width (μm)	59.254 ± 16.5 (5)	173.893 ± 26.5 (3)	**0.0070**
Seed weight	986.82 ± 155.61 (22)	823.25 ± 150.99 (15)	**0.00322**

p-values of Welch's two-sample t-tests test whether the difference in means is significantly different from 0.
Values significant at $p < 0.05$ marked in boldface. Sample sizes in parentheses.

(Djordjevic et al., 2011; Ni et al., 2011), these mutations are likely to disrupt the function of *SvFON2* completely.

Neither mutant allele affects overall plant growth characteristics. Vegetative characteristics of the two *Svfon2* alleles did not differ significantly from each other or from WT in the number of leaves, plant height, and tiller number (**Figures 3B,D–F**; **Table 1A**). Roots of *Svfon2* mutants also grew similarly to WT (**Figure 3C**), suggesting that the root apical meristem was not affected in *Svfon2* mutants. Because of the similarity between the two *Svfon2* alleles, hereafter we refer to them together as *Svfon2*.

Despite the overall similarity of vegetative characteristics, *Svfon2* mutant plants exhibited subtle differences in the size of the SAM at 6 DAS, before its transition to IM (**Figures 3G,H**). Width, height and area of the SAM in *SvFON2* were about 15%, 13% and 9% larger than WT, respectively (**Figures 3I–K**; **Table 1B**). However, the difference was only significant for meristem width ($p = 0.00183$; two-tailed *t*-test).

Reproductive aspects of *Svfon2* differed significantly from WT. Inflorescences in the *Svfon2* mutants emerged from the sheath (headed out) about 1 day earlier than WT (**Figure 4A**), suggesting that the mutants transitioned from vegetative to reproductive growth earlier. Although overall panicle length was not significantly different between *Svfon2.2* mutant plants and WT and only weakly significant between *Svfon2.1* and WT (**Figure 4B**, **Table 1A**), primary branch number per cm (i.e., branch density) was significantly higher in *Svfon2* (**Figure 4C**, **Table 1A**). The number of spikelets per branch was somewhat lower in the mutants, but the values were only significant in the comparison of *Svfon2.1* and WT (**Figure 4D**, **Table 1A**).

The most striking phenotype of *Svfon2* was in the panicle tips (**Figures 4F–I**). Abnormal apices were observed in all mutant panicles including the main inflorescences and those from the tillers. The panicle tips of *Svfon2* were larger than WT, often divided into two or more parts, and contained novel structures that were neither spikelets nor bristles (**Figures 4G,I,J**). Scanning electron microscopy (SEM) of the inflorescence tips showed that terminal sheet-like structures produced prickle hairs, characteristic of bristles (**Figures 4H,I**).

To verify that mutant phenotypes were caused by the mutation in *SvFON2*, we crossed *Svfon2-1* to WT plants. The F1 plants had normal panicles, and nine out of 36 plants had larger panicle tips (25%) in the F2, indicating a single recessive mutation. Genotyping the segregating F2 plants showed complete linkage between the homozygous mutation in *SvFON2* and the larger-tip panicle phenotype, suggesting that the *SvFON2* mutation was indeed responsible for the mutant phenotype.

The abnormal panicle tip phenotype in *Svfon2* suggested a defect in IM control. While IMs of WT inflorescences were more or less conical with clearly organized rows (**Figures 4K,M**, **5A,D**), the IM in *Svfon2* mutants was about three times wider

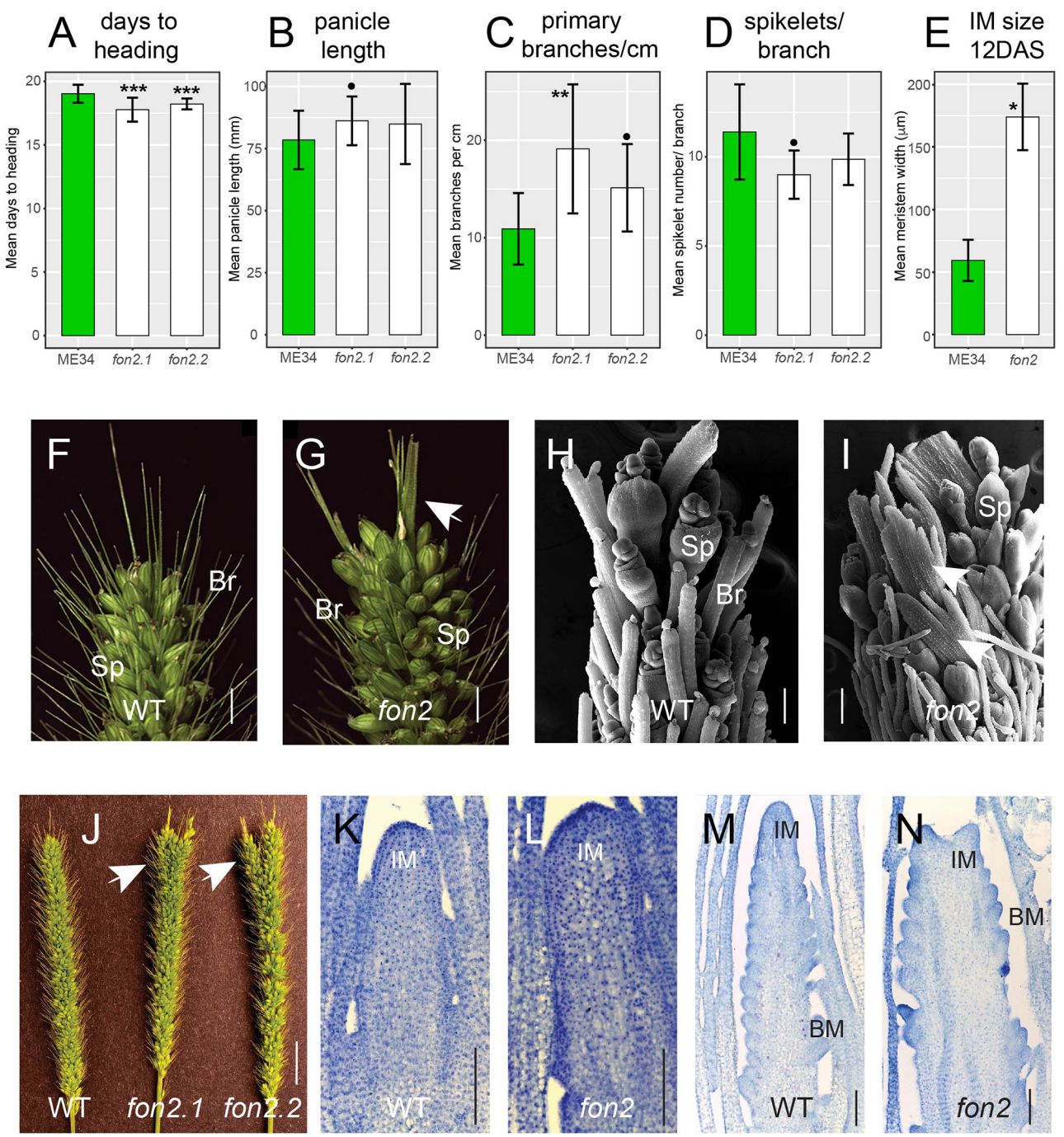

FIGURE 4 | Phenotypic characterization of *fon2* during reproductive development. Days to heading **(A)**, panicle length **(B)**, primary branches/cm **(C)**, spikelets/branch **(D)** of WT (green bars) and *fon2* mutants (*fon2-1* and *fon2-2*; white bars). **(F–I)** Panicle apices from WT **(F,H)** and *Svfon2* **(G,I)**. **(H,I)** Representative SEM images of 17 DAS WT **(H)** and *Svfon2* mutant **(I)**. White arrows show novel sheet-like structures in the mutant. Main panicles **(J)** from WT and mutants. White arrows show that the mutant panicle apices are larger and have more tips. **(K–N)** Toluidine blue stained median sections of inflorescence meristems at nine DAS **(K,L)** and 12 DAS **(M,N)**. **(K,M)**, WT; **(L,N)**, *Svfon2*. Significance values by Welch's *t*-test: $*p < 0.01$; $**p < 0.001$; $***p < 0.0001$; black dot, $p < 0.05$. Numbers of replicates for each statistical comparison listed in **Table 1**. Error bars are ± one standard deviation. IM, inflorescence meristem; BM, branch meristem; Sp, spikelet; Br, bristle (sterile branch). Scale bars: **(F,G)**, 5 mm; **(H,I)**, 100 μm; **(J)**, 1 cm; **(K–N)**, 100 μm.

than WT by 12 DAS (**Figures 4E,N**; **Table 1B**) and formed abnormal shapes (**Figures 4L,N**, **5B,C,E,F**). We looked at many more SEM photos and longitudinal sections than indicated by the sample size for IM width reported in **Table 1B**, and in all cases we observed considerable difference in size between WT and mutant meristems. However, because of the angle of

the SEMs and the fact that the mutant meristems are highly irregular in shape, we could only obtain precise numbers for a small number of samples for which we were confident of our measurements. Nonetheless, the difference was significant ($p = 0.0070$), reflecting the clear distinction in size. Because of a larger IM, more branch meristems were initiated in *Svfon2*, consistent with our observations that the mutants had more primary panicle branches per cm (**Figure 4C**, **Table 1A**). Primary branch meristems were also larger than in WT, but not as markedly so as the IM (**Figures 5E,F**). The slightly reduced number of spikelets per primary branch in the mutants (**Figure 4D**) suggested that the *Svfon2* mutation may have disrupted higher order branching and/or spikelet development. Perhaps because the mutants had fewer spikelets per primary branch and shorter time to flowering, overall seed weight in the main panicle was significantly lower in mutant plants ($p = 0.00322$; **Table 1B**, **Figure 5O**).

SvFON2 Mutations Have No Effect on Floral Organ Number or Morphology

Mutants of the closest homolog of *SvFON2* in rice, *Osfon2*, produced extra anthers and pistils in the flowers (Suzaki et al., 2006). To study whether *Svfon2* gave rise to similar phenotypes, we counted floral organs in *Svfon2*, including the glume, lemma, lodicule, palea, ovary, stigma, and anther. Unlike *Osfon2*, the number and shape of floral organs in *Svfon2* appeared entirely normal (**Figures 5G–N**, **Table 2**), indicating that SvFON2 is not the major CLE peptide controlling the floral meristem.

We cannot rule out the possibility that floral meristems in *Svfon2* mutants are slightly larger or smaller than in WT. Floral meristem size in *S. viridis* is difficult to quantify. The inflorescence has five or six orders of branching and thus bears flowers in many different orientations and stages of development. The precise orientation of the section on any particular floral meristem is not easily controlled to obtain a perfectly medial section; because sections are often more or less oblique, measurements are highly inaccurate. A similar problem exists for SEM photos. The images in **Figures 5G–N** hint that mutant flowers might in fact be smaller than in WT, which would also be consistent with the reduced seed weight per panicle, although a full exploration of this possibility would require extensive measurements of spikelets and floral organs during development. Nonetheless, we are confident that if meristem size and organ number were increased as markedly as in rice *FON2* mutants, we would have detected the change.

SvFON2 Co-expression Network and Its Signaling Components

To identify genes that have a similar expression pattern to that of *SvFON2* and thus potentially identify new factors for inflorescence meristem size determination in *S. viridis* and other panicoid grasses, we defined the *SvFON2* co-expression network using expression data from the IM developmental time series published by Zhu et al. (2018) (**Supplementary Figures 3**, **4**; **Supplementary Table 2**). RNA-seq data were collected in quadruplicate for inflorescences at 10, 12, 14, 15, 16, and 18 DAS, as noted above. The 10 DAS time point captures the IM soon after the transition from the vegetative SAM and the subsequent days capture branching, spikelet formation, and early floral development. For clarity of display, this network was filtered to show only the 26 genes whose expression is most tightly correlated with that of *SvFON2* (weight > 0.185); this set is called "FON2-network" in **Supplementary Table 2**. As expected, the genes in this network showed a pattern nearly identical to that of *SvFON2*, in which expression is low at 10 DAS, increases to 14 or 15 DAS, remains high through 16 DAS and then drops substantially by 18 DAS (**Supplementary Figure 4**). Not surprisingly, the FON2-network included orthologs of *Fasciated ear 4* (*Fea4*, encoding a bZIP transcription factor), and *Ramosa3* (*Ra3*, encoding a trehalose-phosphate phosphatase), genes encoding negative regulators that control IM size and branch initiation without affecting floral organs (Satoh-Nagasawa et al., 2006; Pautler et al., 2015). The *SvFON2* network also contained an ortholog of *Rough sheath1* (*Rs1*) which encodes a class I KNOX homeodomain transcription factor and is important for meristem control and lateral organ initiation (Schneeberger et al., 1995). Identification of known developmental genes for IM control in the *SvFON2* co-expression network is consistent with our finding that *SvFON2* also functions in IM size.

SvFON2 expression is strongly correlated with that of such uncharacterized genes as Sevir.9G527000 and Sevir.5G100000 (**Supplementary Figures 3**, **4**), which exhibit moderate expression during early inflorescence development (**Supplementary Table 2**). These genes contain no annotated domains, and BLASTP searches against plant genomes in Phytozome and against GenBank find no genes of known function. In addition, none of the BLAST hits aligns with more than 64% of the query sequence. These two loci are therefore interesting candidates for future characterization.

The *SvFON2* network also contains five F-box domain-containing genes and one gene encoding a RING-type E3 ligase (**Supplementary Figures 3**, **4**). F-box proteins and E3 ligases are core components of the ubiquitin ligase complex that is responsible for protein degradation, with the F-box protein providing substrate specificity (Sharma et al., 2016). F-box genes can also function in hormone regulation and transcriptional activation (Lippman et al., 2008). Several transcription factors including a zinc finger protein and MADS-box proteins are also in the *SvFON2* network (**Supplementary Figures 3**, **4**). Function of these genes and their genetic relationships remain to be investigated.

In addition to the 21 genes in the tightly correlated FON2-network, 264 additional genes had expression values correlated with those of *SvFON2* but at much lower levels (**Supplementary Table 2**, "FON2_edge_allgenes"). Among these less strongly connected genes were several that were annotated as LRR receptors or *WUS/WOX* genes, as expected in a CLE-gene network. These are shown in **Supplementary Figure 3** as linked to *SvFON2* with dotted lines to indicate that they were added to the diagram manually and are not as tightly connected as the other genes shown in the figure. Five LRR receptor genes were co-expressed with *SvFON2* (**Supplementary Figure 3**,

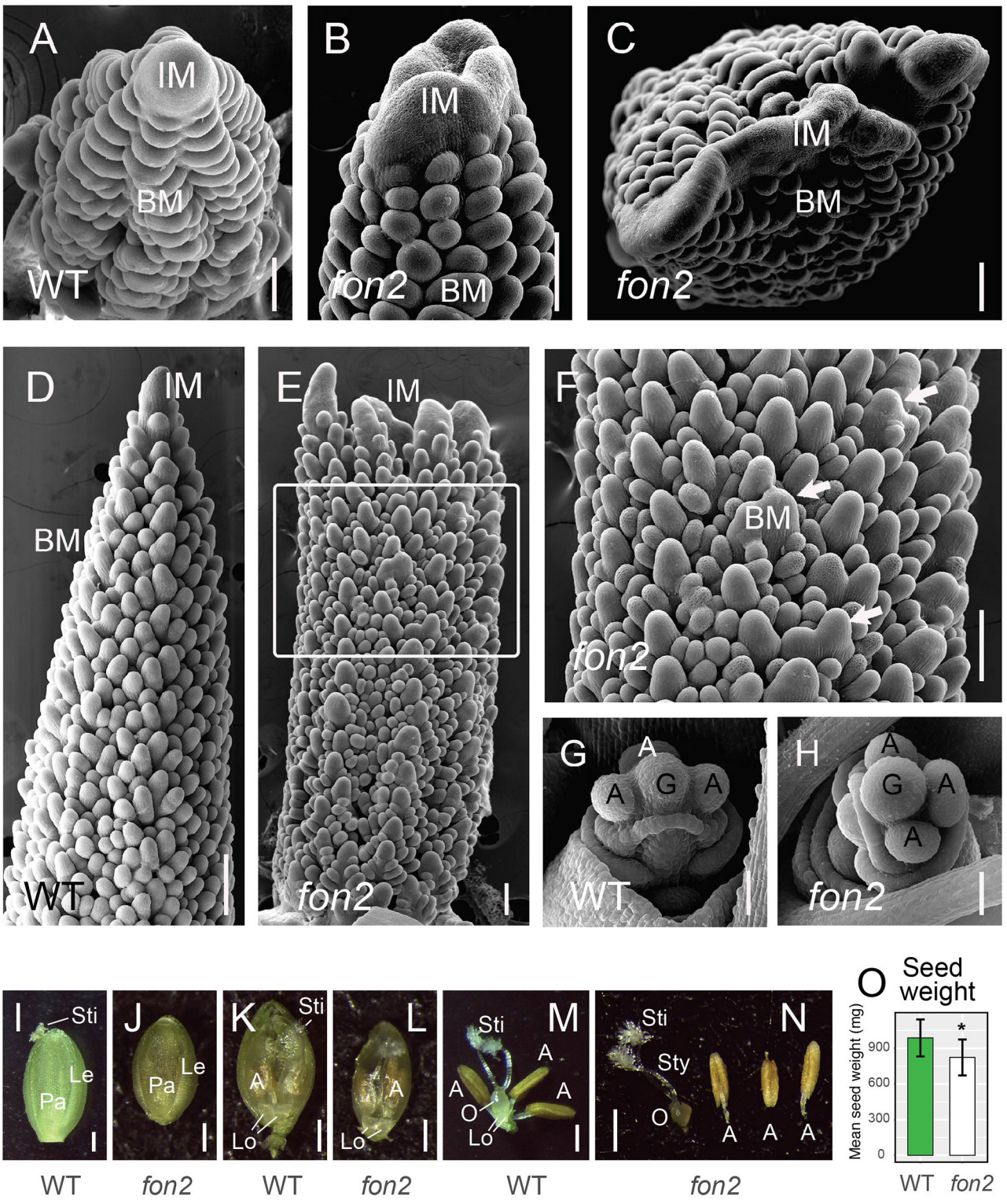

FIGURE 5 | Inflorescence meristems and early floral development of *Svfon2* mutants. **(A–F)** Representative scanning electron microscope images of 12 DAS WT **(A,D)** and *Svfon2* mutants **(B,C,E,F)**. **(F)** corresponds to the area marked by a white box in **(E)**. White arrows show enlarged primary branch meristems.

(Continued)

FIGURE 5 | (G,H) Representative scanning electron microscope images of 17 DAS WT **(G)** and *Svfon2* mutant **(H)**. **(I–N)** Florets of WT **(I,K,M)** and *Svfon2* mutant **(J,L,N)** immediately before anthesis. WT in **(I,M)**, A10; WT in **(K)**, ME34. **(I,J)** Upper (fertile) floret, lemma, and palea, viewed from the adaxial (relative to the floral axis) side. **(K,L)** Glumes and lemmas removed, floret viewed from the abaxial (relative to the floral axis) side, with the floral parts lying on the palea, and partially enveloped by the hyaline margins of the palea. Two normally formed lodicules are clearly visible, and the golden brown anthers can be seen through palea margins. The feathery stigma is slightly exserted from the WT palea, whereas it is still enclosed in the *Svfon2* image. **(M,N)** Floral organs, showing gynoecium with an ovary, two styles and two stigmas, and three anthers on the right. **(O)** Total seed weight in the main panicle of WT (green bar) and *svfon2* (white bar). Significance values by Welch's *t*-test: $^*p < 0.01$. Numbers of replicates for each statistical comparison listed in **Table 1**. Error bars are ± one standard deviation. IM, inflorescence meristem; BM, branch meristem; A, anther; G, gynoecium; Le, upper lemma; Lo, lodicule; O, ovary; Pa, upper palea; Sti, stigma; Sty, style. Scale bars: **(A–H)**, 50 μm; **(I–N)**, 0.5 mm.

TABLE 2 | Numbers of floral organs in WT and *svfon2* mutant flowers.

	Glume	Lemma	Lodicule	Upper Palea	Ovary	Stigma	Anther
WT	2	2	2	1	1	2	3
fon2	2	2	2	1	1	2	3

N > 20.

Supplementary Tables 2, **3**), one of which is homologous to *CLV1/TD1* (Sevir.4G294000/*SvTD1*). Other LRR receptor genes that are co-expressed with *SvFON2* include homologs of EXCESS MICROSPOROCYTES1 (EMS1) which functions in somatic and reproductive cell fates in the *Arabidopsis* anther (Zhao et al., 2002; Li et al., 2017) and HAESA-LIKE 1 (HSL1) that regulates floral organ abscission in *Arabidopsis* (Jinn et al., 2000; Gubert and Liljegren, 2014) (**Supplementary Table 2**). One WUS/WOX gene (Sevir.5G266300) was also co-expressed with *SvFON2* (**Supplementary Figure 3**, **Supplementary Table 2**). The function of the products of these genes in *S. viridis* inflorescence meristems remains to be determined.

We expected that the *SvFON2* co-expression network would include only a subset of the LRR receptors and *WUS/WOX* transcription factors that were expressed during early inflorescence development. Using sequence BLAST and domain searches, we identified homologs of these genes in *S. viridis*. As expected, the LRR receptor family is large, with at least 438 genes in *S. viridis* (**Supplementary Table 3**). Using data from Zhu et al. (2018), we found 247 LRR receptor genes were expressed in early inflorescence development with a collective TPM greater than two across all six stages (**Supplementary Table 3**). Among them were homologs of LRRs that function in the Arabidopsis CLV3 signaling pathway, including *CLV1/TD1*, *CLV2/FEA2*, *FEA3* (Je et al., 2016, 2018), *BARELY ANY MERISTEM 1-3* (*BAM1-3*) (DeYoung et al., 2006), *ERECTA* (*ER*) (Mandel et al., 2014), *CORYNE* (*CRN*) (Muller et al., 2008), *RECEPTOR-LIKE PROTEIN KINASE 2* (*RPK2*) (Kinoshita et al., 2010), and *CLAVATA3 INSENSITIVE RECEPTOR KINASES* (*CIKs*) (Hu et al., 2018; Xu and Jackson, 2018). Expression of these genes was moderate to high (**Supplementary Figure 5**, **Supplementary Table 3**), with *ER* and *BAM* homologs exhibiting the highest and relatively stable expression during these stages (**Supplementary Figure 5**, **Supplementary Table 3**). Several other LRR receptors are also highly expressed, such as Sevir.3G424200, during early inflorescence development (**Supplementary Table 3**), but their roles are unknown in *S. viridis* or other species and thus they are interesting candidate genes for future studies.

Similar analyses found 12 *WUS/WOX* genes in *S. viridis* (**Supplementary Figure 5**, **Supplementary Table 3**), seven of which were expressed in early inflorescences with a collective TPM greater than two. Homologs of *WOX3*, *WOX13*, and *WOX9* had relatively high expression during early inflorescence development (**Supplementary Table 3**).

DISCUSSION

S. viridis FON2 Controls Inflorescence Meristem but Not Floral Meristem Development

Using two independently edited alleles generated by CRISPR-Cas9 technology, we showed that SvFON2 plays a prominent role in IM size control in Setaria, as the co-orthologous protein ZmCLE7 does in maize (Rodríguez-Leal et al., 2019).

Although the basic framework of the signaling pathway involving a CLE ligand and LRR receptors appears conserved among eudicots and monocots, the developmental roles of individual proteins differ. SvFON2 has its major developmental role in the IM but not the FM, different from OsFON2 which specifically regulates the FM without affecting the IM, suggesting that the developmental role of this subgroup of CLEs has become further differentiated between Panicoideae and Oryzoideae. Because the *Svfon2* mutant had normal floral organs, other proteins, likely other CLEs, must control FM and floral organ development in Setaria. *Svfon2* also had a largely normal SAM, again pointing to other CLEs regulating that meristem.

Divergence in the developmental roles of the FON2 CLEs could be caused by differences in (a) gene expression, (b) post-translational modifications, (c) patterns of redundancy and dosage compensation mechanisms, or some combination of the three. In contrast to FCP1 whose genomic regions in different grass species have high degree of collinearity (**Supplementary Figure 6**), the genomic regions encompassing the FON2 orthologs are not perfectly collinear (**Supplementary Figure 7**), suggesting that the regulatory environment may not be conserved for FON2 genes. However, *OsFON2* is expressed in the SAM, IM and FM even though the mutant phenotype is only seen in the FM (Suzaki et al.,

2006). Similarly, *SvFON2* is expressed in a broad spatiotemporal window from IM initiation through to FM and floral organ development but only the IM is substantially altered in the *Svfon2* mutant. Thus, gene regulation alone is unlikely to explain the divergence in developmental roles for this group of CLEs.

Another possibility for *CLE* divergence lies in peptide modifications and interactions with downstream factors. Differences in the processing of the pre-propeptides, amino acid sequences in the CLE domain, and the level and type of modifications (e.g., arabinosylation) of CLE peptides can change their activity and binding affinity to receptors (Ohyama et al., 2009; Xu et al., 2015). CLE domains in grass *FON2* genes differ in several amino acids (**Supplementary Figure 2**), which could affect the number and nature of post-translational modifications.

Third, different degrees of pathway redundancy in different tissues also contribute to divergence. Some tissues are controlled by a single CLE peptide and its pathway, so this CLE plays a predominant role, whereas other tissues are controlled by multiple pathways, so the role of each CLE can be often masked by others (Je et al., 2018; Rodríguez-Leal et al., 2019). All of these factors together constitute a complex yet delicate network controlling IM and FM, which is critical to understand the morphological diversity of grass inflorescences.

Other CLE Genes Function During Inflorescence Development

A total of 23 out of 42 *CLEs* were expressed during early inflorescence development in *S. viridi*s, but only a few of these have been studied in other grasses. The rice FON2 SPARE1 (FOS1) protein functions in FM control. The functional allele of this gene in *indica* varieties acts as a suppressor of *fon2* allele (Suzaki et al., 2009); however, no knock-out of this gene has been reported. The two *S. viridis FOS1* homologs [Sevir.1G144900 (*SvFOS1B*) and Sevir.3G241500 (*SvFOS1A*)] are scarcely expressed in early inflorescence development, even at 18 DAS when most floral meristems should have initiated (TPM collectively from six stages < 0.5) (**Supplementary Table 1**). Thus, FOS1A and FOS1B might have different roles in Setaria than their co-orthologue does in rice. Likewise, overexpression and peptide application studies implicate the rice protein FCP2 in FM and/or IM control (Suzaki et al., 2008; Ohmori et al., 2014), whereas Chu et al. (2013) suggest that rice FCP2 is involved in root meristem maintenance and metaxylem development. *SvFCP2* (Sevir.4G139000) is not expressed at all during early *S. viridis* inflorescence development (**Supplementary Table 1**). Whether the protein functions differently in rice and Setaria is therefore unclear, since no studies of rice or Setaria *FCP2* genes provide evidence from loss of function mutants or responses in mutants lacking putative receptors. With small ligands such as the CLEs, peptide application experiments are hard to interpret, because they may or may not reflect interactions in normal development.

In contrast, several other *CLEs* are far more highly expressed in inflorescences than *SvFON2* (**Supplementary Figure 1**), making it interesting to test their function in inflorescence development in the future. These *CLEs* could also regulate the FM and/or vegetative SAM, as discussed above, but equally likely could be involved in other aspects of inflorescence development.

The genomic context of the CLE genes in grasses has also received scant attention. We show here that while FCP1 orthologs appear in generally collinear regions in several species of grasses (**Supplementary Figure 6**), the region surrounding FON2 is apparently more dynamic (**Supplementary Figure 7**). Whether such local rearrangements affect gene regulation is unknown. The comparative genomic positions of CLE genes in general have not been analyzed, perhaps in part because they are short genes and not always well-annotated.

SvFON2 Co-expression Network and Its Signaling Components

For additional insight into the role of *SvFON2* in signaling, we extracted the *SvFON2* co-expression modules from our published analysis of gene expression during inflorescence development (Zhu et al., 2018). *SvFON2* expression is correlated with expression of the Setaria orthologs of *Fasciated Ear 4* (*SvFEA4*), *Ramosa3* (*SvRA3*), and *RoughSheath1* (*SvRS1*) (**Supplementary Figures 3**, **4**), whose homologs in maize all regulate meristem maintenance or determinacy (Schneeberger et al., 1995; Satoh-Nagasawa et al., 2006; Pautler et al., 2015). In maize, the CLAVATA pathway that involves the FEA2 and FEA3 receptors controls meristem homeostasis (Je et al., 2016, 2018), and FEA4 also negatively controls meristem maintenance, independently of the CLAVATA pathway (Pautler et al., 2015). Since FEA2 function is, at least partially, mediated by *CLE7* (the closest homolog of *SvFON2* and *OsFON2* in maize) (Je et al., 2018), it is possible that *SvFON2* functions in parallel to *SvFEA4* in *S. viridis*, although this remains to be experimentally tested. The genetic relationship between *SvFON2* and *SvRA3* and *SvRS1* has not been explored, and it would be interesting to examine this in *S. viridis* or maize.

The *SvFON2* co-expression network includes a number of F-box containing genes and E3 ligase genes (**Supplementary Figures 3**, **4**). F-box containing genes that function in meristem control and/or inflorescence architecture include *ABERRANT PANICLE ORGANIZATION 1* (*APO1*) (Ikeda et al., 2007) and *LARGER PANICLE* (*LP*) (Li et al., 2011) from rice, *UNUSUAL FLORAL ORGANS* (UFO) from *Arabidopsis* and its ortholog *ANANTHA* (*AN*) from tomato (Lippman et al., 2008), and several F-box genes in wheat (Hong et al., 2012). Similarly, E3 ligases such as *SHOOT APICAL MERISTEM ARREST 1* (*SHA1*) (Sonoda et al., 2007) and *Nicotiana tabacum RING DOMAIN CONTAINING PROTEIN1* (*NtRCP1*) from tobacco (Wang et al., 2015) function in meristem maintenance and/or floral transition. Therefore, we hypothesize that these F-box containing genes and E3 ligases function in meristem regulation during inflorescence development.

Identification of LRR receptors and their expression analyses suggested that homologs of CLV1/TD1, CLV2/FEA2, FEA3, ERECTA (ER), BARELY ANY MERISTEM1-3 (BAM1-3), CORYNE (CRN), RECEPTOR-LIKE PROTEIN KINASE2 (RPK2), and CLAVATA-interacting kinases (CIKs) are expressed in early inflorescences (**Supplementary Figures 3**, **5**,

Supplementary Table 3) and could be receptors of SvFON2. Given that LRR receptors and co-receptors interact in a complex way for various functions (Smakowska-Luzan et al., 2018), SvFON2 could signal through multiple receptors. Among the potential receptors, SvTD1 is most likely because TD1 in maize also functions in the inflorescence meristem (Bommert et al., 2005) similar to SvFON2 in *S. viridis*. In support of this, *SvTD1* is one of the few LRR receptor genes whose expression is correlated with that of *SvFON2* (**Supplementary Table 2**, **Supplementary Figure 5**).

No WOX protein has been functionally characterized in Setaria. Based on their expression (**Supplementary Figure 5**, **Supplementary Table 3**), homologs of *WOX3*, *WOX13*, *WOX9*, and *WUS* are candidates for regulation by the *SvFON2* signaling pathway, although *SvWOX9A* (Sevir.5G266300) is most tightly co-expressed with *SvFON2* and is the best candidate for direct regulation (**Supplementary Figures 3**, **5**). *WOX9* (also called *STIMPY*) functions in embryonic patterning and shoot apical meristem maintenance (Wu et al., 2005, 2007) and its ortholog *COMPOUND INFLORESCENCE* from tomato (Lippman et al., 2008; Zheng and Kawabata, 2017) is essential for inflorescence development and architecture, but roles of their homologs in grasses have not been studied. Specific functions of the two *WOX3* homologs in *S. viridis* (Sevir.3G044600/*SvWOX3A* and Sevir.8G020500/*SvWOX3B*) are unknown. *Arabidopsis WOX3* [also called *PRESSED FLOWER* (*PRS*)] and its orthologs in maize, *narrow sheath1* and *narrow sheath2* (*NS1* and *NS2*), are required for lateral sepal development (Matsumoto and Okada, 2001) and/or leaf development (Nardmann et al., 2004) by recruiting organ founder cells from lateral domains of meristems and promoting cell proliferation (Nardmann et al., 2004; van der Graaff et al., 2009). *WOX13* and its paralog *WOX14* in *Arabidopsis* regulate the floral transition, floral organ development and root development (Deveaux et al., 2008). Since *WOX13* and *WOX14* homologs are highly conserved among land plants (Deveaux et al., 2008), their homolog in *S. viridis* (Sevir.5G365700/*SvWOX13*) may play similar roles. WOX4 is regulated by FCP1 in rice (Ohmori et al., 2013) but appears to be mostly involved in maintenance of vegetative meristems; its expression level in *S. viridis* is low (**Supplementary Table 3**).

Potential Roles of SvFON2 in Flowering Time and Yield

One unexpected result of this study was a significant acceleration of inflorescence development, with the mutant plants heading out about 1 day earlier than WT. We infer that this reflects acceleration of the transition from the vegetative SAM to an IM, although it may or may not affect time to anthesis. We have not found many reports of a similar effect of mutations in CLV3-like genes in other systems, although a change in meristem size might indirectly influence developmental timing. Much of the work on CLV3-like genes has described loss-of-function mutations, in which the effect on the meristem is so dramatic that timing changes may be difficult to disentangle. However, variation in meristem size is associated with variation in days to flowering in maize (Leiboff et al., 2015) and naturally-occurring alleles in a CLV3-like gene are associated with days to flowering in chickpea (*Cicer arietinum*) (Basu et al., 2019).

Any locus that affects inflorescence meristem size has the potential to affect yield. For example, natural variation among *FEA2* and *FEA3* alleles in maize affects inflorescence meristem size and hence kernel row number and number of grains per ear (Je et al., 2016; Trung et al., 2020). Given this information from maize, we may have expected that yield would be higher when *Svfon2* was disrupted, but it was lower. The observation of fewer spikelets per primary branch may help explain this result, as may subtle size differences in florets. Primary branches in wild type *S. viridis* continue to branch multiple times, producing secondary, tertiary, and even higher order branches (Doust and Kellogg, 2002). We speculate that even modest disruption of the primary branch meristems in *Svfon2* mutants may affect these later rounds of branching, which in turn will affect the relative numbers of bristles and spikelets. In addition, as shown in maize (e.g., Rodríguez-Leal et al., 2019), other CLE loci are likely to be involved in control of other meristems. Therefore, when using *CLE* genes such as *SvFON2* to engineer related crops for increased yield, it may be necessary to finetune its expression or function by generating knockdown or weaker alleles, instead of making knockout alleles. In addition, it may be necessary to manipulate other *CLE* genes other than *SvFON2* alone.

In summary, we found that the developmental roles of *FON2* genes have diversified among grasses, with *OsFON2* affecting floral meristems and *SvFON2* affecting inflorescence and branch meristems, similar to its maize homolog. Thus, the *SvFON2* gene regulatory network may be shared among panicoid grasses, but likely does not extend to oryzoids. Our bioinformatic analyses predicted genes that may be involved in the *SvFON2* co-expression network and signaling pathway, focusing on LRR receptors and WUS/WOX genes. Along with rapidly advancing gene editing and transformation technologies (Zhu et al., 2017), studies on the function and evolution of *CLE* genes and their signaling pathway components will be accelerated in *S. viridis* and other grasses.

DATA AVAILABILITY STATEMENT

The datasets presented in this study can be found in online repositories. The names of the repository/repositories and accession number(s) can be found in the article/**Supplementary Material**.

AUTHOR CONTRIBUTIONS

EK and CZ designed the project and produced the figures. HZ did the transformation with input from TB. LL did the *in situ* hybridization with input from DJ. All other experiments and data analysis were carried out by CZ and OC. CZ drafted the paper with subsequent comments and review by EK and DJ. All authors read and approved the final manuscript.

FUNDING

CZ was supported by National Science Foundation (NSF) grant IOS-1413824 to EK. HZ was supported by Central Public-interest Scientific Institution Basal Research Fund for Chinese Academy of Tropical Agricultural Science NO. 1630052017012. DJ and LL were supported by NSF grant IOS-1546837. OC was supported by the Students and Teachers as Research Scientists program at the University of Missouri-St. Louis. Publication fees are covered by funds from the Donald Danforth Plant Science Center.

ACKNOWLEDGMENTS

We thank Carla Coelho, Hui Jiang, and Christine Shyu (Donald Danforth Plant Science Center) for advice on *S. viridis* growth and CRISPR-Cas9 technology. We also thank Daniel Voytas (University of Minnesota) for sending us pMOD_A1110 (pJG471), pMOD_B2518 (pJG310), pMOD_C2616 (pJG338), and pTRANS_250d (pRLG103) constructs for CRISPR-Cas9 cloning. We thank to Paula McSteen (University in Missouri, Columbia) for stimulating discussions on this project and Sona Pandey (Donald Danforth Plant Science Center) for feedback on the manuscript. Dr. Matt Box took the images in **Figures 2A,D**.

SUPPLEMENTARY MATERIAL

The Supplementary Material for this article can be found online at: https://www.frontiersin.org/articles/10.3389/fpls.2021.636749/full#supplementary-material

Supplementary Figure 1 | Expression of CLE genes in *S. viridis* A10 at six developmental stages. Figure includes all but three CLE genes for which at least one stage had TPM > 5 (see all CLE gene in **Supplementary Table 1**). *SvFON2* has elevated expression at 10–12 days after sowing (DAS); the pattern is distinct from that of most other CLEs. Note different scales of the vertical axis for the lower six panels. Leading "Sevir." has been omitted from all gene model names to improve clarity. Each gene model name is followed by the name of the sequence-based cluster to which it was assigned by Goad et al. (2017); color of shading behind names indicates genes from the same cluster. Gene expression in Transcripts Per Million (TPM) at six sequential stages was retrieved from Zhu et al. (2018). The six stages represent IM initiation (10 days after sowing; DAS; see **Figures 2A–C**), primary (12 DAS) and higher order (14 DAS) branch formation, transition to SMs (15 DAS; **Figures 2D–F**), differentiation of spikelets and bristles (16 DAS), and floral organ development (18 DAS).

Supplementary Figure 2 | Comparison of CLE domain sequences from CLV3/FON2 **(A)** and CLE40/FCP1 **(B)** subgroup genes. Genes from *Arabidopsis thaliana* (At) *Brachypodium distachyon* (Bd), *Oryza sativa japonica* (Os), *Setaria viridis* (Sv), and *Zea mays* (Zm) are shown. Vertical line (arrow) indicates position of the CRISPR-Cas9 induced insertions and subsequent disruptions of the reading frame in the two *Svfon2* alleles.

Supplementary Figure 3 | *SvFON2* co-expression network during inflorescence development. Correlations among transcripts in the module containing *SvFON2* from Weighted Gene Co-expression Network Analysis (WGCNA), using data extracted from Zhu et al. (2018); graph constructed in Cytoscape v3.4.10. After filtering by weight > 0.185, connections between key genes involved in plant development (yellow) and the genes that they directly connected with were displayed (**Supplementary Table 2**). "Sevir." is omitted from each gene ID for clarity. Line length is proportional to the weight between the nodes. Green highlighted genes are transcription factors in the MADS-box (MADS) or zinc finger protein (ZFP) families. Pink-purple highlighted genes encode proteins containing an F-box or E3 ligase and may be involved in protein degradation. Other genes are highlighted in blue (functional annotation available) or gray (no sequence similarity to any other annotated genes). Expression of five additional *LRR* genes and one *WOX* gene also correlates with that of *SvFon2* but at a level below the 0.185 cut-off weight; these were added manually to the figure by dotted lines. See also **Supplementary Figure 4** and **Supplementary Table 2**.

Supplementary Figure 4 | Expression of *SvFON2* (upper left) and individual genes in the *SvFON2* co-expression network during inflorescence development. Expression data for genes in colored ovals in **Supplementary Figure 3**. Values are in TPM at six sequential stages (10–18 DAS) retrieved from Zhu et al. (2018). Error bars are standard deviations. Note substantial differences in the scale of the vertical axes, reflecting differences in overall expression level. See also **Supplementary Tables 2**, **3**.

Supplementary Figure 5 | Expression of *SvFON2* and selected LRR receptor and *WUS/WOX* genes during *S. viridis* early inflorescence development. Gene expression data in TPM at six sequential stages (10–18 DAS) retrieved from Zhu et al. (2018). Error bars are standard deviations. Note differences in the scale of the vertical axes, reflecting differences in overall expression level. See also **Supplementary Tables 2**, **3**.

Supplementary Figure 6 | Screenshot of the GEvo analysis from CoGe to compare the ca. 50Kb genomic region around the *FCP1* gene. *FCP1* genes are highlighted in red boxes. Sequences from *Brachypodium distachyon*, *Oryza sativa japonica*, *Setaria viridis*, and *Zea mays* were used for comparison. Each black rectangle represents one sequence and the dashed line in the middle divides the two strands. Gene models are drawn in green, with UTRs in blue, and introns in gray. Colored blocks above or below gene models are regions of similarity between all pairwise sequence comparisons. The more and/or wider colored blocks are, the more collinear or stable the genomic region is. Some connections are shown but connectors are omitted around FCP1 itself for clarity. BdFCP1_Bradi5g13241 is not annotated in the genome of *Brachypodium distachyon* line Bd21(v2.0) for the CoGe analysis so the closest neighboring gene was used to infer the genomic context. Analysis can be regenerated at https://genomevolution.org/r/1fssg.

Supplementary Figure 7 | Screenshot of the GEvo analysis from CoGe to compare the ca. 50 Kb genomic region around the *FON2* gene. *FON2* genes are highlighted in red boxes. Sequences from *Brachypodium distachyon*, *Oryza sativa japonica*, *Setaria viridis*, and *Zea mays* were used for comparison. Each black rectangle represents one sequence and the dashed line in the middle divides the two strands. Gene models are drawn in green, with UTRs in blue and introns in gray. Colored blocks above or below gene models are regions of similarity between all pairwise sequence comparisons. The more and/or wider colored blocks are, the more collinear or stable the genomic region is. Some connections are shown but connectors are omitted around FON2 itself for clarity. Analysis can be regenerated at https://genomevolution.org/r/1fss7.

Supplementary Table 1 | (Sheet 1) Expression of genes in the SvFon2(Sevir.8G183800) network with weight cutoff at 0.185, genes in Transcripts per Million (TPM) at six different stages of inflorescence development. Weight is a value quantifying the co-expression level of a gene pair generated by Weighted Gene Co-expression Network Analysis (WGCNA) in Zhu et al. (2018). For annotation, WikiGene.description and InterPro.description are from Biomart of EnsemblPlants. Best.hit.arabi.name, arabi.symbol, arabi.defline, Best.hit.rice.name and rice.defline are from the annotation file for the S. viridis genome (v1.1) from Phytozome v12.1. **(Sheet 2)** Expression of all genes directly associated with SvFon2 (Sevir.8G183800) in Transcripts per Million (TPM) at six different stages of inflorescence development. Genes were arranged by weight value quantifying the co-expression level of a gene pair generated by Weighted Gene Co-expression Network Analysis (WGCNA) in Zhu et al. (2018). For annotation, Short_name and Short_description are from classic maize genes. WikiGene.description and InterPro.description are from Biomart of EnsemblPlants. Best.hit.arabi.name, arabi.symbol, arabi.defline, Best.hit.rice.name and rice.defline are from the annotation file for the S. viridis genome (v1.1) from Phytozome v12.1.

Supplementary Table 2 | (Sheet 1) Expression of genes homologous to known leucine rich receptors in Transcripts per Million (TPM) at six different stages of inflorescence development. For annotation, WikiGene.description and InterPro.description are from Biomart of EnsemblPlants. Best.hit.arabi.name, arabi.symbol, arabi.defline, Best.hit.rice.name and rice.defline are from the annotation file for the S. viridis genome (v1.1) from Phytozome v12.1. Genes were arranged by their expression value, highest to lowest for the sum of expression

across six stages. **(Sheet 2)** Expression of leucine rich receptors and WOX genes that are coexpressed with SvFon2 (Sevir.8G183800). Weight is a value quantifying the co-expression level of a gene pair generated by Weighted Gene Co-expression Network Analysis (WGCNA) in Zhu et al. (2018). Expression of genes in Transcripts per Million (TPM) at six different stages of inflorescence development. For annotation, WikiGene.description and InterPro.description are from Biomart of EnsemblPlants. Best.hit.arabi.name, arabi.symbol, arabi.defline, Best.hit.rice.name and rice.defline are from the annotation file for the S. viridis genome (v1.1) from Phytozome v12.1. Genes were arranged by their weight value, starting with those whose expression is most closely correlated with SvFON2. **(Sheet 3)** Expression of genes homologous to known leucine rich receptors (LRR) in Transcripts per Million (TPM) at six different stages of inflorescence development. For annotation, WikiGene.description and InterPro.description are from Biomart of EnsemblPlants. Best.hit.arabi.name, arabi.symbol, arabi.defline, Best.hit.rice.name and rice.defline are from the annotation file for the S. viridis genome (v1.1) from Phytozome v12.1. Genes were arranged by their expression value, highest to lowest for the sum of expression across six stages. **(Sheet 4)** Expression of WUS/WOX genes in Transcripts per Million (TPM) at six different stages of inflorescence development. For annotation, WikiGene.description and InterPro.description are from Biomart of EnsemblPlants. Best.hit.arabi.name, arabi.symbol, arabi.defline, Best.hit.rice.name and rice.defline are from the annotation file for the S. viridis genome (v1.1) from Phytozome v12.1. Genes are arranged by their expression value, highest to lowest for the sum of expression across six stages.

REFERENCES

Acharya, B. R., Roy Choudhury, S., Estelle, A. B., Vijayakumar, A., Zhu, C., Hovis, L., et al. (2017). Optimization of phenotyping assays for the model monocot *Setaria viridis*. *Front. Plant Sci.* 8:2172. doi: 10.3389/fpls.2017.02172

Basu, U., Narnoliya, L., Srivastava, R., Sharma, A., Bajaj, D., Daware, A., et al. (2019). CLAVATA signaling pathways genes modulating flowering time and flower number in chickpea. *Theor. Appl. Genet.* 132, 2017–2038. doi: 10.1007/s00122-019-03335-y

Benabdelmouna, A., Abirached-Darmency, M., and Darmency, H. (2001). Phylogenetic and genomic relationships in *Setaria italica* and its close relatives based on the molecular diversity 5S and 18S-5.8S-25S rDNA genes. *Theor. Appl. Genet.* 103, 668–677. doi: 10.1007/s001220100596

Bennetzen, J. L., Schmutz, J., Wang, H., Percifield, R., Hawkins, J., Pontaroli, A. C., et al. (2012). Reference genome sequence of the model plant Setaria. *Nat. Biotechnol.* 30, 555–561. doi: 10.1038/nbt.2196

Bommert, P., Lunde, C., Hardmann, J., Vollbrecht, E., Running, M., Jackson, D., et al. (2005). *Thick tassel dwarf1* encodes a putative maize ortholog of the Arabidopsis CLAVATA1 leucine-rich repeat receptor-like kinase. *Development* 132, 1235–1245. doi: 10.1242/dev.01671

Bommert, P., and Whipple, C. (2018). Grass inflorescence architecture and meristem determinacy. *Semin. Cell Dev. Biol.* 79, 37–47. doi: 10.1016/j.semcdb.2017.10.004

Brutnell, T. P., Wang, L., Swartwood, K., Goldschmidt, A., Jackson, D., Zhu, X.-G., et al. (2010). *Setaria viridis*: a model for C4 photosynthesis. *Plant Cell* 22, 2537–2544. doi: 10.1105/tpc.110.075309

Cermák, T., Curtin, S. J., Gil-Humanes, J., Cegan, R., Kono, T. J. Y., Konecna, E., et al. (2017). A multipurpose toolkit to enable advanced genome engineering in plants. *Plant Cell* 29, 1196–1217. doi: 10.1105/tpc.16.00922

Chu, H., Liang, W., Li, J., Hong, F., Wu, Y., Wang, L., et al. (2013). A CLE-WOX signalling module regulates root meristem maintenance and vascular tissue development in rice. *J. Exp. Bot.* 64, 5359–5369. doi: 10.1093/jxb/ert301

Chu, H., Qian, Q., Liang, W., Yin, C., Tan, H., Yao, X., et al. (2006). The FLORAL ORGAN NUMBER4 gene encoding a putative ortholog of Arabidopsis CLAVATA3 regulates apical meristem size in rice. *Plant Physiol.* 142, 1039–1052. doi: 10.1104/pp.106.086736

Deveaux, Y., Toffano-Nioche, C., Claisse, G., Thareau, V., Morin, H., Laufs, P., et al. (2008). Genes of the most conserved WOX clade in plants affect root and flower development in Arabidopsis. *BMC Evol. Biol.* 8:291. doi: 10.1186/1471-2148-8-291

DeYoung, B. J., Bickle, K. L., Schrage, K. J., Muskett, P., Patel, K., and Clark, S. E. (2006). The CLAVATA1-related BAM1, BAM2 and BAM3 receptor kinase-like proteins are required for meristem function in Arabidopsis. *Plant J.* 45, 1–16. doi: 10.1111/j.1365-313X.2005.02592.x

Djordjevic, M. A., Oakes, M., Wong, C. E., Singh, M., Bhalla, P., Kusumawati, L., et al. (2011). Border sequences of *Medicago truncatula* CLE36 are specifically cleaved by endoproteases common to the extracellular fluids of Medicago and soybean. *J. Exp. Bot.* 62, 4649–4659. doi: 10.1093/jxb/err185

Dodueva, I. E., Yurlova, E. V., Ospina, M. A., and Lutova, L. A. (2011). CLE peptides are universal regulators of meristem development. *Russian J. Plant Phys.* 59, 14–27. doi: 10.1134/S1021443712010050

Doust, A. N., and Kellogg, E. A. (2002). Inflorescence diversification in the panicoid "bristle grass" clade (Paniceae, Poaceae): evidence from molecular phylogenies and developmental morphology. *Am. J. Bot.* 89, 1203–1222. doi: 10.3732/ajb.89.8.1203

Edwards, K., Johnstone, C., and Thompson, C. (1991). A simple and rapid method for the preparation of plant genomic DNA for PCR analysis. *Nucleic Acids Res.* 19, 1349. doi: 10.1093/nar/19.6.1349

Fukunaga, K., Ichitani, K., and Kawase, M. (2006). Phylogenetic analysis of the rDNA intergenic spacer subrepeats and its implication for the domestication history of foxtail millet, *Setaria italica*. *Theor. Appl. Genet.* 113, 261–269. doi: 10.1007/s00122-006-0291-5

Goad, D. M., Zhu, C., and Kellogg, E. A. (2017). Comprehensive identification and clustering of CLV3/ESR-related (CLE) genes in plants finds groups with potentially shared function. *New Phytol.* 2016, 605–616. doi: 10.1111/nph.14348

Gubert, C. M., and Liljegren, S. J. (2014). HAESA and HAESA-LIKE2 activate organ abscission downstream of NEVERSHED and EVERSHED in Arabidopsis flowers. *Plant Signal. Behav.* 9:e29115. doi: 10.4161/psb.29115

Hirakawa, Y., and Bowman, J. L. (2015). A role of TDIF peptide signaling in vascular cell differentiation is conserved among Euphyllophytes. *Front. Plant Sci.* 6:1048. doi: 10.3389/fpls.2015.01048

Hodge, J. G., and Kellogg, E. A. (2016). Abscission zone development in *Setaria viridis* and its domesticated relative, *Setaria italica*. *Am. J. Bot.* 103, 998–1005. doi: 10.3732/ajb.1500499

Hong, M. J., Kim, D. Y., Kang, S. Y., Kim, D. S., Kim, J. B., and Seo, Y. W. (2012). Wheat F-box protein recruits proteins and regulates their abundance during wheat spike development. *Mol. Biol. Rep.* 39, 9681–9696. doi: 10.1007/s11033-012-1833-3

Hu, C., Zhu, Y., Cui, Y., Cheng, K., Liang, W., Wei, Z., et al. (2018). A group of receptor kinases are essential for CLAVATA signalling to maintain stem cell homeostasis. *Nat. Plants* 4, 205–211. doi: 10.1038/s41477-018-0123-z

Hunt, H. V., van der Linden, M., Liu, X., Motuzaite-Matuzeviciute, G., Colledge, S., and Jones, M. K. (2008). Millets across Eurasia: chronology and context of early records of the genera Panicum and Setaria from archaeological sites in the Old World. *Veg. Hist. Archaeobot.* 17, S5–S18. doi: 10.1007/s00334-008-0187-1

Ikeda, K., Ito, M., Nagasawa, N., Kyozuka, J., and Nagato, Y. (2007). Rice ABERRANT PANICLE ORGANIZATION1, encoding an F-box protein, regulates meristem fate. *Plant J.* 51, 1030–1040. doi: 10.1111/j.1365-313X.2007.03200.x

Jackson, D., Veit, B., and Hake, S. (1994). Expression of the maize KNOTTED-1 related homeobox genes in the shoot apical meristem predicts patterns of morphogenesis in the vegetative shoot. *Development* 120, 405–413.

Je, B. I., Gruel, J., Lee, Y. K., Bommert, P., Arevalo, E. D., Eveland, A. L., et al. (2016). Signaling from maize organ primordia via FASCIATED EAR3 regulates stem cell proliferation and yield traits. *Nat. Genet.* 48, 785–791. doi: 10.1038/ng.3567

Je, B. I., Xu, F., Wu, Q., Liu, L., Meeley, R., Gallagher, J. P., et al. (2018). The CLAVATA receptor FASCIATED EAR2 responds to distinct CLE peptides by signaling through two downstream effectors. *Elife* 7:e35673. doi: 10.7554/eLife.35673.031

Jinn, T. L., Stone, J. M., and Walker, J. C. (2000). HAESA, an Arabidopsis leucine-rich repeat receptor kinase, controls floral organ abscission. *Genes Dev.* 14, 108–117. doi: 10.1101/gad.14.1.108

Kinoshita, A., Betsuyaku, S., Osakabe, Y., Mizuno, S., Nagawa, S., Stahl, Y., et al. (2010). RPK2 is an essential receptor-like kinase that transmits the CLV3 signal in Arabidopsis. *Development* 137, 3911–3920. doi: 10.1242/dev.048199

Kitagawa, M., and Jackson, D. (2019). Control of meristem size. *Annu. Rev. Plant Biol.* 70, 269–291. doi: 10.1146/annurev-arplant-042817-040549

Le Thierry d'Ennequin, M., Panaud, O., Toupance, B., and Sarr, A. (2000). Assessment of genetic relationships between Setaria italica and its wild relative *S. viridis* using AFLP markers. *Theor. Appl. Genet.* 100, 1061–1066. doi: 10.1007/s001220051387

Leiboff, S., Li, X., Hu, H. C., Todt, N., Yang, J., Li, X., et al. (2015). Genetic control of morphometric diversity in the maize shoot aplical meristem. *Nat. Commun.* 6:8974. doi: 10.1038/ncomms9974

Li, M., Tang, D., Wang, K., Wu, X., Lu, L., Yu, H., et al. (2011). Mutations in the F-box gene LARGER PANICLE improve the panicle architecture and enhance the grain yield in rice. *Plant Biotechnol. J.* 9, 1002–1013. doi: 10.1111/j.1467-7652.2011.00610.x

Li, Z., Wang, Y., Huang, J., Ahsan, N., Biener, G., Paprocki, J., et al. (2017). Two SERK receptor-like kinases interact with EMS1 to control anther cell fate determination. *Plant Physiol.* 173, 326–337. doi: 10.1104/pp.16.01219

Lian, G., Ding, Z., Wang, Q., Zhang, D., and Xu, J. (2014). Origins and evolution of WUSCHEL-related homeobox protein family in plant kingdom. *Sci. World J.* 2014, 534140. doi: 10.1155/2014/534140

Lippman, Z. B., Cohen, O., Alvarez, J. P., Abu-Abied, M., Pekker, I., Paran, I., et al. (2008). The making of a compound inflorescence in tomato and related nightshades. *PLoS Biol.* 6:e288. doi: 10.1371/journal.pbio.0060288

Liu, H., Ding, Y., Zhou, Y., Jin, W., Xie, K., and Chen, L. L. (2017). CRISPR-P 2.0: an improved CRISPR-Cas9 tool for genome editing in plants. *Mol. Plant* 10, 530–532. doi: 10.1016/j.molp.2017.01.003

Liu, P. L., Du, L., Huang, Y., Gao, S. M., and Yu, M. (2017). Origin and diversification of leucine-rich repeat receptor-like protein kinase (LRR-RLK) genes in plants. *BMC Evol. Biol.* 17:47. doi: 10.1186/s12862-017-0891-5

Lyons, E., and Freeling, M. (2008). How to usefully compare homologous plant genes and chromosomes as DNA sequences. *Plant J.* 53, 661–673. doi: 10.1111/j.1365-313X.2007.03326.x

Lyons, E., Pedersen, B., Kane, J., Alam, M., Ming, R., Tang, H., et al. (2008). Finding and comparing syntenic regions among Arabidopsis and the outgroups papaya, poplar, and grape: CoGe with rosids. *Plant Physiol.* 148, 1772–1781. doi: 10.1104/pp.108.124867

Mamidi, S., Healey, A., Huang, P., Grimwood, J., Jenkins, J., Barry, K., et al. (2020). A genome resource for green millet Setaria viridis enables discovery of agronomically valuable loci. *Nat. Biotechnol.* 38, 1203–1210. doi: 10.1038/s41587-020-0681-2

Mandel, T., Moreau, F., Kutsher, Y., Fletcher, J. C., Carles, C. C., and Eshed Williams, L. (2014). The ERECTA receptor kinase regulates Arabidopsis shoot apical meristem size, phyllotaxy and floral meristem identity. *Development* 141, 830–841. doi: 10.1242/dev.104687

Matsumoto, N., and Okada, K. (2001). A homeobox gene, PRESSED FLOWER, regulates lateral axis-dependent development of Arabidopsis flowers. *Genes Dev.* 15, 3355–3364. doi: 10.1101/gad.931001

Miyawaki, K., Tabata, R., and Sawa, S. (2013). Evolutionarily conserved CLE peptide signaling in plant development, symbiosis, and parasitism. *Curr. Opin. Plant Biol.* 16, 598–606. doi: 10.1016/j.pbi.2013.08.008

Muller, R., Bleckmann, A., and Simon, R. (2008). The receptor kinase CORYNE of Arabidopsis transmits the stem cell-limiting signal CLAVATA3 independently of CLAVATA1. *Plant Cell* 20, 934–946. doi: 10.1105/tpc.107.057547

Nardmann, J., Ji, J., Werr, W., and Scanlon, M. J. (2004). The maize duplicate genes narrow sheath1 and narrow sheath2 encode a conserved homeobox gene function in a lateral domain of shoot apical meristems. *Development* 131, 2827–2839. doi: 10.1242/dev.01164

Ni, J., Guo, Y., Jin, H., Hartsell, J., and Clark, S. E. (2011). Characterization of a CLE processing activity. *Plant Mol. Biol.* 75, 67–75. doi: 10.1007/s11103-010-9708-2

Nimchuk, Z. L., Zhou, Y., Tarr, P. T., Peterson, B. A., and Meyerowitz, E. M. (2015). Plant stem cell maintenance by transcriptional cross-regulation of related receptor kinases. *Development* 142, 1043–1049. doi: 10.1242/dev.119677

Ohmori, Y., Tanaka, W., Kojima, M., Sakakibara, H., and Hirano, H. Y. (2013). WUSCHEL-RELATED HOMEOBOX4 is involved in meristem maintenance and is negatively regulated by the CLE gene FCP1 in rice. *Plant Cell* 25, 229–241. doi: 10.1105/tpc.112.103432

Ohmori, Y., Yasui, Y., and Hirano, H. Y. (2014). Overexpression analysis suggests that FON2-LIKE CLE PROTEIN1 is involved in rice leaf development. *Genes Genet. Syst.* 89, 87–91. doi: 10.1266/ggs.89.87

Ohyama, K., Shinohara, H., Ogawa-Ohnishi, M., and Matsubayashi, Y. (2009). A glycopeptide regulating stem cell fate in *Arabidopsis thaliana*. *Nat. Chem. Biol.* 5, 578–580. doi: 10.1038/nchembio.182

Pautler, M., Eveland, A. L., LaRue, T., Yang, F., Weeks, R., Lunde, C., et al. (2015). FASCIATED EAR4 encodes a bZIP transcription factor that regulates shoot meristem size in maize. *Plant Cell* 27, 104–120. doi: 10.1105/tpc.114.132506

Rodríguez-Leal, D., Xu, C., Kwon, C. T., Soyars, C., Demesa-Arevalo, E., Man, J., et al. (2019). Evolution of buffering in a genetic circuit controlling plant stem cell proliferation. *Nat. Genet.* 51, 786–792. doi: 10.1038/s41588-019-0389-8

Satoh-Nagasawa, N., Nagasawa, N., Malcomber, S., Sakai, H., and Jackson, D. (2006). A trehalose metabolic enzyme controls inflorescence architecture in maize. *Nature* 441, 227–230. doi: 10.1038/nature04725

Schneeberger, R. G., Becraft, P. W., Hake, S., and Freeling, M. (1995). Ectopic expression of the Knox homeobox gene rough sheath1 alters cell fate in the maize leaf. *Genes Dev.* 9, 2292–2304. doi: 10.1101/gad.9.18.2292

Sharma, B., Joshi, D., Yadav, P. K., Gupta, A. K., and Bhatt, T. K. (2016). Role of ubiquitin-mediated degradation system in plant biology. *Front. Plant Sci.* 7:806. doi: 10.3389/fpls.2016.00806

Smakowska-Luzan, E., Mott, G. A., Parys, K., Stegmann, M., Howton, T. C., Layeghifard, M., et al. (2018). An extracellular network of Arabidopsis leucine-rich repeat receptor kinases. *Nature* 553, 342–346. doi: 10.1038/nature25184

Somssich, M., Je, B. I., Simon, R., and Jackson, D. (2016). CLAVATA-WUSCHEL signaling in the shoot meristem. *Development* 143, 3238–3248. doi: 10.1242/dev.133645

Sonoda, Y., Yao, S. G., Sako, K., Sato, T., Kato, W., Ohto, M. A., et al. (2007). SHA1, a novel RING finger protein, functions in shoot apical meristem maintenance in Arabidopsis. *Plant J.* 50, 586–596. doi: 10.1111/j.1365-313X.2007.03062.x

Suzaki, T., Ohneda, M., Toriba, T., Yoshida, A., and Hirano, H. Y. (2009). FON2 SPARE1 redundantly regulates floral meristem maintenance with FLORAL ORGAN NUMBER2 in rice. *PLoS Genet.* 5:e1000693. doi: 10.1371/journal.pgen.1000693

Suzaki, T., Toriba, T., Fujimoto, M., Tsutsumi, N., Kitano, H., and Hirano, H. Y. (2006). Conservation and diversification of meristem maintenance mechanism in *Oryza sativa*: function of the FLORAL ORGAN NUMBER2 gene. *Plant Cell Physiol.* 47, 1591–1602. doi: 10.1093/pcp/pcl025

Suzaki, T., Yoshida, A., and Hirano, H. Y. (2008). Functional diversification of CLAVATA3-related CLE proteins in meristem maintenance in rice. *Plant Cell* 20, 2049–2058. doi: 10.1105/tpc.107.057257

Tang, H., Lyons, E., Pedersen, B., Schnable, J. C., Paterson, A. H., and Freeling, M. (2011). Screening synteny blocks in pairwise genome comparisons through integer programming. *BMC Bioinform.* 12:102. doi: 10.1186/1471-2105-12-102

Thielen, P. M., Pendleton, A. L., Player, R. A., Bowden, K. V., Lawton, T. J., and Wisecaver, J. H. (2020). Reference genome for the highly transformable Setaria viridis ME034V. *G3 (Bethesda)* 10, 3467–3478. doi: 10.1534/g3.120.401345

Trung, K. H., Tran, Q. H., Bui, N. H., Tran, T. T., Luu, K. Q., Tran, N. T. T., et al. (2020). A weak allele of FASCIATED EAR2 (FEA2) increases maize kernel row number (KRN) and yield in elite maize hybrids. *Agronomy* 10:1774. doi: 10.3390/agronomy10111774

van der Graaff, E., Laux, T., and Rensing, S. A. (2009). The WUS homeobox-containing (WOX) protein family. *Genome Biol.* 10:248. doi: 10.1186/gb-2009-10-12-248

Wang, H. Y., Yu, Y., Sun, Y. D., Han, L. B., Wu, X. M., Wu, J. H., et al. (2015). The RING finger protein NtRCP1 is involved in the floral transition in tobacco (*Nicotiana tabacum*). *J. Genet. Genomics* 42, 311–317. doi: 10.1016/j.jgg.2015.03.010

Wu, X., Chory, J., and Weigel, D. (2007). Combinations of WOX activities regulate tissue proliferation during Arabidopsis embryonic development. *Dev. Biol.* 309, 306–316. doi: 10.1016/j.ydbio.2007.07.019

Wu, X., Dabi, T., and Weigel, D. (2005). Requirement of homeobox gene STIMPY/WOX9 for Arabidopsis meristem growth and maintenance. *Curr. Biol.* 15, 436–440. doi: 10.1016/j.cub.2004.12.079

Xu, C., Liberatore, K. L., MacAlister, C. A., Huang, Z., Chu, Y. H., Jiang, K., et al. (2015). A cascade of arabinosyltransferases controls shoot meristem size in tomato. *Nat. Genet.* 47, 784–792. doi: 10.1038/ng.3309

Xu, F., and Jackson, D. (2018). Learning from CIK plants. *Nat. Plants* 4, 195–196. doi: 10.1038/s41477-018-0125-x

Yaginuma, H., Hirakawa, Y., Kondo, Y., Ohashi-Ito, K., and Fukuda, H. (2011). A novel function of TDIF-related peptides: promotion of axillary bud formation. *Plant Cell Physiol.* 52, 1354–1364. doi: 10.1093/pcp/pcr081

Yang, J., Thames, S., Best, N. B., Jiang, H., Huang, P., Dilkes, B. P., et al. (2018). Brassinosteroids modulate meristem fate and differentiation of unique inflorescence morphology in *Setaria viridis*. *Plant Cell* 30, 48–66. doi: 10.1105/tpc.17.00816

Zhao, D. Z., Wang, G. F., Speal, B., and Ma, H. (2002). The excess microsporocytes1 gene encodes a putative leucine-rich repeat receptor protein kinase that controls somatic and reproductive cell fates in the *Arabidopsis anther*. *Genes Dev.* 16, 2021–2031. doi: 10.1101/gad.997902

Zheng, H., and Kawabata, S. (2017). Identification and validation of new alleles of FALSIFLORA and COMPOUND INFLORESCENCE genes controlling the number of branches in tomato inflorescence. *Int. J. Mol. Sci.* 18:1572. doi: 10.3390/ijms18071572

Zhu, C., Yang, J., Box, M. S., Kellogg, E. A., and Eveland, A. L. (2018). A dynamic co-expression map of early inflorescence development in *Setaria viridis* provides a resource for gene discovery and comparative genomics. *Front. Plant Sci.* 9:1309. doi: 10.3389/fpls.2018.01309

Zhu, C., Yang, J., and Shyu, C. (2017). Setaria comes of age: meeting report on the Second International Setaria Genetics Conference. *Front. Plant. Sci.* 8:1562. doi: 10.3389/fpls.2017.01562

Conflict of Interest: The authors declare that the research was conducted in the absence of any commercial or financial relationships that could be construed as a potential conflict of interest.

frontiers in Plant Science

REVIEW
published: 25 February 2021
doi: 10.3389/fpls.2021.641351

Coding of Non-coding RNA: Insights Into the Regulatory Functions of Pri-MicroRNA-Encoded Peptides in Plants

Yi Ren[1], Yue Song[1], Lipeng Zhang[2], Dinghan Guo[2], Juan He[1], Lei Wang[1], Shiren Song[1], Wenping Xu[1], Caixi Zhang[1], Amnon Lers[3], Chao Ma[1] and Shiping Wang[1,4]*

[1] Department of Plant Science, School of Agriculture and Biology, Shanghai Jiao Tong University, Shanghai, China, [2] Department of Horticulture, College of Agriculture, Shihezi University, Shihezi, China, [3] Department of Postharvest Science of Fresh Produce, Volcani Center, Agricultural Research Organization, Bet Dagan, Israel, [4] Key Laboratory of Agro-products Processing Technology of Shandong, Institute of Agro-food Science and Technology, Shandong Academy of Agricultural Sciences, Jinan, China

Peptides composed of a short chain of amino acids can play significant roles in plant growth, development, and stress responses. Most of these functional peptides are derived by either processing precursor proteins or direct translation of small open reading frames present in the genome and sometimes located in the untranslated region sequence of a messenger RNA. Generally, canonical peptides serve as local signal molecules mediating short- or long-distance intercellular communication. Also, they are commonly used as ligands perceived by an associated receptor, triggering cellular signaling transduction. In recent years, increasing pieces of evidence from studies in both plants and animals have revealed that peptides are also encoded by RNAs currently defined as non-coding RNAs (ncRNAs), including long ncRNAs, circular RNAs, and primary microRNAs. Primary microRNAs (miRNAs) have been reported to encode regulatory peptides in *Arabidopsis*, grapevine, soybean, and *Medicago*, called miRNA-encoded peptides (miPEPs). Remarkably, overexpression or exogenous applications of miPEPs specifically increase the expression level of their corresponding miRNAs by enhancing the transcription of the *MIRNA* (*MIR*) genes. Here, we first outline the current knowledge regarding the coding of putative ncRNAs. Notably, we review in detail the limited studies available regarding the translation of miPEPs and their relevant regulatory mechanisms. Furthermore, we discuss the potential cellular and molecular mechanisms in which miPEPs might be involved in plants and raise problems that needed to be solved.

Keywords: miPEP, miRNA-encoded peptide, miRNA, pri-miRNA, non-coding RNA, peptides

OPEN ACCESS

Edited by:
Cao Xu,
Chinese Academy of Sciences, China

Reviewed by:
Hongliang Zhu,
China Agricultural University, China
Xu Fang,
Shandong University, China

****Correspondence:***
Chao Ma
chaoma2015@sjtu.edu.cn

Specialty section:
This article was submitted to Plant Physiology, a section of the journal Frontiers in Plant Science

Received: *14 December 2020*
Accepted: *25 January 2021*
Published: *25 February 2021*

Citation:
Ren Y, Song Y, Zhang L, Guo D, He J, Wang L, Song S, Xu W, Zhang C, Lers A, Ma C and Wang S (2021) Coding of Non-coding RNA: Insights Into the Regulatory Functions of Pri-MicroRNA-Encoded Peptides in Plants. Front. Plant Sci. 12:641351. doi: 10.3389/fpls.2021.641351

INTRODUCTION

For a long time, canonical phytohormones, such as auxin and cytokinin, offer the main perspective in our understanding of regulatory networks modulating plant growth, development, and stress response (Dubois et al., 2018; Kieber and Schaller, 2018). In the last decades, an increasing number of studies have focused on the central role of small peptides, called peptide-hormones, as short- or long-distance signaling molecules to integrate internal cues with external

environment stimuli (Huffaker et al., 2011; Ohkubo et al., 2017; Nakaminami et al., 2018; Olsson et al., 2019). Peptides are typically composed of 2 to 100 amino acid residues (Tavormina et al., 2015) and are commonly secreted into the apoplast. Known peptides usually act as ligands that bind to their receptors to activate downstream signaling cascades involved in plant innate immunity (Huffaker et al., 2006; Yamaguchi et al., 2006; Huffaker and Ryan, 2007), nutrient homeostasis (Okamoto et al., 2016), reproduction process (Kachroo et al., 2001; Okuda et al., 2009; Qu et al., 2015), stress response (Nakaminami et al., 2018; Takahashi et al., 2018), and morphogenesis (Yamaguchi et al., 2016; Qian et al., 2018). Although the majority of the reported functional peptides are derived from the processing of precursor proteins or the coding of small open reading frames (sORFs), numerous pieces of evidence from plants and animals have suggested that previously annotated non-coding RNAs (ncRNAs) may encode peptides, expanding the peptidome complexity (Ruiz-Orera et al., 2014; Lauressergues et al., 2015; Legnini et al., 2017). Primary microRNAs (pri-miRNAs), which are transcribed from the *MIR* genes and subsequently processed to produce the mature miRNAs, can actually encode regulatory miRNA-encoded peptides (miPEPs) in plants (Wang L. and Wang, 2015; Lv et al., 2016; Julkowska, 2020). According to available results, overexpression or external application of miPEPs can positively regulate the mature miRNAs by enhancing the transcription of their associated *MIR* genes, which is similar to the innate immunity system in plants where the endogenous peptides can also increase expression of their encoding precursor genes (Huffaker and Ryan, 2007; Huffaker et al., 2011; Couzigou et al., 2016). In this review, we review the coding of ncRNA, emphatically, focusing on the translation of pri-miRNA and their relevant biological functions and possible regulatory mechanisms.

PEPTIDOME COMPLEXITY IN PLANTS

Since systemin was first characterized in tomato, plant peptides are emerging as significant signaling molecules involved in different physiological processes (Pearce et al., 1991). They are categorized into precursor-derived peptides and non-precursor-derived peptides based on their biogenesis (**Figure 1**). The precursor-derived peptides are further classified into post-translationally modified peptides, cysteine-rich peptides (CRPs), and peptides without rich cysteine or post-translational modification (**Figure 1A**). The non-precursor-derived peptides are mainly encoded by sORFs hidden in the plant genome, additional short ORFs in messenger RNA (mRNA) transcripts, and so-called ncRNAs (**Figures 1B,C**; Hanada et al., 2013; Tavormina et al., 2015; Oh et al., 2018).

Peptides Encoded by Conventional Open Reading Frames

The origins, functions, and functional mechanisms of peptides encoded by conventional ORFs in plants have been well-reviewed (Tavormina et al., 2015; Olsson et al., 2019). Generally, mature precursor-derived peptides are initially translated into larger non-functional prepropeptides and further processed by proteolytic cleavage and modification such as tyrosine (Tyr) sulfation, proline hydroxylation, and hydroxyproline arabinosylation, to yield biologically active peptides (**Figure 1A**; Matsubayashi, 2014; Olsson et al., 2019). The second precursor-derived peptides are the CRPs characterized by a domain with 2–16 cysteine residues (Matsubayashi, 2014). CRPs are also processed, and the typical intramolecular disulfide bonds are catalyzed by protein disulfide isomerases (**Figure 1A**; Tavormina et al., 2015; Olsson et al., 2019). The third group of peptides processed from the non-functional precursors is named "non-Cys-rich/non-modification peptides," which contain several important amino acid residues such as proline, Gly, and lysine critical for biological activity (**Figure 1A**; Tavormina et al., 2015). Additionally, most gene annotation algorithms do not effectively distinguish between coding and non-coding sequences when the coding sequences are small. Therefore, thousands of sORFs are failed to be annotated in the plant genome as coding for proteins (Andrews and Rothnagel, 2014; Takahashi et al., 2019). In *Arabidopsis*, ∼8,000 putative sORFs with high coding potential are identified, of which ∼10% of identified peptides have a function based on the visible phenotypic effects revealed after their overexpression (Hanada et al., 2013). Therefore, it is a reasonable assumption that many functional sORFs are hidden in the plant genome (Hsu and Benfey, 2018; **Figure 1B**). In general, canonical peptides are thought to be phytohormone-like signaling molecules that mediate short- or long-distance intercellular communication and play an important role in regulating growth and development in plants (Ohkubo et al., 2017; Olsson et al., 2019).

Coding of Short Open Reading Frames in Putative Non-coding RNAs

In eukaryotic mRNA, one or more short ORFs may exist in 5× leader sequence [or 5′ untranslated region (UTR)] located in the upstream of the main protein-coding ORF, called upstream open reading frame (uORF) (Chen J. et al., 2020; Kurihara, 2020; **Figure 1C**). The uORF presumably serves as a post-transcriptional *cis*-regulatory element that represses the transcription of main protein-coding ORF by causing ribosome stalling and nonsense-mediated decay (von Arnim et al., 2014). In one case, vitamin C/ascorbate content is determined by the GDP-L-galactose phosphorylase (GGP) enzyme. An uORF located in the upstream UTR of the *GGP* gene, encoding 60-a.a. length peptide, serves as a *cis*-acting element that represses the translation of the downstream *GGP* ORF under high ascorbate concentration (Laing et al., 2015). Editing the uORF of *GGP* increases the vitamin C content by ∼150% (Zhang et al., 2018). In *Arabidopsis*, AtHB1 belongs to the homeodomain-leucine zipper transcription factor family. The translation of *AtHB1* is post-transcriptionally repressed by the uORF located in the upstream of 5' UTR of *AtHB1* through a ribosome stalling mechanism. This uORF encodes a conserved peptide in flowering plants, called CPuORF (Ribone et al., 2017; van der Horst et al., 2019). In addition to uORF in 5' UTR,

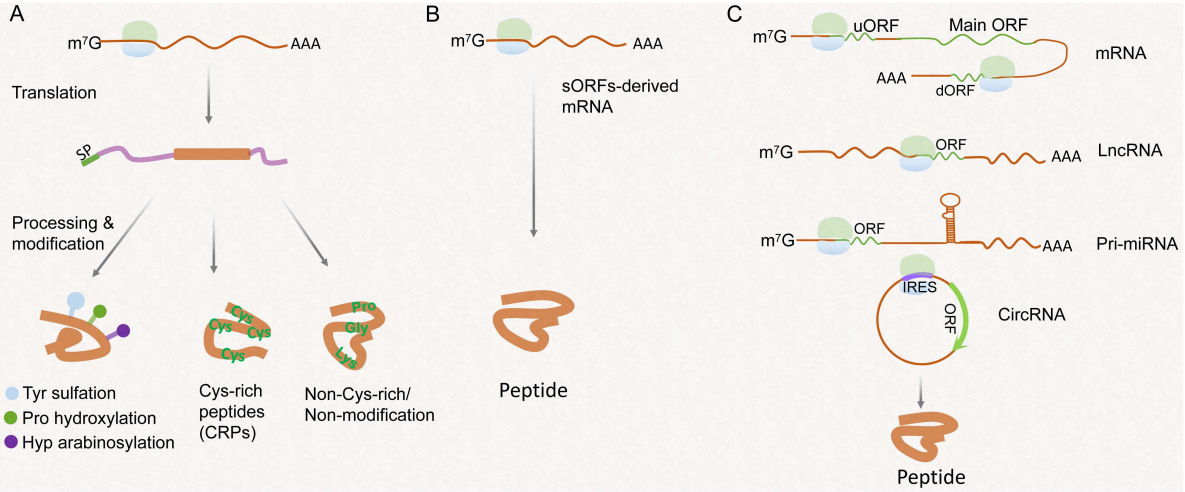

FIGURE 1 | Schematic presentation of the different pathways of peptide synthesis and processing. **(A)** Peptides processed from the precursor containing signaling peptide (SP). Modifications of peptides contain Tyr sulfation, proline hydroxylation, and hydroxyproline arabinosylation. Cys-rich peptides usually contain 2–16 Cys residues. Non-Cys-rich/non-modificational peptides contain several key residues such as proline, Gly, and lysine responsible for biological activity. **(B)** Peptides encoded by sORFs in genome. **(C)** Peptides encoded by an upstream ORF (uORF) or downstream ORF (dORF) of a protein-coding region, non-coding RNAs, including lncRNAs, pri-miRNAs, and circRNAs.

hundreds of sORFs have been identified in 3' UTR, called downstream UTRs (dUTRs), by ribosome profiling sequencing and proteomics analyses in mammalian cell (Chen J. et al., 2020; Wu et al., 2020). Contrary to uORFs, dUTRs were described to enhance the translation of their corresponding main ORF (Wu et al., 2020). Whether translation of dUTRs occurs in plants remains to be shown. Although the translation of sORFs derived from the 5' or 3' UTR of mRNA has been investigated, the biological functions of such peptides are not fully understood yet.

Ribosome profiling sequencing provides a feasible method to explore the coding potential of putative ncRNAs such as long non-coding RNAs (lncRNAs), circular RNAs (circRNAs), and pri-miRNA, although this cue is not sufficient to classify transcripts as coding or non-coding (Ingolia et al., 2012; Guttman et al., 2013). Recently, ncEP, a manually curated database for collecting validated ncRNA-encoded proteins or peptides, is constructed and enriches the repository of coding RNAs (Liu et al., 2020). LncRNAs are usually defined as transcripts that are longer than 200 nt in length and do not encode a discernable protein (Chekanova, 2015). Like the mRNA, lncRNAs are transcribed by Pol II, capped in their 5' termini and poly-adenylated in their 3' termini, and are accumulated in the cytoplasm (van Heesch et al., 2014). Ribosome profiling analyses of six species, including *Arabidopsis*, revealed that a large fraction of the lncRNAs are associated with ribosome protection (Ruiz-Orera et al., 2014). However, most of the known peptides translated from lncRNA were mostly investigated in an animal cell such as HOXB-AS3, a conserved 53-a.a. peptide encoded by lncRNA *HOXB-AS3* that could suppress colon cancer growth (Huang et al., 2017). In *Arabidopsis*, the *POLARIS* (*PLS*) gene encoding a predicted peptide of 36-a.a. residues induced by auxin was located at a 500-nt position of this transcript. PLS is required to regulate auxin–cytokinin homeostasis for modulating root growth and leaf vascular patterning (Casson et al., 2002). In legumes, ENOD40 is expressed in root nodule organogenesis. Unlike canonical mRNA, *ENOD40* is polycistronic RNA that encodes two ORFs and generates two small peptides with 12- and 24-a.a residues responsible for binding to sucrose synthase (Röhrig et al., 2002). These examples suggest that the presence of ORFs encoding for peptides in known lncORFs exists in plants; however, conclusive pieces of evidence require further investigation.

Circular RNAs (circRNAs) are produced by precursor mRNAs back-splicing where a downstream 5' splice site is covalently linked to an upstream 3' splice site in eukaryote (Conn et al., 2017; Li et al., 2018). In grapevine, approximately 91% of circulation events of circRNAs are exon-circulation (Gao et al., 2019), implying that circRNAs may function as a template to direct protein synthesis. In fact, the translation of some circRNAs has been discovered in animals, and the encoded peptides were found to control cell proliferation and play biological roles in disease response (Legnini et al., 2017; Shi et al., 2020). The absence of m^7GpppN caps at the 5' end in circRNAs and lack of poly (A) tails at the 3' end cause cap-independent translation initiation in circRNAs (Diallo et al., 2019). Furthermore, if the circRNAs contain internal ribosome entry sites, the eukaryotic initiation factor (elF4G2) directly binds to the internal ribosome entry site and recruitments 43S pre-initiation complex to initiate translation (Wang Y. and Wang, 2015; Diallo et al., 2019; Shi et al., 2020). In humans, the N^6-methyladenosine (m^6A) of circRNAs drives the efficient initiation of protein translation, and even an m^6A motif, "RRm^6ACH" (R = G or A; H = A, C or U), is characterized (Yang et al., 2017). The coding of circRNAs has not been elucidated in plants, which potentially sheds light on another landscape.

REGULATORY FUNCTIONS OF PRIMARY MICRORNA-DERIVED PEPTIDES

Although there are modest pieces of evidence that endogenous peptides can be encoded by ncRNAs in plants, only the regulatory functions of pri-miRNA-derived peptides are well deciphered in available examples. MiRNAs are ∼22-nt regulatory elements that inhibit the expression of endogenous genes at both the transcriptional and post-transcriptional levels (Voinnet, 2009). The biogenesis of miRNAs is initialized by the Pol II-dependent transcription of intergenic *MIR* genes. Mature miRNAs are processed from the much larger pri-miRNA by the Dicer-like RNase III endonucleases (DCLs) complex and assembled into active RNA-induced silencing complex (RISC) through incorporating into ARGONAUTE1 (AGO1) protein (Rogers and Chen, 2013; Yu et al., 2017). The guide strand (miRNA) guides the RISC to bind the target gene *via* base pairing and mediates gene silencing by target cleavage or translation inhibition (**Figure 2**; Wang et al., 2019). In addition to producing miRNAs, it was found that the pri-miRNAs can contain short ORFs in the 5' upstream of pre-miRNA, which encode for regulatory peptides, called miPEPs. This coding ability of pri-miRNAs has first been discovered in *Arabidopsis* and *Medicago truncatula* and has since been studied in soybeans, grapes, and even mammalian cells (Lauressergues et al., 2015; Couzigou et al., 2016; Fang et al., 2017; Chen Q. J. et al., 2020; Sharma et al., 2020). The endogenous miPEPs have been detected by Western blotting, demonstrating significant levels of peptide accumulation (Lauressergues et al., 2015; Sharma et al., 2020; **Table 1**).

The mature miRNA processing mainly finishes in the nucleus and export to the cytoplasm (Wang et al., 2019). Firstly, the pri-miRNAs could be cut by the DCL complex into three parts in the nucleus: (1) the upstream of a precursor of miRNAs (pre-miRNAs), (2) the pre-miRNAs, and (3) the 3' fragments containing poly (A) tail. The pre-miRNAs are further processed into mature miRNA, and the 3' fragments are possibly degraded (Rogers and Chen, 2013). It is also reasonably speculated that the upstream of pre-miRNAs, which possibly contain sORF, is exported to the cytoplasm for guiding peptide translation (**Figure 2**). For example, the pri-miR171d is mainly accumulated in the nucleus and also slightly detected in the cytoplasm of grape, implying that the coding region of pri-miRNA is possibly transported into the cytoplasm after they are cleaved (Lauressergues et al., 2015; Chen Q. J. et al., 2020). The possibility that the cleaved upstream fragments of the pre-miRNAs are

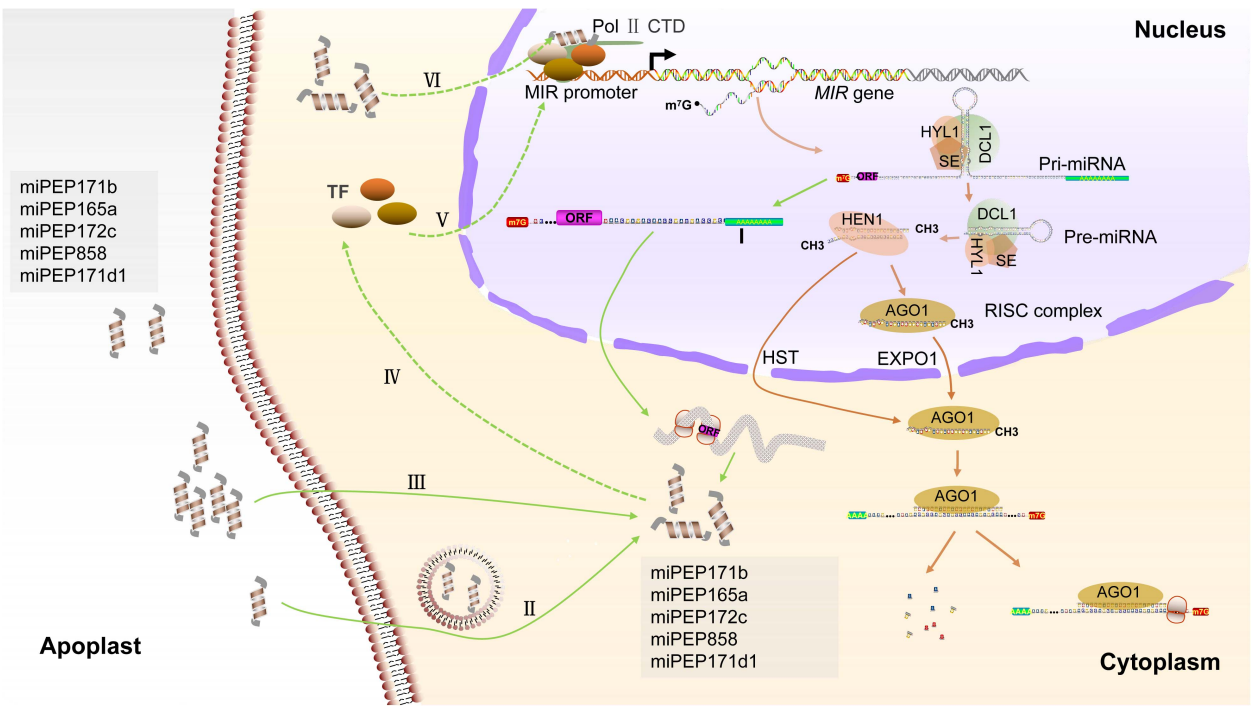

FIGURE 2 | Biogenesis of miRNA and putative regulatory mechanisms of miPEPs in plants. Pri-miRNAs are transcribed by the RNA Pol II from intergenic *MIR* genes and processed by DCL complex, which is generally composed of dicer-like1 (DCL1), hyponasticleaves1 (HYL1), and serrate (SE). On the one hand, these miRNA/miRNA* duplexes that are methylated by the methyltransferase HUA enhancer1 (HEN1) and assembled into RISC in the nucleus or exported by the HST to cytoplasm for RISC assembling. RISC located in the nucleus can be exported by exportin 1 (EXPO1) to the cytoplasm (Wang et al., 2019). On the other hand, the upstream of pre-miRNA containing short ORF is possibly polyadenylated for preventing degradation (I) and is exported to cytoplasm for guiding miPEPs synthesis. External miPEPs are supposed to internalize into cytoplasm by endocytosis-associated processes (II) and passive diffusion (III) (Ormancey et al., 2020; Sharma et al., 2020). MiPEPs maybe function to transcription factors (TFs), which regulate the transcription of *MIR* genes (IV and V), resulting in upregulated expression of associated miRNA. Alternatively, miPEPs maybe serve as a part of "Pol II transcriptional complex" and enhance the transcription of *MIR* genes (VI).

TABLE 1 | Length and biological function of known miPEPs in plant[a].

MiPEP name	MiPEP length (a.a.)	Species	Biological function	References
miPEP171b	20	*Medicago truncatula*	Regulation of root development	Lauressergues et al., 2015
miPEP169d	NA	*Medicago truncatula*	NA	Lauressergues et al., 2015
miPEP171e	NA	*Medicago truncatula*	NA	Lauressergues et al., 2015
MiPEP165a	18	*Arabidopsis thaliana*	Regulation of root development, inflorescence stem, and flowering time	Lauressergues et al., 2015; Ormancey et al., 2020
miPEP160b	24	*Arabidopsis thaliana*	NA	Lauressergues et al., 2015
miPEP164a	37	*Arabidopsis thaliana*	NA	Lauressergues et al., 2015
miPEP319a	50	*Arabidopsis thaliana*	NA	Lauressergues et al., 2015
miPEP858a	44	*Arabidopsis thaliana*	Controlling of flavonoid biosynthesis and development	Sharma et al., 2020
miPEP171c	10	*Arabidopsis thaliana*	Regulation of primary roots	Lauressergues et al., 2015; Chen Q. J. et al., 2020
miPEP171d1	7	*Vitis vinifera*	Regulation of adventitious root formation	Chen Q. J. et al., 2020
miPEP172c	16	*Glycine max*	Stimulating nodulation	Couzigou et al., 2016

[a]*Numerous putative miPEPs identified in A. thaliana are presented in a previous report (Lauressergues et al., 2015).*

protected by re-polyadenylation is still unknown and requires investigation (**Figure 2**). What's more, coupling transcription and translation in nuclear are presumed to be an alternative hypothesis (Prasad et al., 2020). The current researches suggest that plant miPEPs may serve as an endogenous peptide to positively amplify the autoregulatory feedback loop of miRNA generation (Ormancey et al., 2020). They are supposed to specifically activate transcription of their corresponding pri-miRNAs and subsequently to upregulate the expression of mature miRNAs and, meanwhile, to enhance the accumulation of their own levels. The positive regulatory function of miPEPs on *MIR* transcription in the plant has been investigated. In *Arabidopsis*, the positive effect of miPEP165a on pri-miR165a accumulation is inhibited by the cordycepin, which is an inhibitor of RNA synthesis (Lauressergues et al., 2015). In *Arabidopsis*, the promotor of miR858a normally activates the expression of the *GUS* gene in two reporter lines (PromiR858a:ATG^1:GUS and PromiR858a:ORF^1:GUS), which is fused only the start code or entire ORF encoded miPEP858a. Furthermore, the GUS activity is enhanced by the supplement with synthetic miPEP858a in the media, indicating that the miPEP858a acts on the promotor region for enhancing transcription (Sharma et al., 2020). On the one hand, miPEPs possibly, directly or indirectly, function as a *trans*-acting factor such as a transcription factor (TF), which positively regulates the transcription of *MIR* genes (**Figure 2**). Conventional peptides can regulate TF expression levels in the plant. Root meristem growth factor 1 is a secreted and Tyr sulfated peptide and required to maintain the root stem cell niche and transit amplifying cell proliferation in *Arabidopsis*. Root meristem growth factor 1 positively regulates the expression levels of PLT, which is a root-specific TF mediating pattern of the root stem cell niche (Matsuzaki et al., 2010). On the other hand, miPEPs may bind one of the subunits of "Pol II transcriptional complexes" or bind to the Pol II, although there are no direct pieces of evidence to support this hypothesis (**Figure 2**). In plants, peptides can also interact with the subunit of catalyzing enzyme. A representative example is ENOD40 peptides in legumes. Two overlapped ORFs located in 5′ conserved region encode two peptides of 12- and 24-a.a. length residues (peptides A and B); both peptides can specifically bind to nodulin 100 that is a subunit of sucrose synthase (Röhrig et al., 2002). In a word, the strictly regulatory mechanisms of miPEPs remain elusive.

Interestingly, the external application of synthetic miPEPs, which probably do not need additional modification and processing, to plants can produce the same autoregulatory effect. Unlike precursor-derived peptides that usually act as ligand recognized by associated receptors, miPEPs are hypothesized to be internalized by passive diffusion and endocytosis-associated processes (Kachroo et al., 2001; Okuda et al., 2009; Yamaguchi et al., 2010; Oh et al., 2018; Ormancey et al., 2020). In *Arabidopsis*, fluorescently labeled miPEP165a rapidly penetrates into the whole root during 24 h. Loss of function of genes associated with endocytosis or application of endocytosis inhibitor influences the uptake of miPEP165a in the meristematic zone and differentiation zone (Ormancey et al., 2020). Similar to observations of miPEP165a, miPEP858a can be absorbed by the roots and presence inside the plant cell (Sharma et al., 2020). These results indirectly provide pieces of evidence that miPEPs possibly play a role for regulatory functions within intracellular space rather than be transported into the apoplast (**Figure 2**).

An investigation of 50 *Arabidopsis* pri-miRNAs uncovers the presence of at least one putative ORF encoding miPEPs in one pri-miRNA (Lauressergues et al., 2015). These miPEPs have no common signatures, implying that each of these miPEPs is likely specific for their miRNA (Lauressergues et al., 2015). Such a large number of miPEPs form a complex and specific regulatory network that performs different biological functions by positively regulating miRNA expression level. So far, the biological function of numerable miPEPs has been deciphered. MiPEP171b and miPEP165a are 20-a.a. and 18-a.a. peptides produced by *M. truncatula* and *Arabidopsis*, respectively. Overexpression and exogenous supplement of these peptides specifically trigger the accumulation of *miR171b* and *miR165a*, resulting in decreased lateral root formation and stimulation of

main root growth (Lauressergues et al., 2015). Watering plants with synthetic miPEP172c increases nodule number in soybean (Couzigou et al., 2016). In grape, an exogenous supplement of vvimiPEP171d1 can promote adventitious root development by enhancing the expression of *vvi-MIR171d* (Chen Q. J. et al., 2020). MiPEP858a is a 44-a.a. peptide encoded by the first ORF (135 bp) located upstream in the pre-miR858a sequence in *Arabidopsis*. The endogenous miPEP858a is ∼6 kDa in molecular weight (Sharma et al., 2020). MiPEP858a controls flavonoid biosynthesis and plant development by regulating the expression of genes involved in the phenylpropanoid pathway and auxin signaling (Sharma et al., 2020). Although the regulatory functions of several miPEPs have been experimentally validated in different plant species, some key questions remain to be answered. Is miPEPs specific for upregulation of their corresponding pri-miRNAs, and if so, how is it achieved? After all, only a few miRNAs have been used to detect activation specificity (Lauressergues et al., 2015). In grape, the expression level of some miRNAs genes such as *vvi-MIR160c*, *vviMIR171a,* and *vvi-MIR171i* even reduces when grape tissue culture plantlets are treated by synthetic vvi-miPEP171d1, even if it is not definitely clear whether this decrease is caused by the incubation period (Chen Q. J. et al., 2020). In fact, small peptides encoded by lncRNAs produce either inhibitory or stimulatory effects on their target genes in mammals (Anderson et al., 2015; Nelson et al., 2016). Therefore, whether miPEPs exert a negative effect on their corresponding miRNAs or other miRNAs remains to be shown.

PERSPECTIVE

Peptides are regulatory molecules that have received great attention over recent years. In particular, different types of peptides identified from several species were found to be enriched in the peptidome of plants (Tavormina et al., 2015; Olsson et al., 2019; Takahashi et al., 2019). In addition to the conventional peptides derived from the precursor processing and short ORFs, pieces of evidence are emerging for the presence and function of non-conventional peptides translated from 5' UTR or 3' UTR of transcripts and currently defined as ncRNAs (Wang et al., 2020). The function of peptides is diverse, and they are found to be involved in development, growth, and reproduction, senescence and cell death, nutrients balance and nodulation, and biotic and abiotic stress responses. In the past few years, numerous miPEPs derived from pri-miRNAs have been experimentally identified and their function suggested by overexpression studies in different species, implying that coding of pri-miRNAs is ubiquitous among different plant species. Existing pieces of evidence support the regulatory ability of miPEPs in directing an increase in the level of their associated miRNA by enhancing the transcription of pri-miRNAs. Still, several questions remain to be addressed. (1) MiPEPs synthesis and miRNA processing occur in two independent regions of pri-miRNAs; how does coordination occur between the translation in the cytoplasm and the maturation of miRNA in the nucleus? One putative mechanism is that the 5′ upstream of pri-miRNA is transported into the cytoplasm for guiding miPEP synthesis after releasing from the dicing complex and re-polyadenylation (**Figure 2**). (2) How do miPEPs specifically enhance transcription of the *MIR* gene? An analysis of 50 *Arabidopsis* miPEPs uncovered no common structural pattern among them, suggesting that each miPEP probably has a specific regulatory function (Lauressergues et al., 2015). Whether miPEPs directly bind Pol II or trans-acting factors such as TFs remains to be further investigated. (3) Regarding the exogenous application of miPEPs, overexpression and CRISPR-Cas9-editing are required for assessing the biological functions. It is not clear that post-translational modifications of miPEPs can enhance the activity of miPEPs.

In summary, most characterized peptides to date are hypothesized to act as a ligand to mediate plant intercellular communication and response. The identification of peptides that are translated from the transcript of currently defined ncRNAs enriches the plants' peptidome. Particularly, miPEP identification uncovers the dual function of pri-miRNAs combing with coding and non-coding ability. Dissecting the biosynthesis and regulatory mechanism of miPEPs will reveal another miRNA-dependent gene regulation network.

AUTHOR CONTRIBUTIONS

YR integrated the manuscript and drafted the figures. YS, LZ, DG, and JH retrieved and collected the references about miRNA biogenesis, translation of circRNAs, and the translation of lncRNA. LW, SS, WX, and CZ retrieved and collected the literatures about canonical peptides biogenesis, and biological functions. AL and SW revised the manuscript. CM conceived the idea and revised the manuscript. All authors contributed to the article and approved the submitted version.

FUNDING

This work was supported by the Shanghai municipal key task projects of "Prospering Agriculture by Science and Technology Plan" (Grant No. 2020-02-08-00-08-F01458), the National Natural Science Foundation of China (Grant No. 31972383), and the Shanghai Municipal Commission for Science and Technology (Grant No. 19ZR1428000).

REFERENCES

Anderson, D. M., Anderson, K. M., Chang, C. L., Makarewich, C. A., Nelson, B. R., McAnally, J. R., et al. (2015). A micropeptide encoded by a putative long noncoding RNA regulates muscle performance. *Cell* 160, 595–606. doi: 10.1016/j.cell.2015.01.009

Andrews, S. J., and Rothnagel, J. A. (2014). Emerging evidence for functional peptides encoded by short open reading frames. *Nat. Rev. Genet*. 15, 193–204. doi: 10.1038/nrg3520

Casson, S. A., Chilley, P. M., Topping, J. F., Evans, I. M., Souter, M. A., and Lindsey, K. (2002). The POLARIS gene of *Arabidopsis* encodes a predicted peptide required for correct root growth and

leaf vascular patterning. *Plant Cell* 14, 1705–1721. doi: 10.1105/tpc.002618

Chekanova, J. A. (2015). Long non-coding RNAs and their functions in plants. *Curr. Opin. Plant Biol.* 27, 207–216. doi: 10.1016/j.pbi.2015.08.003

Chen, J., Brunner, A. D., Cogan, J. Z., Nuñez, J. K., Fields, A. P., Adamson, B., et al. (2020). Pervasive functional translation of noncanonical human open reading frames. *Science* 367, 1140–1146. doi: 10.1126/science.aay0262

Chen, Q. J., Deng, B. H., Gao, J., Zhao, Z. Y., Chen, Z. L., Song, S. R., et al. (2020). A miRNA-encoded small peptide, vvi-miPEP171d1, regulates adventitious root formation. *Plant Physiol.* 183, 656–670. doi: 10.1104/pp.20.00197

Conn, V. M., Hugouvieux, V., Nayak, A., Conos, S. A., Capovilla, G., Cildir, G., et al. (2017). A circRNA from SEPALLATA3 regulates splicing of its cognate mRNA through R-loop formation. *Nat. Plants* 3:17053. doi: 10.1038/nplants.2017.53

Couzigou, J. M., André, O., Guillotin, B., Alexandre, M., and Combier, J. P. (2016). Use of microRNA-encoded peptide miPEP172c to stimulate nodulation in soybean. *New Phytol.* 211, 379–381. doi: 10.1111/nph.13991

Diallo, L. H., Tatin, F., David, F., Godet, A. C., Zamora, A., Prats, A. C., et al. (2019). How are circRNAs translated by non-canonical initiation mechanisms? *Biochimie* 164, 45–52. doi: 10.1016/j.biochi.2019.06.015

Dubois, M., Van den Broeck, L., and Inze, D. (2018). The pivotal role of ethylene in plant growth. *Trends Plant Sci.* 23, 311–323. doi: 10.1016/j.tplants.2018.01.003

Fang, J., Morsalin, S., Rao, V., and Reddy, E. S. (2017). Decoding of non-coding DNA and non-coding RNA: pri-micro RNA-encoded novel peptides regulate migration of cancer cells. *J. Pharm. Pharmacol.* 3, 23–27. doi: 10.1166/jpsp.2017.1070

Gao, Z., Li, J., Luo, M., Li, H., Chen, Q., Wang, L., et al. (2019). Characterization and cloning of grape circular RNAs identified the cold resistance-related Vv-circATS1. *Plant Physiol.* 180, 966–985. doi: 10.1104/pp.18.01331

Guttman, M., Russell, P., Ingolia, N. T., Weissman, J. S., and Lander, E. S. (2013). Ribosome profiling provides evidence that large noncoding RNAs do not encode proteins. *Cell* 154, 240–251. doi: 10.1016/j.cell.2013.06.009

Hanada, K., Higuchi-Takeuchi, M., Okamoto, M., Yoshizumi, T., Shimizu, M., Nakaminami, K., et al. (2013). Small open reading frames associated with morphogenesis are hidden in plant genomes. *Proc. Natl. Acad. Sci. U.S.A.* 110, 2395–2400. doi: 10.1073/pnas.1213958110

Hsu, P. Y., and Benfey, P. N. (2018). Small but mighty: functional peptides encoded by small ORFs in plants. *Proteomics* 18:e1700038. doi: 10.1002/pmic.201700038

Huang, J. Z., Chen, M., Chen, D., Gao, X. C., Zhu, S., Huang, H., et al. (2017). A peptide encoded by a putative lncRNA HOXB-AS3 suppresses colon cancer growth. *Mol. Cell* 68, 171–184.e176. doi: 10.1016/j.molcel.2017.09.015

Huffaker, A., Dafoe, N. J., and Schmelz, E. A. (2011). ZmPep1, an ortholog of *Arabidopsis* elicitor peptide 1, regulates maize innate immunity and enhances disease resistance. *Plant Physiol.* 155, 1325–1338. doi: 10.1104/pp.110.166710

Huffaker, A., Pearce, G., and Ryan, C. A. (2006). An endogenous peptide signal in *Arabidopsis* activates componenets of the innate immune response. *Proc. Natl. Acad. Sci. U.S.A.* 103, 10098–10103. doi: 10.1073/pnas.0603727103

Huffaker, A., and Ryan, C. A. (2007). Endogenous peptide defense signals in *Arabidopsis* differentially amplify sigbaling for the innate immnue response. *Proc. Natl. Acad. Sci. U.S.A.* 104, 10732–10736. doi: 10.1073/pnas.0703343104

Ingolia, N. T., Brar, G. A., Rouskin, S., McGeachy, A. M., and Weissman, J. S. (2012). The ribosome profiling strategy for monitoring translation *in vivo* by deep sequencing of ribosome-protected mRNA fragments. *Nat. Protoc.* 7, 1534–1550. doi: 10.1038/nprot.2012.086

Julkowska, M. (2020). Small but powerful: microRNA-derived peptides promote grape adventitious root formation. *Plant Physiol.* 183, 429–430. doi: 10.1104/pp.20.00515

Kachroo, A., Schopfer, C. R., Nasrallah, M. E., and Nasrallah, J. B. (2001). Allele-specific receptor-ligand interactions in *Brassica* self-incompatibility. *Science* 293, 1824–1826. doi: 10.1126/science.1062509

Kieber, J. J., and Schaller, G. E. (2018). Cytokinin signaling in plant development. *Development* 145:dev149344. doi: 10.1242/dev.149344

Kurihara, Y. (2020). uORF shuffling fine-tunes gene expression at a deep level of the process. *Plants* 9:608. doi: 10.3390/plants9050608

Laing, W. A., Martinez-Sanchez, M., Wright, M. A., Bulley, S. M., Brewster, D., Dare, A. P., et al. (2015). An upstream open reading frame is essential for feedback regulation of ascorbate biosynthesis in *Arabidopsis*. *Plant Cell* 27, 772–786. doi: 10.1105/tpc.114.133777

Lauressergues, D., Couzigou, J. M., Clemente, H. S., Martinez, Y., Dunand, C., Becard, G., et al. (2015). Primary transcripts of microRNAs encode regulatory peptides. *Nature* 520, 90–93. doi: 10.1038/nature14346

Legnini, I., Di Timoteo, G., Rossi, F., Morlando, M., Briganti, F., Sthandier, O., et al. (2017). Circ-ZNF609 is a circular RNA that can be translated and functions in myogenesis. *Mol. Cell* 66, 22–37 e29. doi: 10.1016/j.molcel.2017.02.017

Li, X., Yang, L., and Chen, L. L. (2018). The biogenesis, functions, and challenges of circular RNAs. *Mol. Cell* 71, 428–442. doi: 10.1016/j.molcel.2018.06.034

Liu, H., Zhou, X., Yuan, M., Zhou, S., Huang, Y. E., Hou, F., et al. (2020). ncEP: a manually curated database for experimentally validated ncRNA-encoded proteins or peptides. *J. Mol. Biol.* 432, 3364–3368. doi: 10.1016/j.jmb.2020.02.022

Lv, S., Pan, L., and Wang, G. (2016). Commentary: primary transcripts of microRNAs encode regulatory peptides. *Front. Plant Sci.* 7:1436. doi: 10.3389/fpls.2016.01436

Matsubayashi, Y. (2014). Posttranslationally modified small-peptide signals in plants. *Annu. Rev. Plant Biol.* 65, 385–413. doi: 10.1146/annurev-arplant-050312-120122

Matsuzaki, Y., Ogawa-Ohnishi, M., Mori, A., and Matsubayashi, Y. (2010). Secreted peptide signals required for maintenance of root stem cell niche in *Arabidopsis*. *Science* 329, 1065–1067. doi: 10.1126/science.1191132

Nakaminami, K., Okamoto, M., Higuchi-Takeuchi, M., Yoshizumi, T., Yamaguchi, Y., Fukao, Y., et al. (2018). AtPep3 is a hormone-like peptide that plays a role in the salinity stress tolerance of plants. *Proc. Natl. Acad. Sci. U.S.A.* 115, 5810–5815. doi: 10.1073/pnas.1719491115

Nelson, B. R., Makarewich, C. A., Anderson, D. M., and Winders, B. R. (2016). A peptide encoded by transcript annotated as long noncoding RNA enhances SERCA activity in muscle. *Science* 351, 271–275. doi: 10.1126/science.aad4076

Oh, E., Seo, P. J., and Kim, J. (2018). Signaling peptides and receptors coordinating plant root development. *Trends Plant Sci.* 23, 337–351. doi: 10.1016/j.tplants.2017.12.007

Ohkubo, Y., Tanaka, M., Tabata, R., Ogawa-Ohnishi, M., and Matsubayashi, Y. (2017). Shoot-to-root mobile polypeptides involved in systemic regulation of nitrogen acquisition. *Nat. Plants* 3:17029. doi: 10.1038/nplants.2017.29

Okamoto, S., Tabata, R., and Matsubayashi, Y. (2016). Long-distance peptide signaling essential for nutrient homeostasis in plants. *Curr. Opin. Plant. Biol.* 34, 35–40. doi: 10.1016/j.pbi.2016.07.009

Okuda, S., Tsutsui, H., Shiina, K., Sprunck, S., Takeuchi, H., Yui, R., et al. (2009). Defensin-like polypeptide LUREs are pollen tube attractants secreted from synergid cells. *Nature* 458, 357–361. doi: 10.1038/nature07882

Olsson, V., Joos, L., Zhu, S., Gevaert, K., Butenko, M. A., and De Smet, I. (2019). Look closely, the beautiful may be small: precursor-derived peptides in plants. *Annu. Rev. Plant Biol.* 70, 153–186. doi: 10.1146/annurev-arplant-042817-040413

Ormancey, M., Le Ru, A., Duboe, C., Jin, H., Thuleau, P., Plaza, S., et al. (2020). Internalization of miPEP165a into *Arabidopsis* roots depends on both passive diffusion and endocytosis-associated processes. *Int. J. Mol. Sci.* 21:2266. doi: 10.3390/ijms21072266

Pearce, G., Strydom, D., JohnsON, S., and Ryan, C. A. (1991). A polypeptide from tomato Leaves induces wound-inducible proteinase inhibitor proteins. *Science* 253, 895–897. doi: 10.1126/science.253.5022.895

Prasad, A., Sharma, N., and Prasad, M. (2020). Noncoding but coding: pri-miRNA into the action. *Trends Plant Sci.* S1360-1385, 30381–30382. doi: 10.1016/j.tplants.2020.12.004

Qian, P., Song, W., Yokoo, T., Minobe, A., Wang, G., Ishida, T., et al. (2018). The CLE9/10 secretory peptide regulates stomatal and vascular development through distinct receptors. *Nat. Plants* 4, 1071–1081. doi: 10.1038/s41477-018-0317-4

Qu, L. J., Li, L., Lan, Z., and Dresselhaus, T. (2015). Peptide signalling during the pollen tube journey and double fertilization. *J. Exp. Bot.* 66, 5139–5150. doi: 10.1093/jxb/erv275

Ribone, P. A., Capella, M., Arce, A. L., and Chan, R. L. (2017). A uORF represses the transcription factor AtHB1 in aerial tissues to avoid a deleterious phenotype. *Plant Physiol.* 175, 1238–1253. doi: 10.1104/pp.17.01060

Rogers, K., and Chen, X. (2013). Biogenesis, turnover, and mode of action of plant microRNAs. *Plant Cell* 25, 2383–2399. doi: 10.1105/tpc.113.113159

Röhrig, H., Schmidt, J., Miklashevichs, E., Schell, J., and John, M. (2002). Soybean ENOD40 encodes two peptides that bind to sucrose synthase. *Proc. Natl. Acad. Sci. U.S.A.* 99, 1915–1920. doi: 10.1073/pnas.022664799

Ruiz-Orera, J., Messeguer, X., Subirana, J. A., and Alba, M. M. (2014). Long non-coding RNAs as a source of new peptides. *ELife* 3:e03523. doi: 10.7554/eLife.03523

Sharma, A., Badola, P. K., Bhatia, C., Sharma, D., and Trivedi, P. K. (2020). Primary transcript of miR858 encodes regulatory peptide and controls flavonoid biosynthesis and development in *Arabidopsis*. *Nat. Plants* 6, 1262–1274. doi: 10.1038/s41477-020-00769-x

Shi, Y., Jia, X., and Xu, J. (2020). The new function of circRNA: translation. *Clin. Transl. Oncol.* 22, 2162–2169. doi: 10.1007/s12094-020-02371-1

Takahashi, F., Hanada, K., Kondo, T., and Shinozaki, K. (2019). Hormone-like peptides and small coding genes in plant stress signaling and development. *Curr. Opin. Plant Biol.* 51, 88–95. doi: 10.1016/j.pbi.2019.05.011

Takahashi, F., Suzuki, T., Osakabe, Y., Betsuyaku, S., Kondo, Y., Dohmae, N., et al. (2018). A small peptide modulates stomatal control via abscisic acid in long-distance signalling. *Nature* 556, 235–238. doi: 10.1038/s41586-018-0009-2

Tavormina, P., De Coninck, B., Nikonorova, N., De Smet, I., and Cammue, B. P. (2015). The plant peptidome: an expanding repertoire of structural features and biological functions. *Plant Cell* 27, 2095–2118. doi: 10.1105/tpc.15.00440

van der Horst, S., Snel, B., Hanson, J., and Smeekens, S. (2019). Novel pipeline identifies new upstream ORFs and non-AUG initiating main ORFs with conserved amino acid sequences in the 5' leader of mRNAs in *Arabidopsis thaliana*. *RNA* 25, 292–304. doi: 10.1261/rna.067983.118

van Heesch, S., van Iterson, M., Jacobi, J., Boymans, S., Essers, P. B., de Bruijn, E., et al. (2014). Extensive localization of long noncoding RNAs to the cytosol and mono- and polyribosomal complexes. *Genome Biol.* 15:R6. doi: 10.1186/gb-2014-15-1-r6

Voinnet, O. (2009). Origin, biogenesis, and activity of plant microRNAs. *Cell* 136, 669–687. doi: 10.1016/j.cell.2009.01.046

von Arnim, A. G., Jia, Q., and Vaughn, J. N. (2014). Regulation of plant translation by upstream open reading frames. *Plant Sci.* 214, 1–12. doi: 10.1016/j.plantsci.2013.09.006

Wang, J., Mei, J., and Ren, G. (2019). Plant microRNAs: biogenesis, homeostasis, and degradation. *Front. Plant Sci.* 10:360. doi: 10.3389/fpls.2019.00360

Wang, L., and Wang, J. W. (2015). Coding function for non-coding RNA in plants-insights from miRNA encoded peptide (miPEP). *Sci. China Life Sci.* 58, 503–505. doi: 10.1007/s11427-015-4854-z

Wang, S., Tian, L., Liu, H., Li, X., Zhang, J., Chen, X., et al. (2020). Large-scale discovery of non-conventional peptides in maize and *Arabidopsis* through an integrated peptidogenomic pipeline. *Mol. Plant* 13, 1078–1093. doi: 10.1016/j.molp.2020.05.012

Wang, Y., and Wang, Z. (2015). Efficient backsplicing produces translatable circular mRNAs. *RNA* 21, 172–179. doi: 10.1261/rna.048272.114

Wu, Q., Wright, M., Gogol, M. M., Bradford, W. D., Zhang, N., and Bazzini, A. A. (2020). Translation of small downstream ORFs enhances translation of canonical main open reading frames. *EMBO J.* 39:e104763. doi: 10.15252/embj.2020104763

Yamaguchi, Y., Huffaker, A., Bryan, A. C., Tax, F. E., and Ryan, C. A. (2010). PEPR2 is a second receptor for the Pep1 and Pep2 peptides and contributes to defense responses in *Arabidopsis*. *Plant Cell* 22, 508–522. doi: 10.1105/tpc.109.068874

Yamaguchi, Y., Pearce, G., and Ryan, C. A. (2006). The cell surface leucine-rich repeat receptor for AtPep1, an endogenous peptide elicitor in *Arabidopsis*, is functional in transgenic tobacco cells. *Proc. Natl. Acad. Sci. U.S.A.* 103, 10104–10109. doi: 10.1073/pnas.0603729103

Yamaguchi, Y. L., Ishida, T., and Sawa, S. (2016). CLE peptides and their signaling pathways in plant development. *J. Exp. Bot.* 67, 4813–4826. doi: 10.1093/jxb/erw208

Yang, Y., Fan, X., Mao, M., Song, X., Wu, P., Zhang, Y., et al. (2017). Extensive translation of circular RNAs driven by N^6-methyladenosine. *Cell Res.* 27, 626–641. doi: 10.1038/cr.2017.31

Yu, Y., Jia, T., and Chen, X. (2017). The 'how' and 'where' of plant microRNAs. *New Phytol.* 216, 1002–1017. doi: 10.1111/nph.14834

Zhang, H., Si, X., Ji, X., Fan, R., Liu, J., and Chen, K. (2018). Genome editing of upstream open reading frames enables translational control in plants. *Nat. Biotechnol.* 36, 894–898. doi: 10.1038/nbt.4202

Conflict of Interest: The authors declare that the research was conducted in the absence of any commercial or financial relationships that could be construed as a potential conflict of interest.

frontiers in Plant Science

ORIGINAL RESEARCH
published: 13 April 2021
doi: 10.3389/fpls.2021.657548

An Evolutionarily Conserved Coreceptor Gene Is Essential for CLAVATA Signaling in *Marchantia polymorpha*

Go Takahashi[1†], Shigeyuki Betsuyaku[2†], Natsuki Okuzumi[1], Tomohiro Kiyosue[1] and Yuki Hirakawa[1†]*

[1] Graduate School of Science, Gakushuin University, Tokyo, Japan, [2] Faculty of Agriculture, Ryukoku University, Otsu, Japan

Growth and development of land plants are controlled by CLAVATA3/EMBRYO SURROUNDING REGION-related (CLE) family of peptide hormones. In contrast to the genetic diversity of CLE family in flowering plants, the liverwort *Marchantia polymorpha* possesses a minimal set of CLE, MpCLE1(TDIF homolog), and MpCLE2 (CLV3 homolog). MpCLE1 and MpCLE2 peptides exert distinct function at the apical meristem of *M. polymorpha* gametophyte via specific receptors, MpTDIF RECEPTOR (MpTDR) and MpCLAVATA1 (MpCLV1), respectively, both belonging to the subclass XI of leucine-rich repeat receptor-like kinases (LRR-RLKs). Biochemical and genetic studies in Arabidopsis have shown that TDR/PXY family and CLV1/BAM family recognize the CLE peptide ligand in a heterodimeric complex with a member of subclass-II coreceptors. Here we show that three LRR-RLK genes of *M. polymorpha* are classified into subclass II, representing three distinct subgroups evolutionarily conserved in land plants. To address the involvement of subclass-II coreceptors in *M. polymorpha* CLE signaling, we performed molecular genetic analysis on one of them, Mp*CLAVATA3 INSENSITIVE RECEPTOR KINASE* (Mp*CIK*). Two knockout alleles for Mp*CIK* formed narrow apical meristems marked by $_{prom}$Mp*YUC2:GUS* marker, which were not expanded by MpCLE2 peptide treatment, phenocopying Mp*clv1*. Loss of sensitivity to MpCLE2 peptide was also observed in gemma cup formation in both Mp*clv1* and Mp*cik*. Biochemical analysis using a *Nicotiana benthamiana* transient expression system revealed weak association between MpCIK and MpCLV1, as well as MpCIK and MpTDR. While MpCIK may also participate in MpCLE1 signaling, our data show that the conserved CLV3-CLV1-CIK module functions in *M. polymorpha*, controlling meristem activity for development and organ formation for asexual reproduction.

Keywords: CLAVATA, coreceptor, Marchantia, meristem, stem cell, gemma cup, LRR-RLK

OPEN ACCESS

Edited by:
Reidunn Birgitta Aalen, University of Oslo, Norway

Reviewed by:
Hiroyasu Motose, Okayama University, Japan
Lin Xu, Chinese Academy of Sciences, China

****Correspondence:***
Yuki Hirakawa
yuki.hirakawa@gakushuin.ac.jp

† These authors have contributed equally to this work

Specialty section:
This article was submitted to Plant Physiology, a section of the journal Frontiers in Plant Science

Received: *23 January 2021*
Accepted: *22 March 2021*
Published: *13 April 2021*

Citation:
Takahashi G, Betsuyaku S, Okuzumi N, Kiyosue T and Hirakawa Y (2021) An Evolutionarily Conserved Coreceptor Gene Is Essential for CLAVATA Signaling in Marchantia polymorpha. Front. Plant Sci. 12:657548. doi: 10.3389/fpls.2021.657548

INTRODUCTION

CLAVATA3/EMBRYO SURROUNDING REGION-related (CLE) peptides are a family of peptide hormones in land plants, mediating cell-to-cell communication in the plant body (Murphy et al., 2012; Hirakawa and Sawa, 2019; Fletcher, 2020). CLE peptides are genetically encoded as a precursor protein possessing a conserved CLE domain(s) at or near the C-terminus. Biosynthesis

of CLE peptide hormone from the CLE domain involves post-translational events including proteolytic cleavage, post-translation modifications and secretion to the apoplast (Ito et al., 2006; Kondo et al., 2006; Ohyama et al., 2009; Tamaki et al., 2013: Matsubayashi, 2014). In flowering plants, a large number of *CLE* genes are encoded in the genome, which have been extensively studied for the past two decades (Cock and McCormick, 2001; Oelkers et al., 2008; Jun et al., 2010; Fletcher, 2020). The function of CLE genes cover a wide range of physiological processes including stem cell homeostasis in meristems, vascular cell differentiation, stomata differentiation and responses to various environmental cues (Fletcher et al., 1999; Suzaki et al., 2008; Okamoto et al., 2009; Stahl et al., 2009; Etchells and Turner, 2010; Hirakawa et al., 2010; Mortier et al., 2010; Kondo et al., 2011; Fiume and Fletcher, 2012; Depuydt et al., 2013; Endo et al., 2013; Araya et al., 2014; Czyzewicz et al., 2015; Gutiérrez-Alanís et al., 2017; Rodríguez-Leal et al., 2017; Qian et al., 2018; Takahashi et al., 2018; Ma et al., 2020). In bryophytes, which are distantly related to flowering plants in the land plant lineage (Morris et al., 2018; Puttick et al., 2018), relatively low number of *CLE* genes are encoded in the genome, providing simplified models to study the function of *CLE* genes (Bowman et al., 2017; Whitewoods et al., 2018). The minimal set of *CLE* genes, Mp*CLE1* (Mp6g07050) and Mp*CLE2* (Mp5g18050), are encoded in the genome of the liverwort *Marchantia polymorpha* (Bowman et al., 2017; Hirakawa et al., 2019; Montgomery et al., 2020; **Figure 1A**). MpCLE1 and MpCLE2 are the orthologs of TDIF (tracheary element differentiation inhibitor factor) and CLV3 (CLAVATA3) of *Arabidopsis thaliana*, respectively, representing the two distinct subgroups of CLE peptide family. In Arabidopsis, specific bioactivities of TDIF and CLV3 are attributed to the difference in a few amino acids between them, which are mediated by two distinct groups of receptors, TDIF RECEPTOR/PHLOEM INTERCALTED WITH XYLEM (TDR/PXY) and CLAVATA1/BARELY ANY MERISTEMs (CLV1/BAMs), respectively (Fletcher et al., 1999; DeYoung et al., 2006; Fisher and Turner, 2007; Hirakawa et al., 2008, 2017; Ogawa et al., 2008; Rodriguez-Villalon et al., 2014; Shimizu et al., 2015; Shinohara and Matsubayashi, 2015; Crook et al., 2020). Since the ligand-receptor pairs are conserved among flowering plants and bryophytes and no CLE homologs were found in sister streptophyte algae, the specific CLE peptide-receptor pairs may have originated in the common ancestor of land plants (Whitewoods et al., 2018; Hirakawa et al., 2019, 2020). In *M. polymorpha*, CLE genes regulate the activity of the apical meristem located at the apical notch of the thalloid gametophyte body. MpCLE1-MpTDR signaling acts as a negative regulator of cell proliferation at the apical notch, while MpCLE2-MpCLV1 signaling functions as a positive regulator of stem cell activity in the apical notch (Hirakawa et al., 2019, 2020).

Both TDR/PXY and CLV1/BAM belong to the subclass XI of leucine-rich repeat receptor-like kinase (LRR-RLK) family. In addition to CLE peptides, a number of peptide ligands have been shown to bind to specific members of subclass-XI receptors, which possess a long extracellular domain (ECD) composed of more than 20 LRRs (Shiu and Bleecker, 2001; Yamaguchi et al., 2006; Hou et al., 2014; Tabata et al., 2014; Ou et al., 2016; Shinohara et al., 2016; Song et al., 2016; Doblas et al., 2017; Nakayama et al., 2017; Toyokura et al., 2019; Doll et al., 2020). Accumulating evidence indicates that subclass-II receptors, such as SOMATIC EMBRYOGENESIS RECEPTOR KINASE/BRASSINOSTEROID INSENSITIVE1-ASSOCIATED KINASE1 (SERK/BAK1) family, participate in the peptide hormone perception by forming a heterodimeric complex with subclass-XI receptors (Hohmann et al., 2017; Gou and Li, 2020). Structural studies have revealed that SERK coreceptors have a short ECD containing five LRRs. The ECD of subclass-II receptors do not interact strongly or at all to the peptide ligand by themselves and rather recognize the ligand-receptor complex (Santiago et al., 2013, 2016; Sun et al., 2013; Wang et al., 2015; Okuda et al., 2020). In line with this scheme, PXY/TDR and SERK2 are reported to form a heterodimeric complex for TDIF recognition, and multiple knockout mutants for Arabidopsis *SERK* genes show reduced TDIF sensitivity in vascular development (Morita et al., 2016; Zhang et al., 2016a,b).

In contrast to TDIF, involvement of SERK family has not been observed in CLV3-type CLEs. Instead, another group of subclass-II receptors, CLAVATA3 INSENSITIVE RECEPTOR KINASEs (CIKs), have been implicated in CLV3 peptide perception. CIK proteins can form protein complexes with CLV1/BAM receptors (Cui et al., 2018; Hu et al., 2018). Quadruple mutants for Arabidopsis *CIK1-4* genes develop enlarged shoot apical meristems, which is similar to those of *clv* mutants. The growth from the enlarged meristems is not arrested by treatment with CLV3 peptide, a negative regulator of stem cells in Arabidopsis (Hu et al., 2018). Furthermore, full activity of Arabidopsis CLE26/CLE45 peptides in root phloem cell differentiation requires *CLE-RESISTANT RECEPTOR KINASE* (*CLERK*)/*CIK2* although biochemical interaction is not detected between the ECDs of CLERK and the subclass-XI receptor BAM3 (Anne et al., 2018). In this study, we searched for the homologs of *CIK* genes in *M. polymorpha* and analyzed their involvement in CLE peptide signaling by molecular genetic approach.

RESULTS

A Single CIK Ortholog in *Marchantia polymorpha*

In the *M. polymorpha* genome, three LRR-RLK genes (Mp7g09160/Mapoly0068s0069, Mp7g14210/Mapoly0009s0106, and Mp7g15980/Mapoly0560s0001) have been classified into subclass II (Sasaki et al., 2007; Bowman et al., 2017; Montgomery et al., 2020). To better understand the evolutionary relationships, we performed phylogenetic analysis of the subclass-II genes from land plants (*A. thaliana*, *Amborella trichopoda*, *Picea abies*, *Selaginella moellendorffii*, *Physcomitrium patens*, *Sphagnum fallax*, *M. polymorpha*) and charophycean algae (*Spirogyra pratensis* and *Coleochaete orbicularis*) based on the amino acid sequence of the kinase domain using a Bayesian method (**Figure 1B**). The tree inferred three subgroups diverged in the land plant lineage, each of which contains a single *M. polymorpha* gene. Mp7g14210, designated as Mp*CIK,* was grouped into a single subgroup with all *CIK* genes from Arabidopsis. Likewise,

A

Species	CLV3	TDIF	CLV1/BAM	TDR/PXY	CIK	SERK/BAK1
Arabidopsis thaliana	28	4	4	3	6	5
Physcomitrium patens	7	0	2	0	3	3
Marchantia polymorpha	1	1	1	1	1	1

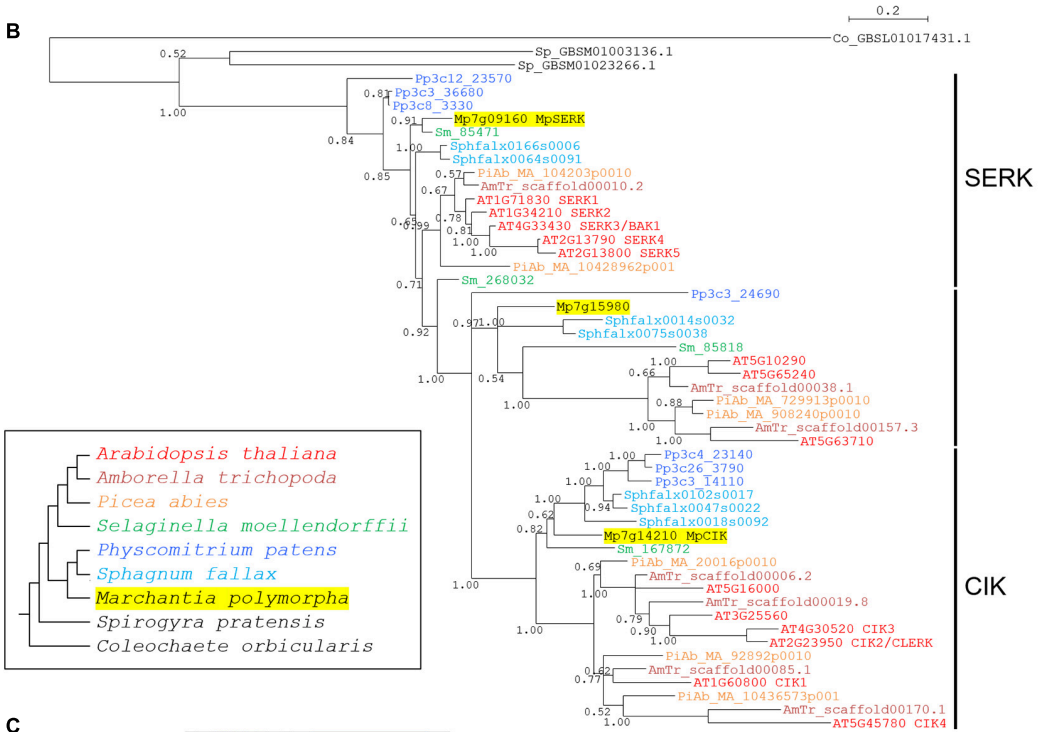

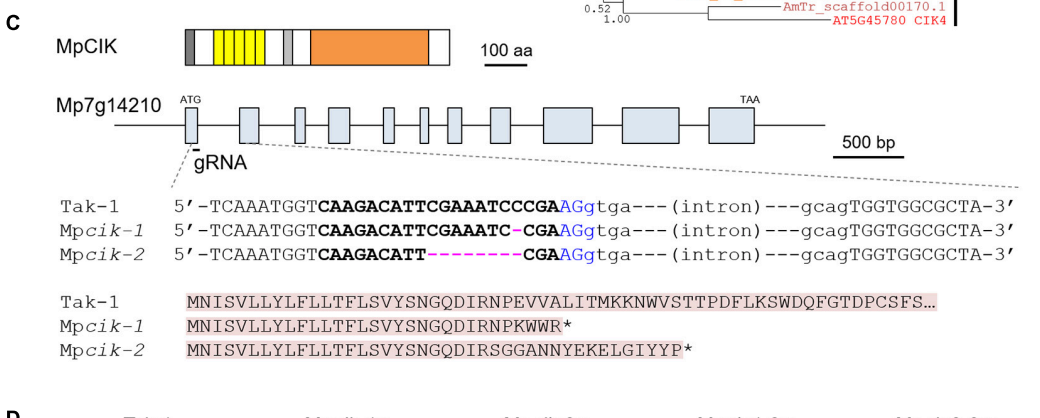

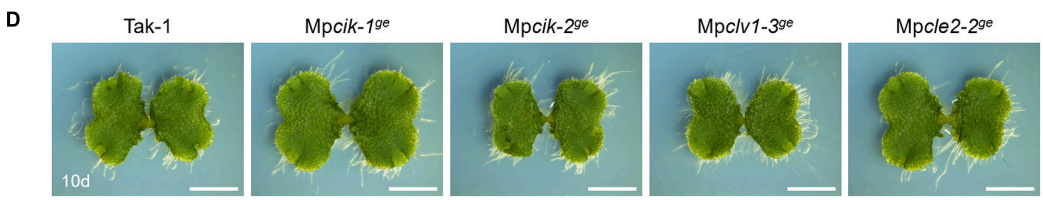

FIGURE 1 | Analysis of LRR-RLK subclass II in *Marchantia polymorpha*. **(A)** The number of CLE-receptor homologs. **(B)** A phylogenetic tree of subclass-II LRR-RLKs, generated with a Bayesian method based on the conserved kinase domain. The posterior probabilities of trees are shown at the nodes. Coleochaete sequence was used as an outgroup. Land plant sequences form a monophyletic clade, which can be divided into three subgroups as indicated on the right. Inset shows the list of species with their phylogenetic relationships. **(C)** Gene/protein structures and genome editing alleles of MpCIK. (top) Protein structure of MpCIK. (middle) Structure of MpCIK/Mp7g14210 locus with the position of a designed guide RNA (gRNA). (bottom) Genotyping of genome editing alleles. Target guide sequence is in bold and PAM sequence is in blue. Deleted bases are indicated with hyphens in magenta. Exon and intron are indicated in capital and small letters, respectively. N-terminal region of WT and mutant proteins deduced from the genomic DNA sequences are indicated below. Asterisks indicate translational termination. **(D)** Overall morphology of 10-day-old plants grown from gemmae. Scale bars represent 0.5 mm.

Mp7g09160/Mp*SERK* was grouped into the SERK subgroup with all Arabidopsis *SERK* genes. Thus, *M. polymorpha* genome may lack redundancy in CLE ligand/receptor/coreceptor orthlogs (**Figure 1A**). In transcriptome of *M. polymorpha*, Mp*CIK* was expressed in thalli, gametangiophores and sporophytes while its expression was relatively low in sporelings. Mp*CLV1* expression showed a similar trend (Bowman et al., 2017).

CRISPR-Cas9 Editing of Mp*CIK* Does Not Affect Overall Growth of Gametophyte

To analyze the physiological function of the *CIK* coreceptor gene in *M. polymorpha*, we generated loss-of-function alleles for Mp*CIK* using CRISPR-Cas9 editing (Sugano et al., 2018). Sanger sequencing revealed that two independent transgenic lines, Mp*cik-1*^{ge} and Mp*cik-2*^{ge}, possess different mutations at the CRISPR/Cas9 target site, both predicted to result in gene knockout due to premature termination of translation (**Figure 1C**). We could not find significant differences in the overall morphology of thalli in 10-day-old Mp*cik-1*^{ge} and Mp*cik-2*^{ge} plants grown from gemmae, compared to any of wild-type (Tak-1), Mp*cle2-2*^{ge} and Mp*clv1-3*^{ge} genotypes (**Figure 1D**).

Mp*CIK* Is Necessary for MpCLE2 Signaling to Control Apical Notch Expansion

To analyze the involvement of Mp*CIK* in MpCLE2 peptide signaling, we examined the apical notch morphology in 4-day-old gemmalings grown on liquid M51C medium supplemented with or without 3 μM MpCLE2 peptide. In wild-type gemmalings, apical notches were expanded by treatment with MpCLE2 peptide, as reported previously (**Figures 2A,B**; Hirakawa et al., 2020). By contrast, apical notches in both Mp*cik-1* and Mp*cik-2* were insensitive to MpCLE2 peptide, which is similar to those in Mp*clv1-3* (**Figures 2A,B**). Importantly, apical notches of the Mp*cik* and Mp*clv1* alleles were narrower than those of wild type in the growth without MpCLE2 peptide. Consistently, *Mpcle2-2*^{ge} developed narrow apical notches but it was sensitive to the

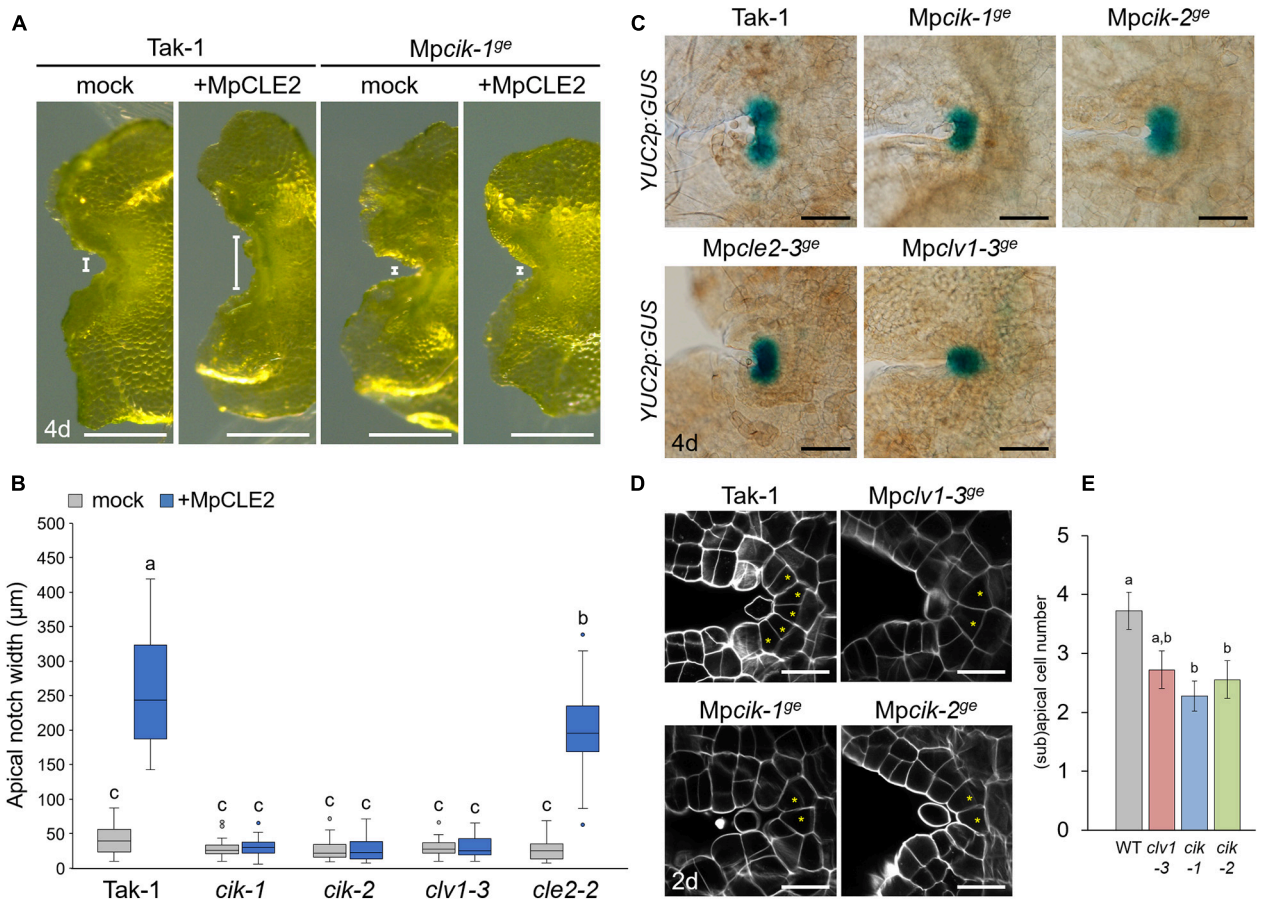

FIGURE 2 | Phenotypes of Mp*CIK* knockout alleles in the apical notch. **(A)** Morphology of 4-day-old gemmalings grown with or without MpCLE2 peptide as indicated above. Width of apical notch is indicated by white lines. **(B)** Quantification of apical notch width. Data sharing superscripts are not significantly different from each other in Tukey's HSD test, $p < 0.05$; $n = 30$. **(C)** $_{pro}$Mp*YUC2:GUS* marker in 4-day-old gemmalings. Genetic background is indicated above each panel. **(D)** Confocal imaging of stem cell zone in 2-day-old gemmalings. Asterisks indicate apical and subapical cells. **(E)** Quantification of the number of apical/subapical cells. Mean and SEM: $n = 18$. Scale bars represent 500 μm in panel **(A)**, 100 μm in panel **(C)** and 20 μm in panel **(D)**.

treatment with the MpCLE2 peptide as reported previously (**Figure 2B**; Hirakawa et al., 2020). $_{pro}$Mp*YUC2(YUCCA2):GUS* is a marker for the tip of apical notch, and $_{pro}$Mp*YUC2:GUS*-positive (Mp*YUC2*$^{+}$) region is affected by MpCLE2-MpCLV1 signaling (Eklund et al., 2015; Hirakawa et al., 2020). Compared to wild-type (Tak-1) background, Mp*YUC2*$^{+}$ region was reduced in Mp*cik* backgrounds, phenocopying Mp*clv1-3* (**Figure 2C**). Confocal imaging in 2-day-old gemmalings showed the number of apical and subapical cells, was reduced in Mp*cik* and Mp*clv1* alleles (**Figures 2D,E**). These data support that MpCIK is an essential component of the MpCLE2 peptide perception.

MpCLE2 Signaling Affects Thallus Branching and Gemma Cup Formation via Mp*CLV1* and Mp*CIK*

To further address the involvement of Mp*CIK* in MpCLE2 signaling, we used $_{pro}$Mp*YUC2*:Mp*CLE2*, a gain of function allele of Mp*CLE2*, which stably develops supernumerary branching from the expanded apical meristems (Hirakawa et al., 2020). We generated Mp*cik* and Mp*clv1* knockout alleles in $_{pro}$Mp*YUC2*:Mp*CLE2-2* background by CRISPR/Cas9-mediated genome editing (**Supplementary Figure 1**). Both Mp*cik-3*^{ge} and Mp*clv1-4*^{ge} suppressed the supernumerary branching phenotype in 16-day-old plants (**Figure 3A**), which is consistent with the results in peptide treatment assay (**Figure 2B**). Furthermore, the number of gemma cup formed on thalli was reduced in $_{pro}$Mp*YUC2*:Mp*CLE2* and it was suppressed in both Mp*cik-3*^{ge} and Mp*clv1-4*^{ge} (**Figure 3A**). Time-course analysis showed that the gemma cup formation was significantly reduced and delayed in $_{pro}$Mp*YUC2*:Mp*CLE2* plants compared to wild type (**Figure 3B**). Meanwhile, all Mp*cik* and Mp*clv1* alleles showed minor increase in gemma cup formation compared to wild type (**Figure 3B**).

Biochemical Interaction of MpCIK and MpCLV1 Proteins

Since the genetic analysis suggests that MpCIK may function as a coreceptor for MpCLV1 for the perception of MpCLE2 peptide, we examined the biochemical interaction between MpCIK and MpCLV1 proteins expressed in a *Nicotiana benthamiana* transient expression system, which has been utilized to analyze the interaction of CLV and CIK receptors of Arabidopsis (Kinoshita et al., 2010; Betsuyaku et al., 2011; Hu et al., 2018). MpCIK, MpCLV1 and MpTDR were expressed under the control of 35S promoter in *N. benthamiana* as proteins C-terminally fused to 3 × HAs-single StrepII or 3 × FLAG (MpCIK-3HS, MpCLV1-3FLAG, MpTDR-3FLAG), respectively (**Figure 4A**). MpTDR, a receptor for MpCLE1, was also included in this interaction assay (Hirakawa et al., 2019). In co-immunoprecipitation experiments using an anti-HA affinity matrix, MpCLV1-3FLAG was detected not strongly but reproducibly in the immunoprecipitates containing MpCIK-3HS, suggesting a weak or transient interaction between MpCIK-3HS and MpCLV1-3FLAG (**Figure 4B**). Similarly, MpTDR-3FLAG was also shown to associate weakly with

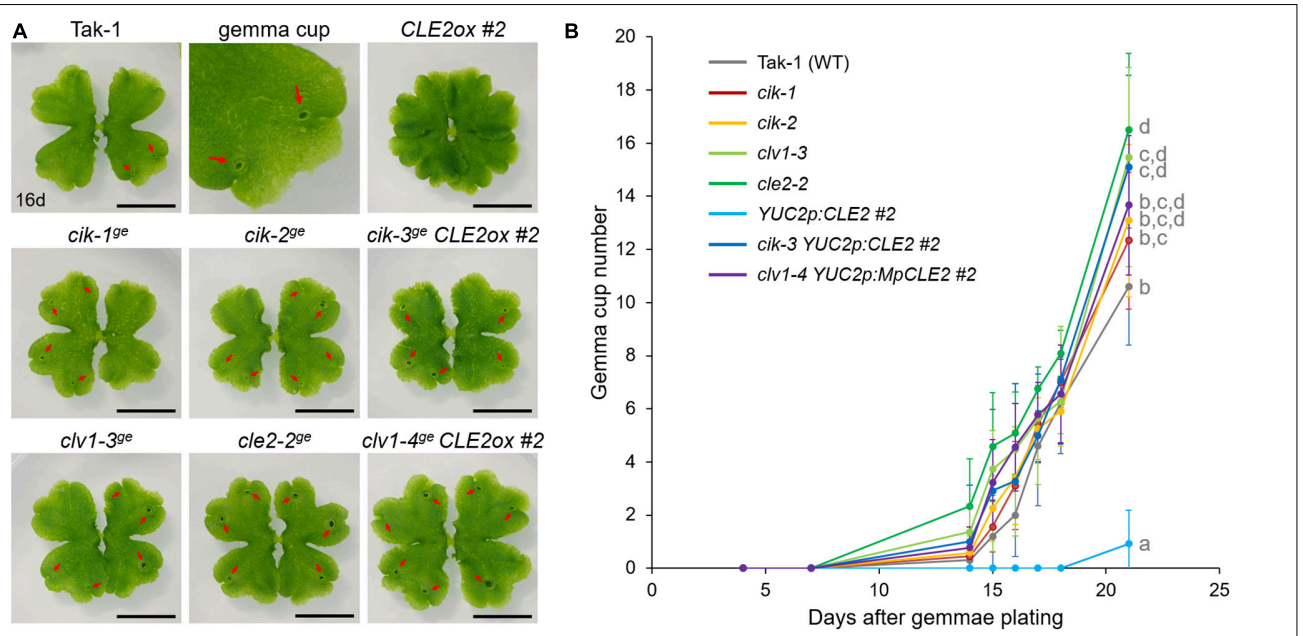

FIGURE 3 | Mp*CIK* knockout suppresses gain-of-function phenotypes of Mp*CLE2*. **(A)** Overall morphology of 16-day-old plants grown from gemmae. Genotypes are indicated above the panels. The upper middle panel shows the magnification of Tak-1 image. Note that $_{pro}$Mp*YUC2*:Mp*CLE2* (*CLE2ox*) exhibits multichotomy and produces no gemmae cups at this age while *cle2*, *clv1*, and *cik* loss-of-function alleles form more gemma cups compared to Tak-1. Arrows indicate gemma cups. Scale bars represent 1 cm. **(B)** Number of gemmae cups (mean and SD; n = 9–12). Data are obtained at 4, 7, 14, 15, 16, 17, 18, and 21 days after gemmae plating. Data of 21-day-old plants sharing the superscripts are not significantly different from each other in Tukey's HSD test, $p < 0.05$. This experiment was repeated twice with similar results.

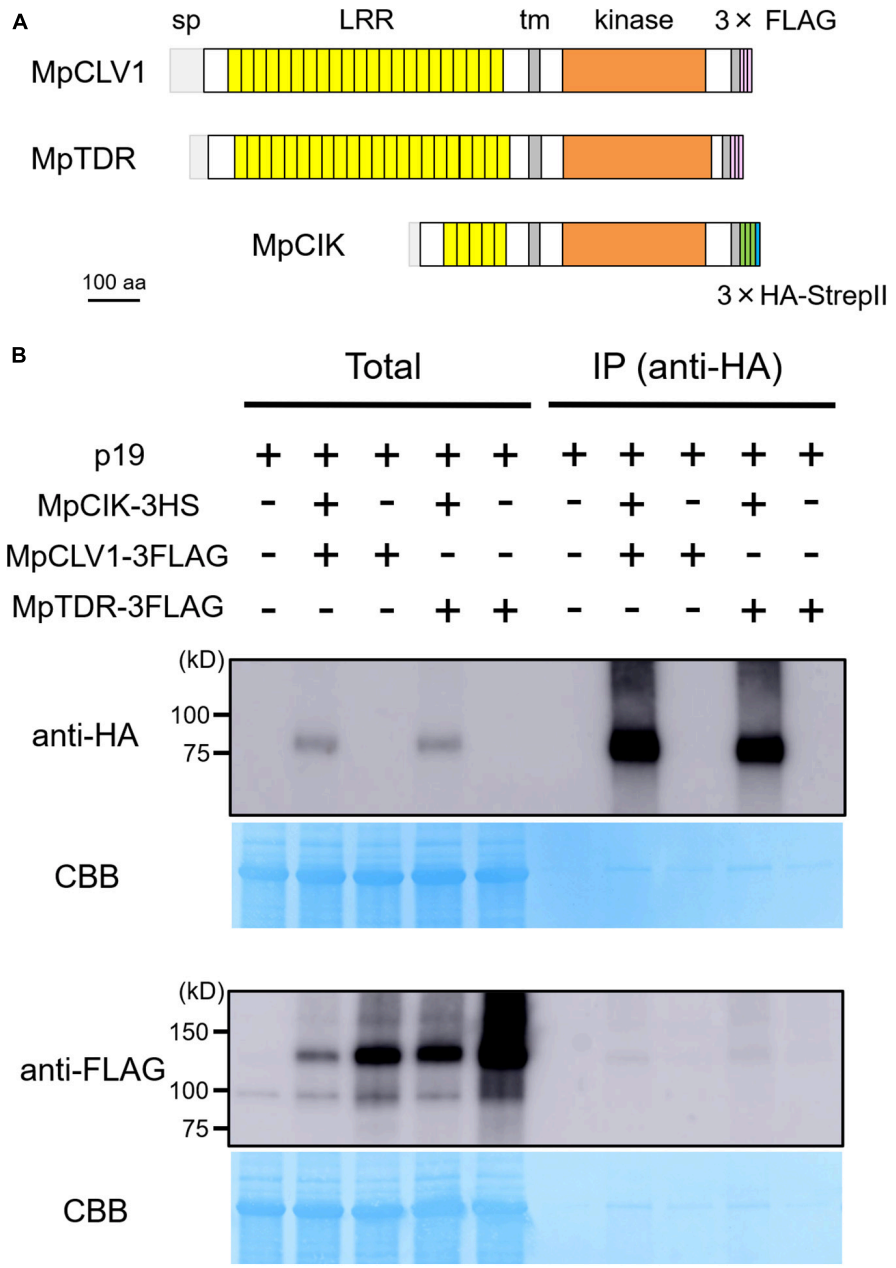

FIGURE 4 | MpCIK weakly associates with MpCLV1 and MpTDR in *N. benthamiana.* **(A)** Schematic illustration of expressed receptors. **(B)** Co-immunoprecipitation experiment using anti-HA affinity matrix. The indicated combinations of MpCIK-3HS, MpCLV1-3FLAG and MpTDR-3FLAG constructs, together with p19 silencing suppressor, were transiently expressed in *N. benthamiana*. Total proteins were extracted and immunoprecipitated with anti-HA affinity matrix. Immunoblot analyses were performed using anti-HA or anti-FLAG antibody. In the presence of MpCIK-3HS, MpCLV1-3FLAG and MpTDR-3FLAG were co-precipitated with anti-HA affinity matrix. This experiment was repeated twice with similar results.

MpCIK-3HS (**Figure 4B**). Thus, MpCLV1 and MpTDR are capable of interacting with MpCIK.

Mp*cik* Is Sensitive to MpCLE1 and TDIF

Our biochemical data suggests that MpCIK could also function as a coreceptor for MpTDR upon the perception of MpCLE1, a TDIF-type CLE peptide. Previously, we showed that synthetic TDIF-type peptides cause slight reduction of overall growth and twisted lobes in *M. polymorpha* thalli (Hirakawa et al., 2019). In order to address the possible involvement of MpCIK in MpCLE1 signaling, we first examined the effects of TDIF, the strongest analog among known TDIF-type CLE peptides including MpCLE1 peptide. In 14-day-old plants grown from gemmae on growth medium supplemented with 3 μM TDIF, both Tak-1 and Mp*cik-1* showed slight reduction of overall growth and twist in the thallus lobes (**Figure 5A**), indicating

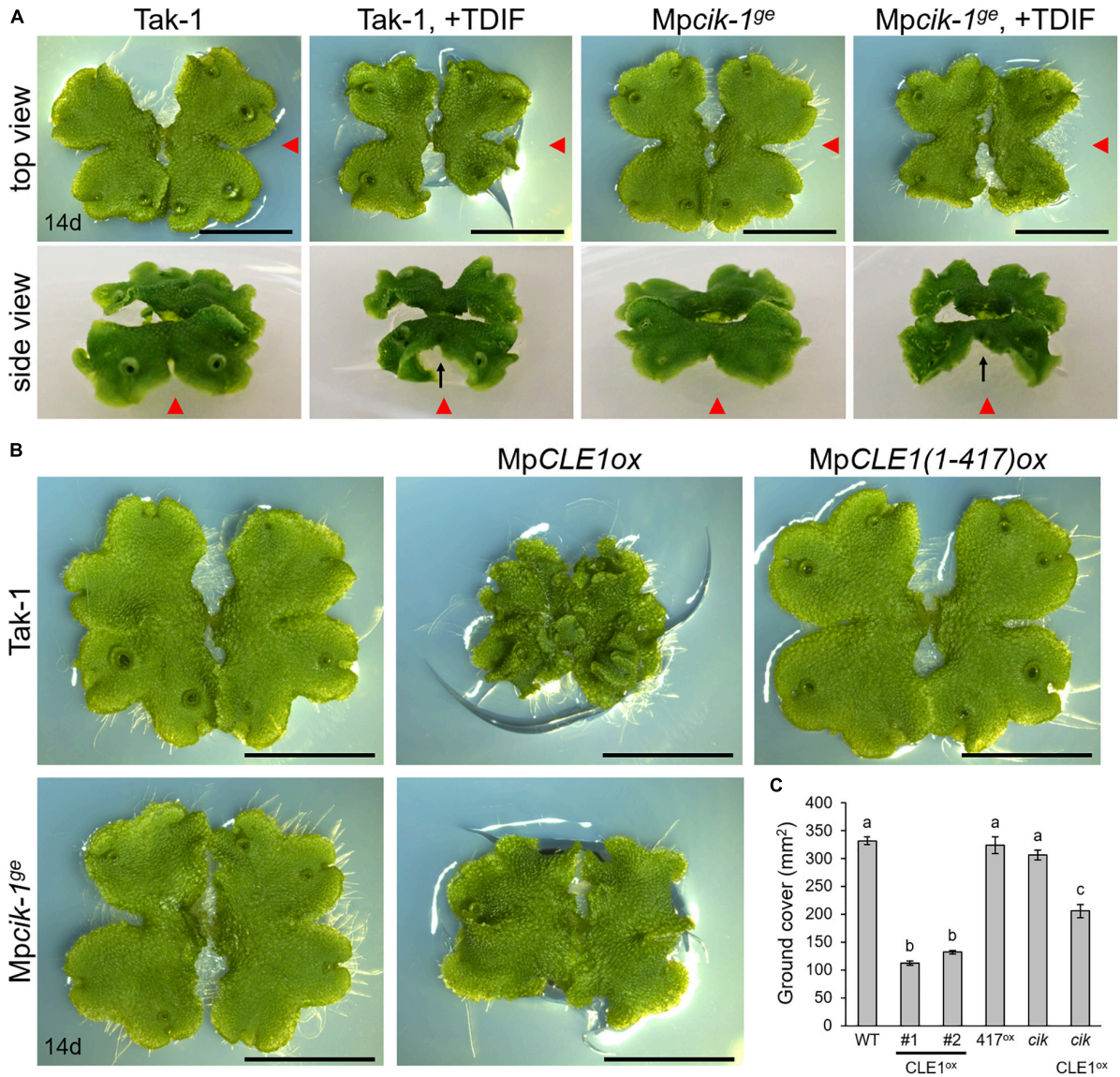

FIGURE 5 | Growth of Mp*cik* thalli is sensitive to MpCLE1/TDIF activity. **(A)** Overall morphology of 14-day-old plants grown from gemmae on medium supplemented with or without TDIF peptide as indicated above. Side view panels show the images taken from the right in the top view panels as indicated by red arrowheads. Note that thalli are twisted in plants treated with TDIF, resulting in the uplift of the thalli from the medium as indicated by arrows. **(B)** Overall morphology of 14-day-old plants grown from gemmae. MpCLE1*ox* indicates overexpression under Mp*YUC2* promoter ($_{pro}$Mp*YUC2*:Mp*CLE1*) in Tak-1 and Mp*cik-1*^{ge} background. Mp*CLE1(1-417)ox*, indicates a truncate version of Mp*CLE1*. **(C)** Ground cover in 14-day-old plants (mean and SD; n = 11–14). Means sharing the superscripts are not significantly different from each other in Tukey's HSD test, $p < 0.05$. Scale bars represent 1 cm in panels **(A)** and **(B)**.

that Mp*CIK* is not necessary for the perception of TDIF. We further analyzed the effects of MpCLE1 overexpression using $_{pro}$Mp*YUC2*:Mp*CLE1* transformants. In the wild-type (Tak-1) background, $_{pro}$Mp*YUC2*:Mp*CLE1* resulted in small, twisted thalli in 14-day-old plants. This phenotype was not observed in $_{pro}$Mp*YUC2*:Mp*CLE1*$^{1-417}$, a truncated version of MpCLE1 lacking an essential asparagine residue in the CLE peptide motif (**Figure 5B**; Hirakawa et al., 2019). In the Mp*cik-1*^{ge} background, $_{pro}$Mp*YUC2*:Mp*CLE1* also resulted in small twisted thalli although the effects on growth was mild compared to the Tak-1 background, as judged from the ground cover area in 14-day-old plants (**Figures 5B,C**). These data suggests that MpCIK could be partially involved in MpCLE1 perception.

DISCUSSION

In this study, we performed functional analysis of Mp*CIK*, the sole *M. polymorpha* ortholog of Arabidopsis *CIK* genes, and showed that MpCIK is essential for MpCLE2 peptide signaling to regulate the apical meristem activity in gametophyte. Biochemical analysis in *N. benthamiana* supports the idea that

the MpCLV1-MpCIK is a receptor–coreceptor pair for MpCLE2 peptide perception. Since the same ligand-receptor–coreceptor relationship of CLV3-CLV1-CIK is consistently observed for multiple paralogs in Arabidopsis (Anne et al., 2018; Cui et al., 2018; Hu et al., 2018), this system is likely an evolutionarily conserved mechanism for the perception of CLV3-type CLE peptide in land plants. In addition, we suggested partial involvement of MpCIK in signaling of TDIF-type CLE peptide, MpCLE1, although MpCIK is not necessary for MpCLE1 signaling. Studies in Arabidopsis have suggested that subclass-II receptors in the SERK subgroup function as coreceptors for TDIF-PXY/TDR signaling (Zhang et al., 2016b). Further studies on MpSERK would clarify the contribution of different coreceptors. The phylogenetic analysis inferred the divergence of CIK and SERK subgroups in the common ancestor of land plants, which coincides with the appearance of subclass-XI genes. Recent studies have also shown that SERK-interacting receptors from subclass X, such as BRI1/BRL and EMS1, are also encoded in bryophytes (Ferreira-Guerra et al., 2020; Furumizu and Sawa, 2021). Interestingly, the two sequences from *S. pratensis* (**Figure 1B**) showed high similarity to the subclass-II genes from land plants. Studies on Zygnematales algae would provide a clue to understand the evolution of these receptors.

Gemma cups are specialized structures for vegetative propagation, found in certain species of Marchantiopsida (Yasui et al., 2019; Kato et al., 2020). Gemma cup formation initiates at the cells in the dorsal epidermis close to the apical cells (Suzuki et al., 2020). We show that gain-of-function of Mp*CLE2* results in the delay of gemma cup formation. Loss-of-function phenotypes support that the intrinsic MpCLE2-MpCLV1-MpCIK signaling module functions as a negative regulator of gemma cup formation. Although it is still unclear if the phenotypes in gemma cup formation can be uncoupled from the defects in the apical/subapical cells, MpCLE2 likely regulates cell fates in both the lateral derivatives of the apical cells and the dorsal derivatives of apical/subapical cells. It is known that hormonal and environmental cues affect the formation of gemma cup (Flores-Sandoval et al., 2015; Aki et al., 2019; Li et al., 2020; Rico-Reséndiz et al., 2020). A possible role for MpCLE2 peptide signaling would be to mediate certain environmental cues to control the timing of gemma cup formation and thus clonal propagation, cooperatively with other hormonal inputs. In addition, involvement of CIK subgroup members into antiviral responses has been suggested in Arabidopsis (Fontes et al., 2004). Further studies of Mp*cik* knockout plants under various environmental conditions would provide a new insight into signals that allowed plants to survive on land.

Our biochemical data reveals that MpCIK is capable of associating with MpCLV1 or MpTDR in an ectopic and transient expression system of *N. benthamiana*. Furthermore, weak associations observed for MpCIK-MpCLV1 as well as MpCIK-MpTDR indicates possible requirement of other components in MpCIK-containing complex formation. For instance, in a ligand-induced dimerization model, receptor–coreceptor interaction can be induced by the perception of ligand at their ectodomains, which in turn allows for their kinase domains to transphosporylate and activate signaling (Jaillais et al., 2011; Hohmann et al., 2018; Perraki et al., 2018). Thus, ligand and/or other membrane receptors could be required for strong MpCIK-MpCLV1/MpTDR association. With its genetic simplicity in CLE signaling, *M. polymorpha* will be a nice experimental system to address this point in future studies.

MATERIALS AND METHODS

Phylogenetic Analysis

Gene sequences of land plants were retrieved from Phytozome v12.1 database[1] except for those of *Arabidopsis thaliana*[2], *Picea abies*[3], and *Marchantia polymorpha*[4]. Sequences of charophycean algae were reported in Bowman et al. (2017), obtained from transcriptome databases for *Spirogyra pratensis*[5] and *Coleochaete orbicularis*[6]. Gene IDs and the protein sequences are listed in **Supplementary Table 1**. Predicted protein sequences were aligned in Clustal W[7]. We excluded ambiguously aligned sequence to produce an alignment of 297 amino acid characters in the conserved cytosolic domain. Bayesian analysis was performed using MrBayes 3.2.7 (Ronquist et al., 2012). Two runs with four chains of Markov chain Monte Carlo (MCMC) iterations were performed for 1,500,000 generations, keeping one tree every 100 generations. The first 25% of the generations were discarded as burn-in and the remaining trees were used to calculate a 50% majority-rule tree. The standard deviation for the two MCMC iteration runs was below 0.01, suggesting that it was sufficient for the convergens of the two runs. Convergence was assessed by visual inspection of the plot of the log likelihood scores of the two runs calculated by MrBayes (Gelman and Rubin, 1992). Character matrix used for the Bayesian phylogenetic analysis is provided in **Supplementary Data Sheet 1**.

Plant Materials and Growth Conditions

Marchantia polymorpha male Takaragaike-1 (Tak-1) accession was used as wild type in this study. *M. polymorpha* plants were grown on half-strength Gamborg B5 medium (pH 5.5) solidified with 1.4% agar at 22°C under continuous white light. *N. benthamiana* seeds were grown on BM2 soil (Berger) in a growth room at 23°C under continuous LED light.

Peptide Treatment

Synthetic peptides used in this study were analytically pure and dissolved in 0.1% TFA (trifluoroacetic acid) solution as stock solutions. For MpCLE2 peptide treatment, approximately 20 mature gemmae were floated on 2 mL liquid M51C medium containing 2% sucrose supplemented with 3 μM MpCLE2 peptide (KEVHypNGHypNPLHN) or mock (TFA)

[1] https://phytozome.jgi.doe.gov/pz/portal.html

[2] https://www.arabidopsis.org/

[3] http://congenie.org/

[4] https://marchantia.info/

[5] http://www.ncbi.nlm.nih.gov/Traces/wgs/wgsviewer.cgi?val=GBSM01&search=GBSM01000000&display=scaffolds

[6] http://www.ncbi.nlm.nih.gov/Traces/wgs/wgsviewer.cgi?val=GBSL01&search=GBSL01000000&display=scaffolds

[7] https://www.genome.jp/tools-bin/clustalw

solution, in 12-well plates as described previously (Hirakawa et al., 2020). For the TDIF treatment, gemmae were plated on half-strength B5 agar plates supplemented with 3 μM TDIF (HEVHypSGHypNPISN) or mock (TFA) solution as described previously (Hirakawa et al., 2019).

Constructs

Primers and plasmids are listed in **Supplementary Tables 2, 3**. All plant transformation vectors were generated using the Gateway cloning system (Thermo Fisher Scientific, Waltham, MA, United States). Gateway destination vectors are described in Kinoshita et al. (2010); Ishizaki et al. (2015), and Sugano et al. (2018), except for pMpGWB301-YUC2p, which was generated in this study. A 3,032 bp DNA flagment of Mp*YUC2* promoter sequence franking the translation initiation site was PCR amplified from pENTR-proMpYUC2 vector (Hirakawa et al., 2020) with a primer pair of MpYUC2prom3k_F_InFusion_*Xba*I and MpYUC2prom_R_InFusion_*Xba*I, and cloned into the *Xba*I digestion site of pMpGWB301 using In-Fusion HD Cloning Kit (Takara Bio, Shiga, Japan). For construction of $_{pro}$Mp*YUC2*:Mp*CLE1*, entry clones, pENTR-MpCLE1 and pENTR-MpCLE(1-417) (Hirakawa et al., 2019), were transferred to the pMpGWB301-YUC2p vector using Gateway LR Clonase II Enzyme mix (Thermo Fisher Scientific). For genome editing of Mp*CIK*, a guide RNA was designed at the first exon/intron junction of Mp7g14210 using CRISPRdirect[8] (Naito et al., 2015) and the plasmid for genome editing was constructed according to Sugano et al. (2018). For the expression of epitope-tagged receptors in *N. benthamiana*, coding sequences of Mp*CIK*, Mp*CLV1*, and Mp*TDR* were PCR amplified from *M. polymopha* cDNA and cloned into pENTR/D-TOPO vector. Resultant entry clones (pENTR-MpCIK, pENTR-MpCLV1, and pENTR-MpTDR) were transferred to pXCSG-3FLAG or pXCSG-3HS vector using Gateway LR Clonase II Enzyme mix (Thermo Fisher Scientific).

Production of Transgenic *Marchantia polymorpha*

Transgenic *M. polymorpha* plants are listed in **Supplementary Table 3**. *Agrobacterium*-mediated transformation of *M. polymorpha* was performed using regenerating thalli according to Kubota et al. (2013). CRISPR/Cas9-based genome editing was performed according to Sugano et al. (2018) and mutations in the guide RNA target loci were examined by direct sequencing of PCR product amplified from genome DNA samples with primers listed in **Supplementary Table 2**. Genome editing of Mp*CLV1* was performed as described previously (Hirakawa et al., 2020). Nomenclature of genes and mutants are according to Bowman et al. (2016).

Plant Imaging and Phenotypic Measurement

Overall morphology of plants was observed under a digital microscope (DMS1000, Leica Microsystems, Wetzlar, Germany) or under a digital camera (TG-6, Olympus, Tokyo, Japan). For the quantification of ground cover area in plant images, blue color was extracted and quantified using ImageJ (Schneider et al., 2012). For the measurement of apical notch width, plants grown on liquid medium were individually transferred onto agar medium and imaged under a digital microscope (DMS 1000, Leica Microsystems). To quantify the apical notch width, distance between the rims of apical notch was measured on the obtained images using ImageJ (Schneider et al., 2012). Confocal imaging of apical notch was performed as described previously (Hirakawa et al., 2020). Briefly, 2-day-old gemmalings were fixed by vacuum infiltration in 4% paraformaldehyde in phosphate buffer (Nacalai Tesque, Kyoto, Japan). After fixation, samples were cleared with ClearSee solution (FUJIFILM Wako Pure Chemical Corporation, Osaka, Japan) and were stained for an hour with SCRI Renaissance 2200 (Renaissance Chemicals, Selby, United Kingdom) in ClearSee solution. Samples were observed under a confocal laser scanning microscopy (Fluoview FV1000, Olympus) using 405-nm excitation. Z-series images were collected at 0.5 μm intervals through the specimens and obtained images were processed using Fiji software to specify apical and subapical cells (Schindelin et al., 2012).

Promoter GUS Assay

Individual plants were stained separately in 30–50 μL GUS staining solution (50 mM sodium phosphate buffer pH 7.2, 1 mM potassium-ferrocyanide, 1 mM potassium-ferricyanide, 10 mM EDTA, 0.01% Triton X-100 and 1 mM 5-bromo-4-chloro-3-indolyl-β-D-glucuronic acid) at 37°C in dark. GUS-stained samples were washed with water, cleared with ethanol and mounted with clearing solution for imaging under a light microscope (BX51, Olympus).

Transient Expression in *Nicotiana benthamiana*

Agrobacterium tumefaciens strains GV3101 MP90RK carrying expression constructs were grown in YEB medium with appropriate antibiotics, harvested by centrifugation at 4,500 rpm for 10 min, and resuspended in infiltration buffer [10 mM MES (pH 5.7), 10 mM MgCl2, 150 μM acetosyringone]. The cultures were adjusted to an OD 600 of 1.0 and incubated at room temperature for at least 3 h prior to infiltration. Equal volumes of cultures of different constructs were mixed for co-infiltration, and then mixed with agrobacterial cultures (OD 600 of 1.0) carrying the p19 silencing suppressor in a 1:1 ratio (Voinnet et al., 1999). The resulting cultures were infiltrated into leaves of 3- to 4-week-old *N. benthamiana*. The leaf samples were harvested 3 days after infiltration for subsequent protein extraction (Betsuyaku et al., 2011).

Protein Extraction

Total protein was extracted from the infiltrated *N. benthamiana* leaves with IP extraction buffer (1:1 w/v, 50 mM Tris–HCl pH 8.0,

[8]https://crispr.dbcls.jp/

150 mM NaCl, 10% glycerol, 1% Triton X-100, 1 × Proteinase inhibitor cocktail SIGMA P9599 and 1 mM EDTA) and incubate the extract at 4°C for 30 min. The lysates were centrifuged at 20,000 × g for 20 min at 4°C and the supernatants were then centrifuged again at 20,000 × *g* for 5 min at 4°C. The resultant supernatants were used as total protein lysates.

Co-immunoprecipitation

For immunoprecipitation, 1 ml of the lysates prepared with IP extraction buffer from 0.5 g of leaves was incubated with anti-HA Affinity Matrix (Roche 11815016) for o/n in a rotary shaker at 4°C. The beads were collected and washed three times with 1 ml of the extraction buffer. Immunoprecipitated proteins were eluted from the beads by boiling in SDS sample buffer at 95°C and analyzed by Western blot using the corresponding antibodies. We used the following antibodies; Anti-HA-Peroxidase High Affinity (3F10) (Roche 12013819001) and Monoclonal ANTI-FLAG M2-Peroxidase (HRP) (SIGMA A8592).

DATA AVAILABILITY STATEMENT

The original contributions presented in the study are included in the article/**Supplementary Material**, further inquiries can be directed to the corresponding author.

AUTHOR CONTRIBUTIONS

YH conceived the study, designed the work with input from all authors, and prepared the manuscript draft. GT, SB, NO, and YH performed the experiments and analyzed the data. All authors contributed to the article and approved the submitted version.

FUNDING

This work was supported by grants from the Japan Science and Technology Agency ERATO (JPMJER1502 to SB) and JSPS KAKENHI (JP19K06727 to YH).

ACKNOWLEDGMENTS

We thank colleagues in the peptide/protein center of WPI-ITbM for peptide synthesis, Eriko Betsuyaku and Ikuko Nakanomyo for technical assistance.

SUPPLEMENTARY MATERIAL

The Supplementary Material for this article can be found online at: https://www.frontiersin.org/articles/10.3389/fpls.2021.657548/full#supplementary-material

REFERENCES

Aki, S. S., Mikami, T., Naramoto, S., Nishihama, R., Ishizaki, K., Kojima, M., et al. (2019). Cytokinin signaling is essential for organ formation in *Marchantia polymorpha*. *Plant Cell Physiol.* 60, 1842–1854. doi: 10.1093/pcp/pcz100

Anne, P., Amiguet-Vercher, A., Brandt, B., Kalmbach, L., Geldner, N., Hothorn, M., et al. (2018). CLERK is a novel receptor kinase required for sensing of root-active CLE peptides in *Arabidopsis*. *Development* 145:dev162354. doi: 10.1242/dev.162354

Araya, T., Miyamoto, M., Wibowo, J., Suzuki, A., Kojima, S., Tsuchiya, Y. N., et al. (2014). CLE-CLAVATA1 peptide-receptor signaling module regulates the expansion of plant root systems in a nitrogen-dependent manner. *Proc. Natl. Acad. Sci. U.S.A.* 111, 2029–2034. doi: 10.1073/pnas.1319953111

Betsuyaku, S., Takahashi, F., Kinoshita, A., Miwa, H., Shinozaki, K., Fukuda, H., et al. (2011). Mitogen-activated protein kinase regulated by the CLAVATA receptors contributes to shoot apical meristem homeostasis. *Plant Cell Physiol.* 52, 14–29. doi: 10.1093/pcp/pcq157

Bowman, J. L., Araki, T., Arteaga-Vazquez, M. A., Berger, F., Dolan, L., Haseloff, J., et al. (2016). The naming of names: guidelines for gene nomenclature in Marchantia. *Plant Cell Physiol.* 57, 257–261.

Bowman, J. L., Kohchi, T., Yamato, K. T., Jenkins, J., Shu, S., Ishizaki, K., et al. (2017). Insights into land plant evolution garnered from the *Marchantia polymorpha* genome. *Cell* 171, 287–304.

Cock, J. M., and McCormick, S. (2001). A large family of genes that share homology with CLAVATA3. *Plant Physiol.* 126, 939–942. doi: 10.1104/pp.126.3.939

Crook, A. D., Willoughby, A. C., Hazak, O., Okuda, S., VanDerMolen, K. R., Soyars, C. L., et al. (2020). BAM1/2 receptor kinase signaling drives CLE peptide-mediated formative cell divisions in *Arabidopsis* roots. *Proc. Natl. Acad. Sci. U.S.A.* 117, 32750–32756. doi: 10.1073/pnas.2018565117

Cui, Y., Hu, C., Zhu, Y., Cheng, K., Li, X., Wei, Z., et al. (2018). CIK receptor kinases determine cell fate specification during early anther development in *Arabidopsis*. *Plant Cell* 30, 2383–2401. doi: 10.1105/tpc.17.00586

Czyzewicz, N., Shi, C. L., Vu, L. D., Van De Cotte, B., Hodgman, C., Butenko, M. A., et al. (2015). Modulation of *Arabidopsis* and monocot root architecture by CLAVATA3/EMBRYO SURROUNDING REGION 26 peptide. *J. Exp. Bot.* 66, 5229–5243. doi: 10.1093/jxb/erv360

Depuydt, S., Rodriguez-Villalon, A., Santuari, L., Wyser-Rmili, C., Ragni, L., and Hardtke, C. S. (2013). Suppression of Arabidopsis protophloem differentiation and root meristem growth by CLE45 requires the receptor-like kinase BAM3. *Proc. Natl. Acad. Sci. U.S.A.* 110, 7074–7079. doi: 10.1073/pnas.1222314110

DeYoung, B. J., Bickle, K. L., Schrage, K. J., Muskett, P., Patel, K., and Clark, S. E. (2006). The CLAVATA1-related BAM1, BAM2 and BAM3 receptor kinase-like proteins are required for meristem function in *Arabidopsis*. *Plant J.* 45, 1–16. doi: 10.1111/j.1365-313x.2005.02592.x

Doblas, V. G., Smakowska-Luzan, E., Fujita, S., Alassimone, J., Barberon, M., Madalinski, M., et al. (2017). Root diffusion barrier control by a vasculature-derived peptide binding to the SGN3 receptor. *Science* 355, 280–284. doi: 10.1126/science.aaj1562

Doll, N. M., Royek, S., Fujita, S., Okuda, S., Chamot, S., Stintzi, A., et al. (2020). A two-way molecular dialogue between embryo and endosperm is required for seed development. *Science* 367, 431–435. doi: 10.1126/science.aaz4131

Eklund, D. M., Ishizaki, K., Flores-Sandoval, E., Kikuchi, S., Takebayashi, Y., Tsukamoto, S., et al. (2015). Auxin produced by the indole-3-pyruvic acid pathway regulates development and gemmae dormancy in the liverwort *Marchantia polymorpha*. *Plant Cell* 27, 1650–1669. doi: 10.1105/tpc.15.00065

Endo, S., Shinohara, H., Matsubayashi, Y., and Fukuda, H. (2013). A novel pollen-pistil interaction conferring high-temperature tolerance during reproduction via CLE45 signaling. *Curr. Biol.* 23, 1670–1676. doi: 10.1016/j.cub.2013.06.060

Etchells, J. P., and Turner, S. R. (2010). The PXY-CLE41 receptor ligand pair defines a multifunctional pathway that controls the rate and orientation of vascular cell division. *Development* 137, 767–774. doi: 10.1242/dev.044941

Ferreira-Guerra, M., Marquès-Bueno, M., Mora-García, S., and Caño-Delgado, A. I. (2020). Delving into the evolutionary origin of steroid sensing in plants. *Curr. Opin. Plant Biol.* 57, 87–95. doi: 10.1016/j.pbi.2020.06.005

Fisher, K., and Turner, S. (2007). PXY, a receptor-like kinase essential for maintaining polarity during plant vascular-tissue development. *Curr. Biol.* 17, 1061–1066. doi: 10.1016/j.cub.2007.05.049

Fiume, E., and Fletcher, J. C. (2012). Regulation of *Arabidopsis* embryo and endosperm development by the polypeptide signaling molecule CLE8. *Plant Cell* 24, 1000–1012. doi: 10.1105/tpc.111.094839

Fletcher, J. C. (2020). Recent advances in *Arabidopsis* CLE peptide signaling. *Trends Plant Sci.* 25, 1005–1016. doi: 10.1016/j.tplants.2020.04.014

Fletcher, J. C., Brand, U., Running, M. P., Simon, R., and Meyerowitz, E. M. (1999). Signaling of cell fate decisions by CLAVATA3 in *Arabidopsis* shoot meristems. *Science* 283, 1911–1914. doi: 10.1126/science.283.5409.1911

Flores-Sandoval, E., Eklund, D. M., and Bowman, J. L. (2015). A simple auxin transcriptional response system regulates multiple morphogenetic processes in the liverwort *Marchantia polymorpha*. *PLoS Genet.* 11:e1005207. doi: 10.1371/journal.pgen.1005207

Fontes, E. P., Santos, A. A., Luz, D. F., Waclawovsky, A. J., and Chory, J. (2004). The geminivirus nuclear shuttle protein is a virulence factor that suppresses transmembrane receptor kinase activity. *Genes. Dev.* 18, 2545–2556. doi: 10.1101/gad.1245904

Furumizu, C., and Sawa, S. (2021). Insight into early diversification of leucine-rich repeat receptor-like kinases provided by the sequenced moss and hornwort genomes. *Plant Mol. Biol.* [Epub ahead of print]. doi: 10.1007/s11103-020-01100-0

Gelman, A., and Rubin, D. B. (1992). Inference from iterative simulation using multiple sequences. *Statist. Sci.* 7, 457–472.

Gou, X., and Li, J. (2020). Paired receptor and coreceptor kinases perceive extracellular signals to control plant development. *Plant Physiol.* 182, 1667–1681. doi: 10.1104/pp.19.01343

Gutiérrez-Alanís, D., Yong-Villalobos, L., Jiménez-Sandoval, P., Alatorre-Cobos, F., Oropeza-Aburto, A., Mora-Macías, J., et al. (2017). Phosphate starvation-dependent iron mobilization induces CLE14 expression to trigger root meristem differentiation through CLV2/PEPR2 signaling. *Dev. Cell* 41, 555–570. doi: 10.1016/j.devcel.2017.05.009

Hirakawa, Y., Fujimoto, T., Ishida, S., Uchida, N., Sawa, S., Kiyosue, T., et al. (2020). Induction of multichotomous branching by CLAVATA peptide in *Marchantia polymorpha*. *Curr. Biol.* 30, 3833–3840. doi: 10.1016/j.cub.2020.07.016

Hirakawa, Y., Kondo, Y., and Fukuda, H. (2010). TDIF peptide signaling regulates vascular stem cell proliferation via the WOX4 homeobox gene in *Arabidopsis*. *Plant Cell* 22, 2618–2629. doi: 10.1105/tpc.110.076083

Hirakawa, Y., and Sawa, S. (2019). Diverse function of plant peptide hormones in local signaling and development. *Curr. Opin. Plant. Biol.* 51, 81–87. doi: 10.1016/j.pbi.2019.04.005

Hirakawa, Y., Shinohara, H., Kondo, Y., Inoue, A., Nakanomyo, I., Ogawa, M., et al. (2008). Non-cell-autonomous control of vascular stem cell fate by a CLE peptide/receptor system. *Proc. Natl. Acad. Sci. U.S.A.* 105, 15208–15213. doi: 10.1073/pnas.0808444105

Hirakawa, Y., Shinohara, H., Welke, K., Irle, S., Matsubayashi, Y., Torii, K. U., et al. (2017). Cryptic bioactivity capacitated by synthetic hybrid plant peptides. *Nat. Commun.* 8:14318.

Hirakawa, Y., Uchida, N., Yamaguchi, Y. L., Tabata, R., Ishida, S., Ishizaki, K., et al. (2019). Control of proliferation in the haploid meristem by CLE peptide signaling in *Marchantia polymorpha*. *PLoS Genet.* 15:e1007997. doi: 10.1371/journal.pgen.1007997

Hohmann, U., Lau, K., and Hothorn, M. (2017). The structural basis of ligand perception and signal activation by receptor kinases. *Annu. Rev. Plant Biol.* 68, 109–137. doi: 10.1146/annurev-arplant-042916-040957

Hohmann, U., Santiago, J., Nicolet, J., Olsson, V., Spiga, F. M., Hothorn, L. A., et al. (2018). Mechanistic basis for the activation of plant membrane receptor kinases by SERK-family coreceptors. *Proc. Natl. Acad. Sci. U.S.A.* 115, 3488–3493. doi: 10.1073/pnas.1714972115

Hou, S., Wang, X., Chen, D., Yang, X., Wang, M., Turrà, D., et al. (2014). The secreted peptide PIP1 amplifies immunity through receptor-like kinase 7. *PLoS Pathog.* 10:e1004331. doi: 10.1371/journal.ppat.1004331

Hu, C., Zhu, Y., Cui, Y., Cheng, K., Liang, W., Wei, Z., et al. (2018). A group of receptor kinases are essential for CLAVATA signalling to maintain stem cell homeostasis. *Nat. Plants* 4, 205–211. doi: 10.1038/s41477-018-0123-z

Ishizaki, K., Nishihama, R., Ueda, M., Inoue, K., Ishida, S., Nishimura, Y., et al. (2015). Development of gateway binary vector series with four different selection markers for the liverwort *Marchantia polymorpha*. *PLoS One* 10:e0138876. doi: 10.1371/journal.pone.0138876

Ito, Y., Nakanomyo, I., Motose, H., Iwamoto, K., Sawa, S., Dohmae, N., et al. (2006). Dodeca-CLE peptides as suppressors of plant stem cell differentiation. *Science* 313, 842–845. doi: 10.1126/science.1128436

Jaillais, Y., Belkhadir, Y., Balsemão-Pires, E., Dangl, J. L., and Chory, J. (2011). Extracellular leucine-rich repeats as a platform for receptor/coreceptor complex formation. *Proc. Natl. Acad. Sci. U.S.A.* 108, 8503–8507. doi: 10.1073/pnas.1103556108

Jun, J., Fiume, E., Roeder, A. H., Meng, L., Sharma, V. K., Osmont, K. S., et al. (2010). Comprehensive analysis of CLE polypeptide signaling gene expression and overexpression activity in Arabidopsis. *Plant Physiol.* 154, 1721–1736. doi: 10.1104/pp.110.163683

Kato, H., Yasui, Y., and Ishizaki, K. (2020). Gemma cup and gemma development in *Marchantia polymorpha*. *New Phytol.* 228, 459–465. doi: 10.1111/nph.16655

Kinoshita, A., Betsuyaku, S., Osakabe, Y., Mizuno, S., Nagawa, S., Stahl, Y., et al. (2010). RPK2 is an essential receptor-like kinase that transmits the CLV3 signal in *Arabidopsis*. *Development* 137, 3911–3920. doi: 10.1242/dev.048199

Kondo, Y., Hirakawa, Y., Kieber, J. J., and Fukuda, H. (2011). CLE peptides can negatively regulate protoxylem vessel formation via cytokinin signaling. *Plant Cell Physiol.* 52, 37–48. doi: 10.1093/pcp/pcq129

Kondo, T., Sawa, S., Kinoshita, A., Mizuno, S., Kakimoto, T., Fukuda, H., et al. (2006). A plant peptide encoded by *CLV3* identified by in situ MALDI-TOF MS analysis. *Science* 313, 845–848. doi: 10.1126/science.1128439

Kubota, A., Ishizaki, K., Hosaka, M., and Kohchi, T. (2013). Efficient Agrobacterium-mediated transformation of the liverwort *Marchantia polymorpha* using regenerating thalli. *Biosci. Biotechnol. Biochem.* 77, 167–172.

Li, D., Flores-Sandoval, E., Ahtesham, U., Coleman, A., Clay, J. M., Bowman, J. L., et al. (2020). Ethylene-independent functions of the ethylene precursor ACC in *Marchantia polymorpha*. *Nat. Plants* 6, 1335–1344. doi: 10.1038/s41477-020-00784-y

Ma, D., Endo, S., Betsuyaku, S., Shimotohno, A., and Fukuda, H. (2020). CLE2 regulates light-dependent carbohydrate metabolism in *Arabidopsis* shoots. *Plant Mol. Biol.* 104, 561–574. doi: 10.1007/s11103-020-01059-y

Matsubayashi, Y. (2014). Posttranslationally modified small-peptide signals in plants. *Annu. Rev. Plant Biol.* 65, 385–413. doi: 10.1146/annurev-arplant-050312-120122

Montgomery, S. A., Tanizawa, Y., Galik, B., Wang, N., Ito, T., Mochizuki, T., et al. (2020). Chromatin organization in early land plants reveals an ancestral association between H3K27me3, transposons, and constitutive heterochromatin. *Curr. Biol.* 30, 573–588. doi: 10.1016/j.cub.2019.12.015

Morita, J., Kato, K., Nakane, T., Kondo, Y., Fukuda, H., Nishimasu, H., et al. (2016). Crystal structure of the plant receptor-like kinase TDR in complex with the TDIF peptide. *Nat. Commun.* 7:12383.

Morris, J. L., Puttick, M. N., Clark, J. W., Edwards, D., Kenrick, P., Pressel, S., et al. (2018). The timescale of early land plant evolution. *Proc. Natl. Acad. Sci. U.S.A.* 115, E2274–E2283.

Mortier, V., Den Herder, G., Whitford, R., Van de Velde, W., Rombauts, S., D'Haeseleer, et al. (2010). CLE peptides control *Medicago truncatula* nodulation locally and systemically. *Plant Physiol.* 153, 222–237. doi: 10.1104/pp.110.153718

Murphy, E., Smith, S., and De Smet, I. (2012). Small signaling peptides in *Arabidopsis* development: how cells communicate over a short distance. *Plant Cell* 24, 3198–3217. doi: 10.1105/tpc.112.099010

Naito, Y., Hino, K., Bono, H., and Ui-Tei, K. (2015). CRISPRdirect: software for designing CRISPR/Cas guide RNA with reduced off-target sites. *Bioinformatics* 31, 1120–1123. doi: 10.1093/bioinformatics/btu743

Nakayama, T., Shinohara, H., Tanaka, M., Baba, K., Ogawa-Ohnishi, M., and Matsubayashi, Y. (2017). A peptide hormone required for Casparian strip diffusion barrier formation in *Arabidopsis* roots. *Science* 355, 284–286. doi: 10.1126/science.aai9057

Oelkers, K., Goffard, N., Weiller, G. F., Gresshoff, P. M., Mathesius, U., and Frickey, T. (2008). Bioinformatic analysis of the CLE signaling peptide family. *BMC Plant Biol.* 8:1. doi: 10.1186/1471-2229-8-1

Ogawa, M., Shinohara, H., Sakagami, Y., and Matsubayashi, Y. (2008). Arabidopsis CLV3 peptide directly binds CLV1 ectodomain. *Science* 319:294. doi: 10.1126/science.1150083

Ohyama, K., Shinohara, H., Ogawa-Ohnishi, M., and Matsubayashi, Y. (2009). A glycopeptide regulating stem cell fate in *Arabidopsis thaliana*. *Nat. Chem. Biol.* 5, 578–580. doi: 10.1038/nchembio.182

Okamoto, S., Ohnishi, E., Sato, S., Takahashi, H., Nakazono, M., Tabata, S., et al. (2009). Nod factor/nitrate-induced CLE genes that drive HAR1-mediated systemic regulation of nodulation. *Plant Cell Physiol.* 50, 67–77. doi: 10.1093/pcp/pcn194

Okuda, S., Fujita, S., Moretti, A., Hohmann, U., Doblas, V. G., Ma, Y., et al. (2020). Molecular mechanism for the recognition of sequence-divergent CIF peptides by the plant receptor kinases GSO1/SGN3 and GSO2. *Proc. Natl. Acad. Sci. U.S.A.* 117, 2693–2703. doi: 10.1073/pnas.1911553117

Ou, Y., Lu, X., Zi, Q., Xun, Q., Zhang, J., Wu, Y., et al. (2016). RGF1 INSENSITIVE 1 to 5, a group of LRR receptor-like kinases, are essential for the perception of root meristem growth factor 1 in *Arabidopsis thaliana*. *Cell Res.* 26, 686–698. doi: 10.1038/cr.2016.63

Perraki, A., DeFalco, T. A., Derbyshire, P., Avila, J., Séré, D., Sklenar, J., et al. (2018). Phosphocode-dependent functional dichotomy of a common co-receptor in plant signalling. *Nature* 561, 248–252. doi: 10.1038/s41586-018-0471-x

Puttick, M. N., Morris, J. L., Williams, T. A., Cox, C. J., Edwards, D., Kenrick, P., et al. (2018). The interrelationships of land plants and the nature of the ancestral embryophyte. *Curr. Biol.* 28, 733–745. doi: 10.1016/j.cub.2018.01.063

Qian, P., Song, W., Yokoo, T., Minobe, A., Wang, G., Ishida, T., et al. (2018). The CLE9/10 secretory peptide regulates stomatal and vascular development through distinct receptors. *Nat. Plants* 4, 1071–1081. doi: 10.1038/s41477-018-0317-4

Rico-Reséndiz, F., Cervantes-Pérez, S. A., Espinal-Centeno, A., Dipp-Álvarez, M., Oropeza-Aburto, A., Hurtado-Bautista, E., et al. (2020). Transcriptional and morpho-physiological responses of *Marchantia polymorpha* upon phosphate starvation. *Int. J. Mol. Sci.* 21:8354. doi: 10.3390/ijms21218354

Rodríguez-Leal, D., Lemmon, Z. H., Man, J., Bartlett, M. E., and Lippman, Z. B. (2017). Engineering quantitative trait variation for crop improvement by genome editing. *Cell* 171, 470–480. doi: 10.1016/j.cell.2017.08.030

Rodriguez-Villalon, A., Gujas, B., Kang, Y. H., Breda, A. S., Cattaneo, P., Depuydt, S., et al. (2014). Molecular genetic framework for protophloem formation. *Proc. Natl. Acad. Sci. U.S.A.* 111, 11551–11556. doi: 10.1073/pnas.1407337111

Ronquist, F., Teslenko, M., van der Mark, P., Ayres, D. L., Darling, A., Höhna, S., et al. (2012). MrBayes 3.2: efficient Bayesian phylogenetic inference and model choice across a large model space. *Syst. Biol.* 61, 539–542. doi: 10.1093/sysbio/sys029

Santiago, J., Brandt, B., Wildhagen, M., Hohmann, U., Hothorn, L. A., Butenko, M. A., et al. (2016). Mechanistic insight into a peptide hormone signaling complex mediating floral organ abscission. *eLife* 5:e15075.

Santiago, J., Henzler, C., and Hothorn, M. (2013). Molecular mechanism for plant steroid receptor activation by somatic embryogenesis co-receptor kinases. *Science* 341, 889–892. doi: 10.1126/science.1242468

Sasaki, G., Katoh, K., Hirose, N., Suga, H., Kuma, K., Miyata, T., et al. (2007). Multiple receptor-like kinase cDNAs from liverwort *Marchantia polymorpha* and two charophycean green algae, *Closterium ehrenbergii* and *Nitella axillaris*: extensive gene duplications and gene shufflings in the early evolution of streptophytes. *Gene* 401, 135–144. doi: 10.1016/j.gene.2007.07.009

Schindelin, J., Arganda-Carreras, I., Frise, E., Kaynig, V., Longair, M., Pietzsch, T., et al. (2012). Fiji: an open-source platform for biological-image analysis. *Nat. Methods* 9, 676–682. doi: 10.1038/nmeth.2019

Schneider, C. A., Rasband, W. S., and Eliceiri, K. W. (2012). NIH Image to ImageJ: 25 years of image analysis. *Nat. Methods* 9, 671–675. doi: 10.1038/nmeth.2089

Shimizu, N., Ishida, T., Yamada, M., Shigenobu, S., Tabata, R., Kinoshita, A., et al. (2015). BAM 1 and RECEPTOR-LIKE PROTEIN KINASE 2 constitute a signaling pathway and modulate CLE peptide-triggered growth inhibition in *Arabidopsis* root. *New Phytol.* 208, 1104–1113. doi: 10.1111/nph.13520

Shinohara, H., and Matsubayashi, Y. (2015). Reevaluation of the CLV3-receptor interaction in the shoot apical meristem: dissection of the CLV3 signaling pathway from a direct ligand-binding point of view. *Plant J.* 82, 328–336. doi: 10.1111/tpj.12817

Shinohara, H., Mori, A., Yasue, N., Sumida, K., and Matsubayashi, Y. (2016). Identification of three LRR-RKs involved in perception of root meristem growth factor in *Arabidopsis*. *Proc. Natl. Acad. Sci. U.S.A.* 113, 3897–3902. doi: 10.1073/pnas.1522639113

Shiu, S. H., and Bleecker, A. B. (2001). Receptor-like kinases from *Arabidopsis* form a monophyletic gene family related to animal receptor kinases. *Proc. Natl. Acad. Sci. U.S.A.* 98, 10763–10768. doi: 10.1073/pnas.181141598

Song, W., Liu, L., Wang, J., Wu, Z., Zhang, H., Tang, J., et al. (2016). Signature motif-guided identification of receptors for peptide hormones essential for root meristem growth. *Cell Res.* 26, 674–685. doi: 10.1038/cr.2016.62

Stahl, Y., Wink, R. H., Ingram, G. C., and Simon, R. (2009). A signaling module controlling the stem cell niche in *Arabidopsis* root meristems. *Curr. Biol.* 19, 909–914. doi: 10.1016/j.cub.2009.03.060

Sugano, S. S., Nishihama, R., Shirakawa, M., Takagi, J., Matsuda, Y., Ishida, S., et al. (2018). Efficient CRISPR/Cas9-based genome editing and its application to conditional genetic analysis in *Marchantia polymorpha*. *PLoS One* 13:e0205117. doi: 10.1371/journal.pone.0205117

Sun, Y., Han, Z., Tang, J., Hu, Z., Chai, C., Zhou, B., et al. (2013). Structure reveals that BAK1 as a co-receptor recognizes the BRI1-bound brassinolide. *Cell Res.* 23, 1326–1329. doi: 10.1038/cr.2013.131

Suzaki, T., Yoshida, A., and Hirano, H. Y. (2008). Functional diversification of CLAVATA3-related CLE proteins in meristem maintenance in rice. *Plant Cell* 20, 2049–2058. doi: 10.1105/tpc.107.057257

Suzuki, H., Harrison, C. J., Shimamura, M., Kohchi, T., and Nishihama, R. (2020). Positional cues regulate dorsal organ formation in the liverwort *Marchantia polymorpha*. *J. Plant Res.* 133, 311–321. doi: 10.1007/s10265-020-01180-5

Tabata, R., Sumida, K., Yoshii, T., Ohyama, K., Shinohara, H., and Matsubayashi, Y. (2014). Perception of root-derived peptides by shoot LRR-RKs mediates systemic N-demand signaling. *Science* 346, 343–346. doi: 10.1126/science.1257800

Takahashi, F., Suzuki, T., Osakabe, Y., Betsuyaku, S., Kondo, Y., Dohmae, N., et al. (2018). A small peptide modulates stomatal control via abscisic acid in long-distance signalling. *Nature* 556, 235–238. doi: 10.1038/s41586-018-0009-2

Tamaki, T., Betsuyaku, S., Fujiwara, M., Fukao, Y., Fukuda, H., and Sawa, S. (2013). SUPPRESSOR OF LLP1 1-mediated C-terminal processing is critical for CLE19 peptide activity. *Plant J.* 76, 970–981. doi: 10.1111/tpj.12349

Toyokura, K., Goh, T., Shinohara, H., Shinoda, A., Kondo, Y., Okamoto, Y., et al. (2019). Lateral inhibition by a peptide hormone-receptor cascade during arabidopsis lateral root founder cell formation. *Dev. Cell* 48, 64–75. doi: 10.1016/j.devcel.2018.11.031

Voinnet, O., Pinto, Y. M., and Baulcombe, D. C. (1999). Suppression of gene silencing: a general strategy used by diverse DNA and RNA viruses of plants. *Proc. Natl. Acad. Sci. U.S.A.* 96, 14147–14152. doi: 10.1073/pnas.96.24.14147

Wang, J., Li, H., Han, Z., Zhang, H., Wang, T., Lin, G., et al. (2015). Allosteric receptor activation by the plant peptide hormone phytosulfokine. *Nature* 525, 265–268. doi: 10.1038/nature14858

Whitewoods, C. D., Cammarata, J., Nemec Venza, Z., Sang, S., Crook, A. D., Aoyama, T., et al. (2018). CLAVATA was a genetic novelty for the morphological innovation of 3D growth in land plants. *Curr. Biol.* 28, 2365–2376. doi: 10.1016/j.cub.2018.05.068

Yamaguchi, Y., Pearce, G., and Ryan, C. A. (2006). The cell surface leucine-rich repeat receptor for AtPep1, an endogenous peptide elicitor in *Arabidopsis*, is functional in transgenic tobacco cells. *Proc. Natl. Acad. Sci. U.S.A.* 103, 10104–10109. doi: 10.1073/pnas.0603729103

Yasui, Y., Tsukamoto, S., Sugaya, T., Nishihama, R., Wang, Q., Kato, H., et al. (2019). GEMMA CUP-ASSOCIATED MYB1, an ortholog of axillary meristem regulators, is essential in vegetative reproduction in *Marchantia polymorpha*. *Curr. Biol.* 29, 3987–3995. doi: 10.1016/j.cub.2019.10.004

Zhang, H., Lin, X., Han, Z., Qu, L. J., and Chai, J. (2016a). Crystal structure of PXY-TDIF complex reveals a conserved recognition mechanism among CLE peptide-receptor pairs. *Cell Res.* 26, 543–555. doi: 10.1038/cr.2016.45

Zhang, H., Lin, X., Han, Z., Wang, J., Qu, L. J., and Chai, J. (2016b). SERK family receptor-like kinases function as co-receptors with PXY for plant vascular development. *Mol. Plant* 9, 1406–1414. doi: 10.1016/j.molp.2016.07.004

Conflict of Interest: The authors declare that the research was conducted in the absence of any commercial or financial relationships that could be construed as a potential conflict of interest.

frontiers in Plant Science

ORIGINAL RESEARCH
published: 16 June 2021
doi: 10.3389/fpls.2021.695439

Genome-Wide Identification and Characterization of Small Peptides in Maize

*Yan Liang†, Wanchao Zhu†, Sijia Chen, Jia Qian and Lin Li**

National Key Laboratory of Crop Genetic Improvement, Huazhong Agricultural University, Wuhan, China

Small peptides (sPeptides), <100 amino acids (aa) long, are encoded by small open reading frames (sORFs) often found in the 5′ and 3′ untranslated regions (or other parts) of mRNAs, in long non-coding RNAs, or transcripts from introns and intergenic regions; various sPeptides play important roles in multiple biological processes. In this study, we conducted a comprehensive study of maize (*Zea mays*) sPeptides using mRNA sequencing, ribosome profiling (Ribo-seq), and mass spectrometry (MS) on six tissues (each with at least two replicates). To identify maize sORFs and sPeptides from these data, we set up a robust bioinformatics pipeline and performed a genome-wide scan. This scan uncovered 9,388 sORFs encoding peptides of 2–100 aa. These sORFs showed distinct genomic features, such as different Kozak region sequences, higher specificity of translation, and high translational efficiency, compared with the canonical protein-coding genes. Furthermore, the MS data verified 2,695 sPeptides. These sPeptides perfectly discriminated all the tissues and were highly associated with their parental genes. Interestingly, the parental genes of sPeptides were significantly enriched in multiple functional gene ontology terms related to abiotic stress and development, suggesting the potential roles of sPeptides in the regulation of their parental genes. Overall, this study lays out the guidelines for genome-wide scans of sORFs and sPeptides in plants by integrating Ribo-seq and MS data and provides a more comprehensive resource of functional sPeptides in maize and gives a new perspective on the complex biological systems of plants.

Keywords: maize, small open reading frame, small peptide, Ribo-seq, mass spectrometry

OPEN ACCESS

Edited by:
Qingyu Wu,
Chinese Academy of Agricultural Sciences (CAAS), China

Reviewed by:
Liuji Wu,
Henan Agricultural University, China
Xu Fang,
Shandong University, China

***Correspondence:**
Lin Li
hzaulilin@mail.hzau.edu.cn

†These authors have contributed equally to this work

Specialty section:
This article was submitted to Plant Physiology, a section of the journal Frontiers in Plant Science

Received: *15 April 2021*
Accepted: *20 May 2021*
Published: *16 June 2021*

Citation:
Liang Y, Zhu W, Chen S, Qian J and Li L (2021) Genome-Wide Identification and Characterization of Small Peptides in Maize. Front. Plant Sci. 12:695439. doi: 10.3389/fpls.2021.695439

INTRODUCTION

Small peptides (sPeptides), which are defined as those peptides shorter than 100 amino acids (aa), represent a class of small molecules with important roles in various biological processes and are translated from small open reading frames (sORFs) shorter than 300 nucleotides (Wang S. et al., 2020). sORFs are widely distributed in the genome and are likely to be located at 5′ and 3′ ends in the untranslated regions of mRNAs [upstream ORFs (uORFs) and downstream ORFs (dORFs)], in the internal regions of annotated ORFs of mRNAs (mORFs) but in a different reading frame, in the short isoforms in spliced mRNAs, and in RNAs produced by transcribed loci in the introns or intergenic regions (Couso and Patraquim, 2017). Although long non-coding RNAs (lncRNAs) are not defined as encoding proteins, some lncRNAs contain sORFs that are engaged by the ribosome, potentially encoding sPeptides (Ruiz-Orera et al., 2018; Ruiz-Orera and Albà, 2019).

sPeptides play important regulatory roles in multiple physiological processes, including growth, development, reproduction, and stress responses (De Coninck and De Smet, 2016). For example, the artificial synthesis and application of the sPeptide hormone insulin were one of the greatest achievements of the twentieth century. Small signaling peptides or peptide hormones in plants, such as cystein-rich peptides, are 5–75 aa long and function as signaling molecules in cell-to-cell communication in defense responses, development, reproduction, and plant–bacteria symbiosis (Marshall et al., 2011; Wang S. et al., 2020). A conserved sORF, *TAS3a*, is associated with the biogenesis of *trans*-acting small-interfering RNAs (tasiRNAs) in *Arabidopsis thaliana*, and a small signaling peptide, *IMMUNE RESPONSE PEPTIDE*, regulates the expression of some defense genes and responds to bacterial or fungal infection in rice (*Oryza sativa*) (Bazin et al., 2017; Wang P. et al., 2020). Multiple sPeptides show high expression in root tissues and a tight association with root growth and absorption. Overexpression of the *C-TERMINALLY ENCODED PEPTIDE1* gene inhibited root growth in *Arabidopsis* (Ohyama et al., 2008). In rice, overexpression of the sPeptide genes, *DROUGHT AND SALT STRESS RESPONSE1*, enhanced drought and stress tolerance, and the knockdown of the sPeptide gene, *OsCADMIUM TOLERANT 3* resulted in a decreased tolerance to aluminum (Xia et al., 2013; Cui et al., 2018).

sORFs and sPeptides have been identified through multiple methods, and their functions have been explored in plants. However, to date, only a few sPeptides have been studied through forward genetic screens because the small size of their encoding sORFs makes them difficult to be targeted by the common mutagenesis methods. Thus, the limited availability of verified sPeptides that can be used as training sets limits the ability of machine learning algorithms to predict sPeptides (Zhou et al., 2013). Further complicating sPeptide identification, many algorithms, such as *de novo* genome annotation, exclude putative proteins of <100 aa in length (Basrai et al., 1997; Claverie, 1997). However, 606,285 potential sORFs (25–250 codons) have been identified in the *A. thaliana* genome (Lease and Walker, 2006).

The bioinformatics and experimental methods have been developed to scan sPeptides encoded by sORFs on a genome-wide level. Bioinformatics approaches based on sequence conservation, functional domains or motifs, gene family clustering, and expression support have been used to search for homologs of known peptides and to predict novel peptides, such as the ROT-FOUR-LIKE/DEVIL (RTFL/DVL) family in *Arabidopsis* (Wen et al., 2004; Guillén et al., 2013; Guo et al., 2015). The transcriptome analysis can reveal the expression of transcripts containing candidate sORFs, but it cannot validate the presence of translational products of these sORFs. The ribosome profiling [also called ribosome sequencing (Ribo-seq)] reveals ribosome footprints by extracting and sequencing RNA that is protected by ribosomes; this can resolve three-nucleotide periodicity, enabling precise definition of translated regions within individual transcripts (Wu et al., 2019). However, several factors introduce contamination in Ribo-seq reads, including structured RNAs and RNAs embedded in protein complexes like rRNA and small nucleolar RNAs (snoRNA), as well as scanning or stalled ribosomes that do not engage in translation (Guttman et al., 2013; Guydosh and Green, 2014; Brar and Weissman, 2015; Archer et al., 2016). Additionally, sPeptides can be directly detected globally using mass spectrometry (MS). For example, an integrated peptidogenomic pipeline using high-throughput MS to probe a customized six-frame translation database was generated and applied to identify non-conventional peptides in maize (*Zea mays*) and *Arabidopsis* (Wang S. et al., 2020). However, since peptides with a bigger size and higher abundance have a better chance of being detected by using MS, the identification of sPeptides solely through MS might miss some of the peptides.

In this study, we collected a large-scale dataset including mRNA sequencing (mRNA-seq), Ribo-seq, and MS data from six tissues (each with two replicates) of maize and performed a *de novo* translatome annotation using the RiboCode software (Xiao et al., 2018). We extracted ORFs of 3–300 nucleotides from the dataset and identified 9,388 sORFs potentially encoding sPeptides. These sORFs showed different Kozak region sequences, higher specificity of translation, and high translational efficiency compared with the canonical protein-coding genes. Furthermore, we searched all sORF sequences in the MS data of the corresponding tissues and verified 2,695 sPeptides. These verified sPeptides clustered perfectly with tissues/replicates, and the verified sPeptides showed higher expression and were longer than the unverified sPeptides. Importantly, the expression in translatome of some annotated sPeptides was positively correlated with that of parental genes, which showed the enrichment of multiple functional gene ontology (GO) terms related to abiotic stress and development. Taken together, the results of this study provide a more comprehensive resource for functional analysis of sPeptides and give helpful information for functional genomics analysis.

MATERIALS AND METHODS

Plant Materials

The seeds of maize (*Z. mays* L.) inbred line B73 were planted in a greenhouse under a temperature and a photoperiod of 30°C for 16 h of light and 25°C for 8 h of darkness. The stem, root, leaf, and whole seedling tissues were collected 14-days after planting, and the ear and tassel tissues were collected in the V12 stage with two biological replicates for each tissue.

Analysis of RNA-Seq and Ribo-Seq Raw Data

The RNA-seq and Ribo-seq data of these plant samples were collected from our previous study (Zhu et al., 2021). A non-coding RNA data set including rRNA, tRNA, and snoRNA sequences were downloaded from the database Rfam (http://rfam.xfam.org/). After removing the adaptors, the collected data were mapped to this dataset using bowtie2 v2.4.1 with default parameters (Langmead and Salzberg, 2012; Kalvari et al., 2018), and the unmapped reads were kept for downstream analysis. The unaligned mRNA-seq and Ribo-seq reads were mapped to the exon sequences and coding sequences (CDSs) of the B73 reference genome (AGPv4), respectively, using STAR v2.7.3 with default parameters (Schnable et al., 2009; Dobin et al., 2013).

Identification of sORFs and Calculation of Transcriptional and Translational Abundance

By comparing the alignment results in the BAM format with the B73 reference genome (AGPv4), we identified ORFs in different tissues using the RiboCode software (https://github.com/xryanglab/RiboCode) with default parameters (Xiao et al., 2018). ORFs identified using the RiboCode were classified into seven types as follows:

1. "annotated": ORFs, overlapping with annotated CDSs, have the same start and stop codon with annotated CDSs.
2. "uORF": ORFs located upstream of annotated CDSs, not overlapping with annotated CDSs.
3. "dORF": ORFs located downstream of annotated CDSs, not overlapping with annotated CDSs.
4. "Overlap_uORF": ORFs located upstream of annotated CDSs and overlapping with annotated CDSs.
5. "Overlap_dORF": ORFs located downstream of annotated CDSs and overlapping with annotated CDSs.
6. "Internal": ORFs located internal regions of annotated CDSs, but in a different reading frame.
7. "novel": ORFs derived from non-coding genes or non-coding transcripts of the coding genes.

The ORFs shorter than 300 nucleotides were considered to be sORFs potentially encoding peptides. Then, the coordinate information of all these sORFs was extracted and merged with the B73 reference genome annotation in the GTF format (https://ftp.ensemblgenomes.org/pub/plants/release-50/gtf/zea_mays/Zea_mays.B73_RefGen_v4.50.gtf.gz) using in-house shell scripts and Stringtie v2.1.4 (parameter: –merge -m 0) (Pertea et al., 2015). The aa sequences of all sORFs were generated by RiboCode and merged together for further analysis.

Using the merged genome annotation, transcriptional and translational abundance was calculated by fragments per kilobase of exon model per million mapped reads (FPKM) using Cufflinks v2.2.1 with parameters: -p 5 -G (Trapnell et al., 2012). Only the unique reads of RNA-seq and Ribo-seq mapped to exons and CDSs were used for the calculation of abundance.

Protein Preparation and MS

The tissue from maize was grounded using liquid nitrogen and then transferred into a 5-mL centrifuge tube with a suitable volume of lysis buffer [1% TritonX-100, 10 mM dithiothreitol, 1% Protease Inhibitor Cocktail, 50 μM 2,6-diamino-3,5-dithiocyanopyridin, 3 μM trichostatin A, 50 mM *N*-arachidonyl maleimide, and 2 mM ethylenediaminetetraacetic acid (EDTA)]. The mixture was sonicated three times on ice using a high-intensity ultrasonic processor (Scientz), and an equal volume of Tris-saturated phenol (pH 8.0) was added and further vortexed for 5 min. The upper phenol phase was transferred to a new centrifuge tube after centrifugation. Then, at least four volumes of ammonium sulfate-saturated methanol were added to precipitate the proteins at −20°C for at least 6 h. After centrifugation, the precipitate with proteins was collected and washed with ice-cold methanol once, followed by ice-cold acetone three times. The protein was redissolved in 8 M urea, and the concentration was determined using a BCA kit based on the instructions of the manufacturer. After digestion with trypsin, the samples were submitted for the MS detection on the Thermo Scientific Q Exactive platform using a label-free method. The resulting MS data were processed with the Maxquant search engine (v.1.5.2.8). Tandem mass spectra were searched against the aa sequences of sORFs identified by RiboCode in the translatome data (Xiao et al., 2018). The mass tolerance for precursor ions was set as 20 ppm in the first search and 5 ppm in the main search, and the mass tolerance for fragment ions was set as 0.02 Da. The false discovery rate (FDR) was adjusted to <1%, and the minimum score for peptides was set to >40.

The MS data of maize leaves sampled from the 14-day-old seedlings were collected from our previous study (Zhu et al., 2021).

Calculation of Shannon Entropy and Translation Efficiency (TE)

To compare the TE of sORFs and other canonical transcripts in different tissues, we selected transcripts expressing in both the transcriptome and translatome (FPKM ≥ 0.5). RPKM for single-end sequencing is the unit to quantify gene's expression level, equivalent to FPKM for pair-end sequencing. The RPKM is defined as follows:

$$RPKM = \frac{\text{Exon Mapper Reads} * 1{,}000{,}000{,}000}{\text{Total Mapped Reads} * \text{Exon Length}}$$

In the pair-end sequencing two paired reads is a fragment. The FPKM is defined as follows:

$$FPKM = \frac{\text{Exon Mapper Fragments} * 1{,}000{,}000{,}000}{\text{Total Mapped Fragments} * \text{Exon Length}}$$

For each transcript, we calculated TE by the following equation:

$$\boldsymbol{TE = \frac{RPKM\ of\ Ribo-seq}{FPKM\ of\ RNA-seq}}$$

We compared the tissue specificity of expression between verified and non-verified peptides by analyzing the Shannon entropy of peptides. For each sORF, we defined the Shannon entropy of expression-level across different tissues as follows: Given expression levels of a sORF in N tissues, the proportion of expression in tissue i out of the sum of all expression-levels in all tissues:

$$\boldsymbol{P(i) = \frac{FPKM(Ti)}{\sum_{i=1}^{N} FPKM(Ti)}}$$

Shannon entropy:

$$\boldsymbol{SE = -\sum_{i=1}^{N} P(i)\log 2\,[P(i)]}$$

Clustering, Gene Ontology Enrichment Analysis, and Statistical Analysis

The verified and previously annotated 501 peptides were clustered into three groups using the gplots package in R with default parameters. For each group of peptides, the GO enrichment analysis was performed on their parental genes using the AgriGO v 2.0 webserver (Tian et al., 2017). The GO terms with an FDR threshold of 0.05 were considered as significant terms.

All of the statistical analyses in this study were performed using R version 4.0.4.

RESULTS

The Widespread Existence of sORFs in Maize

In a previous study by authors, we sampled whole seedlings, roots, stems, and leaves of 14-day-old maize plants, as well as ears and tassels at the V12 stage with two replicates each and used these to perform RNA sequencing (RNA-seq), Ribo-seq, and MS analysis (MS only for leaf samples) (**Figures 1A,B** and **Supplementary Table 1**) (Zhu et al., 2021). We obtained a total of 236 million RNA-seq reads to quantify transcript abundance. We also collected 161.4 million Ribo-seq reads to map ribosome occupancy on genome-wide transcripts (Brar and Weissman, 2015). Additionally, MS was performed to detect and quantify protein abundance for all samples (except the leaf samples) in this study. Taking these results together, we collected a comprehensive transcriptome, translatome, and proteome dataset for the genome-wide identification of sORFs and sPeptides in maize (**Figure 1B**).

After filtering low-quality reads and contaminant reads in the Ribo-seq data (as shown in the "Materials and Methods" section), we mapped the remaining reads to the maize B73 reference genome (Schnable et al., 2009). By applying stringent filters using the RiboCode software, we identified 9,388 sORFs potentially

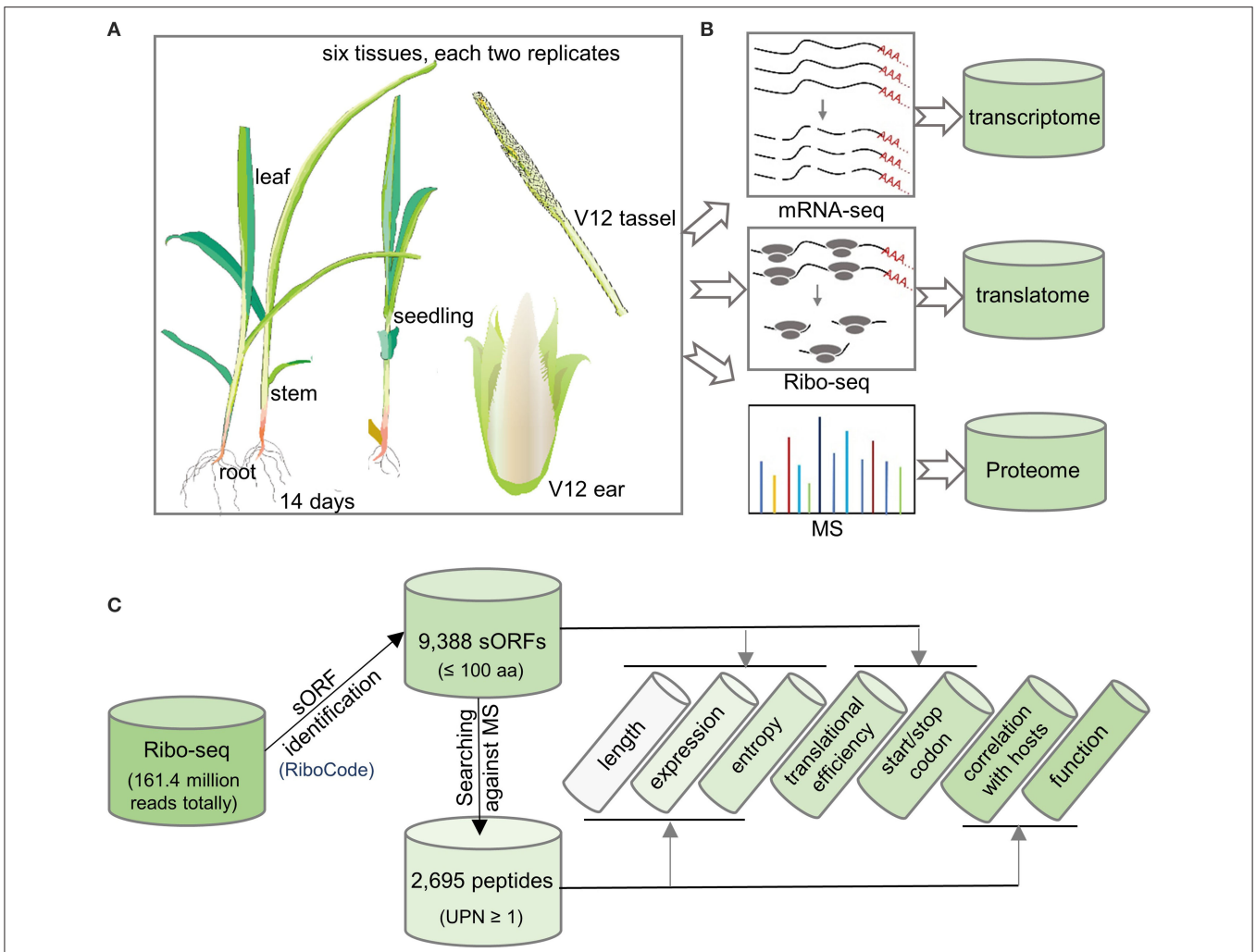

FIGURE 1 | Flowchart of experimentsfor the genome-wide identification of sORFs and sPeptides in maize. **(A)** Six tissues each with two replicates were analyzed in this study. **(B)** Multi-omics data, including transcriptome, translatome, and proteome, were collected for the detection of sORFs and sPeptides. **(C)** Bioinformatics pipeline used in this study to characterize the sORFs and sPeptides.

encoding putative sPeptides (Xiao et al., 2018). Comparison of sORF annotation with the latest maize reference annotation B73 RefGen v4.50 (ensembl) demonstrated 7,589 (80.84%) newly identified sORFs, which complements the functional annotation of the maize genome. Finally, we verified the presence of sPeptides using the MS analysis and identified 2,695 sPeptides, which are supported by the presence of one or more unique peptides (UPN $\geq$ 1) in the MS analysis (**Figure 1C**). These results indicate the widespread existence of sORFs and sPeptides in maize.

Maize sORFs Are a Class of Distinct Translational Elements

By comparing data from this study to the B73 reference genome annotation, we uncovered a total of 2,907 (30.97%) upstream sORFs (uORFs), 485 (5.17%) overlap upstream sORFs (overlap uORFs), 300 (3.2%) internal sORFs, 301 (4.27%) overlap downstream sORFs (overlap dORFs), 3,445 (36.7%) downstream sORFs (dORFs), 1,799 (19.16%) annotated sORFs, and 49 (0.52%) novel sORFs (as shown in the "Materials and methods" section). Similar to genes, sORFs are more likely to be enriched toward the telomeres and depleted in the pericentromeric regions (**Figure 2A**). All sORFs encoded sPeptides shorter than 100 aa in length. However, the different types of sORFs showed distinct length distribution. Annotated sORFs were significantly longer than other types of sORFs ($p <$ 2.2e-16, Mann–Whitney *U* test), while novel and internal sORFs were significantly shorter than the others ($p <$ 2.445e-09, $p <$ 2.2e-16, respectively, Mann–Whitney *U* test) (**Figure 2B**). Interestingly, the three shortest uORFs potentially encode peptides with only 5 aa.

The upstream and downstream sequences of start and stop codon sites might be associated with the translational efficiency of ORFs (Hinnebusch et al., 2016). Thus, we extracted the upstream and downstream 5 bp sequences of start and stop codons of the sORFs as well as canonical transcripts and further performed a motif enrichment using R package ggseqlogo (Wagih, 2017). We found that the sequences of the start and stop codons of sORFs were roughly similar to those of conventional genes. However, the frequency of upstream and downstream sequences of start and stop codons was significantly different between sORFs and other canonical transcripts (**Figures 2C,D**). These results suggest that sORFs exhibit different features (e.g., the frequency of translational start sites) compared with conventional genes.

Moreover, we quantified and compared the expression levels of sORFs and conventional transcripts at the translatome level. Although the translatome abundance of both conventional genes and sORFs could discriminate different tissues, the expression patterns differed dramatically among the different tissues (**Figures 2E,F**). Furthermore, we calculated the Shannon entropy of expression levels across all 12 samples for sORFs and other protein-coding transcripts and demonstrated that sORFs are significantly more likely to be tissue-specific than the canonical transcripts ($p <$ 2.2e-16, Mann–Whitney *U* test) (**Figure 2G**).

Additionally, we checked the difference in translational efficiency between sORFs and canonical protein-coding genes across all tissues. Unexpectedly, sORFs exhibited significantly higher translational efficiency than canonical protein-coding genes for all 11 samples (the sequencing library of ear1 for RNA sequencing was constructed unsuccessfully) (**Figure 2H**), which is likely associated with the different base frequency upstream and downstream of the start and stop codons. All these results indicate that sORFs exhibit distinct genomic and expression features compared with canonical protein-coding genes.

Genome-Wide Classification and Characterization of sPeptides in Maize

To evaluate whether sORFs are able to translate stable peptides in maize, we performed a proteogenomic analysis by searching the aa sequences of sORFs against the MS data (Walley and Briggs, 2015). Consistent with the definition of sPeptides as <100 aa, the sPeptides were mainly concentrated in the range of 0–10 kDa in the MS validation, which corresponds to the length of 5–100 aa (**Figure 3A** and **Supplementary Figure 1A**). By using the MS analysis, we verified 2,596 sPeptides of the 9,388 sORFs identified from Ribo-seq data. Of these sPeptides, ∼85% were detected in more than five tissues (**Supplementary Figure 1B**). Unexpectedly, only about 20% of sPeptides were derived from annotated transcripts of the reference genome, suggesting that the number of sPeptides in maize is largely underestimated (**Figure 3B**). However, the comparison of the validation ratio of sPeptides derived from different types of sORFs demonstrated that sORFs annotated previously in the reference genome are most likely to be validated, while those from novel sORFs are least likely to be validated (**Figure 3C**).

The comparison of Shannon entropy between different kinds of sPeptides and unverified sORFs indicated that sPeptides with MS evidence were more uniformly expressed in the 12 samples (**Supplementary Figure 1C**). Notably, sPeptides exhibit higher translatome abundance and longer CDS in corresponding sORFs than those of the unverified sORFs, which may be due to the limitation of the detection power of MS (**Figures 3D,E**). Then, we clustered the 12 samples based on the expression-level variation of all detectable sPeptides and found that the sPeptides can robustly discriminate tissues, and the replicates of the same tissue were also clustered (**Figure 3F**). Interestingly, we found that many sPeptides are derived from putative-defined lncRNA regions. For example, a long intergenic non-coding RNA (lincRNA) *GRMZM2G117281_T01* annotated in the reference genome of maize was detected to be translated to a sPeptide (**Figure 3G**). A previous study proposed that *GRMZM2G117281* could be responsive to drought stress (Zhang et al., 2014), suggesting a potential functional role of this sPeptide. All these results demonstrate that sPeptides are abundant in the maize genome, exhibit distinct genomic features, and may function in different biological processes.

Annotated sPeptides Are Correlated With Their Corresponding Parental Genes and Might Function in Multiple Processes

A fraction of the ORFs located within annotated genes was shorter than 300 nucleotides. Some of them have been

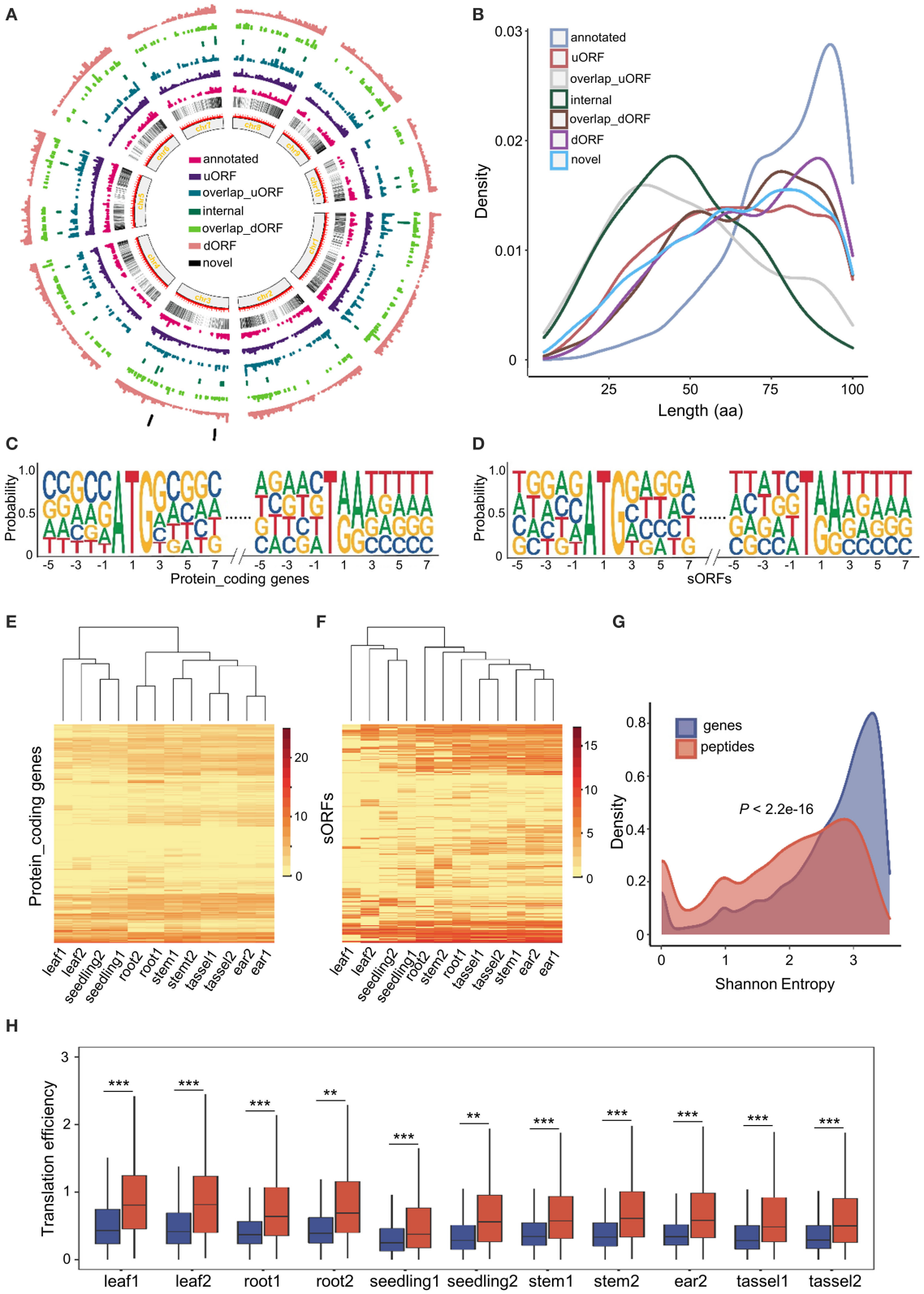

FIGURE 2 | Genome-wide characterization of sORFs in maize. **(A)** Distribution of different kinds of sORFs in the maize genome. **(B)** Length distribution of different kinds of sORFs. **(C,D)** Nucleotide features around start and stop codon sites of conventional genes and sORFs. **(E,F)** Heatmap of expression levels and unsupervised tissue hierarchical trees of conventional genes and sORFs, respectively. **(G)** Shannon entropy distribution of conventional genes (in blue) and sORFs (in red). **(H)** Differentiation of translation efficiency (TE) between conventional genes (mentioned in blue color) and sORFs (mentioned in red color). *,** and *** indicate *P*-values of less than 0.05, 0.01 and 0.001, respectively (Mann–Whitney *U*-test).

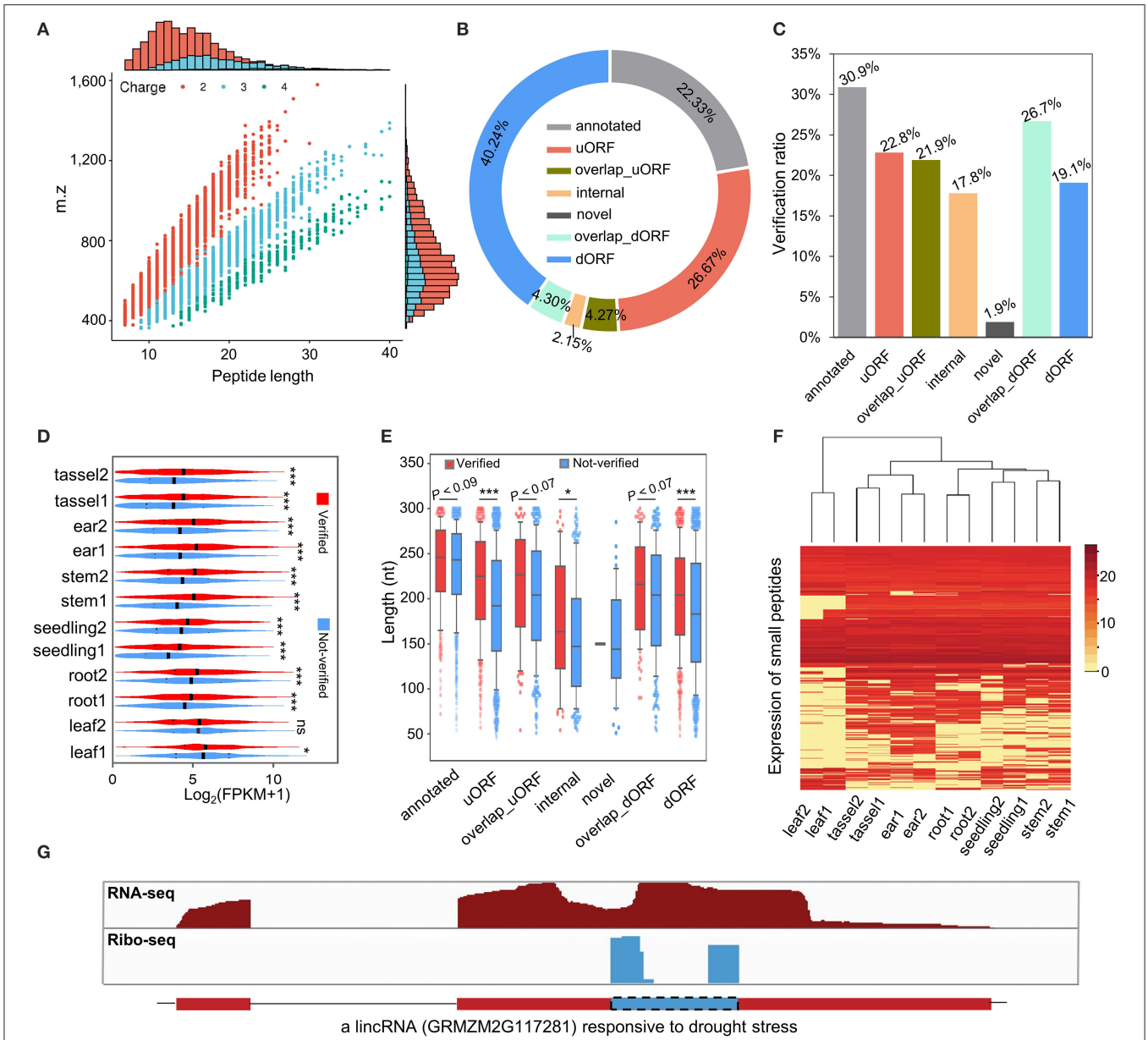

FIGURE 3 | Genome-wide classification and characterization of sPeptides in maize. **(A)** Mass spectrometry (MS) signals discriminate sPeptides and canonical proteins. **(B)** The proportion of different types of sPeptides in maize. **(C)** The validation rate of different kinds of sORFs was detected in this study. **(D)** Comparison of expression abundance between sPeptides and unverified sORFs. *, ** and *** indicate *P*-values of less than 0.05, 0.01 and 0.001, respectively (Mann–Whitney *U*-test). **(E)** Length differentiation between sPeptides and unverified sORFs in maize. *,** and *** indicate *P*-values of less than 0.05, 0.01 and 0.001, respectively (Mann–Whitney *U*-test). **(F)** Expression pattern of sPeptides in the 12 samples. **(G)** Structure of a sPeptide derived from a lincRNA.

demonstrated to be capable of encoding sPeptides with biological functions such as signal peptides (Hsu and Benfey, 2018; Ruiz-Orera and Albà, 2019). In this study, we compared the sPeptides with the functional annotation in the maize B73 RefGen v4 reference genome. A total of 501 out of 2,596 sPeptides identified by Ribo-seq and MS were encoded by sORFs annotated in the reference genome (**Figure 4A**). Based on the expression of the sPeptides quantified by Ribo-seq, we clustered 501 genes into three groups (**Figure 4B**). Furthermore, the translatomic abundance of 501 sPeptides was positively correlated with that of their host genes (**Supplementary Figure 2D**), suggesting that sPeptides might function by orchestrating parental gene expression.

To explore the potential functions of sPeptides, we performed the GO enrichment analysis for the three parental gene sets that correspond to the three different sPeptide groups. Group I parental genes were significantly enriched in the RNA splicing process (**Supplementary Figure 2A**). *Zm00001d010461*, *Zm00001d042725*, and *Zm00001d024593*, enriched in the GO term "RNA splicing," are annotated to encode small nuclear

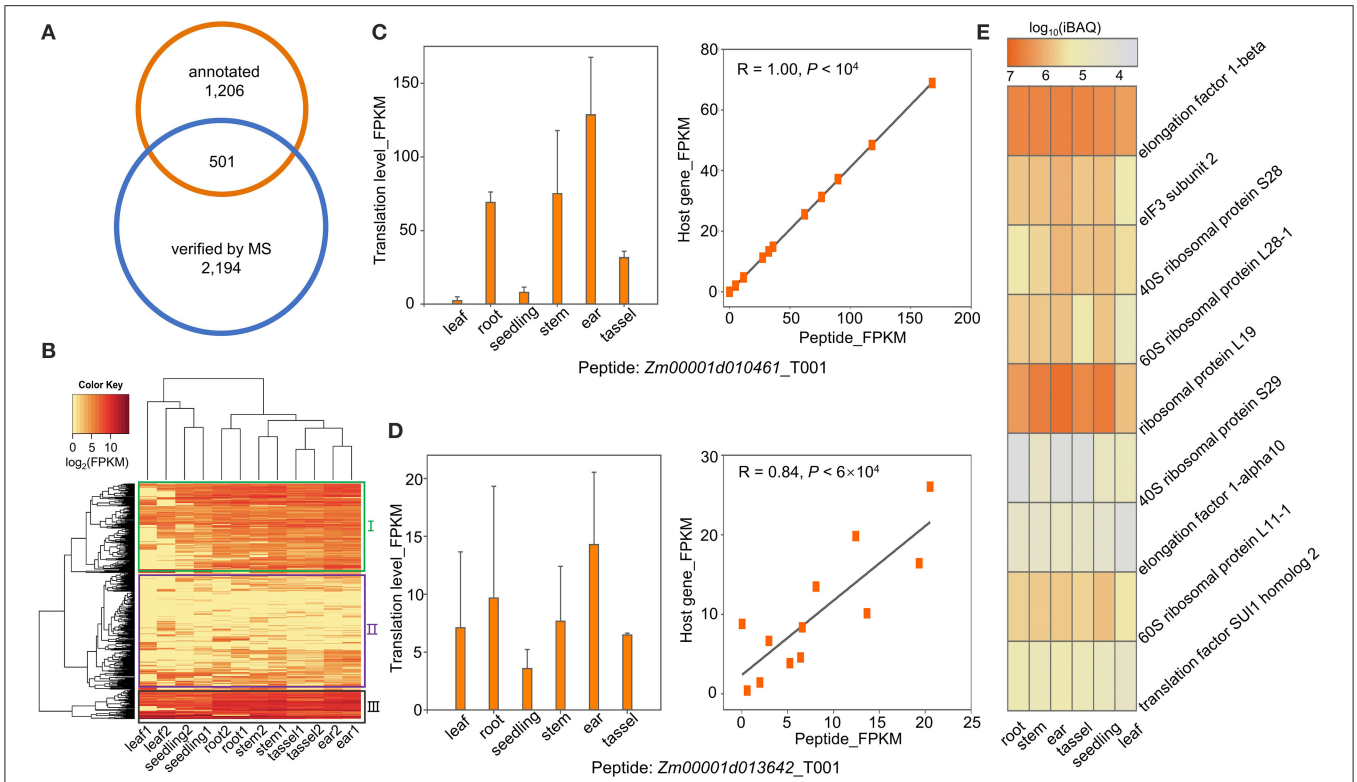

FIGURE 4 | Functional annotation of sPeptides in maize. **(A)** Gene-derived sPeptides were identified by the intersection between annotated genes and sPeptides in this study. **(B)** Gene-derived sPeptides classified different tissues and clustered them into three groups based on their expression patterns. **(C,D)** Translatome abundance variation of sPeptides Zm00001d010461_T001 **(C)** and Zm00001d013642_T001 **(D)** across different tissues shows a high correlation with that of their parental canonical protein-coding gene. **(E)** Proteome abundance of sPeptides across different tissues from Group III.

ribonucleoprotein family-like (LSM) proteins. Generally, LSM proteins are associated with development, response to stress, and abscisic acid signaling *via* mRNA splicing and processing in *Arabidopsis* (Xiong et al., 2001; Perea-Resa et al., 2012; Golisz et al., 2013; Cui et al., 2014; Okamoto et al., 2016). The abundance of the sPeptide, Zm00001d010461_T001 varied dramatically in different tissues and showed a highly positive correlation with the expression of *Zm00001d010461* ($R = 1$, $p <$ 1e-04) (**Figure 4C**). Therefore, we speculated that the sPeptide, Zm00001d010461_T001 could function in stress tolerance and development in maize.

For the second group of parental genes, the GO enrichment showed that these genes are related to organonitrogen compound biosynthetic and metabolic processing (**Supplementary Figure 2B**). Nitrogen is essential for plant growth and development and is also helpful for tolerance against biotic and abiotic stresses (Oh et al., 2017; Zipfel and Oldroyd, 2017; Arora et al., 2020). Notably, *Zm00001d034602* is annotated to function in the organonitrogen compound metabolic process, and its abundance in the translatome was significantly associated with that of the sPeptide Zm00001d034602_T001 (**Figure 4D**). *AT2G22425*, the ortholog of *Zm00001d013642* in *Arabidopsis*, was reported to function in signal peptide processing during *Cabbage leaf curl virus* infection, indicating that the sPeptide Zm00001d013642_T001 may be involved in pathogen response through organonitrogen compound biosynthetic and metabolic processing (Ascencio-Ibáñez et al., 2008).

The sPeptide parental genes in Group III were uniformly expressed across different tissues and showed high abundance at both the translatome and proteome levels (**Figures 4B,E**). These genes are mainly enriched in translation and peptide biosynthetic processes (**Supplementary Figure 2C**). Nine genes with the most significant GO enrichment of translation are annotated as "subunit of ribosome and translation-regulatory factors." These peptides are likely to participate in the fundamental biological pathways and affect multiple agronomic traits.

DISCUSSION

As a new frontier in the study of molecular players in life science, sORFs and sPeptides have been reported to be involved in several biological processes in plants. In this study, we collected RNA-seq, Ribo-seq, and MS data from six tissues of the maize reference inbred B73 with two replicates and performed a genome-wide *de novo* scan of translational elements using the RiboCode software (Xiao et al., 2018). We extracted ORFs encoding peptides with length ranging from 2 to 100 aa and identified 9,388 sORFs potentially encoding sPeptides. Then, we confirmed over 2,000 sPeptides by searching against MS data. Comparison of sORFs/sPeptides with canonical proteins demonstrated the

distinct features of these non-canonical molecules. Finally, the functional GO analyses indicated that these sPeptides are likely to be involved in the response to abiotic stress and plant development (Couso and Patraquim, 2017). This study presents a biological pipeline combining multi-omics data for the genome-wide scan of sORFs and sPeptides in maize, which paves the way for further functional study of sPeptides in maize.

A Robust Bioinformatics Pipeline for the Genome-Wide Scan sORFs and sPeptides Combining Multi-Omics Data of RNA-Seq, Ribo-Seq, and MS

lncRNAs have a low probability of encoding proteins and are more likely to encode sPeptides. lncRNAs have been widely uncovered by RNA-seq in maize (Li et al., 2014). The sORFs or sPeptides are detected by the bioinformatics analyses solely based on RNA-seq data lack representation at the translatome level. Ribosome profiling (Ribo-seq), an RNA sequencing technique focused on the translatome, has been developed and used to monitor translation in real-time during protein biosynthesis (Ingolia et al., 2009). Since ribosomes directly decipher mRNA every three nucleotides, the periodic feature of ribosome footprints can be used to examine unannotated ORFs (Calviello et al., 2016; Hsu et al., 2016). Therefore, sORFs potentially encoding peptides that may not be detected by proteomics-based methods could be uncovered by combining ribosome profiling and bioinformatics analyses (Couso and Patraquim, 2017; Olexiouk et al., 2018; Ruiz-Orera and Albà, 2019).

Due to the presence of reads from the elongating and initiating stage in Ribo-seq experiments, non-AUG start site prediction becomes difficult and false-positive results are introduced (Olexiouk et al., 2018). Wang et al. generated an integrated proteomic pipeline using high-throughput MS to probe a customized six-frame translation database and applied it to a large-scale detection of non-conventional peptides in plants (Wang S. et al., 2020). In total, 1,993 and 1,860 non-conventional peptides were identified in maize and *Arabidopsis*, respectively. However, limited by the systematic error of the technology, in which proteins with higher abundance or larger size have better chances of being detected by the MS, the approaches used to identify peptides based on their mass spectra are likely to have high rates of false negatives (Slavoff et al., 2013; Olexiouk et al., 2018).

Thus, we generated a pipeline for the genome-wide scan of sORFs and sPeptides in maize combining sensitive and real-time Ribo-seq monitoring data as well as less-sensitive but direct MS data. In this study, the annotated sORFs had the highest verification ratio (**Figure 3C**), which may be associated with the fact that annotated sORFs generally have longer length than the other types of sORFs (**Figure 2B**). The corresponding peptides of annotated sORFs are more easily identified by the MS because of their larger molecular mass. We confirmed 2,695 sPeptides by the MS, which accounted for 28.71% of all identified sORFs (9,388). Therefore, Ribo-seq provides an unprecedented chance to detect more potential sPeptides likely with low abundance or smaller relative molecular mass that are difficult to detect by the proteomics-based methods.

To further validate the capacity of pipeline of authors to detect sPeptides, we downloaded and analyzed the MS data from the previous study which identified non-conventional peptides in maize-based on a peptidogenomic method (Wang S. et al., 2020). All sORFs identified from the Ribo-seq data of six different maize tissues were searched against the downloaded MS data that were obtained only from maize leaves at the V3 stage, and 158 sORFs showed peptides evidence. Of these validated sORFs by Wang's MS data, 66 sORFs were also verified in the total MS data (**Supplementary Figure 3**). Although the number and types of tissues are different, there is a proportion of overlapped sPeptides (∼42%) between this study and the previous study based on the non-digestion MS data, reflecting a certain degree of reliability in pipeline of authors. Moreover, the sPeptides, identified in this study, are complementary to previous studies to extend the knowledge of sPeptides in maize.

Potential Functional Roles of sPeptides

Numerous studies have reported that small secreted peptides are involved in different physiological processes including plant growth, development, reproduction, and stress responses (De Coninck and De Smet, 2016). Cysteine-rich peptides, a type of signal peptide, play important roles in developmental patterning as well as in plant–pathogen responses and symbiosis (Hemu et al., 2018). Based on a proteomics method, 1,993 unannotated peptides were identified in maize leaves, which were significantly enriched in regions identified from genome-wide association studies of agronomic traits and appear to be under domestication selection (Wang S. et al., 2020). Thus, the sPeptides identified in this study are likely to function in multiple pathways in maize.

Based on the expression patterns between tissues, the 501 gene-locus-encoded sPeptides annotated in the reference genome and verified by the MS were clustered into three groups through a hierarchical clustering algorithm (**Figure 4B**). Genes in Group I were significantly enriched in the pathway related to mRNA splicing and processing. A large number of studies reported that alternative splicing plays vital roles in growth, development, and responses to stress (de Francisco Amorim et al., 2018; Szakonyi and Duque, 2018; Li et al., 2021). In this study, the sPeptide-associated parental genes, *Zm00001d010461*, *Zm00001d042725*, and *Zm00001d024593*, which are annotated as LSM protein family genes, belong to Group I. In *Arabidopsis*, LSM proteins participate in mRNA splicing and degradation and thus regulate the development and tolerance to stress (Perea-Resa et al., 2012; Golisz et al., 2013; Cui et al., 2014; Okamoto et al., 2016). Moreover, *SAD1*, encoding a polypeptide similar to multifunctional LSM proteins, modulates abscisic acid signal transduction and biosynthesis in *Arabidopsis* through mRNA metabolism (Xiong et al., 2001). The second group (Group II) of sPeptide parental genes was enriched in organonitrogen compound biosynthetic and metabolic processes (**Supplementary Figure 2B**). Signal

molecules, such as reactive oxygen species, calcium, reactive nitrogen species, salicylic acid, and ethylene, are important in plant development and pathogen infection (Oh et al., 2017; Zipfel and Oldroyd, 2017). The form of nitrogen, such as nitrate or ammonium, plays a vital role in the production of these signal molecules (Oh et al., 2017; Arora et al., 2020). The parental genes of the Group II sPeptide, *Zm00001d013642_T001* and *Zm00001d013642*, were annotated in "organonitrogen compound metabolic processing," and its ortholog *AT2G22425* was differentially expressed in *Cabbage leaf curl virus*-infected *Arabidopsis* leaves (Ascencio-Ibáñez et al., 2008). These results imply that *Zm00001d013642_T001* may be involved in signal transduction during the pathogen response through organonitrogen compound biosynthetic and metabolic processes. The last group (Group III) of genes were uniformly expressed in different tissues and with relatively high abundance at the translatome level (**Figure 4B**). There were nine sPeptide parental genes annotated as "subunit of translation start and elongation factors" in Group III. Overall, sPeptides might participate in multiple pathways in different manners to influence the plant life cycle.

Precursors of miRNAs May Encode sPeptides

Some lncRNAs and circular RNAs were detected *in vivo* with evidence for the production of peptides in the shotgun MS data (van Heesch et al., 2019), which implies that non-coding transcripts are likely to play both coding and non-coding roles. A previous study reported that microRNAs (miRNAs) are capable of encoding peptides through the transcripts of their corresponding precursors (Chen et al., 2020). Primary miRNAs have been reported to encode regulatory peptides in *Arabidopsis*, grapevine (*Vitis vinifera*), soybean (*Glycine max*), and *Medicago* sp.; these peptides are named miRNA-encoded peptides (miPEPs) (Ren et al., 2021). For example, miPEP171d1 plays a regulatory role in adventitious root formation and response to stress in plants (Ma et al., 2014; Gao et al., 2019; Chen et al., 2020).

In this study, we aligned the aa sequences of identified sPeptides against the reference sequences of the precursors of miRNAs using BLAST+ (version 2.7.1). Two sPeptides validated by the MS are encoded by pre-miRNAs: ENSRNA049997513-T1 and ENSRNA049997089-T1. In a previous study, zma-miR159d, the mature product of ENSRNA049997513-T1, was predicted to target genes encoding MYB transcription factors (Samad et al., 2017). Moreover, zma-miR159d was found to be involved in the degradation of chlorophyll that induced earlier leaf senescence between different maize inbred lines (Wu et al., 2016). Considering the evidence of their translatome and proteome study, we speculated that zma-miR159d could produce a sPeptide. The other sPeptide is encoded by ENSRNA049997089-T1, which is the primary transcript of *zma-MIR2275d*. *zma-MIR2275*, with a maximum expression in the fertile maize anther, plays an important role in anther development and thereby influencing male reproduction in maize (Zhai et al., 2015; Huang et al., 2019). Furthermore, zma-miR2275 also affects the drought tolerance by directly targeting drought-related mRNAs. The identification of the sPeptide encoded by the pre-miRNA ENSRNA049997089-T1 provides a perspective on the manner of *zma-MIR2275* function as a regulator of development and stress tolerance in maize.

DATA AVAILABILITY STATEMENT

The MS proteomics data for this project have been deposited at the ProteomeXchange Consortium with the dataset identifier PXD025997.

AUTHOR CONTRIBUTIONS

LL designed and supervised this study. YL, WZ, SC, and JQ performed the data analysis. YL, WZ, and LL prepared the manuscript. All authors contributed to the article and approved the submitted version.

FUNDING

This research was supported by the National Natural Science Foundation of China (92035302; 31922068) and the Huazhong Agricultural University Scientific & Technological Self-Innovation Foundation (2662020ZKPY017).

ACKNOWLEDGMENTS

We thank all the contributors in the maize research community for the generosity of sharing the reference maize inbred, B73.

SUPPLEMENTARY MATERIAL

The Supplementary Material for this article can be found online at: https://www.frontiersin.org/articles/10.3389/fpls.2021.695439/full#supplementary-material

Supplementary Figure 1 | Size distribution of peptides in MS and comparison between verified and unverified sORFs. **(A)** Statistics of the mass of peptides. **(B)** Percentage of verified sORFs and their composition. **(C)** Comparison of Shannon entropy between different kinds of verified and unverified sORFs.

Supplementary Figure 2 | The results of GO enrichment analysis of three groups of sPeptide-associated parental genes and correlation of abundance between the 501 sPeptides and their parental genes. **(A–C)** Results of GO enrichment analysis of three clusters of parental genes, respectively. **(D)** The 501 sPeptides positively correlated with their parental genes in the translatome.

Supplementary Figure 3 | The overlapped sPeptides validated by MS data of this study and Wang's study.

Supplementary Table 1 | Tissues used in this study.

Supplementary File 1 | Genome annotation of sPeptides in GTF format.

Supplementary File 2 | Information of sORFs and sPeptides.

REFERENCES

Archer, S. K., Shirokikh, N. E., Beilharz, T. H., and Preiss, T. (2016). Dynamics of ribosome scanning and recycling revealed by translation complex profiling. *Nature* 535, 570–574. doi: 10.1038/nature18647

Arora, R., Singh, P., Kumari, A., Pathak, P. K., and Gupta, K. J. (2020). Using foldscope to monitor superoxide production and cell death during pathogen infection in arabidopsis under different nitrogen regimes. *Methods Mol. Biol.* 2057, 93–102. doi: 10.1007/978-1-4939-9790-9_9

Ascencio-Ibáñez, J. T., Sozzani, R., Lee, T. J., Chu, T. M., Wolfinger, R. D., Cella, R., et al. (2008). Global analysis of Arabidopsis gene expression uncovers a complex array of changes impacting pathogen response and cell cycle during geminivirus infection. *Plant Physiol.* 148, 436–454. doi: 10.1104/pp.108.121038

Basrai, M. A., Hieter, P., and Boeke, J. D. (1997). Small open reading frames: beautiful needles in the haystack. *Genome Res.* 7, 768–771. doi: 10.1101/gr.7.8.768

Bazin, J., Baerenfaller, K., Gosai, S. J., Gregory, B. D., Crespi, M., and Bailey-Serres, J. (2017). Global analysis of ribosome-associated noncoding RNAs unveils new modes of translational regulation. *Proc. Natl. Acad. Sci. U.S.A.* 114, E10018–E10027. doi: 10.1073/pnas.1708433114

Brar, G. A., and Weissman, J. S. (2015). Ribosome profiling reveals the what, when, where and how of protein synthesis. *Nat. Rev. Mol. Cell Biol.* 16, 651–664. doi: 10.1038/nrm4069

Calviello, L., Mukherjee, N., Wyler, E., Zauber, H., Hirsekorn, A., Selbach, M., et al. (2016). Detecting actively translated open reading frames in ribosome profiling data. *Nat. Methods* 13, 165–170. doi: 10.1038/nmeth.3688

Chen, Q. J., Deng, B. H., Gao, J., Zhao, Z. Y., Chen, Z. L., Song, S. R., et al. (2020). A miRNA-encoded small peptide, vvi-miPEP171d1, regulates adventitious root formation. *Plant Physiol.* 183, 656–670. doi: 10.1104/pp.20.00197

Claverie, J. M. (1997). Computational methods for the identification of genes in vertebrate genomic sequences. *Hum. Mol. Genet.* 6, 1735–1744. doi: 10.1093/hmg/6.10.1735

Couso, J. P., and Patraquim, P. (2017). Classification and function of small open reading frames. *Nat. Rev. Mol. Cell Biol.* 18, 575–589. doi: 10.1038/nrm.2017.58

Cui, P., Zhang, S., Ding, F., Ali, S., and Xiong, L. (2014). Dynamic regulation of genome-wide pre-mRNA splicing and stress tolerance by the Sm-like protein LSm5 in Arabidopsis. *Genome Biol.* 15:R1. doi: 10.1186/gb-2014-15-1-r1

Cui, Y., Li, M., Yin, X., Song, S., Xu, G., Wang, M., et al. (2018). OsDSSR1, a novel small peptide, enhances drought tolerance in transgenic rice. *Plant Sci.* 270, 85–96. doi: 10.1016/j.plantsci.2018.02.015

De Coninck, B., and De Smet, I. (2016). Plant peptides - taking them to the next level. *J. Exp. Bot.* 67, 4791–4795. doi: 10.1093/jxb/erw309

de Francisco Amorim, M., Willing, E. M., Szabo, E. X., Francisco-Mangilet, A. G., Droste-Borel, I., Maček, B., et al. (2018). The U1 snRNP subunit LUC7 modulates plant development and stress responses via regulation of alternative splicing. *Plant Cell* 30, 2838–2854. doi: 10.1105/tpc.18.00244

Dobin, A., Davis, C. A., Schlesinger, F., Drenkow, J., Zaleski, C., Jha, S., et al. (2013). STAR: ultrafast universal RNA-seq aligner. *Bioinformatics* 29, 15–21. doi: 10.1093/bioinformatics/bts635

Gao, Z., Li, J., Luo, M., Li, H., Chen, Q., Wang, L., et al. (2019). Characterization and cloning of grape circular RNAs identified the cold resistance-related Vv-circATS1. *Plant Physiol.* 180, 966–985. doi: 10.1104/pp.18.01331

Golisz, A., Sikorski, P. J., Kruszka, K., and Kufel, J. (2013). *Arabidopsis thaliana* LSM proteins function in mRNA splicing and degradation. *Nucleic Acids Res.* 41, 6232–6249. doi: 10.1093/nar/gkt296

Guillén, G., Díaz-Camino, C., Loyola-Torres, C. A., Aparicio-Fabre, R., Hernández-López, A., Díaz-Sánchez, M., et al. (2013). Detailed analysis of putative genes encoding small proteins in legume genomes. *Front. Plant Sci.* 4:208. doi: 10.3389/fpls.2013.00208

Guo, P., Yoshimura, A., Ishikawa, N., Yamaguchi, T., Guo, Y., and Tsukaya, H. (2015). Comparative analysis of the RTFL peptide family on the control of plant organogenesis. *J. Plant Res.* 128, 497–510. doi: 10.1007/s10265-015-0703-1

Guttman, M., Russell, P., Ingolia, N. T., Weissman, J. S., and Lander, E. S. (2013). Ribosome profiling provides evidence that large noncoding RNAs do not encode proteins. *Cell* 154, 240–251. doi: 10.1016/j.cell.2013.06.009

Guydosh, N. R., and Green, R. (2014). Dom34 rescues ribosomes in 3' untranslated regions. *Cell* 156, 950–962. doi: 10.1016/j.cell.2014.02.006

Hemu, X., Serra, A., Darwis, D. A., Cornvik, T., Sze, S. K., and Tam, J. P. (2018). Peptidomic identification of cysteine-rich peptides from plants. *Methods Mol. Biol.* 1719, 379–393. doi: 10.1007/978-1-4939-7537-2_26

Hinnebusch, A. G., Ivanov, I. P., and Sonenberg, N. (2016). Translational control by 5'-untranslated regions of eukaryotic mRNAs. *Science* 352, 1413–1416. doi: 10.1126/science.aad9868

Hsu, P. Y., and Benfey, P. N. (2018). Small but mighty: functional peptides encoded by small ORFs in plants. *Proteomics* 18:e1700038. doi: 10.1002/pmic.201700038

Hsu, P. Y., Calviello, L., Wu, H. L., Li, F. W., Rothfels, C. J., Ohler, U., et al. (2016). Super-resolution ribosome profiling reveals unannotated translation events in Arabidopsis. *Proc. Natl. Acad. Sci. U.S.A.* 113, E7126–E7135. doi: 10.1073/pnas.1614788113

Huang, K., Baldrich, P., Meyers, B. C., and Caplan, J. L. (2019). sRNA-FISH: versatile fluorescent *in situ* detection of small RNAs in plants. *Plant J.* 98, 359–369. doi: 10.1111/tpj.14210

Ingolia, N. T., Ghaemmaghami, S., Newman, J. R., and Weissman, J. S. (2009). Genome-wide analysis *in vivo* of translation with nucleotide resolution using ribosome profiling. *Science* 324, 218–223. doi: 10.1126/science.1168978

Kalvari, I., Nawrocki, E. P., Argasinska, J., Quinones-Olvera, N., Finn, R. D., Bateman, A., et al. (2018). Non-Coding RNA Analysis Using the Rfam Database. *Current Protocols in Bioinformatics* 62, e51. doi: 10.1002/cpbi.51

Langmead, B. and Salzberg, S. L. (2012). Fast gapped-read alignment with Bowtie 2. *Nature Methods* 9, 357–359. doi: 10.1038/nmeth.1923

Lease, K. A., and Walker, J. C. (2006). The Arabidopsis unannotated secreted peptide database, a resource for plant peptidomics. *Plant Physiol.* 142, 831–838. doi: 10.1104/pp.106.086041

Li, L., Eichten, S. R., Shimizu, R., Petsch, K., Yeh, C. T., Wu, W., et al. (2014). Genome-wide discovery and characterization of maize long non-coding RNAs. *Genome Biol.* 15:R40. doi: 10.1186/gb-2014-15-2-r40

Li, Y., Guo, Q., Liu, P., Huang, J., Zhang, S., Yang, G., et al. (2021). Dual roles of the serine/arginine-rich splicing factor SR45a in promoting and interacting with nuclear cap-binding complex to modulate the salt-stress response in Arabidopsis. *New Phytol.* 230, 641–655. doi: 10.1111/nph.17175

Ma, C., Lu, Y., Bai, S., Zhang, W., Duan, X., Meng, D., et al. (2014). Cloning and characterization of miRNAs and their targets, including a novel miRNA-targeted NBS-LRR protein class gene in apple (Golden Delicious). *Mol. Plant* 7, 218–230. doi: 10.1093/mp/sst101

Marshall, E., Costa, L. M., and Gutierrez-Marcos, J. (2011). Cysteine-rich peptides (CRPs) mediate diverse aspects of cell-cell communication in plant reproduction and development. *J. Exp. Bot.* 62, 1677–1686. doi: 10.1093/jxb/err002

Oh, Y., Robertson, S. L., Parker, J., Muddiman, D. C., and Dean, R. A. (2017). Comparative proteomic analysis between nitrogen supplemented and starved conditions in Magnaporthe oryzae. *Proteome Sci.* 15:20. doi: 10.1186/s12953-017-0128-y

Ohyama, K., Ogawa, M., and Matsubayashi, Y. (2008). Identification of a biologically active, small, secreted peptide in Arabidopsis by *in silico* gene screening, followed by LC-MS-based structure analysis. *Plant J.* 55, 152–160. doi: 10.1111/j.1365-313X.2008.03464.x

Okamoto, M., Matsui, A., Tanaka, M., Morosawa, T., Ishida, J., Iida, K., et al. (2016). Sm-like protein-mediated RNA metabolism is required for heat stress tolerance in arabidopsis. *Front. Plant Sci.* 7:1079. doi: 10.3389/fpls.2016.01079

Olexiouk, V., Van Criekinge, W., and Menschaert, G. (2018). An update on sORFs.org: a repository of small ORFs identified by ribosome profiling. *Nucleic Acids Res.* 46, D497–D502. doi: 10.1093/nar/gkx1130

Perea-Resa, C., Hernández-Verdeja, T., López-Cobollo, R., del Mar Castellano, M., and Salinas, J. (2012). LSM proteins provide accurate splicing and decay of selected transcripts to ensure normal Arabidopsis development. *Plant Cell* 24, 4930–4947. doi: 10.1105/tpc.112.103697

Pertea, M., Pertea, G. M., Antonescu, C. M., Chang, T. C., Mendell, J. T., and Salzberg, S. L. (2015). StringTie enables improved reconstruction of a transcriptome from RNA-seq reads. *Nat. Biotechnol.* 33, 290–295. doi: 10.1038/nbt.3122

Ren, Y., Song, Y., Zhang, L., Guo, D., He, J., Wang, L., et al. (2021). Coding of non-coding RNA: insights into the regulatory functions of Pri-MicroRNA-encoded peptides in plants. *Front. Plant Sci.* 12:641351. doi: 10.3389/fpls.2021.641351

Ruiz-Orera, J., and Albà, M. M. (2019). Translation of small open reading frames: roles in regulation and evolutionary innovation. *Trends Genet.* 35, 186–198. doi: 10.1016/j.tig.2018.12.003

Ruiz-Orera, J., Verdaguer-Grau, P., Villanueva-Cañas, J. L., Messeguer, X., and Albà, M. M. (2018). Translation of neutrally evolving peptides provides a basis for *de novo* gene evolution. *Nat. Ecol. Evol.* 2, 890–896. doi: 10.1038/s41559-018-0506-6

Samad, A. F. A., Sajad, M., Nazaruddin, N., Fauzi, I. A., Murad, A. M. A., Zainal, Z., et al. (2017). MicroRNA and transcription factor: key players in plant regulatory network. *Front. Plant Sci.* 8:565. doi: 10.3389/fpls.2017.00565

Schnable, P. S., Ware, D., Fulton, R. S., Stein, J. C., Wei, F., Pasternak, S., et al. (2009). The B73 maize genome: complexity, diversity, and dynamics. *Science* 326, 1112–1115. doi: 10.1126/science.1178534

Slavoff, S. A., Mitchell, A. J., Schwaid, A. G., Cabili, M. N., Ma, J., Levin, J. Z., et al. (2013). Peptidomic discovery of short open reading frame-encoded peptides in human cells. *Nat. Chem. Biol.* 9, 59–64. doi: 10.1038/nchembio.1120

Szakonyi, D., and Duque, P. (2018). Alternative splicing as a regulator of early plant development. *Front. Plant Sci.* 9:1174. doi: 10.3389/fpls.2018.01174

Tian, T., Liu, Y., Yan, H., You, Q., Yi, X., Du, Z., et al. (2017). agriGO v2.0: a GO analysis toolkit for the agricultural community, 2017 update. *Nucleic Acids Res.* 45, W122–W129. doi: 10.1093/nar/gkx382

Trapnell, C., Roberts, A., Goff, L., Pertea, G., Kim, D., Kelley, D. R., et al. (2012). Differential gene and transcript expression analysis of RNA-seq experiments with TopHat and Cufflinks. *Nat. Protoc.* 7, 562–578. doi: 10.1038/nprot.2012.016

van Heesch, S., Witte, F., Schneider-Lunitz, V., Schulz, J. F., Adami, E., Faber, A. B., et al. (2019). The translational landscape of the human heart. *Cell* 178, 242–260.e229. doi: 10.1016/j.cell.2019.05.010

Wagih, O. (2017). ggseqlogo: a versatile R package for drawing sequence logos. *Bioinformatics* 33, 3645–3647. doi: 10.1093/bioinformatics/btx469

Walley, J. W., and Briggs, S. P. (2015). Dual use of peptide mass spectra: protein atlas and genome annotation. *Curr. Plant Biol.* 2, 21–24. doi: 10.1016/j.cpb.2015.02.001

Wang, P., Yao, S., Kosami, K. I., Guo, T., Li, J., Zhang, Y., et al. (2020). Identification of endogenous small peptides involved in rice immunity through transcriptomics- and proteomics-based screening. *Plant Biotechnol. J.* 18, 415–428. doi: 10.1111/pbi.13208

Wang, S., Tian, L., Liu, H., Li, X., Zhang, J., Chen, X., et al. (2020). Large-scale discovery of non-conventional peptides in maize and arabidopsis through an integrated peptidogenomic pipeline. *Mol. Plant* 13, 1078–1093. doi: 10.1016/j.molp.2020.05.012

Wen, J., Lease, K. A., and Walker, J. C. (2004). DVL, a novel class of small polypeptides: overexpression alters Arabidopsis development. *Plant J.* 37, 668–677. doi: 10.1111/j.1365-313X.2003.01994.x

Wu, H. L., Song, G., Walley, J. W., and Hsu, P. Y. (2019). The tomato translational landscape revealed by transcriptome assembly and ribosome profiling. *Plant Physiol.* 181, 367–380. doi: 10.1104/pp.19.00541

Wu, X., Ding, D., Shi, C., Xue, Y., Zhang, Z., Tang, G., et al. (2016). microRNA-dependent gene regulatory networks in maize leaf senescence. *BMC Plant Biol.* 16:73. doi: 10.1186/s12870-016-0755-y

Xia, J., Yamaji, N., and Ma, J. F. (2013). A plasma membrane-localized small peptide is involved in rice aluminum tolerance. *Plant J.* 76, 345–355. doi: 10.1111/tpj.12296

Xiao, Z., Huang, R., Xing, X., Chen, Y., Deng, H., and Yang, X. (2018). *De novo* annotation and characterization of the translatome with ribosome profiling data. *Nucleic Acids Res.* 46:e61. doi: 10.1093/nar/gky179

Xiong, L., Gong, Z., Rock, C. D., Subramanian, S., Guo, Y., Xu, W., et al. (2001). Modulation of abscisic acid signal transduction and biosynthesis by an Sm-like protein in Arabidopsis. *Dev. Cell* 1, 771–781. doi: 10.1016/S1534-5807(01)00087-9

Zhai, J., Zhang, H., Arikit, S., Huang, K., Nan, G. L., Walbot, V., et al. (2015). Spatiotemporally dynamic, cell-type-dependent premeiotic and meiotic phasiRNAs in maize anthers. *Proc. Natl. Acad. Sci. U.S.A.* 112, 3146–3151. doi: 10.1073/pnas.1418918112

Zhang, W., Han, Z., Guo, Q., Liu, Y., Zheng, Y., Wu, F., et al. (2014). Identification of maize long non-coding RNAs responsive to drought stress. *PLoS ONE* 9:e98958. doi: 10.1371/journal.pone.0098958

Zhou, P., Silverstein, K. A., Gao, L., Walton, J. D., Nallu, S., Guhlin, J., et al. (2013). Detecting small plant peptides using SPADA (Small Peptide Alignment Discovery Application). *BMC Bioinformatics* 14:335. doi: 10.1186/1471-2105-14-335

Zhu, W., Xu, J., Chen, S., Chen, J., Liang, Y., Zhang, C., et al. (2021). Large-scale translatome profiling annotates functional genome and reveals the key role of genic 3and#x2b9; untranslated regions in translatomic variation in plants. *Plant Commun.* 2, 100181. doi: 10.1016/j.xplc.2021.100181

Zipfel, C., and Oldroyd, G. E. (2017). Plant signalling in symbiosis and immunity. *Nature* 543, 328–336. doi: 10.1038/nature22009

Conflict of Interest: The authors declare that the research was conducted in the absence of any commercial or financial relationships that could be construed as a potential conflict of interest.

frontiers in Plant Science

MINI REVIEW
published: 19 July 2021
doi: 10.3389/fpls.2021.704490

Signaling Peptides Regulating Abiotic Stress Responses in Plants

*Jin Sun Kim[1,2], Byeong Wook Jeon[3] and Jungmook Kim[1,2]**

[1] Department of Bioenergy Science and Technology, Chonnam National University, Gwangju, South Korea, [2] Department of Integrative Food, Bioscience and Technology, Chonnam National University, Gwangju, South Korea, [3] Kumho Life Science Laboratory, Chonnam National University, Gwangju, South Korea

As sessile organisms, plants are exposed to constantly changing environments that are often stressful for their growth and development. To cope with these stresses, plants have evolved complex and sophisticated stress-responsive signaling pathways regulating the expression of transcription factors and biosynthesis of osmolytes that confer tolerance to plants. Signaling peptides acting like phytohormones control various aspects of plant growth and development via cell-cell communication networks. These peptides are typically recognized by membrane-embedded receptor-like kinases, inducing activation of cellular signaling to control plant growth and development. Recent studies have revealed that several signaling peptides play important roles in plant responses to abiotic stress. In this mini review, we provide recent findings on the roles and signaling pathways of peptides that are involved in coordinating plant responses to abiotic stresses, such as dehydration, high salinity, reactive oxygen species, and heat. We also discuss recent developments in signaling peptides that play a role in plant adaptation responses to nutrient deficiency stress, focusing on nitrogen and phosphate deficiency responses.

Keywords: signaling peptides, receptor-like kinases, dehydration, salt, reactive oxygen species

OPEN ACCESS

Edited by:
Fuminori Takahashi,
Tokyo University of Science, Japan

Reviewed by:
Farida Minibayeva,
Kazan Institute of Biochemistry and Biophysics (RAS), Russia
Linhui Yu,
Brookhaven National Laboratory, United States

****Correspondence:***
Jungmook Kim
jungmkim@jnu.ac.kr

Specialty section:
This article was submitted to Plant Physiology, a section of the journal Frontiers in Plant Science

Received: *14 May 2021*
Accepted: *25 June 2021*
Published: *19 July 2021*

Citation:
Kim JS, Jeon BW and Kim J (2021) Signaling Peptides Regulating Abiotic Stress Responses in Plants. Front. Plant Sci. 12:704490. doi: 10.3389/fpls.2021.704490

INTRODUCTION

As sessile organisms, plants are constantly exposed to a wide range of abiotic stresses, such as drought, high salinity, cold, heat, flooding, and toxic metals in the soil, which negatively affect plant growth, fertility, development, metabolism, photosynthesis, and immune response and impair plant yield and quality in the field (Jeon and Kim, 2013; Suzuki et al., 2014; Ohama et al., 2017; Casal and Balasubramanian, 2019; Hayes et al., 2021). Plants have evolved sophisticated and complex metabolic pathways, signaling modules, such as Ca^{2+}-calcineurin B-like (CBL)-CBL-interacting protein kinases (CIPKs) and mitogen-activated protein kinases (MAPKs) modules, and stress-responsive transcription factors for gaining stress tolerance (Qin et al., 2011; De Zelicourt et al., 2016; Zhu, 2016; Shi et al., 2018; Tang et al., 2020). Recent studies have revealed that signaling peptides acting like phytohormones regulate various biochemical, developmental, and physiological processes to coordinate diverse aspects of plant growth and development (Matsubayashi, 2014; Oh et al., 2018; Fletcher, 2020; Jeon et al., 2021; Kim et al., 2021). Signaling peptides are typically small peptides comprising 5–20 amino acids in length or peptides of 40–100 amino acids; they are processed from precursor proteins or directly translated from small open reading frames without proteolytic processing (Matsubayashi, 2014; Oh et al., 2018).

These peptides can be mobile in a long or short distance or membrane-bound and are typically recognized by the membrane-localized leucine-rich repeat (LRR)-receptor-like kinases (RLKs), mostly in association with shape-complementary coreceptors. This ligand-receptor/coreceptor association initiates intracellular signaling to control plant growth and development. Several peptides controlling adaptation and tolerance mechanisms in response to abiotic stress have been identified. In this review, we summarize the roles and signaling pathways of small peptides involved in coordinating plant responses against abiotic stresses, such as dehydration, high salinity, reactive oxygen species (ROS), and heat, and discuss future directions on the peptide research in abiotic stress response. The roles of signaling peptides regulating plant responses under nitrogen or phosphate deficiency are also discussed.

DEHYDRATION STRESS RESPONSE

CLE Peptides

The CLAVATA3(CLV)/EMBRYO-SURROUNDING REGION-RELATED (CLE) peptides are a major group of signaling peptides in plants (Goad et al., 2017), usually 12–14 amino acids long and processed from a large precursor protein (Strabala et al., 2014). Several CLE peptides play important roles in root meristem maintenance, vasculature tissue and shoot development, and stomata formation and function (Oh et al., 2018; Fletcher, 2020; Jeon et al., 2021). In particular, *CLE25* and *CLE9* mediate dehydration stress tolerance response in *Arabidopsis thaliana* (Arabidopsis) (Takahashi et al., 2018; Zhang et al., 2019; **Figure 1A**).

CLE25 is a mobile peptide that links water deficit to abscisic acid (ABA)-mediated tolerance to dehydration stress (Takahashi et al., 2018; **Figure 1A**). Water deficiency upregulates *CLE25* expression in root vasculature; peptides then migrate to the leaves, inducing stomatal closure (Takahashi et al., 2018; **Figure 1A**). *CLE25* peptides applied to the roots can induce expression of the gene encoding the enzyme NINE-CIS-EPOXYCAROTENOID DIOXYGENASE3 (NCED3), which cleaves an ABA precursor molecule and generates bioactive ABA (**Figure 1A**). The *cle25* knockout mutants are more sensitive to dehydration than wild type (Takahashi et al., 2018). Grafting assays showed that root-derived *CLE25* during dehydration stress is recognized by BARELY ANY MERISTEM1 (BAM1) and BAM2 receptors only in the leaves but not in the roots (Takahashi et al., 2018); the *bam1 bam2* mutants are dehydration-sensitive (Takahashi et al., 2018). These results suggest that *CLE25*–BAM modules convey dehydration signals in the soil from the roots to the leaves in a long-distance signaling to induce ABA accumulation via upregulating *NCED3* expression for stress adaptation and resistance against drought conditions.

CLE9 plays a role in enhancing drought tolerance by regulating stomatal closure (Zhang et al., 2019; **Figure 1A**). Exogenous application of *CLE9* peptides or overexpression of *CLE9* induces stomatal closure and enhances drought tolerance. Genetic analysis showed that *CLE9*-induced stomatal closure requires MITOGEN-ACTIVATED PROTEIN KINASE (MAPK)3 (MPK3)/6 and two guard cell ABA-signaling components–protein kinase OPEN STOMATA 1 (OST1) and anion channel protein SLOW ANION CHANNEL-ASSOCIATED 1 (SLAC1) (Zhang et al., 2019; **Figure 1A**). Moreover, the production of hydrogen peroxide and nitric oxide is stimulated by *CLE9* and disappears in NADPH oxidase-deficient or nitric reductase mutants, respectively (Zhang et al., 2019). These findings indicate that *CLE9* controls stomatal closure in response to drought stress by sharing OST1 and SLAC1, thereby enhancing drought stress tolerance. *CLE9* is specifically expressed in guard cells (Zhang et al., 2019); hence, *CLE9*, unlike *CLE25*, acts locally to control stomatal closure. Further, the *bam*/*clv1* mutants respond normally to *CLE9* peptides in stomatal closure, indicating that BAM receptors are unlikely to be involved in the recognition of *CLE9* peptides (Zhang et al., 2019).

IDA Peptide

The INFLORESCENCE DEFICIENT IN ABSCISSION (IDA) peptide functions in floral organ abscission and lateral root emergence through the LRR-RLKs, HAESA (HAE), and HAESA-LIKE 2 (HSL2) receptors and the MAPK KINASE4 (MKK4)/5-MPK3/6 cascade (Butenko et al., 2003; Stenvik et al., 2006; Cho et al., 2008; Kumpf et al., 2013; Zhu et al., 2019). The extended 20-amino acid Pro-rich motif at the C terminus of IDA, was sufficient to induce floral abscission in Arabidopsis (Stenvik et al., 2008). A 12-amino acid peptide with hydroxylation of a Pro residue at position 7 was identified as the most efficient peptide for signaling activation through HSL2 receptor in *Nicotiana benthamiana* leaf tissue (Butenko et al., 2014). *IDA* is involved in drought-induced cauline leaf abscission (Patharkar and Walker, 2016). Expression of *HAE* and *IDA* is induced in leaf abscission zones when the leaves are subject to drought conditions (Patharkar and Walker, 2016). Mutant analysis showed that *IDA*, *HAE*/*HSL2*, and *MKK4*/*5* are all necessary for drought-induced cauline leaf abscission (**Figure 1B**) as they function in floral organ abscission and lateral root emergence (Patharkar and Walker, 2016). *IDA* induces cell-wall breakdown and thus cell separation, causing these organ abscission events (Stenvik et al., 2006; Zhu et al., 2019; **Figure 1B**).

PSK Peptide

Phytosulfokine-α (PSK-α) is a pentapeptide sulfated at two Tyr residues (Stührwohldt et al., 2011). Seven Arabidopsis loci encode putative *PSK* precursor genes (Kaufmann and Sauter, 2019). PSK-PSK receptor (PSKR)/coreceptor SOMATIC EMBRYOGENESIS RECEPTOR KINASE 3 (SERK3) modules promote cell elongation and primary/lateral root growth (Amano et al., 2007; Ladwig et al., 2015; Wang et al., 2015). PSK and subtilases (SBTs), which cleave PSK precursor protein for generating the PSK pentapeptide, play a role in drought stress tolerance in Arabidopsis (Stührwohldt et al., 2021). Four *PSK* genes–*PSK1*, *PSK3*, *PSK4*, and *PSK5*–and three *SBT* genes–*SBT1.4*, *SBT3.7*, and *SBT3.8*–are significantly upregulated in response to osmotic stress, such as mannitol treatment (Stührwohldt et al., 2021). Shoot and root growth is slower in

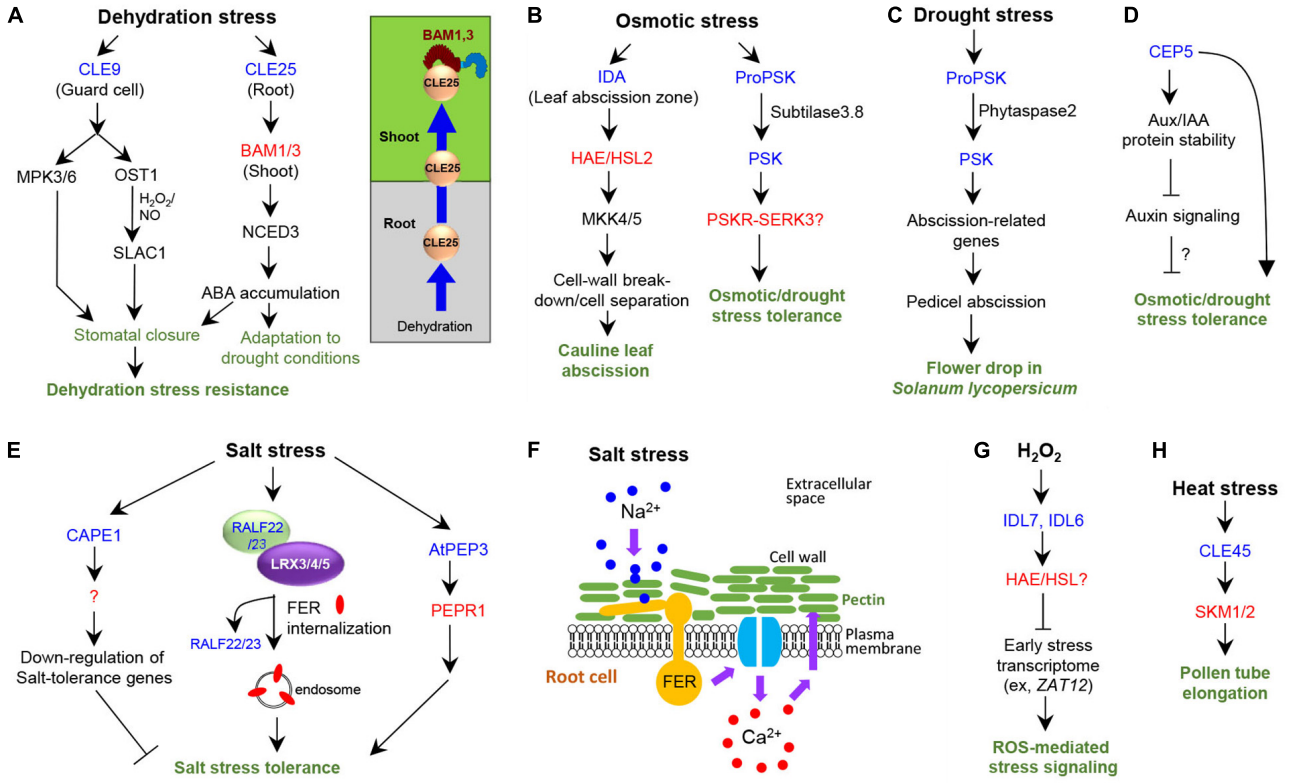

FIGURE 1 | Signaling peptides control abiotic stress responses in plants. Blue and red letters indicate peptides and the cognate receptors, respectively. Plant not specified in the subtitle indicates *Arabidopsis*. **(A)** Roles and signaling pathways of CLE9/25 in dehydration stress response. **(B)** Roles and signaling pathways of IDA and PSK in osmotic stress response. **(C)** Roles of PSK in flower abscission in tomato under drought stress. **(D)** Role of CEP5 in osmotic and drought stress tolerance. **(E)** Roles and signaling pathways in high salinity stress response. **(F)** Role of FER receptor kinase during high salinity stress response to maintain cell-wall integrity in root cells. **(G)** Role of IDL6/7 in ROS-mediated stress signaling. **(H)** Role of CLE45 in pollen tube elongation under heat stress.

sbt3.8 mutant plants than in wild type under osmotic stress, whereas the osmotic stress-induced sensitive phenotype in *sbt3.8* can be recovered by PSK peptide treatment. Arabidopsis plants overexpressing the PSK precursor (*proPSK1*) exhibit enhanced root and hypocotyl growth and osmotic stress tolerance. ProPSK1 is cleaved by SBT3.8 at the C-terminus of the PSK peptide. ProPSK1 processing depends on the Asp residue directly following the cleavage site and is impaired in the *sbt3.8* mutant. Moreover, *SBT3.8* overexpression in Arabidopsis improves osmotic stress tolerance and induces shoot and root growth. These results suggest that SBT3.8 mediates PSK peptide processing from the precursor protein proPSK1, thus contributing to drought stress tolerance (**Figure 1B**).

Phytosulfokine signaling controls drought-induced flower drop in tomato (Reichardt et al., 2020). Overexpression of phytaspase 2 (phyt2), a subtilisin-like protease that cleaves proPSK protein, in tomato plants (*Solanum lycopersicum*) enhances premature flower abscission, whereas *SlPhyt2* knockdown reduces flower drop under drought stress conditions, implying a role of *SlPhyt2* in drought-induced abortion of flower and fruit development (Reichardt et al., 2020). Consistently, *SlPhyt2* expression is induced in response to drought stress in flower pedicels proximal to the abscission zone. Expression of *SlPSK1* and *SlPSK6* is coinduced with that of *SlPhyt2* by drought stress. Using a proteomics assay with a substrate library, the PSK precursor was identified as a candidate substrate for SlPhyt2. Peptides harboring the PSK pentapeptide of varying sizes can be cleaved by SlPhyt2 in an Asp-specific manner, releasing mature PSK *in vitro*. Mature PSK induced pedicel abscission in an inflorescence bioassay. PSK treatment upregulated tomato abscission-related polygalacturonase genes and downregulated genes that maintain the abscission zone in an inactive state, indicating that PSK acts as a signal for pedicel abscission in tomato. These findings suggest that the subtilase SlPhyt2, expressed in the pedicel, produces bioactive PSK, which then triggers abscission by inducing cell wall hydrolases in the abscission zone in response to drought stress (**Figure 1C**).

CEP5 Peptide

The *C-terminally encoded peptide* (*CEP*) genes encode proteins comprising an N-terminal secretion signal, a variable domain, one or more CEP domains, and a short C-terminal extension (Ogilvie et al., 2014). The CEP precursor proteins undergo proteolysis and Pro hydroxylation to become a bioactive 15-amino acid CEP peptide (Ohyama et al., 2008). CEPs and the CEP receptors, CEPR1/2, play diverse roles in plant responses

to changing environmental conditions, such as the systemic N-acquisition response, sucrose-induced lateral root growth enhancement, and primary root growth suppression, under nutrient starvation conditions, such as carbon and nitrogen limitation (Jeon et al., 2021).

CEP5 negatively regulates primary and lateral root development (Roberts et al., 2016) and plays a role in osmotic and drought stress tolerance in Arabidopsis (Smith et al., 2020). Proteome analysis revealed that *CEP5* alters significant portions of the proteins involved in the biological processes "response to stress or to abiotic stimulus", indicating a potential role of *CEP5* in abiotic stress responses. Consistent with this, *CEP5*-overexpression lines or wild type-seedlings treated with hydroxyprolinated *CEP5* peptide exhibit better recovery from drought after re-watering than wild type, indicating that *CEP5* can confer drought stress tolerance. *CEP5*-overexpression line also displays enhanced tolerance in rosette size reduction to osmotic stress and enhanced expression of osmotic stress-inducible transcription factor genes. The *xylem intermixed with phloem (xip)/cepr1 cepr2* double mutant did not display rosette size reduction upon osmotic stress treatment, indicating that CEP5 acts independently of the CEPRs. Notably, *CEP5*-overexpression line displays significant reduction in both *DR5-GUS* or *DR5-LUC* activities and expression of auxin-inducible genes, *LOB DOMAIN-CONTAINING PROTEIN 18* (*LBD18*), *LBD29*, and *PIN-FORMED 1* (*PIN1*). CEP5 stabilizes AUX/IAA proteins, negative regulators of AUXIN RESPONSE FACTORs, by affecting proteasome activity but without altering auxin levels and auxin transport activity (**Figure 1D**). Whether and how the negative regulatory role of CEP5 in auxin response through AUX/IAA stabilization is linked to drought and osmotic stress tolerance need further investigation. Functional analysis of the *cep5* mutants is also necessary to support the results obtained with *CEP5* overexpression.

SALINITY STRESS RESPONSE

CAPE Peptides

CAP-derived peptide 1 (CAPE1) is derived from the C-terminus of PATHOGENESIS-RELATED PROTEIN1b (PR-1b), a member of the cysteine-rich secretory proteins, antigen 5, and pathogenesis-related 1 proteins (CAP) superfamily (Chen et al., 2014). CAPE1 was initially identified using a peptidomics approach from tomato leaves (Chen et al., 2014). CAPE1 induces significant anti-pathogen response in tomato, indicating a role for PR-1 in immune signaling (Chen et al., 2014). In *Arabidopsis*, AtCAPE1, comprising 11 amino acids, negatively regulates salt-stress tolerance (Chien et al., 2015; **Figure 1E**). Nine potential CAPEs from *Arabidopsis* were identified as precursor candidates for CAPEs on the basis of sequence similarity to the precursor of tomato CAPE1 and the C-terminal conserved motif, and were named as the precursor *Arabidopsis thaliana* CAPEs (PROAtCAPEs) (Chien et al., 2015). Among them, *PROAtCAPE1* is down-regulated mainly by salt stress. The *proatcape1* mutant exhibits resistance to growth inhibition under high-salt conditions, whereas exogenous application of synthetic AtCAPE1 peptide or overexpression of *PROAtCAPE1* restores the sensitive phenotype of the mutant, indicating that AtCAPE1 functions as a negative regulator of salt-stress tolerance in *Arabidopsis*. AtCAPE1also negatively regulates salt-inducible genes, such as those involved in osmolyte biosynthesis, detoxification, and dehydration response (Chien et al., 2015). Hence, AtCAPE1 plays a role in the regulation of salt stress responses in *Arabidopsis*.

RALF Peptides

Rapid alkalinization factor (RALF) peptides are 5 kDa cysteine-rich peptides inducing rapid alkalinization of the extracellular compartments of plant cells, thus reducing the proton electrochemical potential required for solute uptake and causing cell growth suppression (Blackburn et al., 2020). RALF peptides are involved in root growth, immune responses, guard cell movement, and pollen tube growth and termination during plant reproductive processes (Ge et al., 2017; Mecchia et al., 2017; Blackburn et al., 2020). They are recognized by the LRR-RLK FERONIA (FER) (Stegmann et al., 2017). RALF22/23-FER module regulates salt tolerance by interacting with the cell-wall LRR extensins (LRX)3/4/5 (Zhao et al., 2018; **Figure 1E**). LRX proteins comprise an N-terminal LRR and a C-terminal extension domain and are localized to the cell wall, playing a role in cell wall-plasma membrane communication (Fabrice et al., 2018). The *lrx3/4/5* triple mutant, *fer* mutant, and *RALF22* or *RALF23*-overexpressing plants all display similar phenotypes, such as reduced plant growth and salt hypersensitivity (Zhao et al., 2018). RALF peptides are physically associated with LRX and FER proteins (Zhao et al., 2018). Salt stress causes dissociation of mature RALF22 peptides from LRX proteins, thereby inducing FER internalization via an endosomal pathway (Zhao et al., 2018; **Figure 1E**). Therefore, RALF22/23-FER and LRX3/4/5 regulate plant growth and salt tolerance via salt-induced cell wall changes.

FERONIA is also necessary for cell-wall integrity, preventing root cells from bursting during growth under high salt stress (Feng et al., 2018). The glycosylphosphatidylinositol-anchored protein (GPI-AP) LORELEI-like GPI-AP1 (LLG1) interacts directly with FER in the endoplasmic reticulum and is required for both FER localization to the plasma membrane and FER-mediated RHO GTPase signaling (Li et al., 2015). *llg1* mutant roots display the same ionic sensitivity and cellular damage caused by a loss of cell-wall integrity as the *fer* mutant (Feng et al., 2018), indicating that FER-LLG1 interaction is important for maintaining cell-wall integrity in the roots. Fortification of pectin cross-links restores growth and cell-wall integrity of *fer* seedlings under salt stress (Feng et al., 2018). The FER extracellular domain binds pectin *in vitro*. FER is necessary for salinity-induced $[Ca^{2+}]$ transients to maintain cell wall integrity during growth recovery, suggesting that FER induces calcium signaling in response to salt stress to maintain cell wall integrity by physically interacting with pectin in the cell wall (**Figure 1F**). Further investigation is needed to identify the calcium channel responsible for FER-mediated induction of calcium transients and how such transients regulate downstream signaling to repair salt stress-induced cell-wall damage. The *ralf1* mutant and a

RALF1 RNAi transgenic line did not show significant root growth inhibition, indicating that RALF1 does not display a critical function in regulating root growth under salt stress (Feng et al., 2018). As RALF22/23-FER module regulates plant growth and salt tolerance via salt-induced cell-wall changes (Zhao et al., 2018), RALF22/23 might play a role in FER-mediated protection of root cells from bursting under salt stress.

AtPEP3

Plant elicitor peptides (Peps) are endogenous elicitors of pattern-triggered immunity against bacteria, fungi, and herbivores (Yamaguchi and Huffaker, 2011; Bartels and Boller, 2015). Among eight members of the *Arabidopsis thaliana* precursor Pep (*AtPROPEP*) family in *Arabidopsis*, AtPep3 plays a role in salinity stress response (Nakaminami et al., 2018). Among the *AtPROPEP* gene family, *AtPROPEP3* displays the greatest induction in response to high salinity. Overexpression of *AtPROPEP3* or exogenous application of synthetic AtPep3 peptide (30 amino acids) derived from the C-terminal region of PROPEP3 induces salt stress tolerance (Nakaminami et al., 2018). Conversely, *AtPROPEP3*-RNAi lines are hypersensitive under salinity stress, which is recovered by AtPep3 peptide application. Endogenous AtPep3 peptide was further identified from NaCl-treated plants via mass spectrometry (Nakaminami et al., 2018). AtPEP1-6 peptides bind to the LRR-RLK PEP RECEPTOR1 (PEPR1) and AtPEP1/2 peptides bind to PEPR2 to initiate immune signaling (Yamaguchi et al., 2006, 2010). Although high-salt treatment significantly reduces plant survival of the *pepr1*, *pepr2*, and *pepr1/2* mutants, exogenous AtPep3 peptide application recovers plant survival only in the *pepr2* mutants (Nakaminami et al., 2018), indicating that AtPep3 is recognized by the PEPR1 receptor to induce salinity stress tolerance in plants (**Figure 1E**). Hence, AtPEP3–PEPR1 module may have a dual function in both salinity stress tolerance and immune responses.

ROS-MEDIATED STRESS SIGNALING

IDA-LIKE (IDL) Peptides

Bioinformatic analyses identified eight *IDL* genes with similarity to IDA (Butenko et al., 2003; Vie et al., 2015). *In silico* analysis showed that *IDL6* and *IDL7* respond to biotic and abiotic stresses, such as cold, salt, and UV light in the root (Vie et al., 2015). Application of IDL6 and IDL7 peptides to *Arabidopsis* reduces the expression of early stress-responsive genes, including *ZINC FINGER PROTEIN* and *WRKY* genes (Vie et al., 2017). *IDL7* expression is rapidly induced by the ROS hydrogen peroxide, and ROS-induced cell death is mitigated in the *idl7* mutant. IDL7 peptides can attenuate the rapid ROS burst induced by the bacterial elicitor flagellin 22 (flg22), whereas *IDL7* mutation enhances flg22-induced ROS burst. Hence, IDL7 acts as a negative regulator of stress-induced ROS signaling in *Arabidopsis* (**Figure 1G**). As *IDL6* displays expression patterns similar to *IDL7* in response to ROS and IDL6 downregulates similar target genes, IDL6 might act like IDL7 in ROS signaling. Although HAE/HSL2 are likely to perceive IDL6 and IDL7 peptides, the receptors of IDL6/7 peptides remain to be experimentally identified (Vie et al., 2017).

HEAT STRESS RESPONSE

CLE45 Peptide

Environmental stresses negatively affect reproductive development of flowering plants and thus the seed yield (Giorno et al., 2013; De Storme and Geelen, 2014). To date, one signaling peptide is reported to play a role in high temperature stress response in plants (Endo et al., 2013), i.e., the *Arabidopsis CLE45*-STERILITY-REGULATING KINASE MEMBER1 (SKM1)/SMK2 receptor module in pollen tube growth (Endo et al., 2013). *CLE45* prolongs pollen tube growth in *in vitro* pollen tube culture. Further, the double mutation in *SKM1/2* encoding LRR–RLKs causes insensitive phenotype in pollen tube growth *in vitro* in response to synthetic CLE45 peptide. Photoaffinity labeling experiment with the SKM1-HaloTag protein demonstrated that SKM1 physically interacts with CLE45 peptides. GUS reporter expression analysis and artificial crossing experiments suggest that heat-inducible *CLE45* in pistils and *SKM1* in pollen function in the same signaling pathway. Suppression of *CLE45* expression by RNAi or expression of a kinase-dead version of SKM1 acting as a dominant negative form of SKM1 in the *skm1* mutant reduces seed number and size at 30°C but not at room temperature (22°C). Collectively, these findings suggest that the *CLE45*–SKM1/2 pathway sustains pollen tube growth under high temperatures, leading to successful seed production (**Figure 1H**).

NUTRIENT DEFICIENCY STRESS RESPONSES

Nitrogen (N) and inorganic phosphate (Pi) are the most important nutrients required by plants, and thus their deficiency profoundly influences the morphology, physiology, growth, and development in plants (Reddy, 2006). Peptides, such as CEPs, CLEs, and RGFs, were identified to play a role in the regulation of nutrient acquisition and to affect plant physiology and growth responses. CEP1 acts as a root-to-shoot mobile signal to promote compensatory N acquisition in the other N-rich parts of the roots (Okamoto et al., 2016). CEP1 peptides originating from the roots under N deficiency are translocated through the xylem to the shoots, where CEP1 peptides are recognized by XIP1/CEPR1 and CEPR2 receptors, generating descending shoot-to-root signals, CEP Downstream 1 (CEPD1) and CEPD2, which belong to the glutaredoxin family (Tabata et al., 2014; Ohkubo et al., 2017; **Figure 2A**). CEPDs are transported to the roots through the phloem to upregulate the nitrate transporter gene *NRT2.1* for promoting N uptake (Ohkubo et al., 2017). CEPD-like 2 originating from the shoots promotes both high-affinity N-uptake in the roots and root-to-shoot transport of nitrate, acting cooperatively with CEPD1/2 (Ota et al., 2020). CEP3 controls nutrient starvation response that suppresses root growth under N-limitation condition, potentially to enhance seedling survival (Delay et al., 2013, 2019; **Figure 2B**).

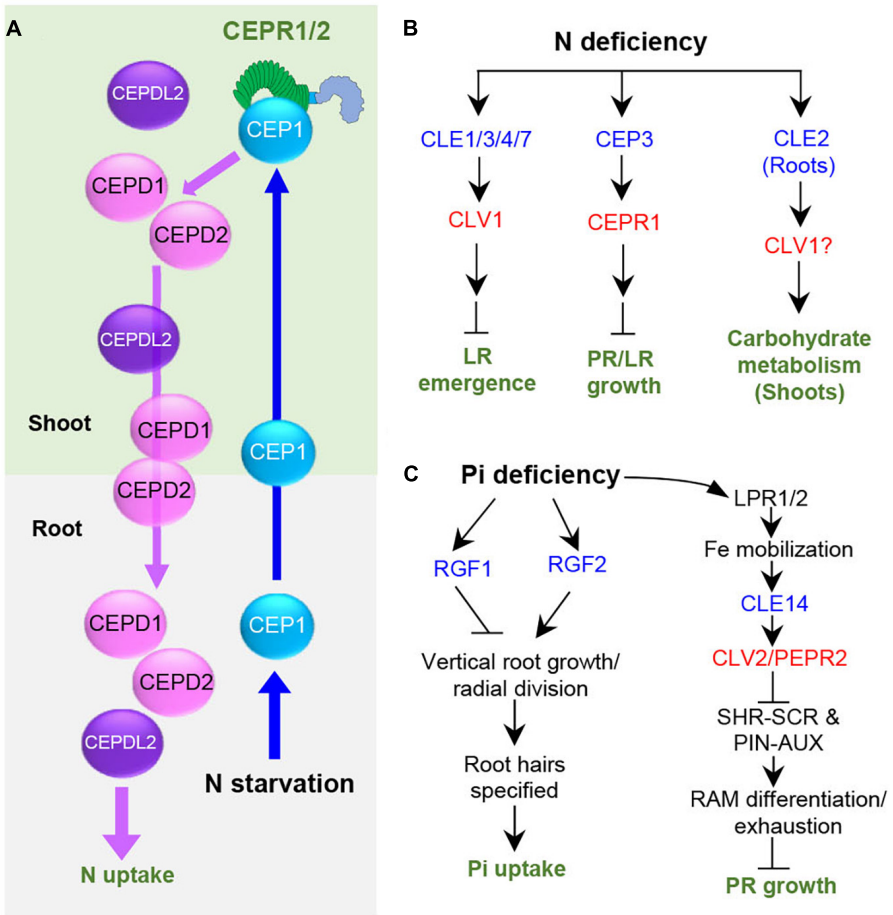

FIGURE 2 | Role and signaling pathways of peptides regulating plant responses under nutritional deficiency stresses in Arabidopsis. Blue and red letters indicate peptides and the cognate receptors, respectively. **(A)** The systemic N-acquisition response. **(B)** Plant responses under nitrogen deficiency. **(C)** Plant responses under phosphate deficiency. N, nitrogen; Pi, inorganic phosphate; LPR, Low Phosphate Root2; LR, lateral root; PR, primary root.

CLE3 inhibits lateral root growth, likely through the receptor CLV1, as the *clv1* mutant displayed longer lateral roots under N deficiency and the inhibitory action of *CLE3* in lateral root formation was compromised in the *clv1* mutant (Araya et al., 2014; **Figure 2B**). *CLE1/3/4/7* genes are upregulated in root pericycle cells by systemic low N levels (Araya et al., 2014), implying that *CLE1/3/4/7* act in the combinatorial manner to control lateral root growth. *CLE2* expression is upregulated by N supply, dark, and sugar starvation (Ma et al., 2020). The *cle2* mutant plants exhibit a severe growth defect with leaf chlorosis under these conditions, whereas *cle3* did not display such growth phenotype under the same condition (Ma et al., 2020). Consistent with this phenotype, overexpression of *CLE2* in roots increased many different genes in shoots, such as dark-inducible genes and the genes involved in metabolite sensing and regulation of carbohydrate metabolism. These results indicate that *CLE2* induced in the roots functions systemically to control carbohydrate metabolism in light-dependent manner (Ma et al., 2020; **Figure 2B**). It is of interest to identify how a single amino acid difference between CLE2 and CLE3 peptides renders these two similar peptides to regulate different plant responses in different tissues. CLE14 mediates low-phosphate stress signal in roots to trigger RAM differentiation and exhaustion through CLV2/PEPR2 receptors via suppressing SCARECROW (SCR)/SHORT-ROOT (SHR) and PIN/auxin pathway, inhibiting primary root growth (Gutiérrez-Alanís et al., 2017; **Figure 2C**). This *CLE14* signaling pathway allows *Arabidopsis* plants to adapt to Pi availability around the roots.

Plants alter root development under Pi scarcity to maximize Pi acquisition. Genetic and microscopic expression analyses suggest that *ROOT GROWTH FACTOR1* (*RGF1*) and *RGF2* regulate different aspects of root development under Pi-deprivation conditions (Cederholm and Benfey, 2015). RGF2 promotes vertical root growth and radial divisions, whereas RGF1 inhibits radial divisions in the root meristem, specifying root hairs for facilitating Pi uptake (Cederholm and Benfey, 2015; **Figure 2C**). RGF1 promotes root meristem activity via a mitogen-activated protein kinase cascade by inducing *RGF1-INDUCIBLE TRANSCRIPTION FACTOR* (*RITF*), which enhances the stability of a master regulator of root stem cells, PLETHORA2, through

ROS signaling (Fernandez et al., 2013; Ou et al., 2016; Shinohara et al., 2016; Song et al., 2016; Fernandez et al., 2020; Lu et al., 2020; Shao et al., 2020; Yamada et al., 2020). It remains to be investigated whether this signaling pathway is involved in RGF-regulated root development caused by Pi deprivation.

CONCLUSION AND PERSPECTIVES

Over recent years, several peptides and signaling pathways have been identified to play roles in coordinating plant responses to abiotic stresses. Although the *Arabidopsis* genome alone encodes several thousands of small coding genes (Takahashi et al., 2019), only few peptides have been reported to be involved in controlling plant abiotic stress responses. Moreover, there exist many questions regarding molecular mechanisms of peptide signaling during abiotic stress responses to be addressed. Functional and molecular understanding on RLKs and the coreceptors that interact with signaling peptides in response to abiotic stress are limited. Questions remain on how peptide precursors are processed into mature peptides, and mature peptides are secreted and transported to the target tissues in long-distance peptide signaling pathways. How peptide-receptor interactions lead to specific developmental controls under abiotic stress need investigation. How peptide-mediated signaling pathways confer plant tolerance to abiotic stresses is also unknown. *CLE25* induces active ABA accumulation in the leaves through long-distance signaling from the roots to the leaves in response to dehydration, and *CLE9* uses ABA signaling components to enhance drought stress tolerance. It will be of interest to investigate how signaling peptides are linked to conventional phytohormone pathways under abiotic stress for obtaining stress resistance. How changes in local concentrations of nutrients and abiotic stressors are sensed in plants for eliciting peptide signaling will be a challenging issue to be explored. As abiotic stresses accelerated by climate changes are a major threat to crop yields and food security, the identification of plant peptides and signaling pathways will provide new strategies to improve stress tolerance in crops for agricultural sustainability.

AUTHOR CONTRIBUTIONS

JiK and BJ wrote the draft manuscript. JuK conceived the review outline and wrote and edited the manuscript. All authors contributed to the article and approved the submitted version.

FUNDING

This work was supported by grants from the Basic Research Lab Program (2020R1A4A2002901) and Mid-Career Researcher Program (2021R1A2C1006296) through the National Research Foundation of Korea (NRF) funded by the Ministry of Science and ICT, and the Next-Generation BioGreen 21 Program from Rural Development Administration, Republic of Korea (PJ013220).

REFERENCES

Amano, Y., Tsubouchi, H., Shinohara, H., Ogawa, M., and Matsubayashi, Y. (2007). Tyrosine-sulfated glycopeptide involved in cellular proliferation and expansion in *Arabidopsis*. *Proc. Natl. Acad. Sci. U.S.A.* 104, 18333–18338. doi: 10.1073/pnas.0706403104

Araya, T., Miyamoto, M., Wibowo, J., Suzuki, A., Kojima, S., Tsuchiya, Y. N., et al. (2014). CLE-CLAVATA1 peptide-receptor signaling module regulates the expansion of plant root systems in a nitrogen-dependent manner. *Proc. Natl. Acad. Sci. U. S. A.* 111, 2029–2034. doi: 10.1073/pnas.1319953111

Bartels, S., and Boller, T. (2015). Quo vadis, Pep? Plant elicitor peptides at the crossroads of immunity, stress, and development. *J. Exp. Bot.* 66, 5183–5193. doi: 10.1093/jxb/erv180

Blackburn, M. R., Haruta, M., and Moura, D. S. (2020). Twenty years of progress in physiological and biochemical investigation of RALF peptides. *Plant Physiol.* 182, 1657–1666. doi: 10.1104/pp.19.01310

Butenko, M. A., Patterson, S. E., Grini, P. E., Stenvik, G. E., Amundsen, S. S., Mandal, A., et al. (2003). Inflorescence deficient in abscission controls floral organ abscission in *Arabidopsis* and identifies a novel family of putative ligands in plants. *Plant Cell* 15, 2296–2307. doi: 10.1105/tpc.014365

Butenko, M. A., Wildhagen, M., Albert, M., Jehle, A., Kalbacher, H., Aalen, R. B., et al. (2014). Tools and strategies to match peptide-ligand receptor pairs. *Plant Cell* 26, 1838–1847. doi: 10.1105/tpc.113.120071

Casal, J. J., and Balasubramanian, S. (2019). Thermomorphogenesis. *Annu. Rev. Plant Biol.* 70, 321–346. doi: 10.1146/annurev-arplant-050718-095919

Cederholm, H. M., and Benfey, P. N. (2015). Distinct sensitivities to phosphate deprivation suggest that RGF peptides play disparate roles in *Arabidopsis* thaliana root development. *New Phytol.* 207, 683–691. doi: 10.1111/nph.13405

Chen, Y. L., Lee, C. Y., Cheng, K. T., Chang, W. H., Huang, R. N., Nam, H. G., et al. (2014). Quantitative peptidomics study reveals that a wound-induced peptide from PR-1 regulates immune signaling in tomato. *Plant Cell* 26, 4135–4148. doi: 10.1105/tpc.114.131185

Chien, P. S., Nam, H. G., and Chen, Y. R. (2015). A salt-regulated peptide derived from the CAP superfamily protein negatively regulates salt-stress tolerance in *Arabidopsis*. *J. Exp. Bot.* 66, 5301–5313. doi: 10.1093/jxb/erv263

Cho, S. K., Larue, C. T., Chevalier, D., Wang, H., Jinn, T. L., Zhang, S., et al. (2008). Regulation of floral organ abscission in *Arabidopsis thaliana*. *Proc. Natl. Acad. Sci. U.S.A.* 105, 15629–15634. doi: 10.1073/pnas.0805539105

De Storme, N., and Geelen, D. (2014). The impact of environmental stress on male reproductive development in plants: biological processes and molecular mechanisms. *Plant Cell Environ.* 37, 1–18. doi: 10.1111/pce.12142

De Zelicourt, A., Colcombet, J., and Hirt, H. (2016). The role of MAPK modules and ABA during abiotic stress signaling. *Trends Plant Sci.* 21, 677–685. doi: 10.1016/j.tplants.2016.04.004

Delay, C., Chapman, K., Taleski, M., Wang, Y., Tyagi, S., Xiong, Y., et al. (2019). CEP3 levels affect starvation-related growth responses of the primary root. *J. Exp. Bot.* 70, 4763–4774. doi: 10.1093/jxb/erz270

Delay, C., Imin, N., and Djordjevic, M. A. (2013). CEP genes regulate root and shoot development in response to environmental cues and are specific to seed plants. *J. Exp. Bot.* 64, 5383–5394. doi: 10.1093/jxb/ert332

Endo, S., Shinohara, H., Matsubayashi, Y., and Fukuda, H. (2013). A novel pollen-pistil interaction conferring high-temperature tolerance during reproduction via CLE45 signaling. *Curr. Biol.* 23, 1670–1676. doi: 10.1016/j.cub.2013.06.060

Fabrice, T. N., Vogler, H., Draeger, C., Munglani, G., Gupta, S., Herger, A. G., et al. (2018). LRX proteins play a crucial role in pollen grain and pollen tube cell wall development. *Plant Physiol.* 176, 1981–1992. doi: 10.1104/pp.17.01374

Feng, W., Kita, D., Peaucelle, A., Cartwright, H. N., Doan, V., Duan, Q., et al. (2018). The FERONIA receptor kinase maintains cell-wall integrity during salt stress through Ca^{2+} signaling. *Curr. Biol.* 28, 666.-675. doi: 10.1016/j.cub.2018.01.023

Fernandez, A., Drozdzecki, A., Hoogewijs, K., Nguyen, A., Beeckman, T., Madder, A., et al. (2013). Transcriptional and functional classification of the GOLVEN/ROOT GROWTH FACTOR/CLE-like signaling peptides reveals their role in lateral root and hair formation. *Plant Physiol.* 161, 954–970. doi: 10.1104/pp.112.206029

Fernandez, A. I., Vangheluwe, N., Xu, K., Jourquin, J., Claus, L. A. N., Morales-Herrera, S., et al. (2020). GOLVEN peptide signalling through RGI receptors and MPK6 restricts asymmetric cell division during lateral root initiation. *Nat. Plants* 6, 533–543. doi: 10.1038/s41477-020-0645-z

Fletcher, J. C. (2020). Recent advances in *Arabidopsis* CLE peptide signaling. *Trends Plant Sci.* 25, 1005–1016. doi: 10.1016/j.tplants.2020.04.014

Ge, Z., Bergonci, T., Zhao, Y., Zou, Y., Du, S., Liu, M. C., et al. (2017). *Arabidopsis* pollen tube integrity and sperm release are regulated by RALF-mediated signaling. *Science* 358, 1596–1600. doi: 10.1126/science.aao3642

Giorno, F., Wolters-Arts, M., Mariani, C., and Rieu, I. (2013). Ensuring reproduction at high temperatures: the heat stress response during anther and pollen development. *Plants (Basel)* 2, 489–506. doi: 10.3390/plants2030489

Goad, D. M., Zhu, C., and Kellogg, E. A. (2017). Comprehensive identification and clustering of CLV3/ESR-related (CLE) genes in plants finds groups with potentially shared function. *New Phytol.* 216, 605–616. doi: 10.1111/nph.14348

Gutiérrez-Alanís, D., Yong-Villalobos, L., Jiménez-Sandoval, P., Alatorre-Cobos, F., Oropeza-Aburto, A., Mora-Macías, J., et al. (2017). Phosphate starvation-dependent iron mobilization induces CLE14 expression to trigger root meristem differentiation through CLV2/PEPR2 signaling. *Dev. Cell* 41, 555–570. doi: 10.1016/j.devcel.2017.05.009

Hayes, S., Schachtschabel, J., Mishkind, M., Munnik, T., and Arisz, S. A. (2021). Hot topic: thermosensing in plants. *Plant Cell Environ.* 44, 2018–2033. doi: 10.1111/pce.13979

Jeon, B. W., Kim, M. J., Pandey, S. K., Oh, E., Seo, P. J., and Kim, J. (2021). Recent advances in peptide signaling during *Arabidopsis* root development. *J. Exp. Bot.* 72, 2889–2902. doi: 10.1093/jxb/erab050

Jeon, J., and Kim, J. (2013). Cold stress signaling networks in *Arabidopsis*. *J. Plant Biol.* 56, 69–76. doi: 10.1007/s12374-013-0903-y

Kaufmann, C., and Sauter, M. (2019). Sulfated plant peptide hormones. *J. Exp. Bot.* 70, 4267–4277. doi: 10.1093/jxb/erz292

Kim, M. J., Jeon, B. W., Oh, E., Seo, P. J., and Kim, J. (2021). Peptide signaling during plant reproduction. *Trends Plant Sci.* doi: 10.1016/j.tplants.2021.02.008 Epub ahead of print.

Kumpf, R. P., Shi, C. L., Larrieu, A., Stø, I. M., Butenko, M. A., Péret, B., et al. (2013). Floral organ abscission peptide IDA and its HAE/HSL2 receptors control cell separation during lateral root emergence. *Proc. Natl. Acad. Sci. U.S.A.* 110, 5235–5240. doi: 10.1073/pnas.1210835110

Ladwig, F., Dahlke, R. I., Stührwohldt, N., Hartmann, J., Harter, K., and Sauter, M. (2015). Phytosulfokine regulates growth in *Arabidopsis* through a response module at the plasma membrane that includes CYCLIC NUCLEOTIDE-GATED CHANNEL17, H+-ATPase, and BAK1. *Plant Cell* 27, 1718–1729. doi: 10.1105/tpc.15.00306

Li, C., Yeh, F. L., Cheung, A. Y., Duan, Q., Kita, D., Liu, M. C., et al. (2015). Glycosylphosphatidylinositol-anchored proteins as chaperones and co-receptors for FERONIA receptor kinase signaling in *Arabidopsis*. *Elife* 4:e06587. doi: 10.7554/eLife.06587

Lu, X., Shi, H., Ou, Y., Cui, Y., Chang, J., Peng, L., et al. (2020). RGF1-RGI1, a peptide-receptor complex, regulates *Arabidopsis* root meristem development via a MAPK signaling cascade. *Mol. Plant* 13, 1594–1607. doi: 10.1016/j.molp.2020.09.005

Ma, D., Endo, S., Betsuyaku, S., Shimotohno, A., and Fukuda, H. (2020). CLE2 regulates light-dependent carbohydrate metabolism in *Arabidopsis* shoots. *Plant Mol. Biol.* 104, 561–574. doi: 10.1007/s11103-020-01059-y

Matsubayashi, Y. (2014). Posttranslationally modified small-peptide signals in plants. *Annu. Rev. Plant Biol.* 65, 385–413. doi: 10.1146/annurev-arplant-050312-120122

Mecchia, M. A., Santos-Fernandez, G., Duss, N. N., Somoza, S. C., Boisson-Dernier, A., Gagliardini, V., et al. (2017). RALF4/19 peptides interact with LRX proteins to control pollen tube growth in *Arabidopsis*. *Science* 358, 1600–1603. doi: 10.1126/science.aao5467

Nakaminami, K., Okamoto, M., Higuchi-Takeuchi, M., Yoshizumi, T., Yamaguchi, Y., Fukao, Y., et al. (2018). AtPep3 is a hormone-like peptide that plays a role in the salinity stress tolerance of plants. *Proc. Natl. Acad. Sci. U.S.A.* 115, 5810–5815. doi: 10.1073/pnas.1719491115

Ogilvie, H. A., Imin, N., and Djordjevic, M. A. (2014). Diversification of the C-TERMINALLY ENCODED PEPTIDE (CEP) gene family in angiosperms, and evolution of plant-family specific CEP genes. *BMC Genomics* 15:870. doi: 10.1186/1471-2164-15-870

Oh, E., Seo, P. J., and Kim, J. (2018). Signaling peptides and receptors coordinating plant root development. *Trends Plant Sci.* 23, 337–351. doi: 10.1016/j.tplants.2017.12.007

Ohama, N., Sato, H., Shinozaki, K., and Yamaguchi-Shinozaki, K. (2017). Transcriptional regulatory network of plant heat stress response. *Trends Plant Sci.* 22, 53–65. doi: 10.1016/j.tplants.2016.08.015

Ohkubo, Y., Tanaka, M., Tabata, R., Ogawa-Ohnishi, M., and Matsubayashi, Y. (2017). Shoot-to-root mobile polypeptides involved in systemic regulation of nitrogen acquisition. *Nat. Plants* 3:17029. doi: 10.1038/nplants.2017.29

Ohyama, K., Ogawa, M., and Matsubayashi, Y. (2008). Identification of a biologically active, small, secreted peptide in *Arabidopsis* by in silico gene screening, followed by LC-MS-based structure analysis. *Plant J.* 55, 152–160. doi: 10.1111/j.1365-313X.2008.03464.x

Okamoto, S., Tabata, R., and Matsubayashi, Y. (2016). Long-distance peptide signaling essential for nutrient homeostasis in plants. *Curr. Opin. Plant Biol.* 34, 35–40. doi: 10.1016/j.pbi.2016.07.009

Ota, R., Ohkubo, Y., Yamashita, Y., Ogawa-Ohnishi, M., and Matsubayashi, Y. (2020). Shoot-to-root mobile CEPD-like 2 integrates shoot nitrogen status to systemically regulate nitrate uptake in *Arabidopsis*. *Nat. Commun.* 11:641. doi: 10.1038/s41467-020-14440-8

Ou, Y., Lu, X., Zi, Q., Xun, Q., Zhang, J., Wu, Y., et al. (2016). RGF1 INSENSITIVE 1 to 5, a group of LRR receptor-like kinases, are essential for the perception of root meristem growth factor 1 in *Arabidopsis thaliana*. *Cell Res.* 26, 686–698. doi: 10.1038/cr.2016.63

Patharkar, O. R., and Walker, J. C. (2016). Core mechanisms regulating developmentally timed and environmentally triggered abscission. *Plant Physiol.* 172, 510–520. doi: 10.1104/pp.16.01004

Qin, F., Shinozaki, K., and Yamaguchi-Shinozaki, K. (2011). Achievements and challenges in understanding plant abiotic stress responses and tolerance. *Plant Cell Physiol.* 52, 1569–1582. doi: 10.1093/pcp/pcr106

Reddy, K. J. (2006). "Nutrient stress," in *Physiology and Molecular Biology of Stress Tolerance in Plants*, eds K. V. Madhava Rao, A. S. Raghavendra, and K. J. Reddy (Dordrecht: Springer), 187–217. doi: 10.1007/1-4020-4225-6_7

Reichardt, S., Piepho, H. P., Stintzi, A., and Schaller, A. (2020). Peptide signaling for drought-induced tomato flower drop. *Science* 367, 1482–1485. doi: 10.1126/science.aaz5641

Roberts, I., Smith, S., Stes, E., De Rybel, B., Staes, A., Van De Cotte, B., et al. (2016). CEP5 and XIP1/CEPR1 regulate lateral root initiation in *Arabidopsis*. *J. Exp. Bot.* 67, 4889–4899. doi: 10.1093/jxb/erw231

Shao, Y., Yu, X., Xu, X., Li, Y., Yuan, W., Xu, Y., et al. (2020). The YDA-MKK4/MKK5-MPK3/MPK6 cascade functions downstream of the RGF1-RGI ligand-receptor pair in regulating mitotic activity in root apical meristem. *Mol. Plant* 13, 1608–1623. doi: 10.1016/j.molp.2020.09.004

Shi, Y., Ding, Y., and Yang, S. (2018). Molecular regulation of CBF signaling in cold acclimation. *Trends Plant Sci.* 23, 623–637. doi: 10.1016/j.tplants.2018.04.002

Shinohara, H., Mori, A., Yasue, N., Sumida, K., and Matsubayashi, Y. (2016). Identification of three LRR-RKs involved in perception of root meristem growth factor in *Arabidopsis*. *Proc. Natl. Acad. Sci. U.S.A.* 113, 3897–3902. doi: 10.1073/pnas.1522639113

Smith, S., Zhu, S., Joos, L., Roberts, I., Nikonorova, N., Dai Vu, L., et al. (2020). The CEP5 peptide promotes abiotic stress tolerance, as revealed by quantitative proteomics, and attenuates the AUX/IAA equilibrium in *Arabidopsis*. *Mol. Cell Proteomics* 19, 1248–1262. doi: 10.1074/mcp.RA119.001826

Song, W., Liu, L., Wang, J., Wu, Z., Zhang, H., Tang, J., et al. (2016). Signature motif-guided identification of receptors for peptide hormones essential for root meristem growth. *Cell Res.* 26, 674–685. doi: 10.1038/cr.2016.62

Stegmann, M., Monaghan, J., Smakowska-Luzan, E., Rovenich, H., Lehner, A., Holton, N., et al. (2017). The receptor kinase FER is a RALF-regulated scaffold controlling plant immune signaling. *Science* 355, 287–289. doi: 10.1126/science.aal2541

Stenvik, G. E., Butenko, M. A., Urbanowicz, B. R., Rose, J. K., and Aalen, R. B. (2006). Overexpression of *INFLORESCENCE DEFICIENT IN ABSCISSION*

activates cell separation in vestigial abscission zones in *Arabidopsis*. *Plant Cell* 18, 1467–1476. doi: 10.1105/tpc.106.042036

Stenvik, G. E., Tandstad, N. M., Guo, Y., Shi, C. L., Kristiansen, W., Holmgren, A., et al. (2008). The EPIP peptide of INFLORESCENCE DEFICIENT IN ABSCISSION is sufficient to induce abscission in *Arabidopsis* through the receptor-like kinases HAESA and HAESA-LIKE2. *Plant Cell* 20, 1805–1817. doi: 10.1105/tpc.108.059139

Strabala, T. J., Phillips, L., West, M., and Stanbra, L. (2014). Bioinformatic and phylogenetic analysis of the CLAVATA3/EMBRYO-SURROUNDING REGION (CLE) and the CLE-LIKE signal peptide genes in the Pinophyta. *BMC Plant Biol.* 14:47. doi: 10.1186/1471-2229-14-47

Stührwohldt, N., Bühler, E., Sauter, M., and Schaller, A. (2021). Phytosulfokine (PSK) precursor processing by subtilase SBT3.8 and PSK signaling improve drought stress tolerance in *Arabidopsis*. *J. Exp. Bot.* 72, 3427–3440. doi: 10.1093/jxb/erab017

Stührwohldt, N., Dahlke, R. I., Steffens, B., Johnson, A., and Sauter, M. (2011). Phytosulfokine-α controls hypocotyl length and cell expansion in *Arabidopsis thaliana* through phytosulfokine receptor 1. *PLoS One* 6:e21054. doi: 10.1371/journal.pone.0021054

Suzuki, N., Rivero, R. M., Shulaev, V., Blumwald, E., and Mittler, R. (2014). Abiotic and biotic stress combinations. *New Phytol.* 203, 32–43. doi: 10.1111/nph.12797

Tabata, R., Sumida, K., Yoshii, T., Ohyama, K., Shinohara, H., and Matsubayashi, Y. (2014). Perception of root-derived peptides by shoot LRR-RKs mediates systemic N-demand signaling. *Science* 346, 343–346. doi: 10.1126/science.1257800

Takahashi, F., Hanada, K., Kondo, T., and Shinozaki, K. (2019). Hormone-like peptides and small coding genes in plant stress signaling and development. *Curr. Opin. Plant Biol.* 51, 88–95. doi: 10.1016/j.pbi.2019.05.011

Takahashi, F., Suzuki, T., Osakabe, Y., Betsuyaku, S., Kondo, Y., Dohmae, N., et al. (2018). A small peptide modulates stomatal control via abscisic acid in long-distance signalling. *Nature* 556, 235–238. doi: 10.1038/s41586-018-0009-2

Tang, R. J., Wang, C., Li, K., and Luan, S. (2020). The CBL-CIPK calcium signaling network: unified paradigm from 20 years of discoveries. *Trends Plant Sci.* 25, 604–617. doi: 10.1016/j.tplants.2020.01.009

Vie, A. K., Najafi, J., Liu, B., Winge, P., Butenko, M. A., Hornslien, K. S., et al. (2015). The IDA/IDA-LIKE and PIP/PIP-LIKE gene families in *Arabidopsis*: phylogenetic relationship, expression patterns, and transcriptional effect of the PIPL3 peptide. *J. Exp. Bot.* 66, 5351–5365. doi: 10.1093/jxb/erv285

Vie, A. K., Najafi, J., Winge, P., Cattan, E., Wrzaczek, M., Kangasjärvi, J., et al. (2017). The IDA-LIKE peptides IDL6 and IDL7 are negative modulators of stress responses in *Arabidopsis thaliana*. *J. Exp. Bot.* 68, 3557–3571. doi: 10.1093/jxb/erx168

Wang, J., Li, H., Han, Z., Zhang, H., Wang, T., Lin, G., et al. (2015). Allosteric receptor activation by the plant peptide hormone phytosulfokine. *Nature* 525, 265–268. doi: 10.1038/nature14858

Yamada, M., Han, X., and Benfey, P. N. (2020). RGF1 controls root meristem size through ROS signalling. *Nature* 577, 85–88. doi: 10.1038/s41586-019-1819-6

Yamaguchi, Y., and Huffaker, A. (2011). Endogenous peptide elicitors in higher plants. *Curr. Opin. Plant Biol.* 14, 351–357. doi: 10.1016/j.pbi.2011.05.001

Yamaguchi, Y., Huffaker, A., Bryan, A. C., Tax, F. E., and Ryan, C. A. (2010). PEPR2 is a second receptor for the Pep1 and Pep2 peptides and contributes to defense responses in *Arabidopsis*. *Plant Cell* 22, 508–522. doi: 10.1105/tpc.109.068874

Yamaguchi, Y., Pearce, G., and Ryan, C. A. (2006). The cell surface leucine-rich repeat receptor for AtPep1, an endogenous peptide elicitor in *Arabidopsis*, is functional in transgenic tobacco cells. *Proc. Natl. Acad. Sci. U.S.A.* 103, 10104–10109. doi: 10.1073/pnas.0603729103

Zhang, L., Shi, X., Zhang, Y., Wang, J., Yang, J., Ishida, T., et al. (2019). CLE9 peptide-induced stomatal closure is mediated by abscisic acid, hydrogen peroxide, and nitric oxide in *Arabidopsis thaliana*. *Plant Cell Environ.* 42, 1033–1044. doi: 10.1111/pce.13475

Zhao, C., Zayed, O., Yu, Z., Jiang, W., Zhu, P., Hsu, C. C., et al. (2018). Leucine-rich repeat extensin proteins regulate plant salt tolerance in *Arabidopsis*. *Proc. Natl. Acad. Sci. U.S.A.* 115, 13123–13128. doi: 10.1073/pnas.1816991115

Zhu, J. K. (2016). Abiotic stress signaling and responses in plants. *Cell* 167, 313–324. doi: 10.1016/j.cell.2016.08.029

Zhu, Q., Shao, Y., Ge, S., Zhang, M., Zhang, T., Hu, X., et al. (2019). A MAPK cascade downstream of IDA-HAE/HSL2 ligand-receptor pair in lateral root emergence. *Nat. Plants* 5, 414–423. doi: 10.1038/s41477-019-0396-x

Conflict of Interest: The authors declare that the research was conducted in the absence of any commercial or financial relationships that could be construed as a potential conflict of interest.

frontiers in Plant Science

ORIGINAL RESEARCH
published: 20 July 2021
doi: 10.3389/fpls.2021.703012

The RGF/GLV/CLEL Family of Short Peptides Evolved Through Lineage-Specific Losses and Diversification and Yet Conserves Its Signaling Role Between Vascular Plants and Bryophytes

Chihiro Furumizu† and Shinichiro Sawa*

Graduate School of Science and Technology, Kumamoto University, Kumamoto, Japan

Short secreted plant peptides act as key signaling molecules and control a plethora of developmental and physiological processes. The ROOT GROWTH FACTOR (RGF)/GOLVEN (GLV)/CLE-Like (CLEL) family of peptides was discovered to be involved in root development in *Arabidopsis thaliana*. In contrast to active research efforts, which have been revealing receptors and downstream signaling components, little attention has been paid to evolutionary processes that shaped the RGF signaling system as we know it in angiosperms today. As a first step toward understanding how RGF signaling emerged and evolved, this study aimed to elucidate the phylogenetic distribution and functional conservation of RGF-like sequences. Using publicly available, genome and transcriptome data, RGF-like sequences were searched in 27 liverworts, 22 mosses, 8 hornworts, 23 lycophytes, 23 ferns, 38 gymnosperms, and 8 angiosperms. This led to the identification of more than four hundreds of RGF-like sequences in all major extant land plant lineages except for hornworts. Sequence comparisons within and between taxonomic groups identified lineage-specific characters. Notably, one of the two major RGF subgroups, represented by *A. thaliana* RGF6/GLV1/CLEL6, was found only in vascular plants. This subgroup, therefore, likely emerged in a common ancestor of vascular plants after its divergence from bryophytes. In bryophytes, our results infer independent losses of RGF-like sequences in mosses and hornworts. On the other hand, a single, highly similar RGF-like sequence is conserved in liverworts, including *Marchantia polymorpha*, a genetically tractable model species. When constitutively expressed, the *M. polymorpha* RGF-like sequence (Mp*RGF*) affected plant development and growth both in *A. thaliana* and *M. polymorpha*. This suggests that MpRGF can exert known RGF-like effects and that Mp*RGF* is under transcriptional control so that its potent activities are precisely controlled. These data suggest that RGFs are conserved

OPEN ACCESS

Edited by:
Fuminori Takahashi,
Tokyo University of Science, Japan

Reviewed by:
Lin Xu,
Center for Excellence in Molecular Plant Sciences, Chinese Academy of Sciences (CAS), China
Hervé Canut,
UMR 5546 Laboratoire de Recherche en Sciences Vegetales (LRSV), France

***Correspondence:**
Chihiro Furumizu
chihiro.furumizu@med.akita-u.ac.jp

†Present address:
Chihiro Furumizu,
Department of Immunology, Graduate School of Medicine, Akita University, Akita, Japan

Specialty section:
This article was submitted to Plant Physiology, a section of the journal Frontiers in Plant Science

Received: *30 April 2021*
Accepted: *28 June 2021*
Published: *20 July 2021*

Citation:
Furumizu C and Sawa S (2021) The RGF/GLV/CLEL Family of Short Peptides Evolved Through Lineage-Specific Losses and Diversification and Yet Conserves Its Signaling Role Between Vascular Plants and Bryophytes. Front. Plant Sci. 12:703012. doi: 10.3389/fpls.2021.703012

as signaling molecules in both vascular plants and bryophytes and that lineage-specific diversification has increased sequence variations of RGFs. All together, our findings form a basis for further studies into RGF peptides and their receptors, which will contribute to our understandings of how peptide signaling pathways evolve.

Keywords: RGF/GLV/CLEL, signaling peptide, land plant evolution, 1KP project, *Marchantia polymorpha*, homology, convergence

INTRODUCTION

Debate is ongoing regarding phylogenetic relationships among land plant lineages. Gaining more support from recent molecular data, one hypothesis proposes that vascular and non-vascular plants are both monophyletic and stem from a deeply rooted split that took place early in land plant evolution (for schematic representation, refer to **Figure 8**). Morphologically, non-vascular plants (i.e., bryophytes) and angiosperms are quite different; homology at the organ level is not generally accepted or remains unresolved between the dominant gametophytic body of bryophytes and dominant sporophytic body of angiosperms. Nevertheless, recent molecular genetics studies have revealed cases where homologous genetic modules control development of functionally analogous organs in the two bodies of different lineages and generations (Koi et al., 2016; Rovekamp et al., 2016; Whitewoods et al., 2018; Yasui et al., 2019; Hirakawa et al., 2020). These observations could be accounted for by a common origin of organs in study or independent recruitment of the same genetic module to analogous organs. Either way, knowledge of molecular bases that underlie biological processes in diverse species is instrumental in understanding genetic mechanisms of how plants evolve and diversify.

Since the first discovery of an endogenous short signaling peptide, genetic, biochemical, and bioinformatic approaches have continued to add new signaling peptide families that act in various biological processes (Olsson et al., 2019; Segonzac and Monaghan, 2019). They mature from short precursor proteins through post-translational modifications and proteolytic cleavage into peptides of typically 10-to-20 amino acid residues (post-translationally modified peptides; PTMPs for short). More than ten PTMP families have been reported to date and all share common gene structures; PTMPs are encoded near the N-terminus. Outside the short PTMP-encoding region, PTMP precursor sequences are highly variable among family members. This structural feature has been hampering confident identification of PTMP homologs especially between two distantly related species. Nonetheless, studies started to reveal conservation of PTMPs across land plants (e.g., Miwa et al., 2009; Ghorbani et al., 2015; Tavormina et al., 2015; Goad et al., 2017).

ROOT GROWTH FACTOR (RGF)/GOLVEN (GLV)/CLE-Like (CLEL) is one of the widely conserved PTMP families (Shinohara, 2021). The RGF/GLV/CLEL (hereafter referred to as RGF for clarity) peptides were discovered independently in *Arabidopsis thaliana* (Matsuzaki et al., 2010; Meng et al., 2012; Whitford et al., 2012). Followed by the identification of their receptors, RGF1-INSENSITIVE (RGI)/RGF1 RECEPTOR (RGFR), the RGF-RGI module has been studied intensively, which in a short period of time has led to the independent elucidation of the downstream events after the receptor activation in *A. thaliana* (Ou et al., 2016; Shinohara et al., 2016; Song et al., 2016; Fernandez et al., 2020; Lu et al., 2020; Shao et al., 2020; Yamada et al., 2020). Gain-of-function alleles and exogenous application of RGF result in developmental defects in the root, and previous studies primarily focus on the roles of RGFs in root development. It has been noted from early on, however, that the expression of the RGF family genes is not restricted to the root (Ghorbani et al., 2016; Busatto et al., 2017). Likewise, although the RGF-RGI module has been studied so far only in angiosperms, bioinformatics analyses identified RGF homologs also in gymnosperm and lycophyte lineages of vascular plants (Strabala et al., 2014; Ghorbani et al., 2015). These limit our view on how this peptide signaling pathway evolved to play their roles as known today. Meanwhile, increasing availability of complete genome sequences enabled larger-scale bioinformatics analyses and led to the identification of RGF homolog in another vascular plant lineage, ferns (Furumizu et al., 2021). An RGF-like sequence was also found in a non-vascular plant, *Marchantia polymorpha* (designated as MpRGF for ROOT GROWTH FACTOR/GOLVEN/CLE-Like-FLAVORED) (Furumizu et al., 2021). These discoveries open up opportunities for studying RGF signaling pathways in different developmental or evolutionary settings. Yet, limiting searches to completely sequenced genomes excludes the possibility to fully consider the large diversity of land plants; a better understanding of the evolution of RGFs comes with a more comprehensive investigation among phylogenetically diverse species.

This study, therefore, searched for RGF-like sequences extensively in all major extant land plant lineages using a large-scale transcriptome data collected by the 1000 Plant Genomes Project (1KP[1]) as well as other valuable genome and transcriptome resources (Rensing et al., 2008; Banks et al., 2011; Goodstein et al., 2012; Amborella Genome Project, 2013; Fernandez-Pozo et al., 2015; Ming et al., 2015; Cheng et al., 2017; Filiault et al., 2018; Dong et al., 2019; One Thousand Plant Transcriptomes Initiative, 2019; Hetherington et al., 2020; Li et al., 2020; Zhang J. et al., 2020; Zhang L. et al., 2020; Geng et al., 2021). As a result, more than four hundreds of RGF-like sequences were retrieved from all major extant land plant lineages excepting hornworts. Mapping these RGF-like sequences on the species phylogeny revealed independent losses in mosses and hornworts and evolution of lineage-specific variations in vascular plants. We further demonstrated that MpRGF possesses known RGF-like activities and can affect plant growth with constitutive expression experiments in *A. thaliana* and *M. polymorpha*. This suggests that a role as a signaling molecule is conserved between

[1]www.onekp.com

vascular plant and bryophyte RGF-like sequences. Our findings form a basis for advancing studies into RGF peptides and their receptors and contribute to our understandings of how peptide signaling pathways evolve.

MATERIALS AND METHODS

Identification of RGF-Like Sequences

Initial BLAST (Basic Local Alignment Search Tool) queries were assembled based on the previously published RGF-like sequences (Furumizu et al., 2021) and used to set up BLASTP or tBLASTn searches. The finalized query file is available as **Supplementary Data Sheet 1**. Fasta files of the published transcriptome and proteome data were downloaded to set up databases for BLAST searches. BLASTP was used to search against the proteome with the following parameters: -task blastp-short -max_target_seqs 30. tBLASTn was used to search against the transcriptome data with the parameters as follows: -word_size 2 -gapopen 9 -gapextend 1 -matrix PAM30 -threshold 16 -comp_based_stats 0 -window_size 15 -max_target_seqs 30. BLAST results were manually examined, and RGF-like candidates were listed. These hits were assessed by the sequence conservation of the presumptive mature peptides, which we defined to begin with the first aspartic acid and second tyrosine residues. When a potential full-length precursor sequence was available, the location of the mature peptide-encoding region and the presence of signal peptide were examined. Given that the processing and secretion modes of RGF-like peptides have not yet been elucidated outside of angiosperms, predicted presence of signal peptide was not considered as prerequisite. All amino acid sequences were aligned with the online version of MAFFT version 7 (Katoh et al., 2019) and manually edited and visualized with Jalview version 2.11.1.3 (Waterhouse et al., 2009). WebLogo version 2.8.2[2] was used to generate sequence logos (Crooks et al., 2004) with the same clustalw color scheme used in Jalview. RGF-like sequences presented in this study are available in **Supplementary Data Sheet 2**.

Plant Materials and Growth Conditions

A. thaliana Col-0 and *M. polymorpha* Tak-1 (Ishizaki et al., 2008) were used as wild type. Plants were grown at 23°C under continuous light. *A. thaliana* seeds were surface-sterilized and germinated on 140 mm × 100 mm × 14.5 mm square dishes (sterile No. 2 square Schale, Eiken Chemical) containing half-strength Murashige and Skoog (MS) Basal Medium (M5519, Sigma-Aldrich) solidified with 1% (w/v) agar (01028-85, Nacalai Tesque). The pH of the medium was adjusted to pH 5.7 with potassium hydroxide. Transformants were selected on half-strength MS plates containing 15 μg/mL glufosinate ammonium (079-05371, FUJIFILM Wako Pure Chemical) and 12.5 μg/mL carbenicillin sodium salt (037-23693, FUJIFILM Wako Pure Chemical). Plates were placed vertically during plant cultivation. For root observation, 1-week-old seedlings were transferred to the half-strength MS medium containing 1.0% sucrose (190-00013, FUJIFILM Wako Pure Chemical) and 1.8% agar, with (for transformants) or without (for Col-0) 15 μg/mL glufosinate ammonium and 12.5 μg/mL carbenicillin sodium salt. Plates were inclined at an angle of approximately 45° to the vertical. *M. polymorpha* plants were grown on 90 mm × 20 mm Petri dishes (BIO-BIK I-90-20, Ina·Optica) containing half-strength Gamborg's B5 Medium (399-00621, FUJIFILM Wako Pure Chemical) solidified with 1.4% (w/v) agar. The pH of the medium was adjusted to pH 5.5 with potassium hydroxide. Transformants were selected on half-strength Gamborg's B5 plates containing 10 μg/mL hygromycin B (085-06153, FUJIFILM Wako Pure Chemical) and 100 μg/mL cefotaxime sodium salt (030-16113, FUJIFILM Wako Pure Chemical). All nutrient agar plates were double wrapped with surgical tape (Micropore Surgical Tape 1530-0, 3M) during plant cultivation. Plant images were obtained by scanning plates using a flat-bed scanner (GT-X830, Epson).

Construction of Plasmids

For constitutive expression in *A. thaliana*, the At*RGF1*, At*RGF6*, and Mp*RGF* coding sequences were PCR amplified from the Col-0 root-derived complementary DNA (cDNA), Col-0 genomic DNA, and Tak-1 gemmae-derived cDNA, respectively, cloned into the pART7 plasmid digested with *Bam*HI and *Xho*I using the In-Fusion HD cloning kit (639649, Takara Bio), and sequenced. The pART7 vector contains the cauliflower mosaic virus 35S promoter sequence and the terminator sequence from the octopine synthase gene. A 15-bp deletion was introduced into pART7 carrying Mp*RGF* by inverse PCR and confirmed by sequencing. Subsequently, the *Not*I fragment of the obtained plasmid was cloned into the *Not*I site of the pMLBART binary vector using the DNA ligation kit, mighty mix (6023, Takara Bio). For constitutive expression in *M. polymorpha*, the Mp*RGF* coding sequence was PCR amplified from the Tak-1 gemmae-derived cDNA, cloned into the pENTR4 dual selection vector (Invitrogen A10561, Thermo Fisher Scientific) digested with *Bam*HI and *Xho*I using the In-Fusion HD cloning kit, and sequenced. Subsequently, the Mp*RGF* coding sequence was subcloned into pMpGWB103 (Ishizaki et al., 2015) using the Gateway LR clonase II enzyme mix (Invitrogen 11791-100, Thermo Fisher Scientific). Sequences of the primers used in this study are listed in **Supplementary Table 1**.

Plant Transformation

Constructs were introduced into the *Agrobacterium tumefaciens* strain GV3101 (pMP90) by electroporation to be used for plant transformation. *A. thaliana* plants were transformed by the floral dip method using surfactant Silwet L-77 (BMS-SL7755, Bio Medical Sciences) (Clough and Bent, 1998). *M. polymorpha* gemmalings were transformed as previously described (Kubota et al., 2013).

RESULTS

RGF-Like Sequences Are Highly Conserved in Liverworts

Mature RGF peptides in *A. thaliana* (hereafter, AtRGFs) share several characteristic residues: the first aspartic acid (D), the

[2]https://weblogo.berkeley.edu

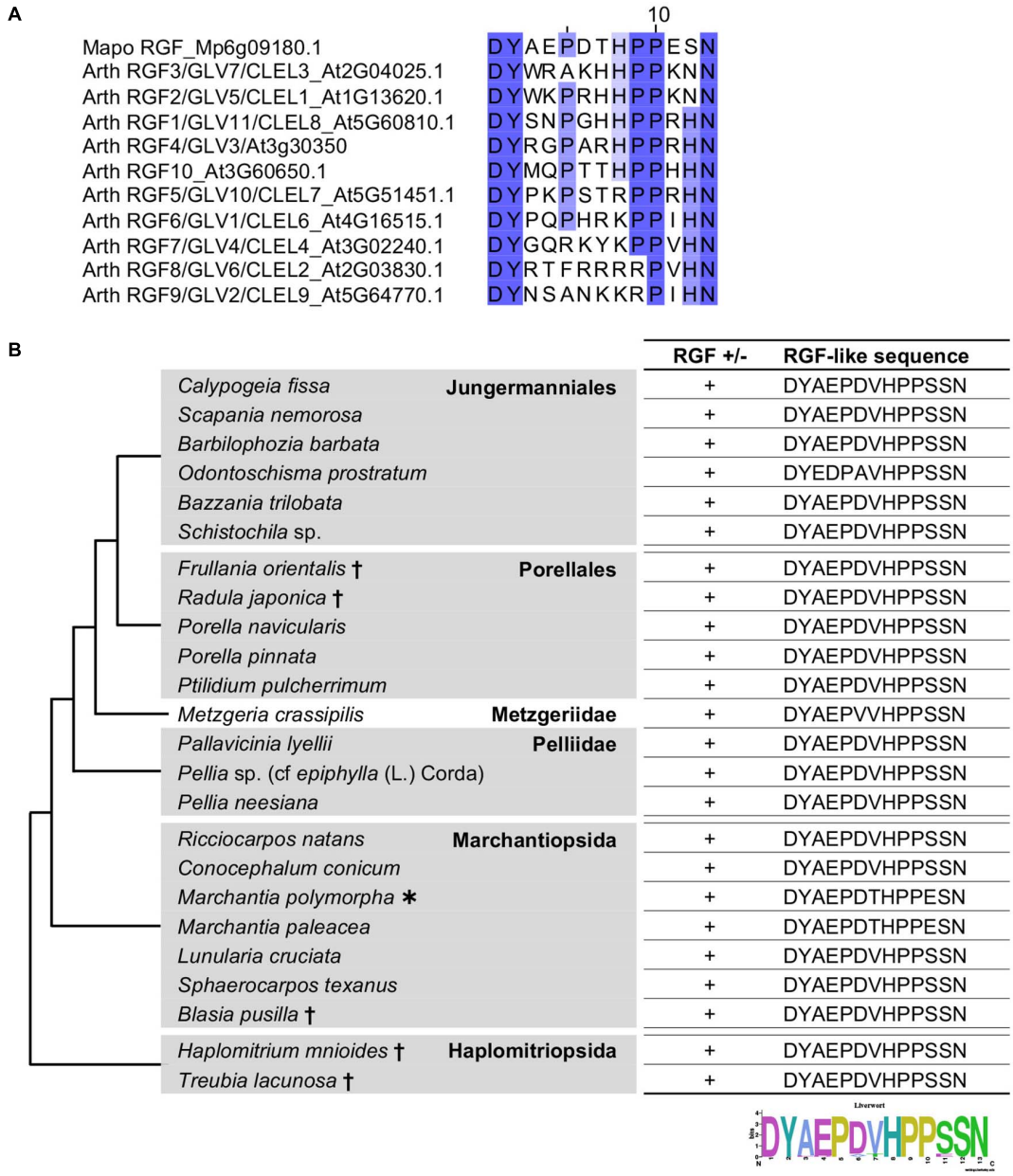

FIGURE 1 | Liverwort RGF-like sequences. **(A)** Alignment of the predicted mature RGF peptides encoded in the *A. thaliana* and *M. polymorpha* genomes. Conserved residues are highlighted with graded shadings. Sequence titles are preceded by the abbreviated species name consisting of the first two letters of the generic and specific names. The sequence of *A. thaliana* RGF4 is based on a previous study (Matsuzaki et al., 2010). **(B)** Shown are the RGF-like peptide sequences identified in the selected liverworts. Phylogenetic relationships of the analyzed species are depicted as a simplified cladogram based on the published phylogenetic analyses (Forrest et al., 2006; Dong et al., 2019). A heavy asterisk indicates that the proteome predicted from the sequenced genome was analyzed for *M. polymorpha* (Bowman et al., 2017). Daggers indicate that the published transcriptome data was analyzed for these species (Dong et al., 2019). The 1KP dataset was analyzed for other species. See also **Supplementary Figure 1**.

second tyrosine (Y) to be sulfated, the tenth proline (P), and the thirteenth asparagine (N). The fifth and ninth P as well as the eighth histidine (H) residues are also highly conserved (**Figure 1A**). All these residues are conserved in the RGF-like sequence found in a liverwort, *M. polymorpha*, MpRGF (Furumizu et al., 2021; **Figure 1A**). A notable difference is the twelfth residue, which is either H or N in AtRGFs but is serine (S) in MpRGF, pointing to RGF sequence diversification between two evolutionary distant lineages. This prompted us to further explore the presence and sequence of putative RGFs in other liverworts.

The liverwort transcriptomes in the 1KP dataset was searched for RGF-like sequences. The 16 amino-acid sequences, encompassing the predicted mature peptide and three preceding

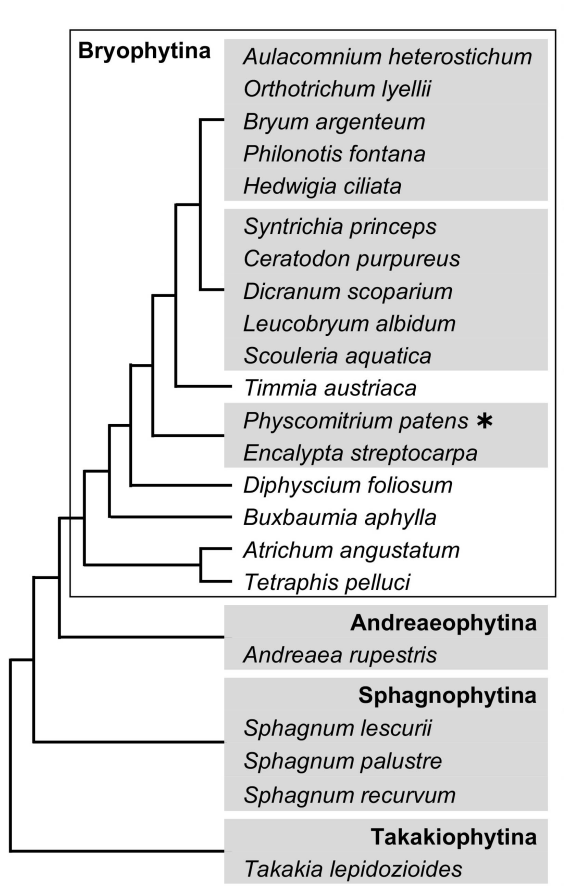

RGF +/-	RGF-like sequences
n.d.	
n.d.	
n.d.	
n.d.	
n.d.	
n.d.	
n.d.	
n.d.	
n.d.	
n.d.	
n.d.	
n.d.	
n.d.	
n.d.	
n.d.	
n.d.	
+	DYMDPQTHPPKGN, DYRQPQMHPPRGN, DYRQPQMHPPRGN
+	DYSQPQTHPPKGN, DYSDPRTHPPRGN, DYKDPQNHPPRSN, DYRDPENHPPRSN
+	DYSDPQTHPPKGN, DYSDPRTHPPRGN, DYSQPQTHPPKGN, DYRDPENHPPRSN, DYKDPQNHPPRSN, DYRDPETHPPKSN, DYRDPQSHPPRSN
+	DYSDPQTHPPKGN, DYSDPRTHPPRGN, DYSQPQTHPPKGN, DYRDPENHPPRSN, DYRDPQSHPPRSN, DYKDPQNHPPRSN
+	DYRDPQTHPPKGN, DYRDPETHPPRGN

FIGURE 2 | Moss RGF-like sequences. The presence (+) or absence (n.d., not detected) of RGF-like sequences was examined in mosses, and the identified, presumptive RGF-like peptide sequences are listed. Phylogenetic relationships of the analyzed species are depicted as a simplified cladogram based on the published phylogenetic analyses (Liu et al., 2019). A heavy asterisk indicates that the proteome predicted from the sequenced genome was analyzed for *P. patens* (Rensing et al., 2008). The 1KP dataset was analyzed for other species. See also **Supplementary Figure 2**.

residues, of AtRGFs and previously identified RGF-like sequences were used as query in the BLAST (Basic Local Alignment Search Tool) searches against the transcriptome data, translated in all six frames. This identified RGF-like sequences in 18 transcriptomes (**Figure 1B**). These findings corroborate the utility of the 1KP dataset in searching signaling peptide-encoding transcripts, which are often expressed at low levels. In the alignment of these sequences, the conservation stretches beyond the presumptive peptide-encoding region (**Supplementary Figure 1**), validating that several partial sequences lacking the N-terminus are indeed homologous to RGFs. In addition, the alignment identified two potential proteolytic cleavage sites in the variable, middle region of nascent polypeptides (**Supplementary Figure 1**). Equivalent residues are targeted by subtilisin-like serine proteases, and these processing events are crucial for the AtRGF biogenesis (Ghorbani et al., 2016; Stuhrwohldt et al., 2020). This suggests that liverwort RGF-like sequences can be processed to PTMPs by molecular machineries shared between vascular plants and bryophytes.

The identified RGF-like sequences are nearly identical. No RGF-like sequences were found in *Radula lindenbergiana*, *Monoclea gottschei*, and *Blasia* species listed in the 1KP dataset. In order to examine the presence of liverwort RGFs more widely, additional BLAST searches were performed using the transcriptome data in an independent study (Dong et al., 2019). This led to the finding of RGF-like sequences in the following five species: *Frullania orientalis*, *Radula japonica*, *Blasia pusilla*, *Haplomitrium mnioides*, and *Treubia lacunosa* (**Figure 1B**). Given that highly similar RGF-like sequences were uniformly conserved across liverworts, the absence of significant hits in the BLAST searches of several 1KP datasets is likely explained by the lack or the loss of low-abundance transcripts in the transcriptome data.

RGF-Like Sequences Were Lost Independently During Moss and Hornwort Evolution

The conservation of RGF between angiosperms and liverworts indicates that the ancestral *RGF* gene(s) should have been present in the common ancestor of vascular plants and bryophytes (liverworts, mosses, and hornworts) while RGF-like sequences were not identified in the sequenced genomes of a moss,

Physcomitrium patens, and *Anthoceros* hornworts (Rensing et al., 2008; Li et al., 2020; Zhang J. et al., 2020; Furumizu et al., 2021). Therefore, we investigated the possibility of finding moss or hornwort RGFs in the 1KP dataset.

RGF-like sequences were found in several but not all moss transcriptomes used in our searches (**Figure 2** and **Supplementary Figure 2**). In order to examine these findings in the evolutionary context, the presence or absence as well as the identified sequences were mapped on the moss species phylogeny. This revealed that the RGF distribution is limited to the species that diverged early during the moss evolution (**Figure 2**). RGF-like sequences were not found in the species that belong to evolutionary younger lineages, collectively known as Bryophytina, suggesting that the RGF-like sequences were lost before the divergence of Bryophytina from Andreaeophytina. This is consistent with the previous report that RGF-like sequences are absent in the sequenced genome of *P. patens*, which belongs to Bryophytina. Alternatively, evolutionary changes in the expression pattern could also account for the lack of RGF-like sequences in Bryophytina in our results, through affecting the amount of RGF transcripts in a given transcriptome.

Searches in the hornwort transcriptomes did not find any RGF-like sequences. Taken together with the previous reports, in which RGF was not identified in the sequenced four genomes of *Anthoceros* species (Li et al., 2020; Zhang J. et al., 2020; Furumizu et al., 2021), these data suggest that during the hornwort evolution, RGF was possibly lost before extant lineages diversified (**Figure 3**). It is still yet possible that the low to zero abundance in the transcriptome data did not allow us to identify hornwort RGFs in this study.

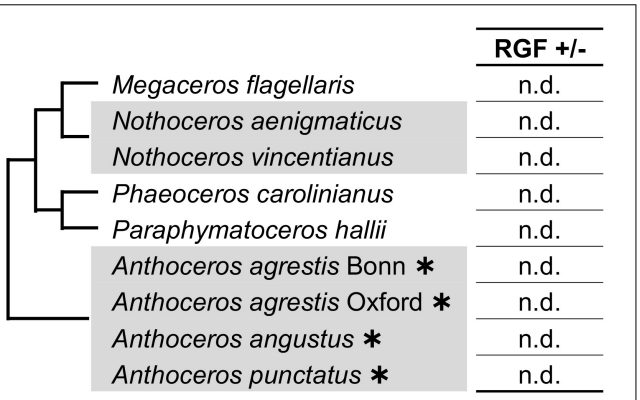

FIGURE 3 | RGF-like sequences were not found in hornworts. Phylogenetic relationships of the analyzed species are depicted as a simplified cladogram based on the published phylogenetic analyses (Frangedakis et al., 2020). Heavy asterisks indicate that the proteome data predicted from the completely sequenced genomes were analyzed for the *Anthoceros* species (Li et al., 2020; Zhang J. et al., 2020). The 1KP dataset was examined for other species.

RGF-Like Sequences Diversified in Lycophytes

The C terminus of the liverwort and moss RGF-like sequences contains SSN and R/K-G/S-N, respectively (**Figures 1**, **2**). These sequence features were not previously recognized for seed plant RGFs and can be explained by lineage-specific gene family evolution (Strabala et al., 2014; Ghorbani et al., 2015). Thus, we examined non-seed vascular plant lineages for hitherto unidentified sequence diversity. Lycophyte is a sister group to the ferns and seed plants and represents the earliest-diverging lineage of extant vascular plants (Spencer et al., 2020). *Selaginella moellendorffii* is the only lycophyte species of which genome was sequenced, and previous studies reported that RGF-like sequences are encoded in its genome (Banks et al., 2011; Ghorbani et al., 2015). To test other lycophyte species, lycophyte transcriptomes were selected from the 1KP dataset so that the large phylogenetic diversity of this lineage was captured and searched for RGF-like sequences. This led to the identification of RGF-like sequences from 17 out of 21 transcriptome data. Additional RGF-like sequences were retrieved by searching against the predicted *Selaginella moellendorffii* proteome and the *Isoetes echinospora* transcriptome data (Banks et al., 2011; Hetherington et al., 2020; **Figure 4** and **Supplementary Figure 3**). No RGF-like sequences were found in four species of Lycopodiaceae (**Figure 4**). In the case of *Huperzia selago* (designated as A in **Figure 4**), a single RGF-like sequence was found in another transcriptome (B). This example suggests that the low transcript level can possibly hinder RGF identification in the 1KP dataset.

The lycophyte RGF-like sequences are classified into two major groups. Group H is characterized by the highly conserved eighth H residue in the predicted mature peptide-encoding region. The last H residue is also conserved with exceptions being five sequences found in the three *Isoetes* transcriptomes (marked with short black vertical line in **Supplementary Figure 3**). Unique residues at the C terminus differentiate these from more canonical Group H sequences. Besides, several Group H sequences have three P residues instead of the otherwise highly conserved two consecutive P residues at the ninth and tenth positions and could generate atypical 14 amino acid-long RGF peptides. The other, Group R, is characterized by the central R/K residues and the invariable twelfth and thirteenth N residues.

Differences between Group H and R are also found in the sequences adjacent to the predicted signaling peptide-encoding region. Most Group H sequences end with the predicted peptide-encoding region whereas additional 9-to-18 residues follow the peptide-encoding region of Group R, suggesting different modes of peptide maturation processes. These distinctive features indicate that two groups underwent significant sequence diversification if they share the same origin and thus are homologous. Pertinent to this is the presence of Group R sequences being limited to Selaginellaceae and Isoetaceae. This observation raises two possibilities: gain of Group R in the lineage leading to Selaginellaceae and Isoetaceae after its split from Lycopodiaceae (Huperzioideae and Lycopodioideae); and loss of Group R in the common ancestor of Lycopodiaceae. It is of note that *A. thaliana* RGFs can also be classified into Group H and Group R (**Figure 1A**). These will be discussed later in conjunction with our findings in other vascular plant lineages.

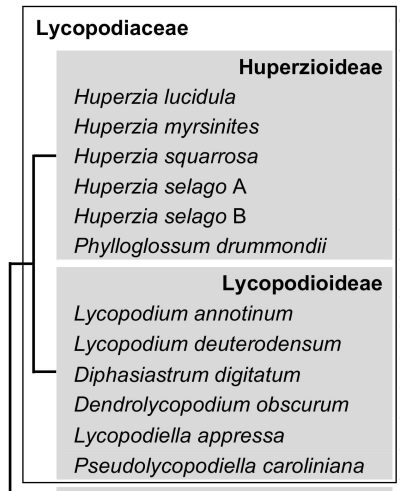

	RGF +/-	H-type RGF-likes	R-type RGF-likes
Lycopodiaceae			
Huperzioideae			
Huperzia lucidula	n.d.		
Huperzia myrsinites	+	DYYRPRTHPPHNH, DYSRPGAHPPHNH, DYVPPANHPPPHGH	n.d.
Huperzia squarrosa	+	DYYRPRTHPPHNH, DYNSPSTHPPHNH, DYSRPGAHPPHNH	n.d.
Huperzia selago A	n.d.		
Huperzia selago B	+	DYYRPRTHPPHNH	n.d.
Phylloglossum drummondii	+	DYTRPGGHPPHNH	n.d.
Lycopodioideae			
Lycopodium annotinum	+	DYVGPQTHPPHSH	n.d.
Lycopodium deuterodensum	+	DYSSPRTHPPHNH, DYAGPGPHPPHSH, DYAGPETHPPQSH, DYAPSGTRPPHSH, DYSGVSTHPPPRPH, DYSGPSTHPPPEGH	n.d.
Diphasiastrum digitatum	n.d.		
Dendrolycopodium obscurum	n.d.		
Lycopodiella appressa	+	DYNPSGTHPPHNH, DYSGPGSHPPHNH, DYSRPGTHPPHNH, DYTPSGTHPPHNH, DYSGPQIHPPKAH	n.d.
Pseudolycopodiella caroliniana	+	DYQGPGTHPPHSH	n.d.
Selaginellaceae			
Selaginella apoda	+	DYTPAAIHPPHSH, DYAGPKRHPPHSH, DYAKVKTHPPHSH	DYAPVRRKPPINN
Selaginella moellendorffii ✱	+	DYTPAAIHPPRSH	DYAPVRRKPPINN, DYTPVHRKPPINN
Selaginella willdenowii	+	DYTNPTYHPPHSH, DYAGPKRHPPHSH	DYAPVRRKPPINN, DYTPVHRKPPINN
Selaginella acanthonota	+	DYYKAKTHPPHSH, DYRGATIHPPPKNH	DYAPVRRRPPINN
Selaginella wallacei	+	DYIRPKTHPPHSH, DYAGPVSHPPHGH	DYAPVRRRPPINN
Selaginella lepidophylla	+	DYTPAAIHPPHSH, DYAKVRTHPPHSH	DYAPVRRKPPINN, DYTPVHRKPPINN
Selaginella kraussiana	+	DYSGPKRHPPQSH, DYREAATHPPPKNH	DYAPVRRRPPINN, DYTPVHRRPPINN
Selaginella selaginoides	+	DYAGPKRHPPHSH, DYPGVSTHPPPKGH	DYAPVRRKPPINN, DYTPVHRKPPINN
Isoetaceae			
Isoetes tegetiformans	+	DYPVPETHPPRQD, DYPYPSTHPPKGD, DYPGPTIHPPRP	DYSHVHRKPPINN, DYTPSHRKPPTNN
Isoetes sp.	+	DYSPPTNHPPHSH, DYPPVGTHPPHSH, DYNQPVPSPPTHN, DYVPSHPPPPHNH	DYSHVHRKPPINN, DYTPSHRKPPTNN
Isoetes echinospora †	+	DYSPPTNHPPHSH, DYPGPTIHPPRPG, DYPVPETHPPRQD	DYTPSHRKPPTNN

FIGURE 4 | Lycophyte RGF-like sequences. The presence (+) or absence (n.d., not detected) of RGF-like sequences was examined in lycophytes. The identified, presumptive RGF-like peptide sequences are classified into two groups and listed. Phylogenetic relationships of the analyzed species are depicted as a simplified cladogram based on the published phylogenetic analyses (Wikstrom and Kenrick, 2000; Field et al., 2016; Weststrand and Korall, 2016; Schafran et al., 2018). A heavy asterisk indicates that the proteome predicted from the sequenced genome was analyzed for *S. moellendorffii* (Banks et al., 2011). A dagger indicates that the published transcriptome data was examined for *Isoetes echinospora* (Hetherington et al., 2020). The 1KP dataset was analyzed for other species. See also **Supplementary Figure 3**.

Fern RGF-Like Sequences All Belong to Group H

The living sister group to lycophytes, euphyllophytes, consists of two major groups: seed plants and ferns. Ferns diverged from the seed plants 400 million years ago, and extant ferns are highly diverse (Plackett et al., 2015). Their early emergence and present-day diversity, however, has not always been sufficiently considered in previous phylogenetic studies, let alone in the studies of plant peptide signaling. It was recently reported that RGF-like sequences are encoded in the sequenced genomes of *Azolla filiculoides* and *Salvinia cucullata* (Furumizu et al., 2021). These are all similar to the Group H sequences in lycophytes, and it was not clear whether ferns have Group R-type sequences. We addressed this question by searching for RGF-like sequences in the selected fern transcriptomes of the 1 KP project as well as in the *Ceratopteris richardii* transcriptome reported independently (Geng et al., 2021).

As shown in **Figure 5** and **Supplementary Figure 4**, nearly all fern RGF-like sequences are characterized by the eighth H residue in the predicted mature form. No sequence was found to carry consecutive R/K residues at the seventh and eighth positions as seen in the lycophyte Group R sequences. The fern RGF-like sequences are classified into two groups according to the last residue of the predicted mature form: N in Group H-N, and P in the other, Group H-P (**Supplementary Figure 4**). These findings were mapped onto the fern species phylogeny (**Figure 5**). Either Group H-N or H-P sequences are absent in several fern species. In particular, Group H-N sequences were not found in *Angiopteris evecta* and *Marattia* sp., both of which belong to Marattiales. Group H-N may have been lost in this lineage, and validation of this possibility requires more species sampling.

Gymnosperms Have Both Group H and Group R RGF-Like Sequences

The lack of Group R sequences in ferns and its presence in lycophytes and angiosperms obscures the evolutionary history of Group R RGF-like sequences in vascular plants. To gain an

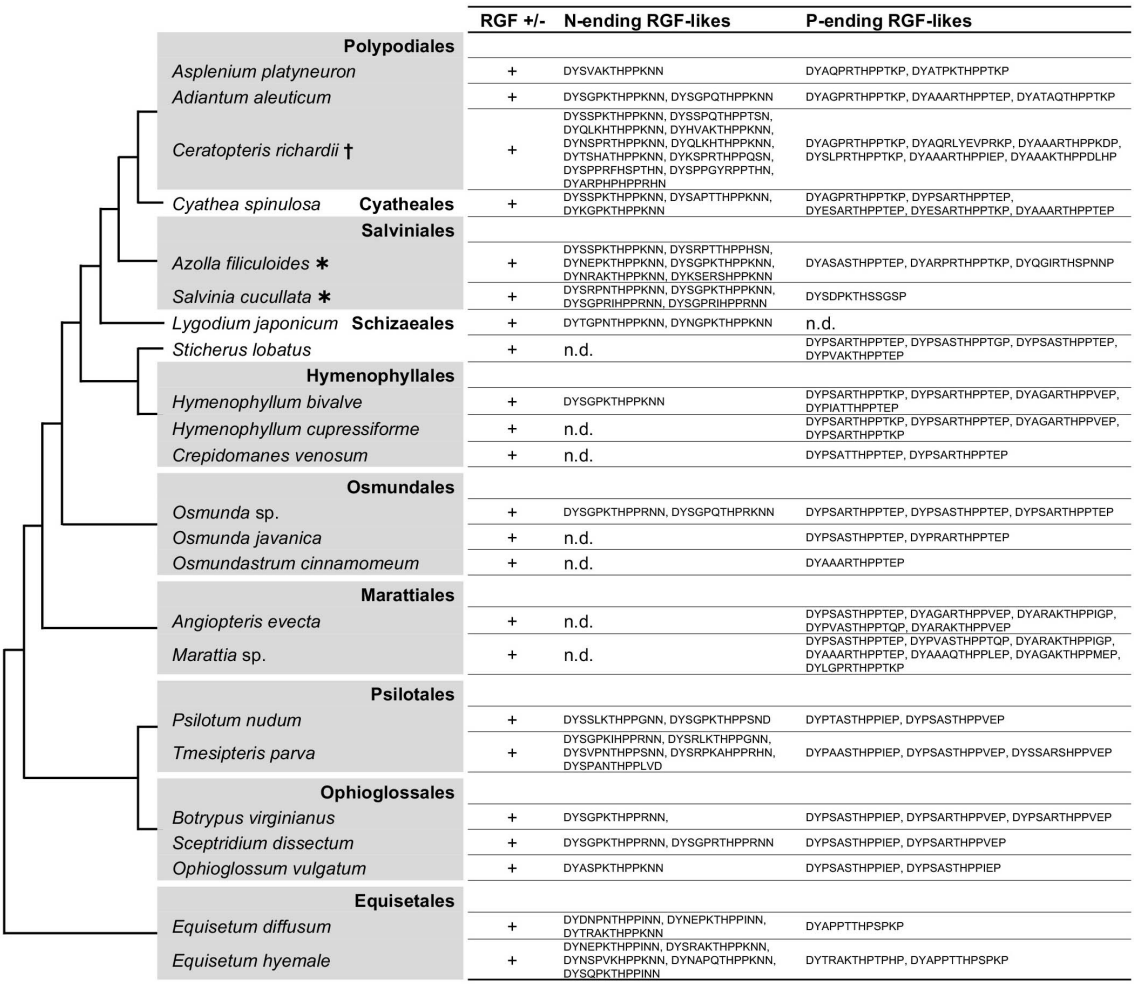

		RGF +/-	N-ending RGF-likes	P-ending RGF-likes
Polypodiales				
Asplenium platyneuron		+	DYSVAKTHPPKNN	DYAQPRTHPPTKP, DYATPKTHPPTKP
Adiantum aleuticum		+	DYSGPKTHPPKNN, DYSGPQTHPPKNN	DYAGPRTHPPTKP, DYAAARTHPPTEP, DYATAQTHPPTKP
Ceratopteris richardii †		+	DYSSPKTHPPKNN, DYSSPQTHPPTSN, DYQLKHTHPPKNN, DYHVAKTHPPKNN, DYNSPRTHPPKNN, DYQLKHTHPPKNN, DYTSHATHPPKNN, DYKSPRTHPPQSN, DYSPPRFHSPTHN, DYSPPGYRPPTHN, DYARPHPHPPRHN	DYAGPRTHPPTKP, DYAQRLYEVPRKP, DYAAARTHPPKDP, DYSLPRTHPPTKP, DYAAARTHPPIEP, DYAAAKTHPPDLHP
Cyathea spinulosa	Cyatheales	+	DYSSPKTHPPKNN, DYSAPTTHPPKNN, DYKGPKTHPPKNN	DYAGPRTHPPTKP, DYPSARTHPPTEP, DYESARTHPPTEP, DYESARTHPPTKP, DYAAARTHPPTEP
Salviniales				
Azolla filiculoides ✱		+	DYSSPKTHPPKNN, DYSRPTTHPPHSN, DYNEPKTHPPKNN, DYSGPKTHPPKNN, DYNRAKTHPPKNN, DYKSERSHPPKNN	DYASASTHPPTEP, DYARPRTHPPTKP, DYQGIRTHSPNNP
Salvinia cucullata ✱		+	DYSRPNTHPPKNN, DYSGPKTHPPKNN, DYSGPRIHPPRNN, DYSGPRIHPPRNN	DYSDPKTHSSGSP
Lygodium japonicum	Schizaeales	+	DYTGPNTHPPKNN, DYNGPKTHPPKNN	n.d.
Sticherus lobatus		+	n.d.	DYPSARTHPPTEP, DYPSASTHPPTGP, DYPSASTHPPTEP, DYPVAKTHPPTEP
Hymenophyllales				
Hymenophyllum bivalve		+	DYSGPKTHPPKNN	DYPSARTHPPTKP, DYPSARTHPPTEP, DYAGARTHPPVEP, DYPIATTHPPTEP
Hymenophyllum cupressiforme		+	n.d.	DYPSARTHPPTKP, DYPSARTHPPTEP, DYAGARTHPPVEP, DYPSARTHPPTKP
Crepidomanes venosum		+	n.d.	DYPSATTHPPTEP, DYPSARTHPPTEP
Osmundales				
Osmunda sp.		+	DYSGPKTHPPRNN, DYSGPQTHPRKNN	DYPSARTHPPTEP, DYPSASTHPPTEP, DYPSARTHPPTEP
Osmunda javanica		+	n.d.	DYPSASTHPPTEP, DYPRARTHPPTEP
Osmundastrum cinnamomeum		+	n.d.	DYAAARTHPPTEP
Marattiales				
Angiopteris evecta		+	n.d.	DYPSASTHPPTEP, DYAGARTHPPVEP, DYARAKTHPPIGP, DYPVASTHPPTQP, DYARAKTHPPVEP
Marattia sp.		+	n.d.	DYPSASTHPPTEP, DYPVASTHPPTQP, DYARAKTHPPIGP, DYAAARTHPPTEP, DYAAAQTHPPLEP, DYAGAKTHPPMEP, DYLGPRTHPPTKP
Psilotales				
Psilotum nudum		+	DYSSLKTHPPGNN, DYSGPKTHPPSND	DYPTASTHPPIEP, DYPSASTHPPVEP
Tmesipteris parva		+	DYSGPKIHPPRNN, DYSRLKTHPPGNN, DYSVPNTHPPSNN, DYSRPKAHPPRHN, DYSPANTHPPLVD	DYPAASTHPPIEP, DYPSASTHPPVEP, DYSSARSHPPVEP
Ophioglossales				
Botrypus virginianus		+	DYSGPKTHPPRNN,	DYPSASTHPPIEP, DYPSARTHPPVEP, DYPSARTHPPVEP
Sceptridium dissectum		+	DYSGPKTHPPRNN, DYSGPRTHPPRNN	DYPSASTHPPIEP, DYPSARTHPPVEP
Ophioglossum vulgatum		+	DYASPKTHPPKNN	DYPSASTHPPIEP, DYPSASTHPPIEP
Equisetales				
Equisetum diffusum		+	DYDNPNTHPPINN, DYNEPKTHPPINN, DYTRAKTHPPKNN	DYAPPTTHPSPKP
Equisetum hyemale		+	DYNEPKTHPPINN, DYSRAKTHPPKNN, DYNSPVKHPPKNN, DYNAPQTHPPKNN, DYSQPKTHPPINN	DYTRAKTHPTPHP, DYAPPTTHPSPKP

FIGURE 5 | Fern RGF-like sequences. The presence (+) or absence (n.d., not detected) of RGF-like sequences was examined in ferns. The identified, presumptive RGF-like peptide sequences are classified into two groups and listed. Phylogenetic relationships of the analyzed species are depicted as a simplified cladogram based on the published phylogenetic analyses (Pryer et al., 2004; Knie et al., 2015; Schuettpelz et al., 2016). Heavy asterisks indicate that the proteome data predicted from the completely sequenced genomes were analyzed (Li et al., 2018). A dagger indicates that the published transcriptome data was examined for *Ceratopteris richardii* (Geng et al., 2021). The 1KP dataset was analyzed for other species. See also **Supplementary Figure 4**.

insight into how Group R sequences emerged and evolved, RGF-like sequences were analyzed in gymnosperms that represent an informative node, bridging seed-free vascular plants and angiosperms. Gymnosperms comprise only 1,000 species but consist of a wide variety of groups. Species were therefore sampled broadly from the available 1 KP dataset.

Collected gymnosperm RGF-like sequences include both Group H and Group R sequences (**Figure 6** and **Supplementary Figure S5**). This is consistent with a previous study, which also identified RGF-like genes of both types in coniferous species (Strabala et al., 2014). Several transcriptomes lack Group R sequences. The corresponding species do not belong to specific taxonomic groups, and Group R includes sequences from all major taxonomic lineages. This suggests that lower expression levels but not their absence in the genome accounts for the lack of Group R sequences in these transcriptomes. In fact, the sequenced *Picea abies* genome encodes seven RGF-like sequences in total, four of which belong to Group R. A mere number of zero-to-two in other species appears consistent with the hypothesis of lower transcript accumulation levels of Group R sequences in general.

Gymnosperm Group H sequences were further classified into five subgroups (**Supplementary Figure 5**). Subgroup H1 sequences were found only in Cupressaceae and Taxaceae, possibly having originated recently in the common ancestor of these evolutionary young lineages. Similar to Group R, other subgroups are more uniformly distributed in gymnosperms. Exceptions to this are subgroup H3 lacking cycad and Ginkgo sequences and subgroup H5 without Araucariaceae sequences. Given the lack of completely sequenced genomes in these lineages and the large size of gymnosperm genomes, it requires additional investigation to confirm lineage-specific sequence variations. Group H as a whole comprises sequences from all major gymnosperm lineages. Therefore, both Group H and R

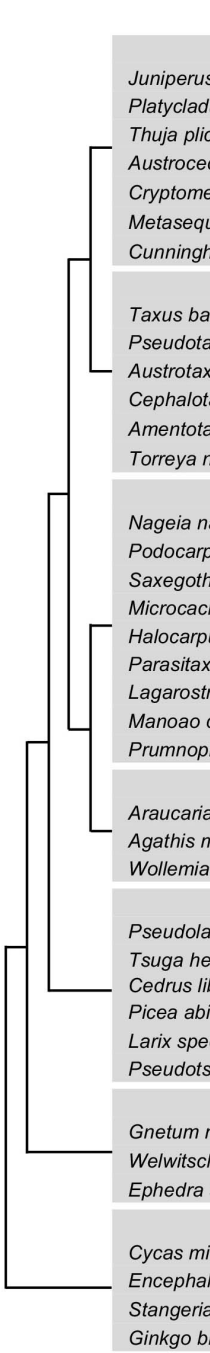

	RGF +/-	H-type RGF-likes	R-type RGF-likes
Cupressaceae			
Juniperus scopulorum	+	DYAGATTHPPSEP, DYSGPQTHGPKHH, DYRDPTTHPVTPS	DYTPAQRKPPIHN
Platycladus orientalis	+	DYAGATTHPPSEP, DYSGPQTHGPKHH, DYRDPTTHPVTPS	DYTPAQRKPPIHN, DYGKVHRKPPIHN
Thuja plicata	+	DYAGATTHPPSEP, DYSGPQTHGPKHH	DYTPAQRKPPIHN
Austrocedrus chilensis	+	DYAGATTHPPSEP, DYSGPQTHGPKHH, DYSAPKTHPPKNN, DYHDPTTHPVTPS	DYGKVHRKPPIHN, DYSAAKKRPPIHN
Cryptomeria japonica	+	DYAGATTHPPSEP, DYHGPTTHPPATP, DYSGPQTHGPKHH, DYSAPKTHPPKNN, DYHDPTTHPVTPS	DYTPAQRKPPIHN, DYGKVHRKPPIHN
Metasequoia glyptostroboides	+	DYAGATTHPPSEP, DYHGPTTHPPATP, DYSGPQTHGPKHH, DYKDPTTHPIIPS	DYTPAQRKPPIHN
Cunninghamia lanceolata	+	DYAGATTHPPSEP, DYSGPQTHGPKHH, DYSAPKTHPPKNN, DYHGPTTHPPATP	DYTPAQRKPPIHN
Taxaceae			
Taxus baccata	+	DYAGATTHPPSEP, DYHGPTTHPPATP, DYSAPQTHPPKNN	DYSPAHKRPPIHN
Pseudotaxus chienii	+	DYAGATTHPPSEP, DYHGPTTHPPATP	n.d.
Austrotaxus spicata	+	DYAGATTHPPSEP, DYHGPTTHPPATP	n.d.
Cephalotaxus harringtonia	+	DYAGATTHPPSEP, DYHGPTTHPPATP, DYSGPQTHGPKHH, DYSAPKTHPPKNN	DYSPAHKRPPIHN
Amentotaxus argotaenia	+	DYAGATTHPPTEP, DYSAPKTHPPKNN, DYSAPQTHPPKNN, DYSGPQTHGPKHH	DYSPAHKRPPIHN
Torreya nucifera	+	DYAGATTHPPTEP, DYHGPTTHPPATP, DYSGPKTHPPKNN, DYQNPKTHPVTPSP	n.d.
Podocarpaceae			
Nageia nagi	+	DYAGATTHPPSEP	n.d.
Podocarpus coriaceus	+	DYAGATTHPPSEP, DYHGPTTHPPANP, DYSGPGSHDPQHH, DYSGPRTHPPKNN	DYSPAHKRPPIHN
Saxegothaea conspicua	+	DYAGATTHPPSEP, DYHGPTTHPPSTP	DYSPAHKRPPIHN
Microcachrys tetragona	+	DYAGATTHPPSEP, DYHGPTTHPPATP, DYSGPRTHPPKNN	DYSPAHKRPPIHN
Halocarpus bidwillii	+	DYAGATTHPPSEP, DYHGPTTHPPASP, DYSGPRTHPPKNN	n.d.
Parasitaxus usta	+	DYAGATTHPPSEP, DYHGPTTHPPNPQ	DYSPAQKRPPIHN
Lagarostrobos franklinii	+	DYAGATTHPPSEP	n.d.
Manoao colensoi	+	DYAGATTHPPSEP, DYHGPTTHPPATP, DYSGPRTHPPKNN, DYSGPQTHGPKHH	DYSPAQKRPPIHN, DYRHVRRNPPIHN
Prumnopitys andina	+	DYAGATTHPPSEP, DYHGPTTHPPATP, DYNGPKTHPPKNN	DYTPAQKRPPIHN
Araucariaceae			
Araucaria rulei	+	DYAGATTHPPSEP, DYHGPTTHPPATP	DYTPAQRRPPIHN
Agathis macrophylla	+	DYAGATTHPPSEP, DYHGPTTHPPATP	DYTPAQRRPPIHN
Wollemia nobilis	+	DYAGATTHPPSEP, DYHGPTTHPPATP, DYSGPQTHGPKHH	DYTPAQRRPPIHN, DYSPAHKRPPIHN
Pinaceae			
Pseudolarix amabilis	+	DYAGATTHPPNEP	n.d.
Tsuga heterophylla	+	DYAGATTHPPNEP, DYTGPKTHPPKNN	DYAPAHRKPPIHN
Cedrus libani	+	DYAGASTHPPNEP, DYSGPKTHSPKHH	DYTPAQKKPPIHN
Picea abies ✱	+	DYAGATTHPPNEP, DYSGPKTHPPKNN, DYHGATTHPPAPP	DYTPAQKKPPIHN, DYAPAHKKPPIHN, DYGRARRNPPIHN, DYGRARRNPHIHN
Larix speciosa	+	DYSGPKTHNPKHH	DYTPARKNPPIHN
Pseudotsuga wilsoniana	+	DYAGATTHPPNEP, DYHGATTHPPTPP, DYSGPKTHNPKHH	DYAPAHKKPPIHN
Gnetales			
Gnetum montanum	+	DYAGATTHPPIEP, DYQGPKTHPDKPP	n.d.
Welwitschia mirabilis	+	DYAGATTHPPIEP, DYQGPKTHPPRPP, DYSAPKTHPPKNN, DYSKPKTHKPTHD, DYKGPETHVSPRP	DYSPAQKRPPIHH
Ephedra sinica	+	DYAVATTHPPVQP, DYTPAHKNPPIHH, DYQRPKTHPPNPP	n.d.
Cycads & *Ginkgo*			
Cycas micholitzii	+	DYAGATTHPPIEP, DYSGPKTHSAKHH	n.d.
Encephalartos barteri	+	DYAGATTHPPIEP	DYSPARKKPPIHN
Stangeria eriopus	+	DYAGATTHPPIEP, DYSGPKTHPPKNN, DYSAPKTHPPKNN, DYNGPKTHRPKHH	DYSPARKKPPIHN
Ginkgo biloba	+	DYAGATTHPPIEP	n.d.

FIGURE 6 | Gymnosperm RGF-like sequences. The presumptive RGF-like peptide sequences identified in gymnosperms are classified into two groups and listed. Sequences in magenta in a given species share similar N-terminal sequences, suggesting the common origin. R-type sequences were not found in several species (n.d., not detected). Phylogenetic relationships of the analyzed species are depicted as a simplified cladogram based on the published phylogenetic analyses (Lu et al., 2014; Ran et al., 2018; One Thousand Plant Transcriptomes Initiative, 2019). Names of taxonomic groups are color coded consistently with **Supplementary Figure 5**. A heavy asterisk indicates that the proteome predicted from the genome sequence was analyzed (Nystedt et al., 2013). The 1KP dataset was analyzed for other species. See also **Supplementary Figures 5, 6**.

sequences must have been present in the common ancestor of extant gymnosperm species.

Manual curation of gymnosperm RGF-like precursor sequences revealed that several group H and R sequences show striking similarities (**Supplementary Figures 5** and **6**). These paired sequences were recognized so far only in several gymnosperm lineages in our searches and could possibly result from alternative splicing as reported by Strabala et al. (2014).

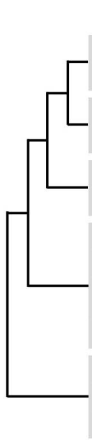

	RGF +/-	H-type RGF-likes (H + H-PP)	R-type RGF-likes
Rosid			
Arabidopsis thaliana	+	DYMQPTTHPPHHN, DYSNPGHHPPRHN, DYWKPRHHPPKNN, DYWRAKHHPPKNN, DYRGPARHPPRHN	DYPQPHRKPPIHN, DYRTFRRRRPVHN, DYNSANKKRPIHN, DYPKPSTRPPRHN, DYGQRKYKPPVHN
Asterid			
Solanum lycopersicum	+	DYLPPRTHPPIHN, DYLPARTHPPVHN, DYHVATTHPPRNN, DYKSPRHHPPRHN, DYRGPETHTKMPP, DYRGPETHTYIPP	DYSPAKRKPPIHN, DYAQPHRKPPIHN, DYDPPQRKPPIHN, DYHWVRRRRPIHN, DYTPARKKPPIHN
Ranunculid			
Aquilegia coerulea	+	DYNVPKPHPPKNN, DYHVPKEHPPKHN, DYYGPKIHKPKHH, DYRGPETHSFVPP, DYIPPRTHPPGPP	DYSPARRKPPIHN, DYEPPHRRPPIHN, DYSHVRRRRPVHN
Monocot			
Ananas comosus	+	DYDPPRSHSPHHN, DYQGPETHSLPPP	DYSPAKRKPPIHN
Brachypodium distachyon	+	DYAGPITHPPSHN, DYRIPKCHPPRNN, DYTPPKSHPPQHN, DYYGPRGHIPSHN, DYGMPRRHTPRHN, DYYGPRGHNPRHH, DYYGPSDHSPRHH	DYTPANRKPPIHN, DYTPVHRRTPKHN
Zea mays	+	DYAGPRTHTPSHN, DYVGPKTHPPSHN, DYRSPRKHPPKNN, DYHSVHRHPPTHN, DYAGPRTHPHDPP	DYSPAARKPPIHN, DYAPWRRRVPKHN, DYAPWHRRVPKHN, DYASARRHTPRNN,
ANA grade			
Nymphaea colorata	+	DYNSPTTHLPINN, DYAPPKIHPPSHN, DYKGPETHAFLPP, DYKGPETHFFPPP	DYSPVAKKPPIHN, DYPQPHRKPPINN, DYSSARKSTPNHN, DYSAAAKNSPVHN, DYSPEAKKSPIHN
Amborella trichopoda	+	DYSPPLTHPPIHN, DYRGPETHSHVPP	DYSPARRKTPIHN, DYVHARKRRPIHN, DYTPAGKKKPIHN

FIGURE 7 | Angiosperm RGF-like sequences. The presumptive RGF-like peptide sequences identified in the sequenced genomes of angiosperms are classified into two groups and listed. Sequences in dull yellow belong to the group H-PP. Phylogenetic relationships of the analyzed species are depicted as a simplified cladogram based on the published phylogenetic analyses (One Thousand Plant Transcriptomes Initiative, 2019). See also **Supplementary Figure 7**.

Cross comparison between paired examples of different taxonomic groups did not show sequence conservation beyond mature-peptide encoding regions. This suggests their possible independent origins and raises a question as to what drove their evolution. Further investigations are needed to elucidate how commonly these pairs exist both within and outside gymnosperms.

Cryptic Sequence Diversity in Angiosperm RGFs

RGF-like sequences were originally identified in *A. thaliana* and has since been reported in other angiosperm species (Matsuzaki et al., 2010; Meng et al., 2012; Whitford et al., 2012; Ghorbani et al., 2015; Tadiello et al., 2016). These angiosperm sequences, however, have not been characterized from an evolutionary perspective by comparing their profiles with those of RGF-like sequences from non-flowering plants. In view of the rapidly growing availability of plant genome data, RGF-like sequences were searched in diverse angiosperm species (Goodstein et al., 2012; Amborella Genome Project, 2013; Fernandez-Pozo et al., 2015; Ming et al., 2015; Cheng et al., 2017; Filiault et al., 2018; Zhang L. et al., 2020; **Figure 7** and **Supplementary Figure 7**). This resulted in identifying both Group H and R sequences in all species examined. In addition, similar but distinct sequences were found to constitute a new subclass of Group H. Their presumptive mature forms in 13 amino acids end with PP and are hereby named Group H-PP. Some Group H-PP sequences have a C-terminal extension longer than 20 amino acids. It remains to be tested whether they encode secreted short peptides.

Conserved and Lineage-Specific Features of RGF-Like Sequences

As summarized in **Figure 8**, RGF-like sequences show both conserved and lineage-specific characteristics. Group H sequences are found in all major lineages of extant land plants, suggesting an early origin of Group H in the common ancestor of land plants. Group R sequences, on the other hand, are present only in vascular plants. It is possible Group R evolved early in vascular plant lineage and was subsequently lost in ferns. Alternatively, Group R sequences may have evolved independently at least twice in ancestral lycophytes and seed plants. The latter could explain the difference in the twelfth position of predicted, mature RGF-like peptides, which is dominated by N in lycophytes and H in seed plants. Other sequence characteristics are highly similar between seed plant and lycophyte Group R sequences, in favor of their common origin.

Compared with Group R, Group H sequences show more diversity. This is of particularly the case in vascular plants. It has to be emphasized that except for *A. thaliana* RGFs, secreted, bioactive forms have not been determined (Matsuzaki et al., 2010; Whitford et al., 2012). Such structural information will be critical to delve into the sequence diversity of RGF-like sequences.

M. polymorpha RGF-Like Sequence Elicits RGF-Like Activities in *A. thaliana*

As a first step toward understanding biological functions of RGF-like sequences in non-flowering plants, the *M. polymorpha* RGF-like sequence was chosen for molecular experiments for the following reasons. First, liverworts including *M. polymorpha* and other bryophyte groups form a presumably monophyletic lineage sister to vascular plants and serve as an informative reference to complement our knowledge on angiosperm RGFs (**Figure 8**). Second, a single, highly similar RGF-like sequence is present in the liverwort species analyzed in this study (**Figure 1**). This observation points to a conserved role for liverwort RGF-like sequences. Third, canonical proteolytic cleavage sites are identified at similar positions in the liverwort and *A. thaliana* RGF precursors (Ghorbani et al., 2016; Stuhrwohldt et al., 2020; **Supplementary Figure 1**). This led us to reason that conserved molecular players or analogous mechanisms for the biogenesis of RGF-like peptides could exist in *M. polymorpha* and *A. thaliana*. Fourth, the predicted

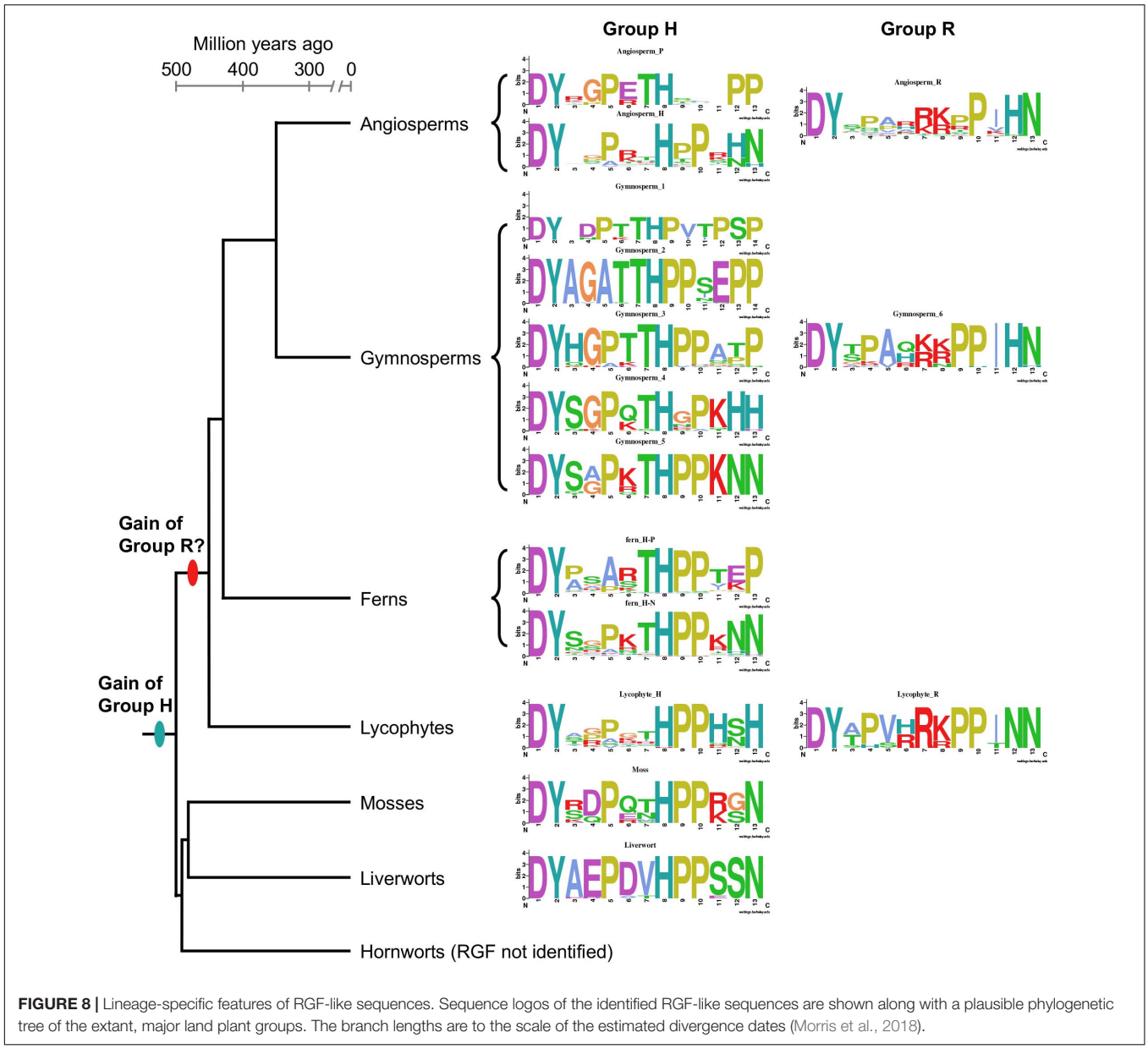

FIGURE 8 | Lineage-specific features of RGF-like sequences. Sequence logos of the identified RGF-like sequences are shown along with a plausible phylogenetic tree of the extant, major land plant groups. The branch lengths are to the scale of the estimated divergence dates (Morris et al., 2018).

M. polymorpha RGF-like sequence has several residues not found in angiosperm RGFs (**Figures 1**, **7**, **8**). These variations could possibly affect ligand-receptor interactions, which can be tested by heterologous expression.

In *A. thaliana*, it has been reported that constitutive expression and exogenous application of RGFs affect root development (Matsuzaki et al., 2010; Meng et al., 2012; Whitford et al., 2012; Fernandez et al., 2013, 2015). We generated transgenic *A. thaliana* plants constitutively expressing either *A. thaliana* RGF (At*RGF1*/*GLV11*/*CLEL8* of Group H or At*RGF6*/*GLV1*/*CLEL6* of Group R) or *M. polymorpha* RGF (Mp*RGF*, Group H) and compared their root morphologies (**Figure 9**). In order to circumvent differences in the number and expression level of the transgene among independent lines, plants in the T1 generation were used. When grown on inclined, hard-agar plates, Mp*RGF*-expressing plants showed enhanced wavy growth. The overall direction of their root growth was bended. These phenotypes are similar to those caused by At*RGF1*/*GLV11*/*CLEL8* over-expression (Meng et al., 2012). At*RGF1*/*GLV11*/*CLEL8*-expressing plants formed irregular waves including loops as previously reported (Whitford et al., 2012). These morphologies are hardly observed in Mp*RGF*-expressing plants. Common to all three transgenic lines are the phenotypes such as shorter roots and lower density of lateral roots (Fernandez et al., 2013; **Figure 9B**). These phenotypes were not observed in *A. thaliana* plants constitutively expressing a mutated form of Mp*RGF*, of which predicted mature form lacks the first five amino acids (Mp*rgf*, **Figure 9A**). Therefore, the observed biological activities of MpRGF in *A. thaliana* are attributable to the putative peptide-encoding region. Despite notable sequence differences

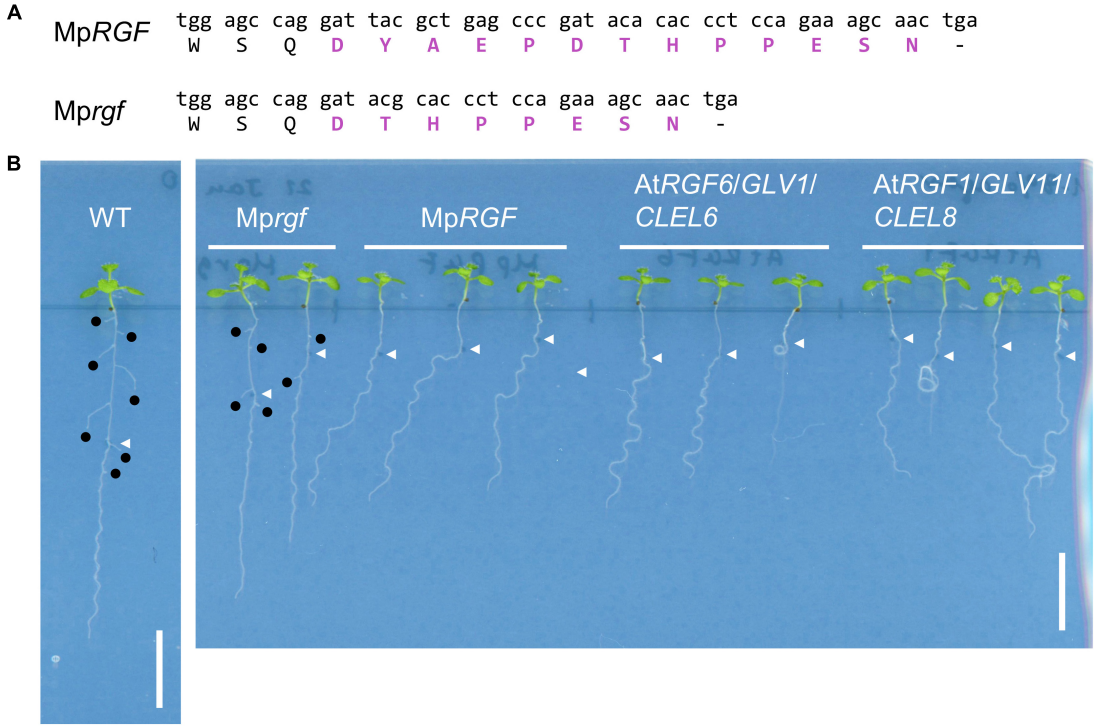

FIGURE 9 | Overexpression of Mp*RGF* in *A. thaliana*. **(A)** A mutated form of Mp*RGF*, designated as Mp*rgf*, used in this experiment. Shown are the nucleotide and translated amino acid sequences encompassing the mature peptide encoding region. The deduced mature peptide sequences are highlighted in bold magenta letters. **(B)** Constitutive expression of At*RGF1/GLV11/CLEL8*, At*RGF6/GLV1/CLEL6*, Mp*RGF*, or its mutated form, Mp*rgf* in *A. thaliana* seedlings. A Col-0 plant is shown for comparison. Note the difference in plant vigor due to the chemicals added in the medium for selecting transgenic plants. White arrow heads indicate the position of the root tip at the time of seedling transfer to the hard agar medium plate. Emerged lateral roots are marked with black circles. Scale bars: 1 cm.

from angiosperm RGFs, our finding suggests that MpRGF can signal through the *A. thaliana* RGF receptors.

Over-Expression of Mp*RGF* Results in Dwarfing in *M. polymorpha*

Our current understanding of the roles of RGFs is based on the previous studies focusing on the sporophytic organs of angiosperms, and it has not been reported to date that RGFs have any roles during gametophyte development. In contrast to angiosperms, in which the sporophyte generation is dominated, liverworts have a life cycle with the dominant gametophytic phase. It is thus more feasible to study RGF functions in the gametophyte using liverworts. Detection of RGF-like sequences in the 1KP dataset (**Figure 1**) corroborates that liverwort RGF-like sequences are expressed in their gametophytic bodies, from which samples are typically collected for transcriptome analyses (One Thousand Plant Transcriptomes Initiative, 2019). In *M. polymorpha*, a genetically tractable liverwort model (Bowman et al., 2017; Kohchi et al., 2021), publicly available RNA-Seq data shows that the Mp*RGF* transcript (Mp6g09180.1) is detected both in vegetative and reproductive organs with higher mRNA abundance in gametophytic tissues than in sporophytic tissues (MarpolBase[3]).

[3]https://marchantia.info

To explore gametophytic RGF roles, the impact of activated RGF signaling was evaluated. For this purpose, transgenic M. *polymorpha* plants expressing Mp*RGF* under the constitutive Mp*EF1* promoter (Althoff et al., 2014) were generated by transforming regenerating thalli. Independent twelve T1 lines were distinguishable from wild-type plants by their small size. Gemma cup and gemmae formation was delayed but eventually observed in the Mp*RGF* overexpressors. This allowed us to grow wild-type and transgenic G1 gemmae simultaneously, which confirmed the observations in the T1 generation (**Figure 10**). That is, excessive MpRGF interfers with normal growth and development. We infer that Mp*RGF* is under strict transcriptional regulation so that its potent activities are controlled tightly.

DISCUSSION

Framing Sequence Diversity of Signaling Peptides in the Context of Land Plant Evolution

Despite being as short as a chain of 10-20 amino acids, plant signaling peptides carry a large amount of information for binding with interacting partners to induce downstream signaling events. Much attention has been paid to understand

the effect of peptide sequence variation on ligand-receptor interactions and resultant signaling responses within a few model species. These efforts have been contributing to an understanding of signaling peptide language, so to say, and even to the creation of a new one or a new word (peptide). The latter, for instance, was realized through a serendipitous discovery using a chemical synthetic approach (Hirakawa et al., 2017). These previous studies were driven by collecting, comparing, and clustering peptide sequences based on similarities. There exist, however, potential pitfalls associated with the common features found in signaling peptide encoding genes; namely, except for the short mature peptide encoding region, a large part of precursor proteins lack sequence conservation. This poses a challenge when identifying signaling peptides and analyzing their sequence variation with conventional homology-based and molecular phylogenetic approaches. As an attempt to overcome these shortcomings, we placed RGF-like peptides in a species phylogeny as summarized in **Figure 8**. This offers an opportunity to decipher evolutionary trajectories of RGF-like peptides and lay a foundation for further exploration of driving forces that underlie changes in peptide sequences.

Challenges in Translating Bioinformatic Knowledge Into an Understanding of Living Systems

The unparalleled 1KP project as well as other valuable resources allowed us to identify more than four hundreds of RGF-like sequences in all major extant land plant lineages excepting hornworts. The absence of RGF-like sequences in our searches can result from the nature of the original transcriptome data, such as the lack or the loss of low-abundance transcripts in the tissue used for RNA extraction. Therefore, additional investigation by PCR-based homolog detection and ultimately by genome sequencing is necessary to confirm the lack of RGF-like sequences in a given species. This poses an intrinsic limitation to the transcriptome data. Moreover, a question remains unsolved as to whether these genes are all homologous due to the overall low sequence similarity. Homology itself is not a clear-cut concept (Inkpen and Doolittle, 2016), which one confronts when assessing similarities of sequences found in distantly related species. Pertinent to this is likely independent evolution of sequences similar to plant signaling peptides in animals and microbes (Mitchum et al., 2012; Ronald and Joe, 2018). To our knowledge, horizontal gene transfer has not been demonstrated in any of these cases of so-called peptide mimics, which can hijack the host peptide-receptor signaling pathways. A problem will thus linger of how to define a signaling peptide family, for instance, by homology or by interacting receptor.

Experimental validations are fundamental to confirm that the newly identified genes encode secreted short peptides and to determine amino acid sequences of their bioactive forms before postulating mechanisms that drive and generate a peptide sequence diversity. These biochemical analyses, however, are not always feasible in every species. We took an alternative and complementary approach, heterologous expression in *A. thaliana*, and demonstrated that the *M. polymorpha* RGF sequence shows RGF-like activities in plants (**Figure 9**). The result also showed that Mp*RGF*-induced responses are more similar to the phenotypes caused by constitutively expressing At*RGF6*/*GLV1*/*CLEL6* than At*RGF1*/*GLV11*/*CLEL8*, while MpRGF resembles the latter *A. thaliana* RGF in sequence (**Figure 1**). Such discrepancies at first glance can result from differences in expression levels or heterologous nature of the experiment; they could be reconciled in future studies if we gain a better understanding of ligand-receptor interactions both in *A. thaliana* and in *M. polymorpha*.

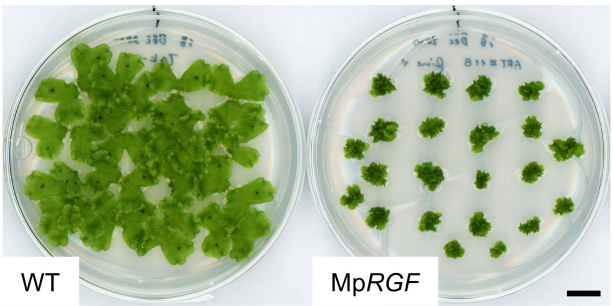

FIGURE 10 | Overexpression of Mp*RGF* in *M. polymorpha*. *M. polymorpha* plants ectopically expressing the Mp*RGF* cDNA are shown with wild-type Tak-1 plants. G1 gemmalings plated simultaneously were observed. Scale bar: 1 cm.

Evolutionary Understanding Facilitates Mechanistic Studies in Model Species

In *A. thaliana*, multiple receptors have been reported for RGF peptides (Ou et al., 2016; Shinohara et al., 2016; Song et al., 2016). As pointed out previously, it remains unknown whether the RGF receptors have different affinities for specific RGF peptides *in vivo* (Pruitt et al., 2017). It was reported, however, that one of the *A. thaliana* RGF receptors (At4g26540) interacts with RGFs *in vitro* with different binding affinities (Song et al., 2016). Overall, H-type RGFs have higher affinities than R-type RGFs, suggestive of inherent differences among RGF ligand-receptor pairs in signaling outputs. Functional differences among RGFs have been noted since their discovery. For example, the H-type, and not R-type, acts as primary RGF in maintaining the meristematic activities in the *A. thaliana* root (Matsuzaki et al., 2010). Given that Group H RGF-like sequences are more widely conserved across land plants, with its emergence predating the split between vascular plants and bryophytes (**Figure 8**), when studying roles of RGFs in biological processes of interest, it can be helpful to keep in mind evolutionary differences between two major RGF subgroups; they show structural differences as well as changes in expression patterns. A recent study reported a novel role for R-type RGF, *A. thaliana* RGF7, in triggering innate immunity through interactions with a subset of RGF receptors (Wang et al., 2021). This opens up a new avenue to dissect how RGF signaling diversified.

Mechanisms Underlying Functional Evolution of Peptide Ligand-Receptor Signaling

In the two examples of known RGF functions described above, the angiosperm root possibly evolved in the common ancestor of ferns and seed plants. Innate immunity in non-flowering plants is just beginning to be addressed (Ponce de León and Montesano, 2017; Carella et al., 2019; Matsui et al., 2020; Poveda, 2020). Therefore, it is not yet straightforward to transfer these knowledges in *A. thaliana* into studies on bryophyte and non-flowering vascular plant RGFs. In order to understand the evolution of RGF signaling, it is crucial to reveal biological roles of RGFs especially in the non-vascular plant lineage, bryophytes. Losses of RGF in hornworts and the moss lineage including *P. patens* directed our attention to the liverwort, *M. polymorpha*. Our results indicate that RGF-like sequences exist possibly as a single gene in liverworts. The high sequence similarities suggest their conserved roles in this lineage. The altered growth and development of Mp*RGF*-overexpressing plants indeed verifies its potency as a signaling molecule (**Figure 10**).

In future studies, it is of critical importance to identify MpRGF receptor(s). Homologs of *A. thaliana* RGF receptors are strong candidates as demonstrated for another signaling peptide family (Whitewoods et al., 2018; Hirakawa et al., 2019, 2020). In accordance, when expressed in *A. thaliana*, MpRGF appears to activate RGF receptor signaling (**Figure 9**). Assigning receptors to conserved signaling peptides in diverse lineages helps us dissect pairing rules of peptide ligands and receptors (Song et al., 2016; Zhang et al., 2016). The understanding of ligand-receptor interactions, in turn, provides insight into how they co-evolve.

Contrasting phylogenetically widespread RGFs, several signaling peptide families, such as LURE, PEP, and SCR/SP11, appear less conserved (Bartels and Boller, 2015; Nasrallah, 2017; Takeuchi, 2021). These presumably evolutionary-young families share intertwined features in common: rapid sequence diversification and participation in inter- or intra-species interactions with each influenced by the other (Takeuchi and Higashiyama, 2012; Lori et al., 2015; Ma et al., 2016; Murase et al., 2020). Understanding structural details of the evolving interface of homologous ligand-receptor pairs as well as underlying genetic changes has been advanced (Ma et al., 2016; Durand et al., 2020; Murase et al., 2020). Studies into RGF-like molecules and their receptors could offer opportunities to study ligands and receptors co-evolving over a longer period of time, from which related yet functionally distinct ligand-receptor pairs may emerge, for instance (van Kesteren et al., 1996).

In addition to ligand-receptor binding, other protein-protein interactions are also indispensable for functional peptide signaling and fine-tuning its activities; processing and modification enzymes involved in RGF peptide maturation have been studied in *A. thaliana* (Matsuzaki et al., 2010; Ghorbani et al., 2016; Stuhrwohldt et al., 2020). Assuming that the nascent MpRGF protein produces a short secreted peptide similar to mature AtRGFs, our finding supports that similar processing machineries are responsible for the MpRGF biogenesis (**Supplementary Figure 1**). Consequently, residues needed to interact with processing or modification enzymes should be conserved in the variable region of peptide precursors, where sequence similarities are seldom recognized, thereby constraining the primary and possibly higher structures of peptide precursors. Alternatively, changes in interactions can add new moieties to the signaling peptidome. These point to potential values of comparative evolutionary approaches in studying signaling peptide biogenesis.

Another key issue is to determine whether angiosperm and liverwort RGF signaling pathways involve any conserved cellular processes both in the sporophyte (dominant in angiosperms) and gametophyte (dominant in liverworts) generations (Fernandez et al., 2020; Lu et al., 2020; Shao et al., 2020; Yamada et al., 2020). Answers to this question will shed light on molecular mechanisms underlying diversification of land plants and, along with elucidation of RGF signaling components, will contribute to our understandings of how peptide signaling pathways evolve.

DATA AVAILABILITY STATEMENT

The datasets presented in this study can be found in online repositories. The names of the repository/repositories and accession number(s) can be found in the article/**Supplementary Material**.

AUTHOR CONTRIBUTIONS

CF conceived and designed the study and collected and analyzed the data. SS contributed to the materials. CF wrote the article with contributions from SS. Both authors contributed to the article and approved the submitted version.

FUNDING

This work was supported by JSPS KAKENHI (17H03967, 18H04841, 18H04625, 18H05487, and 20H00422 to SS and 20K06770 to CF) and Grant for Basic Science Research Projects from the Sumitomo Foundation to CF (200078).

ACKNOWLEDGMENTS

The authors would like to thank John L. Bowman for his help in identifying RGF homologs in liverworts, Eduardo Flores-Sandoval and Facundo Romani for stimulating discussions, and Reira Suzuki for providing the *Arabidopsis thaliana* cDNA.

SUPPLEMENTARY MATERIAL

The Supplementary Material for this article can be found online at: https://www.frontiersin.org/articles/10.3389/fpls.2021.703012/full#supplementary-material

REFERENCES

Althoff, F., Kopischke, S., Zobell, O., Ide, K., Ishizaki, K., Kohchi, T., et al. (2014). Comparison of the MpEF1alpha and CaMV35 promoters for application in Marchantia polymorpha overexpression studies. *Transgenic Res.* 23, 235–244. doi: 10.1007/s11248-013-9746-z

Amborella Genome Project (2013). The *Amborella* genome and the evolution of flowering plants. *Science* 342:1241089. doi: 10.1126/science.1241089

Banks, J. A., Nishiyama, T., Hasebe, M., Bowman, J. L., Gribskov, M., dePamphilis, C., et al. (2011). The *Selaginella* genome identifies genetic changes associated with the evolution of vascular plants. *Science* 332, 960–963. doi: 10.1126/science.1203810

Bartels, S., and Boller, T. (2015). Quo vadis, Pep? Plant elicitor peptides at the crossroads of immunity, stress, and development. *J. Exp. Bot.* 66, 5183–5193. doi: 10.1093/jxb/erv180

Bowman, J. L., Kohchi, T., Yamato, K. T., Jenkins, J., Shu, S., Ishizaki, K., et al. (2017). Insights into land plant evolution garnered from the *Marchantia polymorpha* genome. *Cell* 171, 287–304.e15. doi: 10.1016/j.cell.2017.09.030

Busatto, N., Salvagnin, U., Resentini, F., Quaresimin, S., Navazio, L., Marin, O., et al. (2017). The peach RGF/GLV signaling peptide pCTG134 is involved in a regulatory circuit that sustains auxin and ethylene actions. *Front. Plant Sci.* 8:1711. doi: 10.3389/fpls.2017.01711

Carella, P., Gogleva, A., Hoey, D. J., Bridgen, A. J., Stolze, S. C., Nakagami, H., et al. (2019). Conserved biochemical defenses underpin host responses to oomycete infection in an early-divergent land plant lineage. *Curr. Biol.* 29, 2282–2294.e5. doi: 10.1016/j.cub.2019.05.078

Cheng, C. Y., Krishnakumar, V., Chan, A. P., Thibaud-Nissen, F., Schobel, S., and Town, C. D. (2017). Araport11: a complete reannotation of the *Arabidopsis thaliana* reference genome. *Plant J.* 89, 789–804. doi: 10.1111/tpj.13415

Clough, S. J., and Bent, A. F. (1998). Floral dip: a simplified method for *Agrobacterium*-mediated transformation of *Arabidopsis thaliana*. *Plant J.* 16, 735–743. doi: 10.1046/j.1365-313x.1998.00343.x

Crooks, G. E., Hon, G., Chandonia, J. M., and Brenner, S. E. (2004). WebLogo: a sequence logo generator. *Genome Res.* 14, 1188–1190. doi: 10.1101/gr.849004

Dong, S., Zhao, C., Zhang, S., Wu, H., Mu, W., Wei, T., et al. (2019). The amount of RNA editing sites in liverwort organellar genes is correlated with GC content and nuclear PPR protein diversity. *Genome Biol. Evol.* 11, 3233–3239. doi: 10.1093/gbe/evz232

Durand, E., Chantreau, M., Le Veve, A., Stetsenko, R., Dubin, M., Genete, M., et al. (2020). Evolution of self-incompatibility in the Brassicaceae: lessons from a textbook example of natural selection. *Evol. Appl.* 13, 1279–1297. doi: 10.1111/eva.12933

Fernandez, A. I., Vangheluwe, N., Xu, K., Jourquin, J., Claus, L. A. N., Morales-Herrera, S., et al. (2020). GOLVEN peptide signalling through RGI receptors and MPK6 restricts asymmetric cell division during lateral root initiation. *Nat. Plants* 6, 533–543. doi: 10.1038/s41477-020-0645-z

Fernandez, A., Drozdzecki, A., Hoogewijs, K., Nguyen, A., Beeckman, T., Madder, A., et al. (2013). Transcriptional and functional classification of the GOLVEN/ROOT GROWTH FACTOR/CLE-like signaling peptides reveals their role in lateral root and hair formation. *Plant Physiol,* 161, 954–970. doi: 10.1104/pp.112.206029

Fernandez, A., Drozdzecki, A., Hoogewijs, K., Vassileva, V., Madder, A., Beeckman, T., et al. (2015). The GLV6/RGF8/CLEL2 peptide regulates early pericycle divisions during lateral root initiation. *J. Exp. Bot.* 66, 5245–5256. doi: 10.1093/jxb/erv329

Fernandez-Pozo, N., Menda, N., Edwards, J. D., Saha, S., Tecle, I. Y., Strickler, S. R., et al. (2015). The sol genomics network (SGN)–from genotype to phenotype to breeding. *Nucleic Acids Res.* 43, D1036–D1041. doi: 10.1093/nar/gku1195

Field, A. R., Testo, W., Bostock, P. D., Holtum, J. A. M., and Waycott, M. (2016). Molecular phylogenetics and the morphology of the Lycopodiaceae subfamily Huperzioideae supports three genera: *Huperzia*, *Phlegmariurus* and *Phylloglossum*. *Mol. Phylogenet. Evol.* 94(Pt B), 635–657. doi: 10.1016/j.ympev.2015.09.024

Filiault, D. L., Ballerini, E. S., Mandakova, T., Akoz, G., Derieg, N. J., Schmutz, J., et al. (2018). The *Aquilegia* genome provides insight into adaptive radiation and reveals an extraordinarily polymorphic chromosome with a unique history. *eLife* 7:e36426. doi: 10.7554/eLife.36426

Forrest, L. L., Davis, E. C., Long, D. G., Crandall-Stotler, B. J., Clark, A., and Hollingsworth, M. L. (2006). Unraveling the evolutionary history of the liverworts (Marchantiophyta): multiple taxa, genomes and analyses. *Bryologist* 109, 303–334.

Frangedakis, E., Shimamura, M., Villarreal, J. C., Li, F. W., Tomaselli, M., Waller, M., et al. (2020). The hornworts: morphology, evolution and development. *New Phytol.* 229, 735–754. doi: 10.1111/nph.16874

Furumizu, C., Krabberød, A. K., Hammerstad, M., Alling, R. M., Wildhagen, M., Sawa, S., et al. (2021). The sequenced genomes of non-flowering land plants reveal the innovative evolutionary history of peptide signaling. *Plant Cell* 173. doi: 10.1093/plcell/koab173

Geng, Y., Cai, C., McAdam, S. A. M., Banks, J. A., Wisecaver, J. H., and Zhou, Y. (2021). A De Novo transcriptome assembly of *Ceratopteris richardii* provides insights into the evolutionary dynamics of complex gene families in land plants. *Genome Biol. Evol.* 13:evab042. doi: 10.1093/gbe/evab042

Ghorbani, S., Hoogewijs, K., Pecenkova, T., Fernandez, A., Inze, A., Eeckhout, D., et al. (2016). The SBT6.1 subtilase processes the GOLVEN1 peptide controlling cell elongation. *J. Exp. Bot.* 67, 4877–4887. doi: 10.1093/jxb/erw241

Ghorbani, S., Lin, Y. C., Parizot, B., Fernandez, A., Njo, M. F., Van de Peer, Y., et al. (2015). Expanding the repertoire of secretory peptides controlling root development with comparative genome analysis and functional assays. *J. Exp. Bot.* 66, 5257–5269.

Goad, D. M., Zhu, C., and Kellogg, E. A. (2017). Comprehensive identification and clustering of CLV3/ESR-related (CLE) genes in plants finds groups with potentially shared function. *New Phytol.* 216, 605–616. doi: 10.1111/nph.14348

Goodstein, D. M., Shu, S., Howson, R., Neupane, R., Hayes, R. D., Fazo, J., et al. (2012). Phytozome: a comparative platform for green plant genomics. *Nucleic Acids Res.* 40, D1178–D1186. doi: 10.1093/nar/gkr944

Hetherington, A. J., Emms, D. M., Kelly, S., and Dolan, L. (2020). Gene expression data support the hypothesis that *Isoetes* rootlets are true roots and not modified leaves. *Sci. Rep.* 10:21547. doi: 10.1038/s41598-020-78171-y

Hirakawa, Y., Fujimoto, T., Ishida, S., Uchida, N., Sawa, S., Kiyosue, T., et al. (2020). Induction of multichotomous branching by CLAVATA peptide in *Marchantia polymorpha*. *Curr. Biol.* 30, 3833–3840e3834. doi: 10.1016/j.cub.2020.07.016

Hirakawa, Y., Shinohara, H., Welke, K., Irle, S., Matsubayashi, Y., Torii, K. U., et al. (2017). Cryptic bioactivity capacitated by synthetic hybrid plant peptides. *Nat. Commun.* 8:14318. doi: 10.1038/ncomms14318

Hirakawa, Y., Uchida, N., Yamaguchi, Y. L., Tabata, R., Ishida, S., Ishizaki, K., et al. (2019). Control of proliferation in the haploid meristem by CLE peptide signaling in *Marchantia polymorpha*. *PLoS Genet.* 15:e1007997. doi: 10.1371/journal.pgen.1007997

Inkpen, S. A., and Doolittle, W. F. (2016). Molecular phylogenetics and the perennial problem of homology. *J. Mol. Evol.* 83, 184–192. doi: 10.1007/s00239-016-9766-4

Ishizaki, K., Chiyoda, S., Yamato, K. T., and Kohchi, T. (2008). *Agrobacterium*-mediated transformation of the haploid liverwort *Marchantia polymorpha* L., an emerging model for plant biology. *Plant Cell Physiol.* 49, 1084–1091. doi: 10.1093/pcp/pcn085

Ishizaki, K., Nishihama, R., Ueda, M., Inoue, K., Ishida, S., Nishimura, Y., et al. (2015). Development of gateway binary vector series with four different selection markers for the liverwort *Marchantia polymorpha*. *PLoS One* 10:e0138876. doi: 10.1371/journal.pone.0138876

Katoh, K., Rozewicki, J., and Yamada, K. D. (2019). MAFFT online service: multiple sequence alignment, interactive sequence choice and visualization. *Brief. Bioinform.* 20, 1160–1166. doi: 10.1093/bib/bbx108

Knie, N., Fischer, S., Grewe, F., Polsakiewicz, M., and Knoop, V. (2015). Horsetails are the sister group to all other monilophytes and Marattiales are sister to leptosporangiate ferns. *Mol. Phylogenet. Evol.* 90, 140–149. doi: 10.1016/j.ympev.2015.05.008

Kohchi, T., Yamato, K. T., Ishizaki, K., Yamaoka, S., and Nishihama, R. (2021). Development and molecular genetics of *Marchantia polymorpha*. *Annu. Rev. Plant Biol.* 72, 677–702. doi: 10.1146/annurev-arplant-082520-094256

Koi, S., Hisanaga, T., Sato, K., Shimamura, M., Yamato, K. T., Ishizaki, K., et al. (2016). An evolutionarily conserved plant RKD factor controls germ cell differentiation. *Curr. Biol.* 26, 1775–1781. doi: 10.1016/j.cub.2016.05.013

Kubota, A., Ishizaki, K., Hosaka, M., and Kohchi, T. (2013). Efficient *Agrobacterium*-mediated transformation of the liverwort *Marchantia*

polymorpha using regenerating thalli. *Biosci. Biotechnol. Biochem.* 77, 167–172. doi: 10.1271/bbb.120700

Li, F. W., Brouwer, P., Carretero-Paulet, L., Cheng, S., de Vries, J., Delaux, P. M., et al. (2018). Fern genomes elucidate land plant evolution and cyanobacterial symbioses. *Nat. Plants* 4, 460–472. doi: 10.1038/s41477-018-0188-8

Li, F. W., Nishiyama, T., Waller, M., Frangedakis, E., Keller, J., Li, Z., et al. (2020). *Anthoceros* genomes illuminate the origin of land plants and the unique biology of hornworts. *Nat. Plants* 6, 259–272. doi: 10.1038/s41477-020-0618-2

Liu, Y., Johnson, M. G., Cox, C. J., Medina, R., Devos, N., Vanderpoorten, A., et al. (2019). Resolution of the ordinal phylogeny of mosses using targeted exons from organellar and nuclear genomes. *Nat. Commun.* 10:1485. doi: 10.1038/s41467-019-09454-w

Lori, M., van Verk, M. C., Hander, T., Schatowitz, H., Klauser, D., Flury, P., et al. (2015). Evolutionary divergence of the plant elicitor peptides (Peps) and their receptors: interfamily incompatibility of perception but compatibility of downstream signalling. *J. Exp. Bot.* 66, 5315–5325. doi: 10.1093/jxb/erv236

Lu, X., Shi, H., Ou, Y., Cui, Y., Chang, J., Peng, L., et al. (2020). RGF1-RGI1, a peptide-receptor complex, regulates *Arabidopsis* root meristem development via a MAPK signaling cascade. *Mol. Plant* 13, 1594–1607. doi: 10.1016/j.molp.2020.09.005

Lu, Y., Ran, J. H., Guo, D. M., Yang, Z. Y., and Wang, X. Q. (2014). Phylogeny and divergence times of gymnosperms inferred from single-copy nuclear genes. *PLoS One* 9:e107679. doi: 10.1371/journal.pone.0107679

Ma, R., Han, Z., Hu, Z., Lin, G., Gong, X., Zhang, H., et al. (2016). Structural basis for specific self-incompatibility response in *Brassica*. *Cell Res.* 26, 1320–1329. doi: 10.1038/cr.2016.129

Matsui, H., Iwakawa, H., Hyon, G. S., Yotsui, I., Katou, S., Monte, I., et al. (2020). Isolation of natural fungal pathogens from *Marchantia polymorpha* reveals antagonism between salicylic acid and jasmonate during liverwort-fungus interactions. *Plant Cell Physiol.* 61:442. doi: 10.1093/pcp/pcz214

Matsuzaki, Y., Ogawa-Ohnishi, M., Mori, A., and Matsubayashi, Y. (2010). Secreted peptide signals required for maintenance of root stem cell niche in *Arabidopsis*. *Science* 329, 1065–1067. doi: 10.1126/science.1191132

Meng, L., Buchanan, B. B., Feldman, L. J., and Luan, S. (2012). CLE-like (CLEL) peptides control the pattern of root growth and lateral root development in *Arabidopsis*. *Proc. Natl. Acad. Sci. U.S.A.* 109, 1760–1765. doi: 10.1073/pnas.1119864109

Ming, R., VanBuren, R., Wai, C. M., Tang, H., Schatz, M. C., Bowers, J. E., et al. (2015). The pineapple genome and the evolution of CAM photosynthesis. *Nat. Genet.* 47, 1435–1442. doi: 10.1038/ng.3435

Mitchum, M. G., Wang, X., Wang, J., and Davis, E. L. (2012). Role of nematode peptides and other small molecules in plant parasitism. *Annu. Rev. Phytopathol.* 50, 175–195. doi: 10.1146/annurev-phyto-081211-173008

Miwa, H., Tamaki, T., Fukuda, H., and Sawa, S. (2009). Evolution of CLE signaling: origins of the CLV1 and SOL2/CRN receptor diversity. *Plant Signal. Behav.* 4, 477–481. doi: 10.4161/psb.4.6.8391

Morris, J. L., Puttick, M. N., Clark, J. W., Edwards, D., Kenrick, P., Pressel, S., et al. (2018). The timescale of early land plant evolution. *Proc. Natl. Acad. Sci. U.S.A.* 115, E2274–E2283. doi: 10.1073/pnas.1719588115

Murase, K., Moriwaki, Y., Mori, T., Liu, X., Masaka, C., Takada, Y., et al. (2020). Mechanism of self/nonself-discrimination in *Brassica* self-incompatibility. *Nat. Commun.* 11:4916. doi: 10.1038/s41467-020-18698-w

Nasrallah, J. B. (2017). Plant mating systems: self-incompatibility and evolutionary transitions to self-fertility in the mustard family. *Curr. Opin. Genet. Dev.* 47, 54–60. doi: 10.1016/j.gde.2017.08.005

Nystedt, B., Street, N. R., Wetterbom, A., Zuccolo, A., Lin, Y. C., Scofield, D. G., et al. (2013). The Norway spruce genome sequence and conifer genome evolution. *Nature* 497, 579–584. doi: 10.1038/nature12211

Olsson, V., Joos, L., Zhu, S., Gevaert, K., Butenko, M. A., and De Smet, I. (2019). Look closely, the beautiful may be small: precursor-derived peptides in plants. *Annu. Rev. Plant Biol.* 70, 153–186. doi: 10.1146/annurev-arplant-042817-040413

One Thousand Plant Transcriptomes Initiative (2019). One thousand plant transcriptomes and the phylogenomics of green plants. *Nature* 574, 679–685. doi: 10.1038/s41586-019-1693-2

Ou, Y., Lu, X., Zi, Q., Xun, Q., Zhang, J., Wu, Y., et al. (2016). RGF1 INSENSITIVE 1 to 5, a group of LRR receptor-like kinases, are essential for the perception of root meristem growth factor 1 in *Arabidopsis thaliana*. *Cell Res.* 26, 686–698. doi: 10.1038/cr.2016.63

Plackett, A. R., Di Stilio, V. S., and Langdale, J. A. (2015). Ferns: the missing link in shoot evolution and development. *Front. Plant Sci.* 6:972. doi: 10.3389/fpls.2015.00972

Ponce de León, I., and Montesano, M. (2017). Adaptation mechanisms in the evolution of moss defenses to microbes. *Front. Plant Sci.* 8:366. doi: 10.3389/fpls.2017.00366

Poveda, J. (2020). *Marchantia polymorpha* as a model plant in the evolutionary study of plant-microorganism interactions. *Curr. Plant Biol.* 23:100152. doi: 10.1016/j.cpb.2020.100152

Pruitt, R. N., Joe, A., Zhang, W. G., Feng, W., Stewart, V., Schwessinger, B., et al. (2017). A microbially derived tyrosine-sulfated peptide mimics a plant peptide hormone. *New Phytol.* 215, 725–736. doi: 10.1111/nph.14609

Pryer, K. M., Schuettpelz, E., Wolf, P. G., Schneider, H., Smith, A. R., and Cranfill, R. (2004). Phylogeny and evolution of ferns (monilophytes) with a focus on the early leptosporangiate divergences. *Am. J. Bot.* 91, 1582–1598. doi: 10.3732/ajb.91.10.1582

Ran, J. H., Shen, T. T., Wang, M. M., and Wang, X. Q. (2018). Phylogenomics resolves the deep phylogeny of seed plants and indicates partial convergent or homoplastic evolution between Gnetales and angiosperms. *Proc. Biol. Sci.* 285:20181012. doi: 10.1098/rspb.2018.1012

Rensing, S. A., Lang, D., Zimmer, A. D., Terry, A., Salamov, A., Shapiro, H., et al. (2008). The *Physcomitrella* genome reveals evolutionary insights into the conquest of land by plants. *Science* 319, 64–69. doi: 10.1126/science.1150646

Ronald, P., and Joe, A. (2018). Molecular mimicry modulates plant host responses to pathogens. *Ann. Bot.* 121, 17–23. doi: 10.1093/aob/mcx125

Rovekamp, M., Bowman, J. L., and Grossniklaus, U. (2016). Marchantia MpRKD regulates the gametophyte-sporophyte transition by keeping egg cells quiescent in the absence of fertilization. *Curr. Biol.* 26, 1782–1789. doi: 10.1016/j.cub.2016.05.028

Schafran, P. W., Zimmer, E. A., Taylor, W. C., and Musselman, L. J. (2018). A whole chloroplast genome phylogeny of diploid species of isoetes (Isoetaceae, Lycopodiophyta) in the Southeastern United States. *Castanea* 83, 224–235. doi: 10.2179/17-132

Schuettpelz, E., Schneider, H., Smith, A. R., Hovenkamp, P., Prado, J., Rouhan, G., et al. (2016). A community-derived classification for extant lycophytes and ferns. *J. Syst. Evol.* 54, 563–603. doi: 10.1111/jse.12229

Segonzac, C., and Monaghan, J. (2019). Modulation of plant innate immune signaling by small peptides. *Curr. Opin. Plant Biol.* 51, 22–28. doi: 10.1016/j.pbi.2019.03.007

Shao, Y., Yu, X., Xu, X., Li, Y., Yuan, W., Xu, Y., et al. (2020). The YDA-MKK4/MKK5-MPK3/MPK6 cascade functions downstream of the RGF1-RGI ligand-receptor pair in regulating mitotic activity in the root apical meristem. *Mol. Plant* 13, 1608–1623. doi: 10.1016/j.molp.2020.09.004

Shinohara, H. (2021). Root meristem growth factor RGF, a sulfated peptide hormone in plants. *Peptides* 142:170556. doi: 10.1016/j.peptides.2021.170556

Shinohara, H., Mori, A., Yasue, N., Sumida, K., and Matsubayashi, Y. (2016). Identification of three LRR-RKs involved in perception of root meristem growth factor in *Arabidopsis*. *Proc. Natl. Acad. Sci. U.S.A.* 113, 3897–3902.

Song, W., Liu, L., Wang, J., Wu, Z., Zhang, H., Tang, J., et al. (2016). Signature motif-guided identification of receptors for peptide hormones essential for root meristem growth. *Cell Res.* 26, 674–685. doi: 10.1038/cr.2016.62

Spencer, V., Venza, Z. N., and Harrison, C. J. (2020). What can lycophytes teach us about plant evolution and development? Modern perspectives on an ancient lineage. *Evol. Dev.* 23, 174–196. doi: 10.1111/ede.12350

Strabala, T. J., Phillips, L., West, M., and Stanbra, L. (2014). Bioinformatic and phylogenetic analysis of the CLAVATA3/EMBRYO-SURROUNDING REGION (CLE) and the CLE-LIKE signal peptide genes in the Pinophyta. *BMC Plant Biol.* 14:47. doi: 10.1186/1471-2229-14-47

Stuhrwohldt, N., Scholl, S., Lang, L., Katzenberger, J., Schumacher, K., and Schaller, A. (2020). The biogenesis of CLEL peptides involves several processing events in consecutive compartments of the secretory pathway. *eLife* 9:e55580. doi: 10.7554/eLife.55580

Tadiello, A., Ziosi, V., Negri, A. S., Noferini, M., Fiori, G., Busatto, N., et al. (2016). On the role of ethylene, auxin and a GOLVEN-like peptide hormone in the regulation of peach ripening. *BMC Plant Biol.* 16:44. doi: 10.1186/s12870-016-0730-7

Takeuchi, H. (2021). The role of diverse LURE-type cysteine-rich peptides as signaling molecules in plant reproduction. *Peptides* 142:170572. doi: 10.1016/j.peptides.2021.170572

Takeuchi, H., and Higashiyama, T. (2012). A species-specific cluster of defensin-like genes encodes diffusible pollen tube attractants in *Arabidopsis*. *PLoS Biol.* 10:e1001449. doi: 10.1371/journal.pbio.1001449

Tavormina, P., De Coninck, B., Nikonorova, N., De Smet, I., and Cammue, B. P. A. (2015). The plant peptidome: an expanding repertoire of structural features and biological functions. *Plant Cell* 27, 2095–2118. doi: 10.1105/tpc.15.00440

van Kesteren, R. E., Tensen, C. P., Smit, A. B., van Minnen, J., Kolakowski, L. F., Meyerhof, W., et al. (1996). Co-evolution of ligand-receptor pairs in the vasopressin/oxytocin superfamily of bioactive peptides. *J. Biol. Chem.* 271, 3619–3626. doi: 10.1074/jbc.271.7.3619

Wang, X. Y., Zhang, N., Zhang, L. N., He, Y. X., Cai, C., Zhou, J. G., et al. (2021). Perception of the pathogen-induced peptide RGF7 by the receptor-like kinases RGI4 and RGI5 triggers innate immunity in *Arabidopsis thaliana*. *New Phytol.* 230, 1110–1125. doi: 10.1111/nph.17197

Waterhouse, A. M., Procter, J. B., Martin, D. M., Clamp, M., and Barton, G. J. (2009). Jalview version 2–a multiple sequence alignment editor and analysis workbench. *Bioinformatics* 25, 1189–1191. doi: 10.1093/bioinformatics/btp033

Weststrand, S., and Korall, P. (2016). Phylogeny of Selaginellaceae: there is value in morphology after all! *Am. J. Bot.* 103, 2136–2159. doi: 10.3732/ajb.1600156

Whitewoods, C. D., Cammarata, J., Nemec Venza, Z., Sang, S., Crook, A. D., Aoyama, T., et al. (2018). CLAVATA was a genetic novelty for the morphological innovation of 3D growth in land plants. *Curr. Biol.* 28, 2365–2376.e5. doi: 10.1016/j.cub.2018.05.068

Whitford, R., Fernandez, A., Tejos, R., Perez, A. C., Kleine-Vehn, J., Vanneste, S., et al. (2012). GOLVEN secretory peptides regulate auxin carrier turnover during plant gravitropic responses. *Dev. Cell* 22, 678–685. doi: 10.1016/j.devcel.2012.02.002

Wikstrom, N., and Kenrick, P. (2000). Phylogeny of epiphytic *Huperzia* (Lycopodiaceae): paleotropical and neotropical clades corroborated by rbcL sequences. *Nord. J. Bot.* 20, 165–171. doi: 10.1111/j.1756-1051.2000.tb01561.x

Yamada, M., Han, X., and Benfey, P. N. (2020). RGF1 controls root meristem size through ROS signalling. *Nature* 577, 85–88. doi: 10.1038/s41586-019-1819-6

Yasui, Y., Tsukamoto, S., Sugaya, T., Nishihama, R., Wang, Q., Kato, H., et al. (2019). GEMMA CUP-ASSOCIATED MYB1, an ortholog of axillary meristem regulators, is essential in vegetative reproduction in *Marchantia polymorpha*. *Curr. Biol.* 29, 3987–3995e3985. doi: 10.1016/j.cub.2019.10.004

Zhang, H., Han, Z., Song, W., and Chai, J. (2016). Structural insight into recognition of plant peptide hormones by receptors. *Mol. Plant* 9, 1454–1463. doi: 10.1016/j.molp.2016.10.002

Zhang, J., Fu, X. X., Li, R. Q., Zhao, X., Liu, Y., Li, M. H., et al. (2020). The hornwort genome and early land plant evolution. *Nat. Plants* 6, 107–118. doi: 10.1038/s41477-019-0588-4

Zhang, L., Chen, F., Zhang, X., Li, Z., Zhao, Y., Lohaus, R., et al. (2020). The water lily genome and the early evolution of flowering plants. *Nature* 577, 79–84. doi: 10.1038/s41586-019-1852-5

Conflict of Interest: The authors declare that the research was conducted in the absence of any commercial or financial relationships that could be construed as a potential conflict of interest.

frontiers in Plant Science

MINI REVIEW
published: 03 September 2021
doi: 10.3389/fpls.2021.719606

Peptide Signaling Pathways Regulate Plant Vascular Development

*Bingjian Yuan[1] and Huanzhong Wang[1,2]**

[1]Department of Plant Science and Landscape Architecture, University of Connecticut, Storrs, CT, United States, [2]Institute for System Genomics, University of Connecticut, Storrs, CT, United States

Plant small peptides, including CLAVATA3/EMBRYO SURROUNDING REGION-RELATED (CLE) and Epidermal Patterning Factor-Like (EPFL) peptides, play pivotal roles in coordinating developmental processes through cell-cell communication. Recent studies have revealed that the phloem-derived CLE peptides, CLE41/44 and CLE42, promote (pro-)cambial cell proliferation and inhibit xylem cell differentiation. The endodermis-derived EPFL peptides, EPFL4 and EPFL6, modulate vascular development in the stem. Further, several other peptide ligands CLE9, CLE10, and CLE45 play crucial roles in regulating vascular development in the root. The peptide signaling pathways interact with each other and crosstalk with plant hormone signals. In this mini-review, we summtarize the recent advances on peptides function in vascular development and discuss future perspectives for the research of the CLE and EPFL peptides.

Keywords: vascular development, peptide, cambium, signaling, *Arabidopsis*

OPEN ACCESS

Edited by:
Qingyu Wu,
Chinese Academy of Agricultural Sciences (CAAS), China

Reviewed by:
Yuki Hirakawa,
Gakushuin University, Japan
Guodong Wang,
Shaanxi Normal University, China

****Correspondence:***
Huanzhong Wang
huanzhong.wang@uconn.edu
orcid.org/0000-0002-9004-3420

Specialty section:
This article was submitted to Plant Physiology, a section of the journal Frontiers in Plant Science

Received: *02 June 2021*
Accepted: *06 August 2021*
Published: *03 September 2021*

Citation:
Yuan B and Wang H (2021) Peptide Signaling Pathways Regulate Plant Vascular Development. Front. Plant Sci. 12:719606. doi: 10.3389/fpls.2021.719606

INTRODUCTION

Intercellular communication and interaction are fundamentally important for plants to fine-tune growth and development in response to ever-changing environmental conditions (Kucukoglu and Nilsson, 2015). Secreted signaling peptides play crucial roles in regulating vascular development by short-range intercellular communication (Fukuda et al., 2007). Peptides are often referred to as proteins smaller than 100 amino acids and derived from precursor proteins or directly translated from short open reading frames embedded in longer transcripts (Tavormina et al., 2015). The CLAVATA3/EMBRYO SURROUNDING REGION-RELATED (CLE) peptides are essential for plant development and stress responses (Wang and Fiers, 2010; Tavormina et al., 2015). The *Arabidopsis* genome contains 32 *CLE* genes encoding 27 unique peptides (Yamaguchi et al., 2016; Fukuda and Hardtke, 2020). These CLE peptides are recognized at the cell surface by transmembrane receptors and activate intracellular signal transduction, therefore regulating plant growth and development (Fletcher, 2020). In this mini-review, we summarize the function and interaction of peptide signaling pathways in vascular development (**Table 1**) and discuss the gaps in current knowledge and provide perspective for future research.

Vascular Development

Plant vasculatures transport water and nutrients to all developing organs. In the *Arabidopsis* stem, the vascular tissues are organized as bundles, in which the procambium or cambium resides in the middle, xylem inside, and phloem outside of the bundle (**Figure 1A**). At the shoot tip, vascular bundles are well separated along the stem periphery (**Figure 1A**). In the

TABLE 1 | CLAVATA3/EMBRYO SURROUNDING REGION-RELATED (CLE) peptides and their receptors in regulating vascular development.

Peptide	Receptors	Function
CLE41/44	PXY/TDR and SERKs	Cambial cell division, xylem differentiation, and vascular patterning
EPFL4/6	ER and ERL1	Vascular cambial cell division
CLE9/10	BAMs	Xylem differentiation
CLE25	CLV2-CLERK	Phloem initiation
CLE45	BAM3, CLV2-CRN	Phloem cell differentiation

more mature stem, cambium starts developing in positions between bundles, connects vascular cambium, and forms a ring of cambial cells (**Figure 1A**). At the bottom of the stem, cambium cells divide and form xylem precursor cells inward and phloem precursor cells outward of the stem. Eventually, these precursors differentiate into secondary xylem and secondary phloem, respectively (**Figure 1A**). Other plant organs, such as the root and hypocotyls, also go through secondary growth depending on the activity of cambium cells (Wang, 2020). Regulation of vascular development is vital for plant secondary growth and crop production and therefore remains a critical research area in plant biology.

TDIF-PXY Signaling Regulates Vascular Development

The proliferation of cambial stem cells is essential for vascular development and the mechanical strength of the plant stem. Peptide signals play crucial roles in regulating vascular development through cell-to-cell communication (Fukuda and Hardtke, 2020). The tracheary element differentiation inhibitory factor (TDIF) peptide is so far the best-understood peptide in this process (Fletcher, 2020; Wang, 2020). Tracheary element differentiation inhibitory factor is synthesized from the phloem and travels to the cambium, where TDIF binds to its receptor PHLOEM INTERCALATED WITH XYLEM/TDIF RECEPTOR (PXY/TDR) on the plasma membrane (Hirakawa et al., 2008; Etchells et al., 2016). Overexpression of TDIF coding genes *CLE41* and *CLE44* or exogenous application of synthetic TDIF peptide promote procambial cells proliferation and inhibit xylem cell differentiation (Hirakawa et al., 2008; Whitford et al., 2008; Etchells and Turner, 2010). These experiments established the function of the TDIF-PXY module in cambial cell proliferation, xylem differentiation, and vascular patterning (Hirakawa et al., 2008; Etchells and Turner, 2010). Downstream of the TDIF-PXY module is two WUSCHEL-related HOMEOBOX (WOX) transcription factors, WOX4 and WOX14 (Hirakawa et al., 2010; Etchells et al., 2013; Wang et al., 2013). WOX4 is expressed mainly in the procambium and cambium, and its expression level is upregulated by applying CLE ligand (Hirakawa et al., 2010). WOX14 acts redundantly with WOX4 in regulating vascular cell division (Etchells et al., 2013). The TDIF-PXY-WOX signaling plays a crucial role in the maintenance of the vascular meristem during secondary growth (Hirakawa et al., 2010; Yamaguchi et al., 2016).

The crystal structure of the extracellular domain of PXY/TDR in complex with TDIF peptide has been determined (Morita et al., 2016; Zhang et al., 2016a). The extracellular domain of PXY/TDR adopts a super-helical structure comprising 22 leucine-rich repeats (LRRs) and specifically recognizes TDIF by its inner concave surface (Morita et al., 2016). The TDIF peptide mainly adopts a "Ω"-like conformation binding the inner surface of the LRRs (Zhang et al., 2016a). The highly conserved amino acids of TDIF, including Hyp4, G6, Hyp7, and P9, are critical for the interaction with PXY/TDR (Zhang et al., 2016a). However, there are some discrepancies regarding which amino acids of PXY/TDR are essential to the interaction with TDIF (Morita et al., 2016; Zhang et al., 2016a). Structure-based sequence alignment showed that the TDIF-interacting motifs are conserved among plant species, suggesting a conserved TDIF-PXY recognition mechanism (Morita et al., 2016).

The TDIF-PXY-WOX4 signaling is conserved in plants. The TDIF peptide was first discovered from an analysis in zinnia (Ito et al., 2006). Later, TDIF peptide was found in *Arabidopsis* (Hirakawa et al., 2008) and the genomes of Euphyllophytes (Hirakawa and Bowman, 2015). The function of TDIF-PXY-WOX4 signaling has been investigated in poplar. Transgenic studies showed that the tissue-specific expression of *PttPXY* and *PttCLE41* genes resulted in enhanced secondary growth in hybrid aspen, indicating that TDIF-PXY signaling is conserved in poplar (Etchells et al., 2015). Consistent with this study, *PttWOX4* gene is specifically expressed in the cambial region and controls cell division activity in the vascular cambium (Kucukoglu et al., 2017).

In a recent study, a regulatory network downstream of TDIF-PXY was identified using an enhanced yeast one-hybrid system (Smit et al., 2020). Among the transcription factor-promoter interactions, WOX14 positively regulated the expression of *TARGET OF MONOPTEROS 6* (*TMO6*), which encodes a Dof-type transcription factor (Schlereth et al., 2010). In addition, WOX4 and TMO6 both positively regulate the expression of a third transcription factor gene, *LATERAL ORGAN BOUNDARIES DOMAIN4* (Smit et al., 2020). These data support a mechanism that this feed-forward loop controls vascular stem cell proliferation and helps to define the function of PXY signaling in determining the shape of the vascular bundle (Fletcher, 2020; Smit et al., 2020).

The TDIF-PXY signaling module regulates cell division in the (pro-)cambium and controls vascular organization *via* interacting with other factors (Etchells et al., 2016). The SOMATIC EMBRYOGENESIS RECEPTOR KINASE (SERK) family regulates plant growth and development, as well as many other biological processes (Albrecht et al., 2008). The SERK genes are expressed in procambial cells, suggesting that the SERK family may have a function in regulating vascular development (Kwaaitaal and De Vries, 2007). Indeed, the TDIF receptor PXY forms heterodimers with SERKs, including SERK1, SERK2, and SERK3 (BAK1), in regulating procambial cell proliferation (Zhang et al., 2016b). A NAC domain transcription factor XVP is localized on the plasma membrane and forms a complex with TDIF co-receptor PXY-BAK1 (Yang et al., 2020a). The XVP is expressed in the cambium and regulates xylem differentiation and vascular patterning (Yang et al., 2020a). Further study showed that XVP regulates xylem differentiation through a crucial factor VASCULAR-RELATED

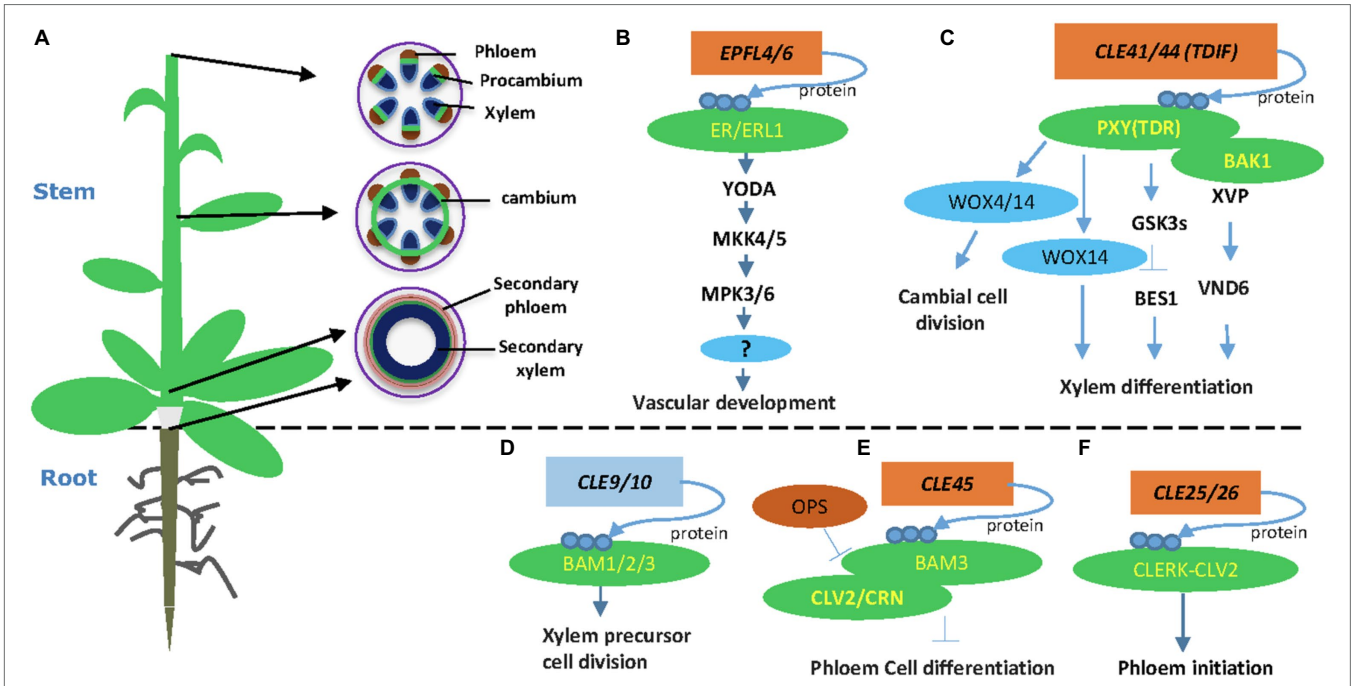

FIGURE 1 | Plant-specific CLE and Epidermal Patterning Factor-Like (EPFL) peptide signaling pathways in vascular development. **(A)** An *Arabidopsis* plant and different stages of vascular developmental in the stem. A young stem develops discrete vascular bundles that are comprised of phloem, xylem, and intervening procambium. In developing stems, cambial cells from vascular and interfascicular regions form a closed ring structure. Secondary growth produces secondary phloem and secondary xylem in both mature stem and hypocotyls. **(B)** The EPFL4 and EPFL6 peptides regulate stem vascular development in *Arabidopsis*. **(C)** CLE41/44 regulates vascular cambial cell division and xylem differentiation in the stem. **(D)** The CLE9/10 peptide regulates xylem formation. **(E)** The CLE45-BAM3 peptide inhibits root protophloem cell differentiation. **(F)** The CLE25 peptide promotes root protophloem cell differentiation. Arrows depict positive regulatory relationships and bars depict negative regulatory relationships.

NAC-DOMAIN6. The XVP promotes the expression of TDIF-encoding gene *CLE44*, whereas TDIF negatively regulates the expression of *XVP*, suggesting a feedback regulating loop (**Figure 1**). However, it is still not clear whether and how XVP proteins are translocated to the nucleus.

EPFL4/6-ER Signaling in the Regulation of Vascular Cambium

The EPIDERMAL PATTERNING FACTOR-LIKE 4 (EPFL4) and EPFL6/CHALLAH (CHAL) secretory peptides were first identified as regulators of inflorescence development through activating the ER signaling (Uchida et al., 2012). Two additional ER paralogs, ER-LIKE 1 (ERL1) and ERL2, together with ER, play crucial roles in regulating inflorescence architecture, organ shape, and epidermal stomatal patterning in *Arabidopsis* (Shpak et al., 2004; Uchida et al., 2012). In vascular development, the endodermis-produced EPFL4 and EPFL6 peptides function as ligands for phloem-located ER in regulating procambial cell division and stem elongation (Fischer and Teichmann, 2017; Ikematsu et al., 2017). Therefore, the cell-to-cell communication between the endodermis and the phloem plays a crucial role in procambial development (Ikematsu et al., 2017). Both *ER* and *ERL1* are expressed in inflorescence stem and function redundantly in regulating procambial development and xylem differentiation (Ikematsu et al., 2017; Tameshige et al., 2017). The *mpk3/mpk6* and mkk4/*mkk5* mutants showed short pedicels and a corymb-like inflorescence similar to the phenotypes of the *er* mutant (Meng et al., 2013). Further evidence showed that the MAPK cascade functions downstream of the ER receptor in regulating pedicel length and inflorescence architecture (Meng et al., 2013). Therefore, the MAPK cascade, involving YDA-MKK4/MKK5-MPK3/MPK6, functions downstream of ER in regulating cell proliferation and plant organ development (**Figure 1**). It would be interesting to investigate if this MAPK pathway also regulates procambium development in the stem and hypocotyl.

Other CLE Peptide Signaling Pathways in Vascular Development

Besides CLE41/CLE44, EPFL4, and EPFL6, other peptides, including CLE9/10, CLE25, and CLE45, also play critical roles in vascular development (Fukuda and Hardtke, 2020). The *CLE9* and *CLE10* genes are preferentially expressed in xylem precursor cells of the root vasculature (Kondo et al., 2011). Interestingly, the peptide CLE9/10 forms a complex with the receptor kinase HAESA-LIKE 1 (HSL1) to regulate stomatal lineage cell division. In the root xylem development, CLE9/10 is perceived by BARELY ANY MERISTEM (BAM) class receptor kinases in regulating periclinal cell division (**Figure 1**; Qian et al., 2018). BARELY ANY MERISTEM 1 and its homologs, BAM2 and BAM3, are class XI LRR receptor-like kinases similar to CLV1 and PXY (DeYoung et al., 2006). The *bam1 bam2*

and *bam1 bam3* mutants exhibited increased xylem files similarly to the *cle9* mutant (Qian et al., 2018). Indeed, physical interaction between CLE9/10 and BAM1 was demonstrated by three independent approaches (Shinohara et al., 2012; Anne et al., 2018; Qian et al., 2018), confirming the BAMs as CLE9 receptors in root xylem development.

The CLE45 peptide forms a complex with BARELY ANY MERISTEM 3 (BAM3) to regulate *Arabidopsis* protophloem differentiation (Depuydt et al., 2013). Protophloem consists of narrow thin-walled cells and is developed from procambium. Studies revealed that CLE45 is expressed from protophloem sieve elements in root meristems and perceived fully by CLAVATA 2 (CLV2) and the CORYNE (CRN) receptor proteins (Hazak et al., 2017). CRN is required for BAM3-mediated CLE45 signaling *via* stabilizing BAM3 expression. In addition, a protophloem-specific CRN expression rescues the resistance of the *crn* mutant to root-active CLE peptides (Hazak et al., 2017). Collectively, these data support a vital function of the CLE45 and CLV/BAM receptors in vascular development (Hazak et al., 2017). Downstream of BAM3, a MEMBRANE-ASSOCIATED KINASE REGULATOR protein, positively regulates CLE45 signaling (Kang and Hardtke, 2016). Further, OCTOPUS (OPS), a polarly localized membrane-associated protein, promotes root protophloem differentiation by antagonizing CLE45 signaling through direct interference with BAM3 and CLV2-CRN (**Figure 1**; Truernit et al., 2012; Rodriguez-Villalon et al., 2014; Breda et al., 2019).

The CLE25 and CLE26 play crucial roles in regulating root protophloem development (Czyzewicz et al., 2015; Anne et al., 2018; Ren et al., 2019). CLE25 expression is tightly associated with phloem initiation, and the loss-of-function mutant *cle25* shows a delayed protophloem differentiation phenotype (Ren et al., 2019). Genetic screening for suppressors identified CLV2 as a potential receptor for CLE25 (Ren et al., 2019). Further peptide assay and protein interaction experiment found that CLE-RESISTANT RECEPTOR KINASE (CLERK) interacts with CLV2 and possibly forms a receptor complex for CLE25 (Ren et al., 2019). However, direct binding between CLE25 and the CLERK-CLV2 receptor complex remains to be established experimentally.

The CLE45 and CLE25/26 peptides are all expressed in root and repress phloem development as shown by expression analyses and synthetic peptides treatment experiments (Kinoshita et al., 2007; Jun et al., 2010). CLE25 may be involved in the formative cell division during protophloem differentiation. It is still unclear which division step is regulated by CLE25 in the two successive formative cell division steps during protophloem development (Rodriguez-Villalon et al., 2014; Ren et al., 2019). In addition, there are some differences in terms of perception of these peptides. The CLE25 and CLE26 peptides could be perceived by CLERK (Anne et al., 2018; Ren et al., 2019), while CLE45 is perceived by BAM3 (Kang and Hardtke, 2016; Hazak et al., 2017). Further, CLE25 may be involved in response to detrimental environmental signals (Takahashi et al., 2018). Further investigation is needed to clarify the functional difference of these peptides in protophloem development.

The Crosstalk Between TDIF-TDR Signaling and Other Signaling Pathways

The development of vascular tissue involves interactions between TDIF-PXY and other peptide signaling pathways. The receptor kinases PXY and ER genetically interact to coordinate cell division and organization (Uchida and Tasaka, 2013; Etchells et al., 2016; Wang et al., 2019). Gene expression analysis suggested that *PXL1* and *PXL2* expression is upregulated in *er* mutant stems (Wang et al., 2019). The expression of *EPFL4* and *EPFL6* is altered in *pxf* (mutation of the PXY family, including *pxy*, *pxl1*, and *pxl2*) and *er pxy* mutants (Wang et al., 2019). Further study showed that the mutant of *er pxf* had considerably fewer cells per vascular bundle than either *pxf*, *er*, or *pxy* er, suggesting that *PXL1* and *PXL2* are functionally redundant with *ER* to regulate vascular proliferation in the stem (Wang et al., 2019). These results demonstrate that PXY and ER coordinately regulate vascular proliferation and organization *via* inter-tissue signaling (Wang et al., 2019).

TDFI-PXY signaling also interacts with plant hormonal signals, such as brassinosteroids (BR), auxin, and ethylene signaling. The GLYCOGEN SYNTHASE KINASE 3 (GSK3) family members, including BRASSINOSTEROID-INSENSITIVE 2 (BIN2), are crucial downstream components of the TDIF signaling pathway in suppressing xylem differentiation (Kondo et al., 2014). The PXY/TDR receptor interacts with GSK3s on the plasma membrane and activates GSK3s in a TDIF-dependent fashion (Kondo et al., 2014). The interaction between PXY/TDR and BIN2 inhibits the transcription factor BES1 to prevent procambial cell differentiation into the xylem (Kondo et al., 2014). Recently, an additional study showed that the GSK3 protein BIN2-LIKE 1 (BIL1) integrates the PXY/TDR signaling through phosphorylating the auxin response factor MP/ARF5, which limits the effect of MP/ARF5 on ARR7 and ARR15 expression, thus enhancing vascular cambial activity (Han et al., 2018). Together, these results suggest that BIL1 mediated the crosstalk between peptide signaling and hormone signaling to maintain the cambial activity (**Figure 1**; Han et al., 2018). Ethylene promotes cambium activity (Love et al., 2009; Yang et al., 2020b) and interacts with TDIF-PXY signaling (Etchells et al., 2012). The interaction between TDIF-PXY and plant hormone may help plants better perceive and respond to long-distance developmental and environmental signals.

The Crosstalk Between EPFL4/6-ER Signaling and Other Signaling Pathways

The LRR receptor-like kinase ER is a stem growth regulator and involves in diverse developmental processes, including epidermal and mesophyll development, stomatal density, and vascular development (Tameshige et al., 2017). For example, hydrogen peroxide induces cortex proliferation, while SPINDLY, an O-linked glucosamine acetyltransferase, functions downstream of ER to fine-tune cortex proliferation, indicating a connection between ER signaling and cellular redox homeostasis (Cui et al., 2014). Another study showed that an LRR receptor-like kinase SUPPRESSOR OF BIR1-1, previously known to control plant immune responses and abscission, appears downstream

of BREVIPEDICELLUS (BP) and ER to regulate the precocious differentiation of xylem fiber (Milhinhos et al., 2019). In addition, ER signaling pathway and the SWR1 chromatin remodeling complex jointly regulate inflorescence architecture by promoting the expression of the PACLOBUTRAZOL RESISTANCE (PRE) gene family (Cai et al., 2017). Further study showed that a growth-related transcription factor HOMOLOG OF BEE2 INTERACTING WITH IBH1 (HBI1) functions downstream of PRE1 to regulate inflorescence architecture by promoting pedicel elongation (Cai et al., 2021). These studies indicate potential crosstalks between ERFL4/6 and other pathways in regulating vascular development.

CONCLUSION

Significant progress has been made in our understanding of peptide signaling, including the TDIF-PXY/TDR module and the EPFL4/6–ER/ERL1 module, in regulating vascular development (Fukuda and Hardtke, 2020; Wang, 2020; Wang and Wang, 2020). While the TDIF-PXY signaling in vascular development has been the subject of much research since the discovery of TDIF, many questions remain. For instance, compared to the wild type, *pxy* mutants showed more fiber cells indicating that PXY has a potential function in regulating xylem development (Fisher and Turner, 2007). Moreover, environmental factors, including light, carbon dioxide concentration, and drought, all affect the expression pattern of several EPFL family genes, indicating that ER signaling could respond to external environmental stimuli (Richardson and Torii, 2013). Therefore, studying the crosstalk between environmental factors and peptide signaling in vascular development is an exciting field in the future.

Further, the EPFL4/6–ER/ERL1 module regulates procambial maintenance in inflorescence stems (Uchida et al., 2012), and a MAPK signaling module YDA-MKK4/5-MPK3/6 functions downstream of ER (Meng et al., 2013). Identification of the substrates of MPK3/6 would be crucial to understand the molecular mechanism of the EPFL-ER signaling. The crosstalk between TDIF-PXY and EPFL-ER signaling has been proposed, but the mechanistic interaction has not been established. It is possible that a common downstream signaling hub may connect both pathways in regulating cambial activity.

In addition, the BAM1 receptor can potentially bind both CLV3 and CLE25 peptides, indicating that the same receptors can perceive different CLE peptides in various biological contexts (Takahashi et al., 2018; Fletcher, 2020). In contrast, the CLE9/10 peptide ligand is recognized by two different receptor kinases HSL1 and BAM3 in regulating stomatal lineage cell division and periclinal cell division of xylem precursor cells, respectively (Qian et al., 2018). Therefore, the same receptor can perceive different CLE peptides, while the same peptide can bind to different receptors, indicating extremely complex peptide signal transduction networks in plants. The complexity may be necessary for peptide signaling to have developmental and organ-specific functions. Further dissection of the peptide signaling pathways will provide new insight into our understanding of vascular development.

AUTHOR CONTRIBUTIONS

BY and HW wrote the review. All authors contributed to the article and approved the submitted version.

FUNDING

This work is supported by the National Science Foundation (IOS-1453048) and in part, by USDA NIFA Hatch project #CONS00990 to HW.

REFERENCES

Albrecht, C., Russinova, E., Kemmerling, B., Kwaaitaal, M., and De Vries, S. C. (2008). Arabidopsis Somatic Embryogenesis receptor kinase proteins serve brassinosteroid-dependent and -independent signaling pathways. *Plant Physiol.* 148, 611–619. doi: 10.1104/pp.108.123216

Anne, P., Amiguet-Vercher, A., Brandt, B., Kalmbach, L., Geldner, N., Hothorn, M., et al. (2018). CLERK is a novel receptor kinase required for sensing of root-active CLE peptides in arabidopsis. *Development* 145:dev162354. doi: 10.1242/dev.162354

Breda, A. S., Hazak, O., Schultz, P., Anne, P., Graeff, M., Simon, R., et al. (2019). A cellular insulator against CLE45 peptide signaling. *Curr. Biol.* 29, 2501–2508.e3. doi: 10.1016/j.cub.2019.06.037

Cai, H., Chai, M., Chen, F., Huang, Y., Zhang, M., He, Q., et al. (2021). HBI1 acts downstream of ERECTA and SWR1 in regulating inflorescence architecture through the activation of the brassinosteroid and auxin signaling pathways. *New Phytol.* 229, 414–428. doi: 10.1111/nph.16840

Cai, H., Zhao, L., Wang, L., Zhang, M., Su, Z., Cheng, Y., et al. (2017). ERECTA signaling controls Arabidopsis inflorescence architecture through chromatin-mediated activation of PRE1 expression. *New Phytol.* 214, 1579–1596. doi: 10.1111/nph.14521

Cui, H., Kong, D., Wei, P., Hao, Y., Torii, K. U., Lee, J. S., et al. (2014). SPINDLY, ERECTA, and its ligand STOMAGEN have a role in redox-mediated cortex proliferation in the arabidopsis root. *Mol. Plant* 7, 1727–1739. doi: 10.1093/mp/ssu106

Czyzewicz, N., Shi, C.-L., Vu, L. D., Van De Cotte, B., Hodgman, C., Butenko, M. A., et al. (2015). Modulation of Arabidopsis and monocot root architecture by CLAVATA3/EMBRYO SURROUNDING REGION 26 peptide. *J. Exp. Bot.* 66, 5229–5243. doi: 10.1093/jxb/erv360

Depuydt, S., Rodriguez-Villalon, A., Santuari, L., Wyser-Rmili, C., Ragni, L., and Hardtke, C. S. (2013). Suppression of Arabidopsis protophloem differentiation and root meristem growth by CLE45 requires the receptor-like kinase BAM3. *Proc. Natl. Acad. Sci. U. S. A.* 110, 7074–7079. doi: 10.1073/pnas.1222314110

DeYoung, B. J., Bickle, K. L., Schrage, K. J., Muskett, P., Patel, K., and Clark, S. E. (2006). The CLAVATA1-related BAM1, BAM2 and BAM3 receptor kinase-like proteins are required for meristem function in Arabidopsis. *Plant J.* 45, 1–16. doi: 10.1111/j.1365-313X.2005.02592.x

Etchells, J. P., Mishra, L. S., Kumar, M., Campbell, L., and Turner, S. R. (2015). Wood formation in trees is increased by manipulating PXY-regulated cell division. *Curr. Biol.* 25, 1050–1055. doi: 10.1016/j.cub.2015.02.023

Etchells, J. P., Provost, C. M., Mishra, L., and Turner, S. R. (2013). WOX4 and WOX14 act downstream of the PXY receptor kinase to regulate plant vascular proliferation independently of any role in vascular organisation. *Development* 140, 2224–2234. doi: 10.1242/dev.091314

Etchells, J. P., Provost, C. M., and Turner, S. R. (2012). Plant vascular cell division is maintained by an interaction between PXY and ethylene signalling. *PLoS Genet.* 8:e1002997. doi: 10.1371/journal.pgen.1002997

Etchells, J. P., Smit, M. E., Gaudinier, A., Williams, C. J., and Brady, S. M. (2016). A brief history of the TDIF-PXY signalling module: balancing

meristem identity and differentiation during vascular development. *New Phytol.* 209, 474–484. doi: 10.1111/nph.13642

Etchells, J. P., and Turner, S. R. (2010). The PXY-CLE41 receptor ligand pair defines a multifunctional pathway that controls the rate and orientation of vascular cell division. *Development* 137, 767–774. doi: 10.1242/dev.044941

Fischer, U., and Teichmann, T. (2017). The ERECTA and ERECTA-like genes control a developmental shift during xylem formation in Arabidopsis. *New Phytol.* 213, 1562–1563. doi: 10.1111/nph.14440

Fisher, K., and Turner, S. (2007). PXY, a receptor-like kinase essential for maintaining polarity during plant vascular-tissue development. *Curr. Biol.* 17, 1061–1066. doi: 10.1016/j.cub.2007.05.049

Fletcher, J. C. (2020). Recent advances in Arabidopsis CLE peptide signaling. *Trends Plant Sci.* 25, 1005–1016. doi: 10.1016/j.tplants.2020.04.014

Fukuda, H., and Hardtke, C. S. (2020). Peptide signaling pathways in vascular differentiation. *Plant Physiol.* 182, 1636–1644. doi: 10.1104/pp.19.01259

Fukuda, H., Hirakawa, Y., and Sawa, S. (2007). Peptide signaling in vascular development. *Curr. Opin. Plant Biol.* 10, 477–482. doi: 10.1016/j.pbi.2007.08.013

Han, S., Cho, H., Noh, J., Qi, J., Jung, H. J., Nam, H., et al. (2018). BIL1-mediated MP phosphorylation integrates PXY and cytokinin signalling in secondary growth. *Nat. Plants* 4, 605–614. doi: 10.1038/s41477-018-0180-3

Hazak, O., Brandt, B., Cattaneo, P., Santiago, J., Rodriguez-Villalon, A., Hothorn, M., et al. (2017). Perception of root-active CLE peptides requires CORYNE function in the phloem vasculature. *EMBO rep.* 18, 1367–1381. doi: 10.15252/embr.201643535

Hirakawa, Y., and Bowman, J. L. (2015). A role of TDIF peptide signaling in vascular cell differentiation is conserved among euphyllophytes. *Front. Plant Sci.* 6:1048. doi: 10.3389/fpls.2015.01048

Hirakawa, Y., Kondo, Y., and Fukuda, H. (2010). TDIF peptide signaling regulates vascular stem cell proliferation via the WOX4 homeobox gene in Arabidopsis. *Plant Cell* 22, 2618–2629. doi: 10.1105/tpc.110.076083

Hirakawa, Y., Shinohara, H., Kondo, Y., Inoue, A., Nakanomyo, I., Ogawa, M., et al. (2008). Non-cell-autonomous control of vascular stem cell fate by a CLE peptide/receptor system. *Proc. Natl. Acad. Sci. U. S. A.* 105, 15208–15213. doi: 10.1073/pnas.0808444105

Ikematsu, S., Tasaka, M., Torii, K. U., and Uchida, N. (2017). ERECTA-family receptor kinase genes redundantly prevent premature progression of secondary growth in the Arabidopsis hypocotyl. *New Phytol.* 213, 1697–1709. doi: 10.1111/nph.14335

Ito, Y., Nakanomyo, I., Motose, H., Iwamoto, K., Sawa, S., Dohmae, N., et al. (2006). Dodeca-CLE as peptides as suppressors of plant stem cell differentiation. *Science* 313, 842–845. doi: 10.1126/science.1128436

Jun, J., Fiume, E., Roeder, A. H. K., Meng, L., Sharma, V. K., Osmont, K. S., et al. (2010). Comprehensive analysis of CLE polypeptide signaling gene expression and overexpression activity in arabidopsis. *Plant Physiol.* 154, 1721–1736. doi: 10.1104/pp.110.163683

Kang, Y. H., and Hardtke, C. S. (2016). Arabidopsis MAKR 5 is a positive effector of BAM 3-dependent CLE 45 signaling. *EMBO Rep.* 17, 1145–1154. doi: 10.15252/embr.201642450

Kinoshita, A., Nakamura, Y., Sasaki, E., Kyozuka, J., Fukuda, H., and Sawa, S. (2007). Gain-of-function phenotypes of chemically synthetic CLAVATA3/ESR-related (CLE) peptides in Arabidopsis thaliana and Oryza sativa. *Plant Cell Physiol.* 48, 1821–1825. doi: 10.1093/pcp/pcm154

Kondo, Y., Hirakawa, Y., Kieber, J. J., and Fukuda, H. (2011). CLE peptides can negatively regulate protoxylem vessel formation via cytokinin signaling. *Plant Cell Physiol.* 52, 37–48. doi: 10.1093/pcp/pcq129

Kondo, Y., Ito, T., Nakagami, H., Hirakawa, Y., Saito, M., Tamaki, T., et al. (2014). Plant GSK3 proteins regulate xylem cell differentiation downstream of TDIF-TDR signalling. *Nat. Commun.* 5:3504. doi: 10.1038/ncomms4504

Kucukoglu, M., Nilsson, J., Zheng, B., Chaabouni, S., and Nilsson, O. (2017). WUSCHEL-RELATED HOMEOBOX4 (WOX4)-like genes regulate cambial cell division activity and secondary growth in Populus trees. *New Phytol.* 215, 642–657. doi: 10.1111/nph.14631

Kucukoglu, M., and Nilsson, O. (2015). CLE peptide signaling in plants - the power of moving around. *Physiol. Plant.* 155, 74–87. doi: 10.1111/ppl.12358

Kwaaitaal, M. A. C. J., and De Vries, S. C. (2007). The SERK1 gene is expressed in procambium and immature vascular cells. *J. Exp. Bot.* 58, 2887–2896. doi: 10.1093/jxb/erm103

Love, J., Björklund, S., Vahala, J., Hertzberg, M., Kangasjärvi, J., and Sundberg, B. (2009). Ethylene is an endogenous stimulator of cell division in the cambial meristem of Populus. *Proc. Natl. Acad. Sci.* 106, 5984–5989. doi: 10.1073/PNAS.0811660106

Meng, X., Wang, H., He, Y., Liu, Y., Walker, J. C., Torii, K. U., et al. (2013). A MAPK cascade downstream of ERECTA receptor-like protein kinase regulates Arabidopsis inflorescence architecture by promoting localized cell proliferation. *Plant Cell* 24, 4948–4960. doi: 10.1105/tpc.112.104695

Milhinhos, A., Vera-Sirera, F., Blanco-Touriñán, N., Mari-Carmona, C., Carrió-Seguí, À., Forment, J., et al. (2019). SOBIR1/EVR prevents precocious initiation of fiber differentiation during wood development through a mechanism involving BP and ERECTA. *Proc. Natl. Acad. Sci. U. S. A.* 116, 18710–18716. doi: 10.1073/pnas.1807863116

Morita, J., Kato, K., Nakane, T., Kondo, Y., Fukuda, H., Nishimasu, H., et al. (2016). Crystal structure of the plant receptor-like kinase TDR in complex with the TDIF peptide. *Nat. Commun.* 7:12383. doi: 10.1038/ncomms12383

Qian, P., Song, W., Yokoo, T., Minobe, A., Wang, G., Ishida, T., et al. (2018). The CLE9/10 secretory peptide regulates stomatal and vascular development through distinct receptors. *Nat. Plants* 4, 1071–1081. doi: 10.1038/s41477-018-0317-4

Ren, S. C., Song, X. F., Chen, W. Q., Lu, R., Lucas, W. J., and Liu, C. M. (2019). CLE25 peptide regulates phloem initiation in Arabidopsis through a CLERK-CLV2 receptor complex. *J. Integr. Plant Biol.* 61, 1043–1061. doi: 10.1111/jipb.12846

Richardson, L. G. L., and Torii, K. U. (2013). Take a deep breath: peptide signalling in stomatal patterning and differentiation. *J. Exp. Bot.* 64, 5243–5251. doi: 10.1093/jxb/ert246

Rodriguez-Villalon, A., Gujas, B., Kang, Y. H., Breda, A. S., Cattaneo, P., Depuydt, S., et al. (2014). Molecular genetic framework for protophloem formation. *Proc. Natl. Acad. Sci. U. S. A.* 111, 11551–11556. doi: 10.1073/pnas.1407337111

Schlereth, A., Möller, B., Liu, W., Kientz, M., Flipse, J., Rademacher, E. H., et al. (2010). MONOPTEROS controls embryonic root initiation by regulating a mobile transcription factor. *Nature* 464, 913–916. doi: 10.1038/nature08836

Shinohara, H., Moriyama, Y., Ohyama, K., and Matsubayashi, Y. (2012). Biochemical mapping of a ligand-binding domain within Arabidopsis BAM1 reveals diversified ligand recognition mechanisms of plant LRR-RKs. *Plant J.* 70, 845–854. doi: 10.1111/j.1365-313X.2012.04934.x

Shpak, E. D., Berthiaume, C. T., Hill, E. J., and Torii, K. U. (2004). Synergistic interaction of three ERECTA-family receptor-like kinases controls Arabidopsis organ growth and flower development by promoting cell proliferation. *Development* 131, 1491–1501. doi: 10.1242/dev.01028

Smit, M. E., McGregor, S. R., Sun, H., Gough, C., Bågman, A. M., Soyars, C. L., et al. (2020). A PXY-mediated transcriptional network integrates signaling mechanisms to control vascular development in Arabidopsis. *Plant Cell* 32, 319–335. doi: 10.1105/tpc.19.00562

Takahashi, F., Suzuki, T., Osakabe, Y., Betsuyaku, S., Kondo, Y., Dohmae, N., et al. (2018). A small peptide modulates stomatal control via abscisic acid in long-distance signaling. *Nature* 556, 235–238. doi: 10.1038/s41586-018-0009-2

Tameshige, T., Ikematsu, S., Torii, K. U., Uchida, N., and Etchells, P. (2017). Stem development through vascular tissues: EPFL-ERECTA family signaling that bounces in and out of phloem. *J. Exp. Bot.* 68, 45–53. doi: 10.1093/jxb/erw447

Tavormina, P., De Coninck, B., Nikonorova, N., De Smet, I., and Cammuea, B. P. A. (2015). The plant peptidome: an expanding repertoire of structural features and biological functions. *Plant Cell* 27, 2095–2118. doi: 10.1105/tpc.15.00440

Truernit, E., Bauby, H., Belcram, K., Barthélémy, J., and Palauqui, J. C. (2012). OCTOPUS, a polarly localised membrane-associated protein, regulates phloem differentiation entry in Arabidopsis thaliana. *Development* 139, 1306–1315. doi: 10.1242/dev.072629

Uchida, N., Lee, J. S., Horst, R. J., Lai, H. H., Kajita, R., Kakimoto, T., et al. (2012). Regulation of inflorescence architecture by intertissue layer ligand-receptor communication between endodermis and phloem. *Proc. Natl. Acad. Sci. U. S. A.* 109, 6337–6342. doi: 10.1073/pnas.1117537109

Uchida, N., and Tasaka, M. (2013). Regulation of plant vascular stem cells by endodermisderived EPFL-family peptide hormones and phloemexpressed ERECTA-family receptor kinases. *J. Exp. Bot.* 64, 5335–5343. doi: 10.1093/jxb/ert196

Wang, G., and Fiers, M. (2010). CLE peptide signaling during plant development. *Protoplasma* 240, 33–43. doi: 10.1007/s00709-009-0095-y

Wang, H. (2020). Regulation of vascular cambium activity. *Plant Sci.* 291:110322. doi: 10.1016/j.plantsci.2019.110322

Wang, J., Kucukoglu, M., Zhang, L., Chen, P., Decker, D., Nilsson, O., et al. (2013). The Arabidopsis LRR-RLK, PXC1, is a regulator of secondary wall formation correlated with the TDIF-PXY/TDR-WOX4 signaling pathway. *BMC Plant Biol.* 13:94. doi: 10.1186/1471-2229-13-94

Wang, N., Bagdassarian, K. S., Doherty, R. E., Kroon, J. T., Connor, K. A., Wang, X. Y., et al. (2019). Organ-specific genetic interactions between paralogues of the PXY and ER receptor kinases enforce radial patterning in Arabidopsis vascular tissue. *Development* 146:dev177105. doi: 10.1242/dev.181750

Wang, S., and Wang, H. (2020). Coordination of Multilayered Signalling Pathways on Vascular Cambium Activity. *Annu. Plant Rev. Online* 3, 457–472. doi: 10.1002/9781119312994.APR0754.

Whitford, R., Fernandez, A., De Groodt, R., Ortega, E., and Hilson, P. (2008). Plant CLE peptides from two distinct functional classes synergistically induce division of vascular cells. *Proc. Natl. Acad. Sci. U. S. A.* 105, 18625–18630. doi: 10.1073/pnas.0809395105

Yamaguchi, Y. L., Ishida, T., and Sawa, S. (2016). CLE peptides and their signaling pathways in plant development. *J. Exp. Bot.* 67, 4813–4826. doi: 10.1093/jxb/erw208

Yang, J. H., Lee, K. H., Du, Q., Yang, S., Yuan, B., Qi, L., et al. (2020a). A membrane-associated NAC domain transcription factor XVP interacts with TDIF co-receptor and regulates vascular meristem activity. *New Phytol.* 226, 59–74. doi: 10.1111/nph.16289

Yang, S., Wang, S., Li, S., Du, Q., Qi, L., Wang, W., et al. (2020b). Activation of ACS7 in Arabidopsis affects vascular development and demonstrates a link between ethylene synthesis and cambial activity. *J. Exp. Bot.* 71, 7160–7170. doi: 10.1093/jxb/eraa423

Zhang, H., Lin, X., Han, Z., Qu, L. J., and Chai, J. (2016a). Crystal structure of PXY-TDIF complex reveals a conserved recognition mechanism among CLE peptide-receptor pairs. *Cell Res.* 26, 543–555. doi: 10.1038/cr.2016.45

Zhang, H., Lin, X., Han, Z., Wang, J., Qu, L. J., and Chai, J. (2016b). SERK family receptor-like kinases function as co-receptors with PXY for plant vascular development. *Mol. Plant* 9, 1406–1414. doi: 10.1016/j.molp.2016.07.004

Conflict of Interest: The authors declare that the research was conducted in the absence of any commercial or financial relationships that could be construed as a potential conflict of interest.

Publisher's Note: All claims expressed in this article are solely those of the authors and do not necessarily represent those of their affiliated organizations, or those of the publisher, the editors and the reviewers. Any product that may be evaluated in this article, or claim that may be made by its manufacturer, is not guaranteed or endorsed by the publisher.

frontiers in Plant Science

ORIGINAL RESEARCH
published: 23 September 2021
doi: 10.3389/fpls.2021.737219

Influence of Switchgrass *TDIF-like* Genes on *Arabidopsis* Vascular Development

Dongdong Tian[1,2], *Jingwen Tang*[1], *Liwen Luo*[1], *Zhe Zhang*[1], *Kebing Du*[1,3], *Robert M. Larkin*[1], *Xueping Shi*[1,3]* and *Bo Zheng*[1,3]*

[1] Key Laboratory of Horticultural Plant Biology of Ministry of Education, College of Horticulture and Forestry Sciences, Huazhong Agricultural University, Wuhan, China, [2] Tobacco Research Institute, Chinese Academy of Agricultural Science, Qingdao, China, [3] Hubei Engineering Technology Research Center for Forestry Information, Huazhong Agricultural University, Wuhan, China

As a member of the CLAVATA3 (CLV3)/EMBRYO SURROUNDING REGION (CLE) family, the dodecapeptide tracheary element differentiation inhibitory factor (TDIF) has a major impact on vascular development in plants. However, the influence of polymorphisms in the TDIF peptide motif on activity remains poorly understood. The model plant, *Arabidopsis* provides a fast and effective tool for assaying the activity of *TDIF* homologs. Five *TDIF* homologs from a group of 93 *CLE* genes in switchgrass (*Panicum virgatum*), a perennial biomass crop, named *PvTDIF-like* (*PvTDIFL*) genes were studied. The expression levels of *PvTDIFL1*, *PvTDIFL3*^{MR3}, and *PvTDIFL3*^{MR2} were relatively high and all of them were expressed at the highest levels in the rachis of switchgrass. The precursor proteins for PvTDIFL1, PvTDIFL3^{MR3}, and PvTDIFL3^{MR2} contained one, three, and two TDIFL motifs, respectively. Treatments with exogenous PvTDIFL peptides increased the number of stele cells in the hypocotyls of *Arabidopsis* seedlings, with the exception of PvTDIFL_4p. Heterologous expression of *PvTDIFL1* in *Arabidopsis* strongly inhibited plant growth, increased cell division in the vascular tissue of the hypocotyl, and disrupted the cellular organization of the hypocotyl. Although heterologous expression of *PvTDIFL3*^{MR3} and *PvTDIFL3*^{MR2} also affected plant growth and vascular development, PvTDIFL activity was not enhanced by the multiple TDIFL motifs encoded by *PvTDIFL3*^{MR3} and *PvTDIFL3*^{MR2}. These data indicate that in general, PvTDIFLs are functionally similar to *Arabidopsis* TDIF but that the processing and activities of the PvTDIFL peptides are more complex.

Keywords: switchgrass, CLE, TDIF, vascular development, biomass

OPEN ACCESS

Edited by:
Qingyu Wu,
Chinese Academy of Agricultural Sciences (CAAS), China

Reviewed by:
Alison W. Roberts,
University of Rhode Island, United States
Guodong Wang,
Shaanxi Normal University, China

***Correspondence:**
Xueping Shi
xpshi@mail.hzau.edu.cn
Bo Zheng
bo.zheng@mail.hzau.edu.cn

Specialty section:
This article was submitted to Plant Physiology, a section of the journal Frontiers in Plant Science

Received: *06 July 2021*
Accepted: *17 August 2021*
Published: *23 September 2021*

Citation:
Tian D, Tang J, Luo L, Zhang Z, Du K, Larkin RM, Shi X and Zheng B (2021) Influence of Switchgrass TDIF-like Genes on Arabidopsis Vascular Development. Front. Plant Sci. 12:737219. doi: 10.3389/fpls.2021.737219

INTRODUCTION

In plants, the *CLAVATA3 (CLV3)/EMBRYO SURROUNDING REGION (CLE)* gene family plays a vital role in cell division and cell differentiation by mediating intercellular communication (Fletcher et al., 1999; Fiers et al., 2005, 2007). *CLE* peptides are derived from a pre-propeptide containing an N-terminal signal peptide and a conserved C-terminal motif of 12-13 amino acids. A few *CLE* genes encode multiple CLE motifs in rice, wheat (*Triticum aetivum*), *Picea*, and *Amborella*, etc. (Goad et al., 2017). *CLE* genes are ubiquitous in the plant kingdom, and have been comprehensively studied in eudicots (*Arabidopsis thaliana*, *Glycine max*, *Lycopersicon esculentum*,

Gossypium hirsutum, *Populus trichocarpa*, and *Vitis vinifera*), monocots (*Oryza sativa*, *T. aestivum*, and *Zea mays*), and gymnosperms (*Picea abies* and *P. glauca*) (Cock and McCormick, 2001; Sawa et al., 2008; Strabala et al., 2014; Han et al., 2016; Goad et al., 2017; Wang et al., 2019). In *A. thaliana*, at least 32 *CLE* genes have been identified (Ito et al., 2006; Kondo et al., 2006; Ohyama et al., 2009; Ogawa-Ohnishi et al., 2013). Based on their biological functions, the *Arabidopsis* CLE peptides were grouped into two major classes. The A-type CLE peptides which maintain the apical meristems in shoots and roots and include CLV3, CLE1-27, and CLE40. The B-type/H-type CLE peptides, on the other hand, suppress xylem differentiation and promote vascular procambial cell division and include CLE41, CLE42, and CLE44 (Schoof et al., 2000; Ito et al., 2006; Whitford et al., 2008; Stahl et al., 2009; Hirakawa et al., 2010a,b).

One member of the CLE family, a dodecapeptide (H-E-V-P-S-G-P-N-P-I-S-N) named tracheary element differentiation inhibitory factor (TDIF) was first identified in a *Zinnia elegans* mesophyll cell xylogenesis system. H^1 is unique among CLE peptides with TDIF activity, and V^3, N^8, and N^{12} are essential for TDIF activity (Ito et al., 2006). In *Arabidopsis*, TDIF is encoded by two genes, *CLE41* and *CLE44*. *CLE42* and *CLE46* are classified as *TDIF-like* (*TDIFL*) genes, because their CLE motifs (H-G-V-P-S-G-P-N-P-I-S-N and H-K-H-P-S-G-P-N-P-T-G-N, respectively) are highly homologous to the TDIF motif. The *TDIF* genes are mainly involved in the regulation of vascular development. The TDIF signaling pathway in the vascular meristem has been well-studied (Ito et al., 2006; Ohyama et al., 2008). The TDIF RECEPTOR/PHLOEM INTERCALATED WITH XYLEM (TDR/PXY), a member of the leucine-rich repeat receptor-like kinase (LRR-RLK) family, is the TDIF receptor in procambial cells (Fisher and Turner, 2007; Hirakawa et al., 2008). The TDIF peptide that is produced in the phloem controls vascular procambial or cambial cell proliferation and xylem differentiation by activating TDR/PXY in the procambium or cambium. Two transcription factors, WUSCHEL HOMEOBOX RELATED 4 (WOX4) and WOX14, regulate the proliferation of plant vascular tissue by acting downstream of the TDIF–TDR/PXY signaling pathway (Hirakawa et al., 2010a,b; Etchells et al., 2013; Kucukoglu et al., 2017; Li et al., 2018). In addition, an NAC domain transcription factor, XVP, fine-tunes the TDIF signaling that contributes to vascular development by serving as a negative regulator (Kucukoglu, 2020; Yang et al., 2020). Current reports on TDIF/TDIFL have focused on genes encoding a single motif. Little is known about the function of TDIF/TDIFL genes encoding multiple motifs.

Switchgrass (*P. virgatum*) is a highly productive herbaceous perennial that thrives in diverse environments and is, therefore, a model perennial biomass crop (PBC) (Sanderson et al., 1996; McLaughlin and Adams Kszos, 2005). It has been a feedstock for the biofuels and specialty chemicals (Parrish and Fike, 2005; Sanderson et al., 2006; Keshwani and Cheng, 2009). Among the four PBCs (poplar, switchgrass, *Miscanthus,* and *Salix*), molecular regulation of lignocellulosic formation has been comprehensively studied in poplar trees (Clifton-Brown et al., 2019). Increasing vascular cambial activity results in incremental xylem and phloem, therefore increasing the biomass of wood. The division of vascular cambial cells was stimulated by manipulating CLE41–PXY signaling in hybrid poplar (Etchells and Turner, 2010; Etchells et al., 2015). The WOX4 controls the rate of cambial cell division and hence, the growth of stem girth in a TDIF-dependent manner (Kucukoglu et al., 2017). In a recent report, the *CLE* gene family in switchgrass, including three *PvTDIFL* genes, was defined. The statistical analysis demonstrated that no common TDIF/TDIFL motif is shared between monocots and dicots and that the contribution of TDIF/TDIFL to the development of vascular tissue has probably been diverged in monocots and dicots (Zhang et al., 2020). However, the knowledge of TDIF/TDIFL peptide functions in switchgrass remains limited.

Studying the mechanisms that drive rapid growth in switchgrass and other PBCs may help to introduce biomass-related genes, pathways or regulatory modules into dicotyledonous plants. *Arabidopsis* is widely used in the study of secondary cell wall formation and vascular development because although *Arabidopsis* is an annual herbaceous plant, it has most of the cell types associated with secondary growth (Zhang et al., 2011; Ursache et al., 2013; Ragni and Hardtke, 2014). The TDIF–TDR/PXY signaling pathway has been well-studied in *Arabidopsis* (Etchells and Turner, 2010; Hirakawa et al., 2010a,b; Etchells et al., 2013, 2016; Wang et al., 2013; Kondo and Fukuda, 2015; Zhang et al., 2016; Kucukoglu, 2020). Thus, *Arabidopsis* is suitable for activity screening and functional analysis of *TDIF*/*TDIFL* genes from various plants. This study aimed to use bioinformatics tools to identify the CLE gene family, including *TDIF*/*TDIFL* genes, at the whole genome level in *P. virgatum*. Treatment of *Arabidopsis* with exogenous TDIF/TDIFL peptides and heterologous expression of *TDIF*/*TDIFL* genes in *Arabidopsis* allowed the researchers of this study to test whether particular PvTDIFL peptides influenced plant growth and vascular development. Rapid characterization of PvTDIFL peptides in *Arabidopsis* can provide a preliminary understanding of the biological activities of PvTDIFL peptides and indicate potential biotechnological applications related to wood formation and biomass improvement. This is not practical to achieve with switchgrass because the genetic transformation of switchgrass is still time-consuming and laborious (Xi et al., 2009; Chen and Song, 2019; Ondzighi-Assoume et al., 2019).

MATERIALS AND METHODS

Identification of *CLE* Genes in *P. virgatum*

The amino acid sequences of *Arabidopsis* CLE proteins were downloaded from The *Arabidopsis* Information Resource (TAIR) (https://www.Arabidopsis.org/). The 12-amino acid CLE motifs were used as queries in TBLASTN search of the *P. virgatum* v1.1 genome with a threshold e-value of 500 in the Phytozome v12.1 database (https://phytozome.jgi.doe.gov/pz/portal.html) (Goodstein et al., 2012). Repeated hits were removed and only one hit at each chromosomal location was kept. Genes at each chromosomal location were identified as potential *CLE* genes. If there was no annotated gene at the target location, a 5-kb genome fragment with the target location in the center was then retrieved and subjected to an analysis with the online software, FGENESH,

for gene predictions on the softberry website (http://linux1.softberry.com/) (Solovyev et al., 2006). Amino acid sequences encoded by each of the potential *CLE* genes were checked for the C-terminal conserved CLE motifs. All of the newly identified motifs were used as queries in TBLASTN searches, as described in the preceding steps. The analysis was iterated until no more *CLE* candidate could be identified. All of the *CLE* candidates were compared with the previously reported *CLE* genes in *P. virgatum* (Zhang et al., 2020). The final *TDIF/TDIFL* gene sequences were obtained using cloning based on the nucleotide sequences from Phytozome (**Supplementary Figure 1**).

Bioinformatics Analysis

To classify *PvCLE* genes, all 12-aa CLE motifs encoded by *AtCLE* and *PvCLE* genes were extracted, including the *PvCLE* genes encoding multiple CLE motifs. Phylogenetic trees containing the 12-aa CLE motif sequences were constructed as previously described (Zhang et al., 2020). Based on the clustering of CLE motifs, *PvCLE* genes in the same group as *AtTDIF*/*TDIFL* genes were predicted as *PvTDIFL* genes. To further analyze the evolutionary relationship between *PvTDIFL* and *AtTDIF*/*TDIFL* genes, phylogenetic trees containing the full-length amino acid sequences for TDIF/TDIFL from both *P. virgatum* and *Arabidopsis* were constructed using the MEGA 5.05 software (Hall, 2013) with the following parameters: alignment, Muscle, phylogeny construct or test, Maximum Likelihood Tree, and number of bootstrap replication $= 1000$. Signal peptides that target the TDIF/TDIFL proteins to the secretary pathway were predicted with the SMART Server using a normal model (http://smart.embl-heidelberg.de/smart/set_mode.cgi?NORMAL=1) (Letunic and Bork, 2018). Gene structure analysis was performed using the Gene Structure Display Server 2.0 (http://gsds.cbi.pku.edu.cn/) (Hu et al., 2015). The Format of Gene Features was set as fast-all (FASTA) Sequence. Other features containing signal peptides and motifs were uploaded in Browser Extensible Data (BED) format. Phylogenetic Tree was uploaded in Newick format based on full-length amino acid sequences (Hu et al., 2015). Multiple alignments were performed using the DNAMAN v6.0 software (Lynnon Biosoft, Quebec, Canada). Weblogo-Create Sequence Logos (http://weblogo.berkeley.edu/logo.cgi) was used for comparative analysis of motif conservation and for conservation analysis of each amino acid site of TDIF/TDIFL motifs in *Arabidopsis* and switchgrass (Crooks et al., 2004). Isoelectric point (*p*I) and molecular weight (MW) were calculated using the ExPASy-ProtParam tool (http://web.expasy.org/protparam/) (Bjellqvist et al., 1993).

Plant Materials and Growth Conditions

Arabidopsis thaliana ecotype Columbia-0 (Col-0) and *P. virgatum* were used in this study. *Arabidopsis* seeds were surface sterilized in 75% (v/v) ethanol for 1 min and 5% (v/v) sodium hypochlorite for 15 min, with occasional gentle shaking. The seeds were then washed five times with sterilized distilled H_2O (dH_2O). After stratification at 4°C for 2 days, the seeds were placed in liquid Murashige and Skoog (MS) medium (pH 5.8) containing 1.5% sucrose (w/v) or on solid MS medium (pH 5.8) containing 1.5% sucrose (w/v) and 0.7% plant agar (w/v). The conical flasks containing liquid medium and the plates containing solid medium were placed in a tissue culture room maintained at 23°C and grown in a photoperiod containing 16 h of light at a fluence rate of 100 μmol photons m^{-2} s^{-1} followed by 8 h of dark. The conical flasks were placed on an orbital shaker at a rotational speed of 80 rpm. The plates were positioned vertically. *Arabidopsis* were grown in soil under the same temperature and light conditions, except that light intensity was set as 150 μmol photons m^{-2} s^{-1}. The *P. virgatum* plants used in this study were grown at Huazhong Agricultural University, Wuhan, China.

Exogenous Peptide Treatment

The TDIF/TDIFL peptides derived from *Arabidopsis* TDIF and PvTDIFL motifs (**Supplementary Table 1**) were chemically synthesized by GenScript Biotech Corporation (Nanjing, China). Twenty milligrams of each peptide was provided at a purity ≥ 90% (w/w). Peptides were dissolved in double distilled water (ddH_2O) at a stock concentration of 1 mg/ml and stored at −80°C for future use. Synthetic TDIF and PvTDIFL peptides were added to liquid medium at a final concentration of 10 μM as previously described (Whitford et al., 2008). *Arabidopsis* seeds were treated with 10 ml of medium in conical flasks on an orbital shaker at a rotational speed of 80 rpm for 10 days. Each treatment required six flasks, with six seeds per flask.

RNA Extraction and qRT-PCR Analysis of *PvTDIFL* Genes

Five different tissues of *P. virgatum*, namely, seed (mature seeds), rachis (bearing mature seeds), leaf (fully expanded leaf), stem (middle internode of seedling), and root were sampled in triplicates and immediately frozen in liquid nitrogen. Total RNA was extracted using the 2 × CTAB method (Li et al., 2008). The pellet was dissolved in 30 μl of RNase free ddH_2O. The concentration and quality of RNA were measured with a NanoDrop® 2000 spectrophotometer (Thermo Scientific, Wilmington, Delaware, USA). The RNA samples with A_{260}/A_{280} ratios that ranged from 1.8 to 2.1 and A_{260}/A_{230} ratios ≥2 were stored at −80°C for future use.

To quantify the relative expression levels of *PvTDIFL* genes in different samples, 1 μg of total RNA was used as a template to synthesize cDNA using the PrimeScript™ RT reagent Kit with gDNA Eraser (Perfect Real Time) (TaKaRa, Dalian, China). The qRT-PCR reactions were then prepared using 2 × HSYBR qPCR Mix without ROX (ZOMANBIO, Beijing, China). A standard 2-step amplification protocol was run in a LightCycler® 96 Real-Time PCR System (Roche, USA). The comparative C_T method (ΔΔCt method) was used for relative quantification of real-time PCR (Pfaffl, 2001). *PvUBQ6* (Pavir.5NG345900) was used as the reference gene (Gimeno et al., 2014). All gene specific primers (**Supplementary Table 2**) were designed using the Primer Premier 5.0 software (www.PremierBiosoft.com). All real-time PCR reactions were run in three biological replicates and two technical replicates.

Plasmid Construction and Generation of Transgenic Plants

The coding sequences (CDS) from *PvTDIFL3*^{MR3} and *PvTDIFL3*^{MR2} were amplified using PCR with gene specific primers (**Supplementary Table 2**). The CDS of *PvTDIFL1* was artificially synthesized (Sunny Technology, Shanghai, China). The products were cloned into a Gateway™ entry vector *pDONR201* using the BP recombination reaction (Invitrogen). The clones were analyzed using DNA sequencing. The correct fragments were subsequently recombined into the destination vector, *pK2GW7* (Karimi et al., 2002). Transformation of *A. thaliana* was performed using the *Agrobacterium tumefaciens*-mediated floral dip method (Clough and Bent, 1998).

Morphological and Histological Analysis of *Arabidopsis* Seedlings

Arabidopsis seedlings were photographed with a Canon EOS 7D digital camera to obtain high-resolution images. Root length was measured by using the ImageJ software (http://imagej.nih.gov/ij). The images presented in the figures were representative images from images of 24 individual seedlings for each line for the plate-grown plants and 10 individual seedlings for each line for the soil-grown plants, respectively.

Histological analysis of the vasculature was performed by using semi-thin sections. The upper part of the hypocotyl, 2–3 mm in length, was cut with a scalpel. A small amount of tissue from the stem and petiole of the rosette was kept to mark the upper end of the hypocotyl segment. The hypocotyl segments were fixed in formalin-acetic acid-alcohol (FAA) fixative (50% ethanol, 10% glacial acetic acid, 5% formaldehyde, v/v/v) at 4°C for 24 h. Dehydration was carried out by immersing the specimen in an ascending series of ethanol. Lastly, the specimens were infiltrated and embedded with Technovit® 7100 resin (www.kulzer-technik.com). The hypocotyl specimens were transversely sectioned at a thickness of 2.5 μm using a RM2265 Microtome (Leica BIOSYSTEMS, Nussloch, Germany) beginning from the upper end. The rosette tissues were first trimmed and monitored by sectioning and microscopy. The 10th to 20th sections of the hypocotyls were stained with 0.05% (w/v) aqueous toluidine blue and visualized with a BX53 light microscope (OLYMPUS, Tokyo, Japan). The cells in the stele were marked by using the ImageJ software and the number of cells was counted manually.

Statistical analysis was performed with six biological replicates and a *t*-test was used with double sample variance assumption. The letters a, b, and c and asterisks indicate statistically significant differences relative to the control.

Accession Numbers

Sequence data from this article are from the *P. virgatum* v1.1 genome in the Phytozome v12.1 database and TAIR10 associated with the following accession numbers: *AtEF1-α* (At5G60390), *PvUBQ6* (Pavir.5NG345900), *AtCLE41* (AT3G24770), *AtCLE42* (AT2G34925), *AtCLE44* (AT4G13195), *AtCLE46* (AT5G59305), *PvTDIFL1* (Pavir.Ab03264), *PvTDIFL2* (Pavir.Aa00134), and *PvTDIFL4* (Pavir.J06189). The sequence data for PvTDIFL3^{MR3} and PvTDIFL3^{MR2} has been submitted to GenBank and are associated with accession numbers MZ463198 and MZ463199, respectively.

RESULTS

Identification of *CLE* Genes in *P. virgatum*

To identify *CLE* genes in *P. virgatum* (*PvCLE*), sequences similar to the *Arabidopsis* CLE motifs were identified in the *P. virgatum* v1.1 genome (https://phytozome.jgi.doe.gov/pz/portal.html). The *PvCLE* genes were predicted and clustered using the recently reported method (Zhang et al., 2020). In total, 93 *PvCLE* genes were identified, including 91 annotated *PvCLE*s in the *P. virgatum* v1.1 genome and two novel *PvCLE*s identified in this study (**Figure 1**, **Supplementary Table 3**). Since there were three *PvCLE*s that encoded multiple CLE motifs, all *PvCLE*s encoded a total of 97 CLE motifs. The total number of *PvCLE*s was nearly three times of the number of *AtCLE*s. Based on the clustering, *PvCLE*s were divided into six groups (**Figure 1A**, **Supplementary Figure 2**). The Weblogo of CLE motifs showed that Group 1, including eight *AtCLE*s (*AtCLE1-7*, and *AtCLV3*) and 21 *PvCLE*s, had two conserved amino acids, namely, Asp (D) at the 8th residue and His (H) at 12th residue. These two residues were replaced with Asn (N) in Group 3, which contained 13 *AtCLE*s (*AtCLE8-14*, *AtCLE16-17*, and *AtCLE19-22*) and 38 *PvCLE*s. Residue number 12 was Asn (N) in Group 2, which contained five *AtCLE*s (*AtCLE18*, *AtCLE25-27*, and *AtCLE45*) and 20 *PvCLE*s (**Supplementary Figure 2**). The Pavir.Fa00904.1 from Group 2 encoded two repeats of RRVRRGSDPIHN, therefore the Group 2 *PvCLE*s encoded a total of 21 CLE motifs. Group 4 was comprised of nine *TDIF*/*TDIFL* genes, with four members from *Arabidopsis* (*AtCLE41*, *42*, *44*, and *46*) and five genes from *P. virgatum*. In Group 4, there were two *PvCLE*s encoding multiple TDIFL motifs (see the next paragraph for details), and the total number of TDIFL motifs encoded in *P. virgatum* was as many as eight. Group 5 had two *Arabidopsis* members (*AtCLE40* and *AtCLE43*) and three *PvCLE*s. In general, the motif conservation in Group 5 was lower relative to groups 1 through 4. Six *PvCLE* genes were found upon encoding CLE motifs that are very different from the AtCLE motifs and thus, fell into "Group others" (**Figure 1A**, **Supplementary Table 3**). The CLE motifs are rather conserved between the AtCLEs and PvCLEs (**Figures 1B,C**).

In total, five *TDIF* homologous genes were identified in the *P. virgatum* genome (**Figure 2**, **Supplementary Figure 1**, **Table 1**). The three *TDIF* homologs that were annotated are Pavir.Ab03264, Pavir.Aa00134, and Pavir.J06189, namely *PvTDIF-like1* (*PvTDIFL1*), *PvTDIFL2,* and *PvTDIFL4* in this study, respectively. A novel *TDIFL* gene, *PvTDIFL3*, was identified from TBLASTN searches of the *P. virgatum* v1.1 genome with a threshold e-value of 500. The predicted PvTDIFL3 protein product contained three potential TDIFL motifs and hence named PvTDIFL3^{MR3}. The MR3 is referring to that it has three motif repeats (**Figure 2**, **Table 1**). When gene-specific primers were used to amplify the CDS of *PvTDIFL*s, a shorter fragment derived from *PvTDIFL3*^{MR3} was also cloned that was

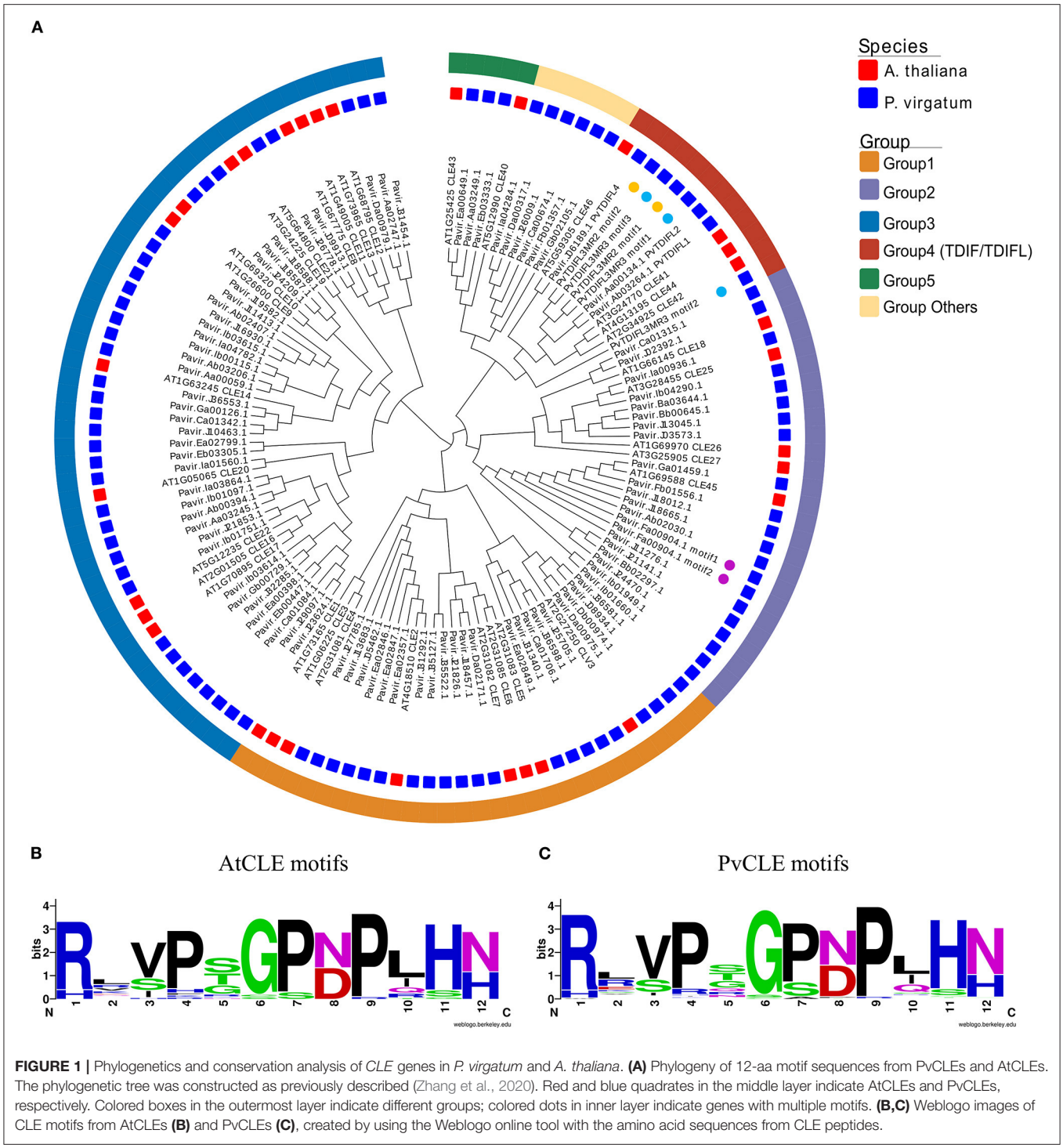

FIGURE 1 | Phylogenetics and conservation analysis of *CLE* genes in *P. virgatum* and *A. thaliana*. **(A)** Phylogeny of 12-aa motif sequences from PvCLEs and AtCLEs. The phylogenetic tree was constructed as previously described (Zhang et al., 2020). Red and blue quadrates in the middle layer indicate AtCLEs and PvCLEs, respectively. Colored boxes in the outermost layer indicate different groups; colored dots in inner layer indicate genes with multiple motifs. **(B,C)** Weblogo images of CLE motifs from AtCLEs **(B)** and PvCLEs **(C)**, created by using the Weblogo online tool with the amino acid sequences from CLE peptides.

named *PvTDIFL3*^{MR2} (**Figures 2A–C**). The amino acid sequence of PvTDIFL3^{MR2} is identical to that of PvTDIFL3^{MR3}, except that 47 amino acid residues are missing from the middle. The missing 47 amino acid residues constitute the second TDIFL motif and its flanking sequences of PvTDIFL3^{MR3} (**Figure 2C**). The *PvTDIFL3*^{MR2} matched to the same chromosomal location as *PvTDIFL3*^{MR3} in TBLASTN search of the *P. virgatum* v1.1 genome. In a phylogenetic analysis, amino acid sequences from the five *PvTDIFL* genes clustered in the same clade as the amino acid sequences from *Arabidopsis TDIF/TDIFL* genes (**Figures 1**, **2A**). The nucleotide sequences were subjected to the online gene prediction program FGENESH on the Softberry website (http://linux1.softberry.com/), to evaluate the genomic sequence and gene structure of these five genes.

All the TDIF/TDIFL proteins from *Arabidopsis* and switchgrass contained a signal peptide for the secretory pathway

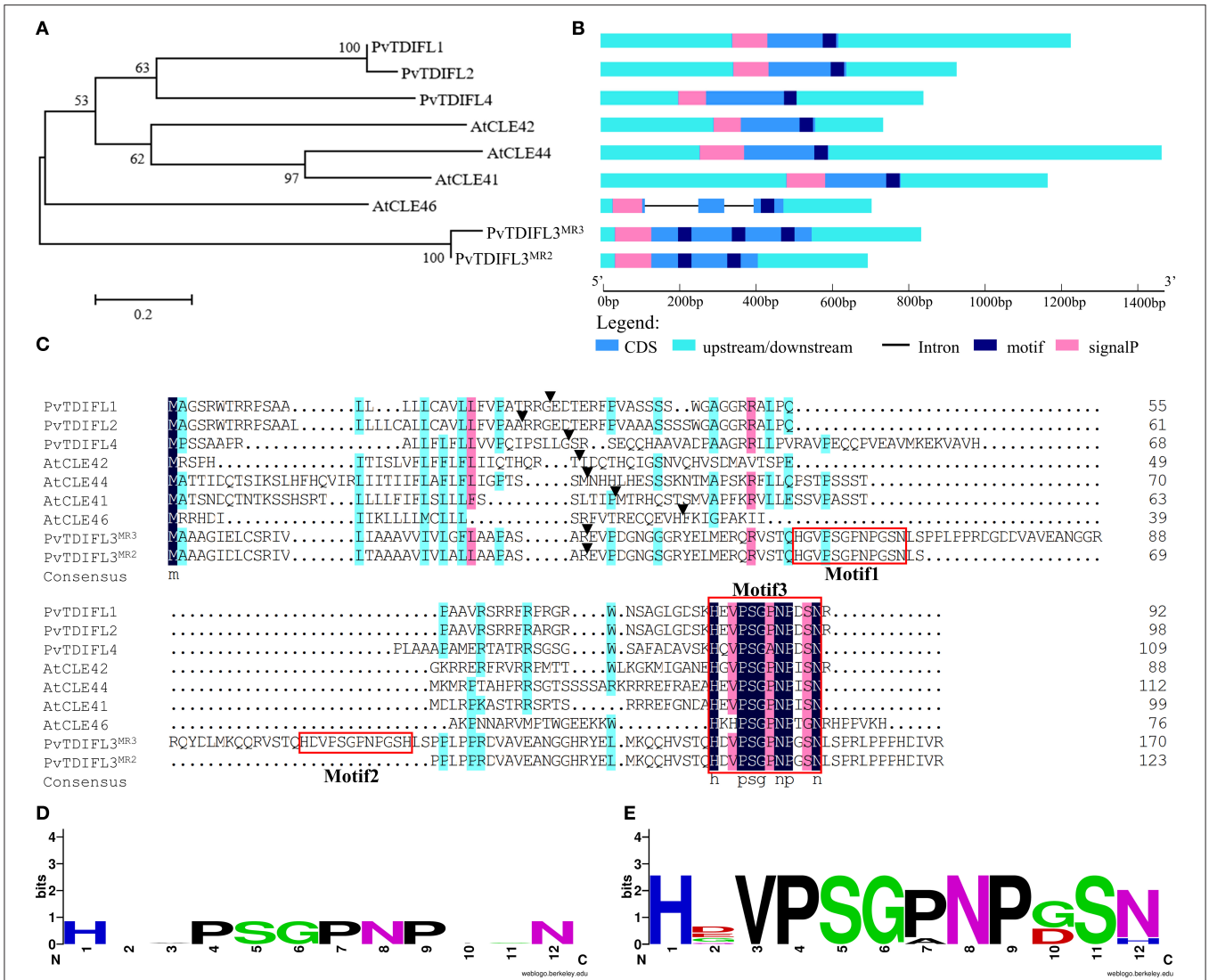

FIGURE 2 | Phylogenetic analysis and genomic organization of tracheary element differentiation inhibitory factor (TDIF) in *P. virgatum* and *A. thaliana*. **(A)** Phylogeny of full-length protein sequences from PvTDIFLs and AtTDIF. The alignment was generated by using Muscle with the Maximum Likelihood method and 1,000 bootstrap iterations. Numbers on the nodes indicate clade credibility values. **(B)** Gene structures of *PvTDIFLs* and *AtTDIF* from nucleotide sequences. Gene structure analysis was performed using the gene structure display server 2.0. Cyan box, 3′ UTR and 5′ UTR; blue box, CDS; pink box, signal peptide; navy-blue box, TDIF peptide; black line, intron. **(C)** Multiple amino acid sequence alignment of PvTDIFL and AtTDIF proteins. Multiple alignments were performed using the DNAMAN v6.0 software. TDIF peptides are boxed in red. Black triangles indicate the SignalP cleavage site. **(D,E)** Weblogo images of AtTDIF **(D)** and PvTDIFL **(E)**. The images were created by using the Weblogo online tool with the amino acid sequences from AtTDIF and PvTDIFL peptides, respectively.

at the N-terminus (**Figures 2B,C**). Similar to the *Arabidopsis* TDIF proteins, PvTDIFL1, 2, and 4 had a single TDIFL motif at the C-terminus. However, PvTDIFL3^{MR3} and PvTDIFL3^{MR2} had three and two TDIFL motifs, respectively (**Figures 2B,C**). The PvTDIFL proteins ranged from 92 to 175 amino acid residues in length. Their theoretical molecular weights (MW) and isoelectric points (*p*I) ranged from 10.01 to 18.50 kDa and from 5.81 to 11.94, respectively (**Table 1**).

A multiple sequence alignment analysis revealed that PvTDIFL1 and 2 proteins shared the same motif, HEVPSGPNPDSN, which is different from the *Arabidopsis* TDIF motif at the 10th residue in that an Ile (I) residue is changed to an Asp (D) residue. Motif 1 and motif 3 of PvTDIFL3^{MR3}/PvTDIFL3^{MR2} were different at the 2nd and 10th residues relative to the TDIF motif. The 12th residue of Motif 2 from PvTDIFL3^{MR3} had an Asn (N) to His (H) substitution. The 2nd, 7th, and 10th residues of the motif from PvTDIFL4 were different from the TDIF motif (**Figure 2C**). The conserved TDIF/TDIFL dodecapeptides in *Arabidopsis* and switchgrass were compared by using a WebLogo analysis. Similar to the *Arabidopsis* TDIF, the 4th and 7th residues of the TDIFL motifs in PvTDIFL proteins were conserved Pro (P) residues.

TABLE 1 | Information of PvTDIFL peptides used in this study.

Protein symbol	Gene ID	Protein length (AA)	SignalP cleavage site	Position of motif (AA)	PvTDIFL motif
PvTDIFL1	Pavir.Ab03264	92	31	80-91	HEVPSGPNPDSN
PvTDIFL2	Pavir.Aa00134	98	31	86-97	HEVPSGPNPDSN
PvTDIFL3^{MR3}	NA	171	32	56-67	HGVPSGPNPGSN
				103-114	HDVPSGPNPGSH
				146-157	HDVPSGPNPGSN
PvTDIFL3^{MR2}	NA	124	32	56-67	HGVPSGPNPGSN
				99-110	HDVPSGPNPGSN
PvTDIFL4	Pavir.J06189	109	26	98-109	HQVPSGANPDSN

NA, indicates no annotation.

However, their 2nd, 10th and 12th residues were less conserved (**Figures 2D,E**).

Tissue-Specific Expression Analysis of *PvTDIFL* Genes in *P. virgatum*

In *Arabidopsis*, *CLE41* is expressed in the phloem and the neighboring pericycle cells in the root and hypocotyl. *CLE44* is expressed in the phloem, pericycle and endodermal cells (Hirakawa et al., 2008). To analyze the expression pattern of *PvTDIFL* genes in the different tissues of switchgrass, *in silico* expression analysis and qRT-PCR were both performed.

The *in silico* expression data for *PvTDIFL1*, *2*, and *4* were downloaded from Phytozome. *PvTDIFL1* and *2* were both expressed at the highest levels in the inflorescence panicle, rachis and shoot. The *PvTDIFL3^{MR3}* and *PvTDIFL3^{MR2}* were not annotated in Phytozome and thus, no *in silico* expression data was available. The expression of *PvTDIFL4* was barely detectable in the tissues studied (**Figure 3A**).

For qRT-PCR, five switchgrass tissue samples were collected in triplicates. These tissues included seed, rachis, leaf, stem, and root. The *PveEF-1α*, *PvACT12*, and *PvUBQ6* were evaluated as internal reference genes (Gimeno et al., 2014). The *PvUBQ6* was selected because of its uniform expression levels in different tissues. The qRT-PCR results showed that the expression levels of *PvTDIFL1* were in the rachis, which is consistent with the *in silico* data (**Figure 3B**). The expression of *PvTDIFL3^{MR3}* was relatively high in the rachis and leaf. In contrast, the expression of *PvTDIFL3^{MR2}* was more specific to the rachis (**Figures 3C,D**). However, the expression of *PvTDIFL2* and *PvTDIFL4* was undetectable, probably due to low levels of expression. The relatively high levels of expression in the rachis provides evidence for *PvTDIFL* genes contributing to vascular development, similar to the *Arabidopsis TDIF* genes.

In vitro PvTDIFL Peptide Treatment Increased Hypocotyl Stele Cell Numbers in *Arabidopsis*

Exogenous TDIF peptide promotes procambial cell divisions, which leads to a remarkable increase in the vascular development of the hypocotyl in *Arabidopsis* (Hirakawa et al., 2010a). To study the activity and functional conservation of PvTDIFL peptides, four types of PvTDIFL peptides corresponding to the TDIFL motifs from PvTDIFL1, PvTDIFL3^{MR3} and PvTDIFL3^{MR2} were chemically synthesized and exogenously applied to *Arabidopsis* seedlings, at a concentration of 10 μM. The *Arabidopsis* TDIF peptide was used as the positive control (Whitford et al., 2008).

Arabidopsis seedlings were grown in liquid MS media either with or without TDIF/TDIFL peptides for 10 d. To test whether these peptide treatments affected the vasculature of the hypocotyl, semi-thin transverse sections were prepared. The results showed that the application of *Arabidopsis* TDIF peptides induced increases in the size of the stele with significant increases in cell numbers, as previously reported (**Figures 4A,B,G**) (Whitford et al., 2008). Similarly, the number of cells in the stele increased significantly in the seedlings treated with PvTDIFL_1p, 2p, and 3p, but not as much as in the TDIF-treated seedlings (**Figures 4A–E,G**). In contrast, the PvTDIFL_4p treatment caused an unexpected decrease in the number of cells in the stele, due to the His (H) substitution for Asn (N) at the 12th residue of PvTDIFL_4p (**Figures 4A,F,G**). These data indicate that the activities of the three peptides (PvTDIFL_2p, 3p, and 4p) encoded by *PvTDIFL3* diverged.

Influence of Heterologous Expression of *PvTDIFL* Genes on Plant Morphology and Vascular Development in *Arabidopsis*

As described above, *PvTDIFL1*, *3^{MR3}* and *3^{MR2}* differ in their motif numbers, motif sequences and peptide activities. To further investigate their functions in plant development, the 35S promoter was used to drive the expression of *PvTDIFL1*, *3^{MR3}* and *3^{MR2}* in *Arabidopsis*. The relative expression levels of the *PvTDIFL* transgenes in *Arabidopsis* were analyzed by RT-PCR (**Figure 5A**). The transgene expression levels and morphologies of two representative lines for each transgene were compared to Col-0. Four-week-old soil-grown plants were photographed (**Figures 5B–H**). In comparison with the wild-type plants (**Figure 5B**). Both lines harboring the *35S:PvTDIFL1* transgene developed smaller rosettes with small, round, and bushy leaves relative to Col-0 (**Figures 5B–D**). Similar results were obtained when *AtCLE42* and *44* were overexpressed in *Arabidopsis* (Strabala et al., 2006). In contrast, the morphological changes of *35S:PvTDIFL3^{MR3}* and *35S:PvTDIFL3^{MR2}* plants were less severe and less consistent (**Figures 5E–H**).

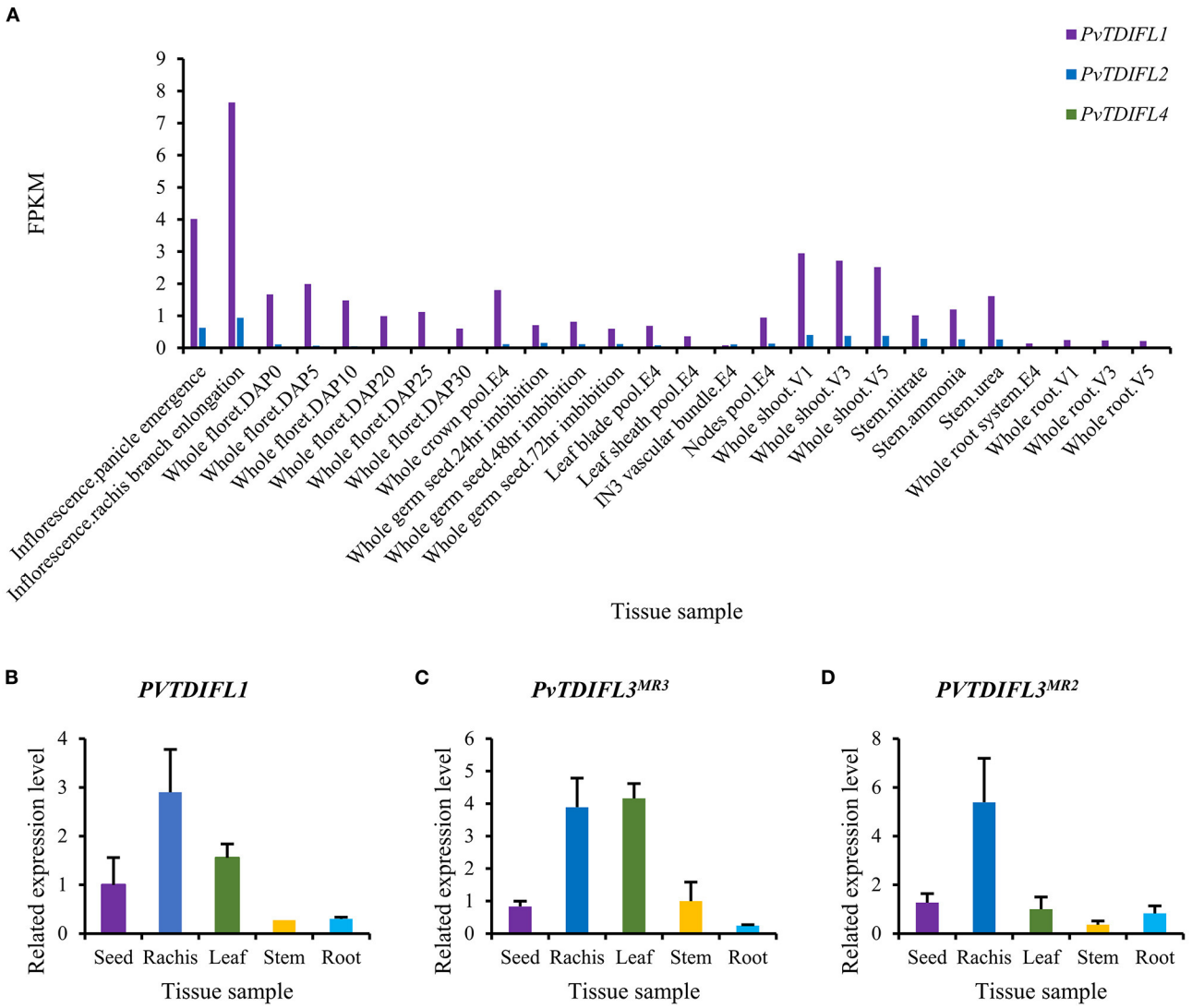

FIGURE 3 | Expression analysis of *PvTDIFL* genes in *P. virgatum*. **(A)** Expression of *PvTDIFL1*, *2* and *4* in different samples of *P. virgatum*. Fragments Per Kilobase per Million (FPKM) values of *PvTDIFL1*, *2*, and *4* were obtained from *in silico* expression data in Phytozome. Samples listed are as follows: Inflorescence.Panicle emergence, Inflorescence.rachis branch elongation, Whole floret.DAP0, 5, 10, 20, 25, 30, Whole crown pool.E4, Whole germ seed 24 h imbibition, 48 h imbibition, 72 h imbibition, Leaf blade pool.E4, Leaf sheath pool.E4, IN3 vascular bundle.E4, Nodes pool.E4, Whole shoot.V1, 3, 5, Stem.nitrate, Stem.ammonia, Stem.urea, Whole root system.E4, Whole root.V1, 3, 5. **(B–D)** Relative expression levels of *PvTDIFL1* **(B)**, *PvTDIFL3*^{MR3} **(C)**, and *PvTDIFL3*^{MR2} **(D)** quantified using qRT-PCR. Seed (mature), rachis (bearing mature seeds), leaf (fully expanded leaf), stem (middle internode), and root of switchgrass grown on campus were collected in triplicate in July. *PvUBQ6* was used as the reference gene. The comparative C_T method (ΔΔCt method) was used for relative quantification of real-time PCR.

To further quantify the phenotypic changes of the *35S:PvTDIFL* plants, the above-mentioned lines were grown on vertical plates for 2 weeks to observe the morphological changes in roots. A significant decrease in the length of the primary root was observed in all heterologous expression lines, except for line *35S:PvTDIFL3*^{MR2}*-1* (**Figures 6A–G,O**). Similar short-root phenotypes were observed in rice and pine after treatments with synthetic TDIF peptides (Kinoshita et al., 2007; Strabala et al., 2014). The heights of the inflorescence of *35S:PvTDIFL* plants were measured after 6 weeks of growth in soil, 2 weeks after the initiation of flowering. Extreme dwarfism was observed in the lines harboring the *35S:PvTDIFL1* transgene. The heights of their inflorescences were 40% of the wild-type plants ($p \leq 0.001$, $n = 10$). The height of the inflorescence was also decreased in the lines harboring the *35S:PvTDIFL3*^{MR3} transgene. The heights of the inflorescence from the line *35S:PvTDIFL3*^{MR3}*-1* and *-2* were 54% ($p \leq 0.001$, $n = 10$) and 34% ($p \leq 0.001$, $n = 10$) of the wild type plants, respectively. In contrast, no significant decrease in the height of the inflorescence was observed in the lines harboring the *35S:PvTDIFL3*^{MR2} transgene (**Figures 6H–N,P**).

To investigate the functions of *PvTDIFL* genes in vascular development, the hypocotyls of 6-week-old *Arabidopsis* were

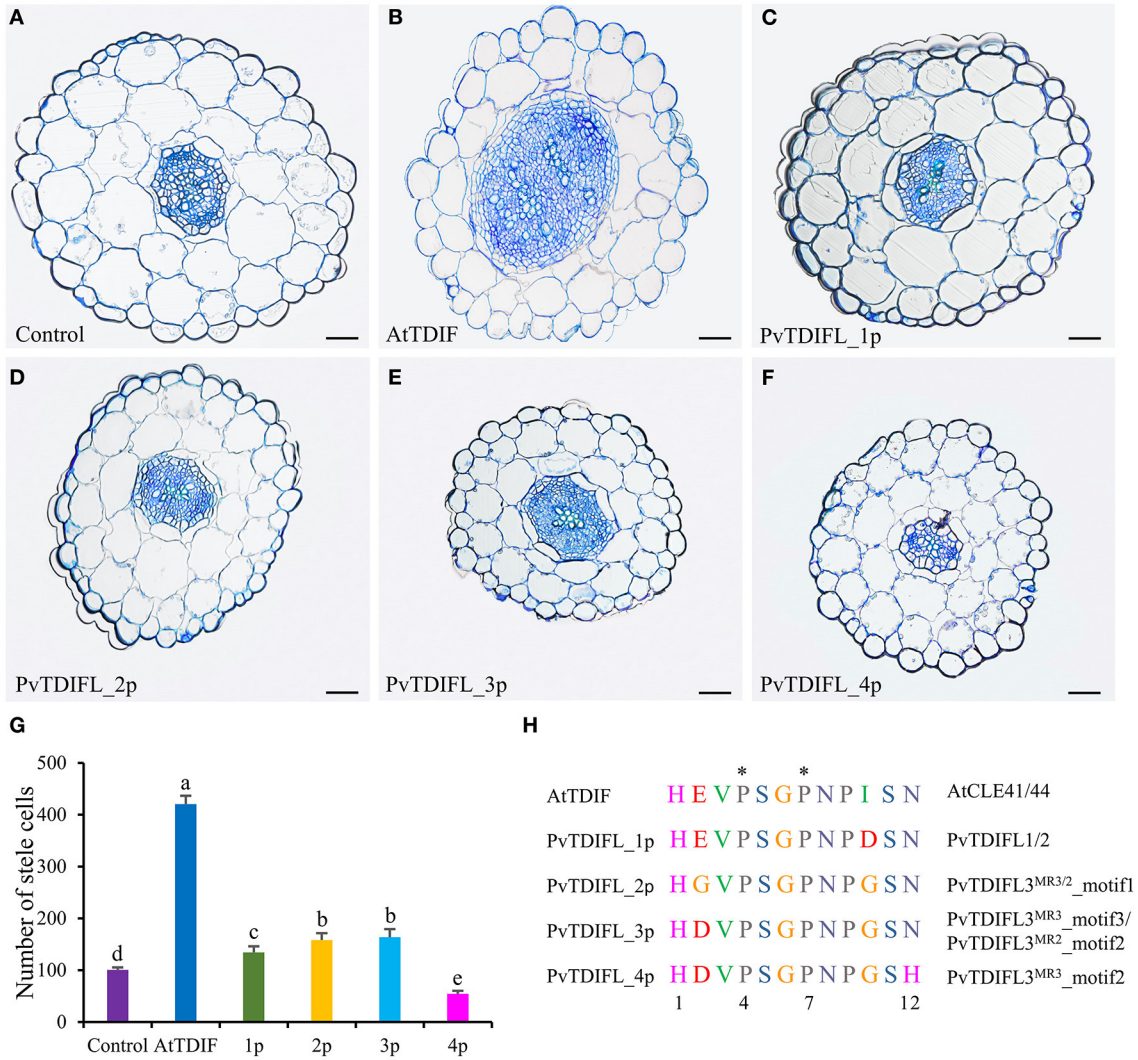

FIGURE 4 | Effects of AtTDIF and PvTDIFL peptides on stele development of 10-day-old *Arabidopsis* hypocotyls grown in liquid media. **(A)** Transverse section of hypocotyl from *Arabidopsis* plants without peptide-treatment. **(B–F)** Transverse sections of hypocotyls from *Arabidopsis* plants treated with the AtTDIF **(B)**, PvTDIFL_1p **(C)**, PvTDIFL_2p **(D)**, PvTDIFL_3p **(E)**, and PvTDIFL_4p **(F)** synthetic peptides. Sections were 2.5 μm thick and stained with 0.05% (w/v) aqueous toluidine blue. Bar = 50 μm. **(G)** Numbers of stele cells in the hypocotyls of non-treated and synthetic peptide-treated plants. Biological replicates were sections from 6 different hypocotyls. Different letters indicate statistically significant differences ($p < 0.05$), $n = 6$. **(H)** Sequences and modifications of AtTDIF and PvTDIFL peptides. Peptide names are indicated at the left. Proteins containing the indicated peptides are indicated at the right. The asterisk indicates hydroxyproline.

sectioned and analyzed using light microscopy. In comparison with Col-0 (**Figures 7A,E**), heterologous expression of *PvTDIFL1* induced a drastic increase in the number of cells in the stele, suppressed the differentiation of xylem and disrupted the organization of the vascular tissue (**Figures 7B,F**). Heterologous expression of $PvTDIFL3^{MR3}$ induced a reduction in the size of xylem and an increase in the size of phloem without disrupting the organization of the vascular tissue and did not influence the diameter of the hypocotyl (**Figures 7C,G**). Heterologous expression of $PvTDIFL3^{MR2}$ led to a similar albeit somewhat attenuated phenotype relative to the heterologous expression of *PvTDIFL1*. For instance, the size of treachery elements was not reduced in the plants expressing $PvTDIFL3^{MR2}$ (**Figures 7D,H**). The above results are consistent with the previous reports on the *TDIF* genes in *Arabidopsis* and *Populus* (Hirakawa et al., 2008; Whitford et al., 2008; Etchells and Turner, 2010; Etchells et al., 2015; Li et al., 2018). Although PvTDIFL1 contains only one single TDIFL motif, it had the greatest influence on vascular development. On the contrary, multiple TDIFL motifs did not increase the activity of either $PvTDIFL3^{MR3}$ or $PvTDIFL3^{MR2}$ relative to PvTDIFL1.

DISCUSSION

Identification of *TDIF*/*TDIFL* Genes in *P. virgatum*

In this study, 93 putative *CLE* genes were identified in the genome of *P. virgatum*, by using a novel method that was

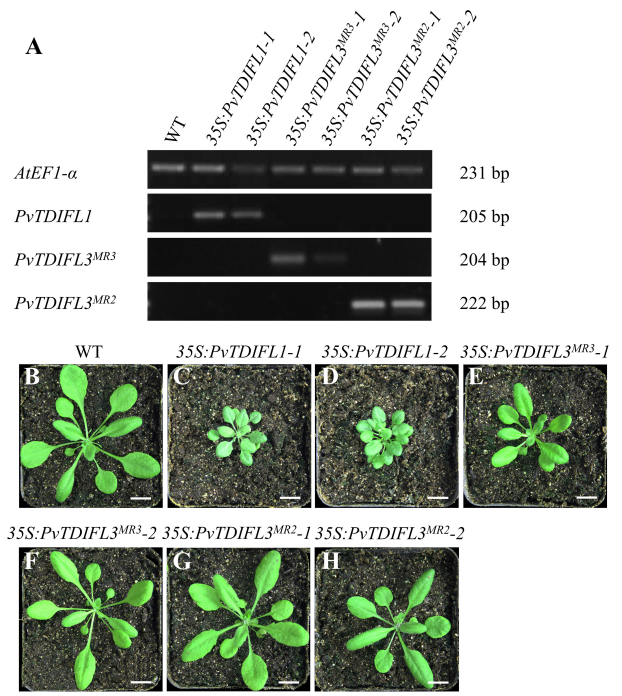

FIGURE 5 | Reverse Transcription PCR (RT-PCR) analysis and morphology of 4-week-old *Arabidopsis* seedlings expressing *PvTDIFL*s. **(A)** RT-PCR analysis of *35S:PvTDIFL* lines used in this study. *AtEF1-α* was used as the reference gene. **(B)** 4-week-old wild type plant. **(C–H)** 4-week-old transgenic plants harboring *35S:PvTDIFL1-1* **(C)**, *35S:PvTDIFL1-2* **(D)**, *35S:PvTDIFL3^{MR3}-1* **(E)**, *35S:PvTDIFL3^{MR3}-2* **(F)**, *35S:PvTDIFL3^{MR2}-1* **(G)**, and *35S:PvTDIFL3^{MR2}-2* **(H)** transgenes grown in soil. Bar = 1 cm in **(B–H)**.

recently developed (Zhang et al., 2020) followed by gene cloning. In *Arabidopsis*, all of the 32 *CLE* genes encode proteins with a single CLE motif, except for CLE18, which contains a second CLEL motif (Meng et al., 2012). Surprisingly, five CLE proteins containing multiple CLE motifs were identified in *O. sativa*, *T. aestivum,* and *Medicago truncatula* (Oelkers et al., 2008). A total of 59 CLE proteins in 27 plant species contain multiple CLE motifs (Goad et al., 2017). Genes encoding proteins containing multiple CLE motifs have been recently identified in various plants, despite that the CLE motifs from the same protein might or might not be identical to each other (Goad et al., 2017). Most functional studies on *CLE* genes have been conducted with genes encoding a single CLE motif. The knowledge of the *CLE* genes encoding multiple motifs remains limited. In this study of *CLE* genes in *P. virgatum*, it was found that three *PvCLE* genes—*Pavir.Fa00904.1*, *PvTDIFL3^{MR3}*, and *PvTDIFL3^{MR2}* encode proteins containing multiple CLE motifs, which allowed the functions of the CLE motif-containing proteins encoded by these genes to be studied.

Among the three *PvCLEs* that encode multiple CLE motifs, *PvTDIFL3^{MR3}* and *3^{MR2}* appear to encode CLE peptides that are homologous to the TDIF peptide. The function of the TDIF peptide in vascular development has been well-studied in several species, such as *Arabidopsis*, *Populus*, *Marchantia polymorpha* (Ito et al., 2006; Hirakawa et al., 2008, 2010a,b; Etchells and Turner, 2010; Etchells et al., 2015; Kondo and Fukuda, 2015). However, these previously studied *TDIF*/*TIDFL* genes encode a single TDIF/TDIFL motif. Therefore, functional analysis of the TDIFL peptides from the PvTDIFL3^{MR3} and 3^{MR2} proteins could provide a better understanding of the regulatory activities of TDIF/TDIFL peptides.

In total, five PvTDIFL-encoding genes were identified in *P. virgatum*. The motif sequences of PvTDIFL1/2 and TDIF are very similar. Indeed, only the 10th amino acid residue of the motif is different between PvTDIFL1/2 and TDIF. The TDIFL peptide from PvTDIFL1/2 represents the largest group of TDIF/TIDFL peptides in monocots (Zhang et al., 2020). The number of different residues in the TDIFL motifs of PvTDIFL3^{MR3}, 3^{MR2}, and 4 ranges from two to three (**Figures 2B,C**). The PvTDIFL3^{MR3} and 3^{MR2} contain three and two TDIFL motifs, respectively. Sequence alignments of PvTDIFL proteins show that PvTDIFL3^{MR3} had one more repeat of the TDIFL motif within its flanking sequence relative to PvTDIFL3^{MR2}. The *PvTDIFL3^{MR2}* was a "byproduct" of cloning *PvTDIFL3^{MR3}* by using gene specific primers for *PvTDIFL3^{MR3}*. Meanwhile, *PvTDIFL3^{MR3}* and *3^{MR2}* were matched to the same chromosomal locus, which provides evidence that these two genes could be alleles. An alternative explanation is that *PvTDIFL3^{MR2}* is simply missing from the v1.1 genome sequence of *P. virgatum*.

Activities of PvTDIFL Peptides in *Arabidopsis*

Alanine scanning mutagenesis indicated that the 2nd, 5th, 7th, 10th, and 11th residues of the TDIF motif do not contribute to its activity. However, the H^1, V^3, G^6, N^8, P^9, and N^{12} substitutions caused severe losses of TDIF activity (Ito et al., 2006). In order to investigate the activities of PvTDIFL peptides based on the predicted motifs, four PvTDIFL peptides were synthesized and applied to *Arabidopsis* seedlings. The peptide activities were evaluated based on their ability to influence cell numbers and cell arrangement in the vasculature of the hypocotyl.

The results showed that PvTDIFL_1p, 2p, and 3p had similar and significant activities in promoting cell division, disrupting vascular cell patterns and inhibiting xylem development, although their activities were weaker than the *Arabidopsis* TDIF peptide (**Figures 4A–E,G**). On the contrary, PvTDIFL_4p (corresponding to the 2nd motif of PvTDIFL3^{MR3}) had no TDIF activity. Instead, PvTDIFL_4p induced a 50% reduction in the number of cells in the hypocotyl, which is consistent with PvTDIFL_4p serving as an antagonist of peptides that possess TDIF activity (**Figures 4F,G**). The sequence alignment of the PvTDIFL peptides that included the TDIF peptide showed that PvTDIFL_1p, 2p, and 3p have different residues at the 2nd and/or 10th residues, which are not critical positions for TDIF activity (Ito et al., 2006). The PvTDIFL_4p has an extra substitution, with a His (H) instead of an Asn (N) at the 12th residue (**Figure 4H**), which is one of the critical positions (Ito et al., 2006). This H-to-N substitution is consistent with its inhibitory activity in the exogenous peptide treatment experiments.

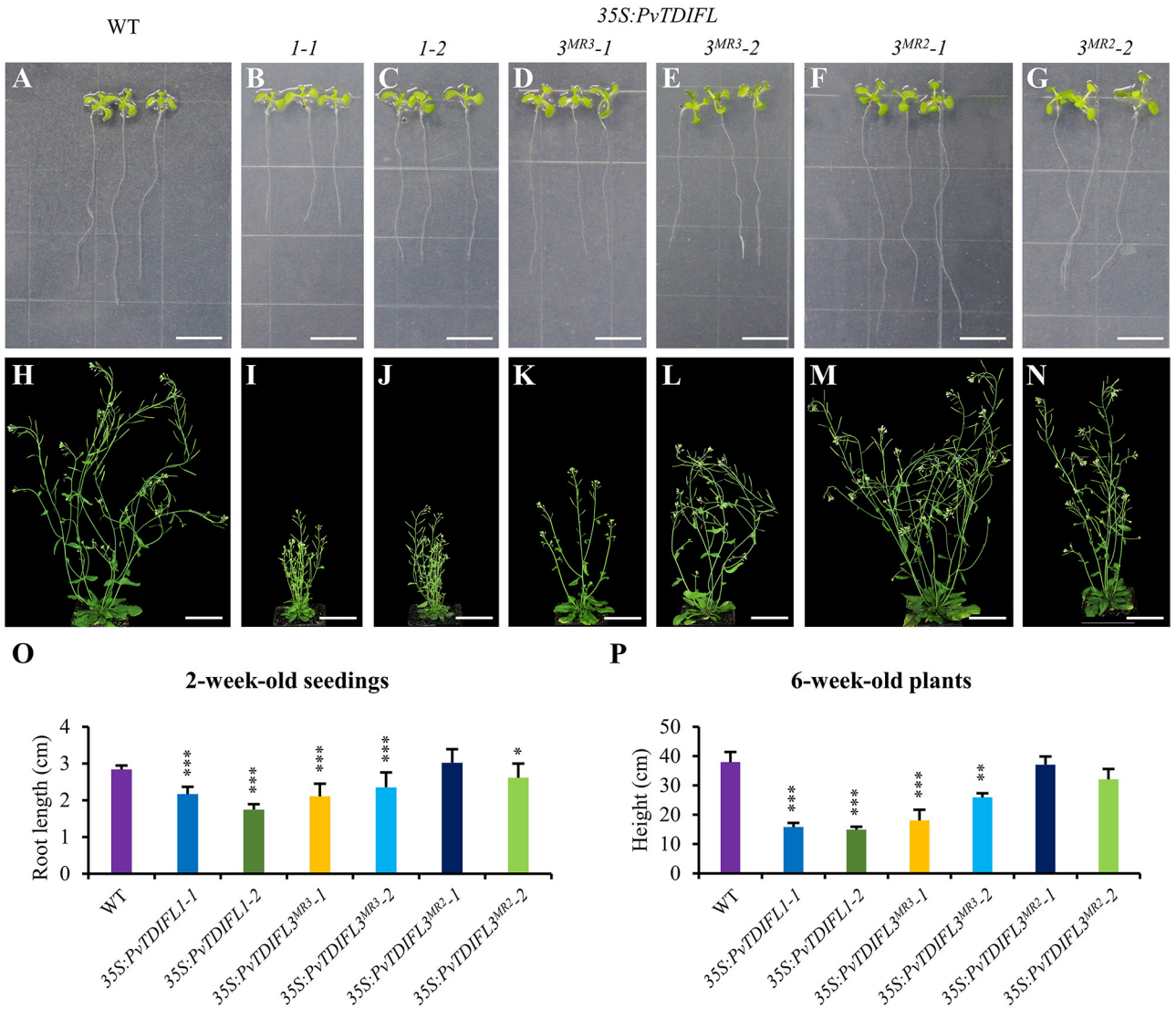

FIGURE 6 | Morphology of 2 and 6-week-old *Arabidopsis* expressing *PvTDIFL* transgenes. **(A–G)** Morphological observations of 2-week-old seedlings from WT **(A)**, and transgenic plants harboring *35S:PvTDIFL1-1* **(B)**, *35S:PvTDIFL1-2* **(C)**, *35S:PvTDIFL3^{MR3}-1* **(D)**, *35S:PvTDIFL3^{MR3}-2* **(E)**, *35S:PvTDIFL3^{MR2}-1* **(F)**, *35S:PvTDIFL3^{MR2}-2* **(G)** transgenes grown on vertical plates. **(H–N)** Morphological observation of 6-week-old seedlings from WT **(H)** and transgenic plants harboring *35S:PvTDIFL1-1* **(I)**, *35S:PvTDIFL1-2* **(J)**, *35S:PvTDIFL3^{MR3}-1* **(K)**, *35S:PvTDIFL3^{MR3}-2* **(L)**, *35S:PvTDIFL3^{MR2}-1* **(M)**, *35S:PvTDIFL3^{MR2}-2* **(N)** transgenes grown in soil. **(O)** Quantitation analysis of root length of 2-week-old seedlings. **(P)** Heights of 6-week-old plants. *, **, and *** indicates statistically significant differences from WT at $p < 0.05$, $p < 0.01$, and $p < 0.001$, respectively. Sample size $n = 24$ (biological replicates) for the vertical plates and $n = 10$ (biological replicates) for plants grown in soil. Bar = 1 and 5 cm in **(A–G)** and **(H–N)**, respectively.

Functional Analysis of *PvTDIFL* Genes in *Arabidopsis*

It has been hypothesized that a full CLE protein precursor carrying multiple motifs can release several active peptides after processing, which could play an amplification effect (Oelkers et al., 2008). To better understand the function of *PvTDIFL* genes, *PvTDIFL1* (one motif), *PvTDIFL3^{MR3}* (three motifs), and *PvTDIFL3^{MR2}* (two motifs) were expressed in *Arabidopsis*. Heterologous expression of *PvTDIFL1* mimicked the phenotypes of the *Arabidopsis* plants that overexpressed the endogenous *TDIF* genes, such as *CLE41* and *CLE44* (Strabala et al., 2006; Etchells and Turner, 2010). However, heterologous expression of *PvTDIFL3^{MR3}* and *3^{MR2}* produced more subtle phenotypes than the heterologous expression of *PvTDIFL1* (**Figures 5**–**7**). An amplification of TDIFL activity in *Arabidopsis* plants expressing *PvTDIFL3^{MR3}* or *3^{MR2}* was not observed although these genes encode peptides with multiple motifs. The lack of the amplification effect has several possible explanations. Firstly, *PvTDIFL3^{MR3}* and *3^{MR2}* were heterologously expressed in *Arabidopsis*. Because *Arabidopsis* does not have any CLE proteins with multiple CLE motifs, it might not be able to process PvTDIFL3^{MR3} or 3^{MR2} protein precursors efficiently. Secondly,

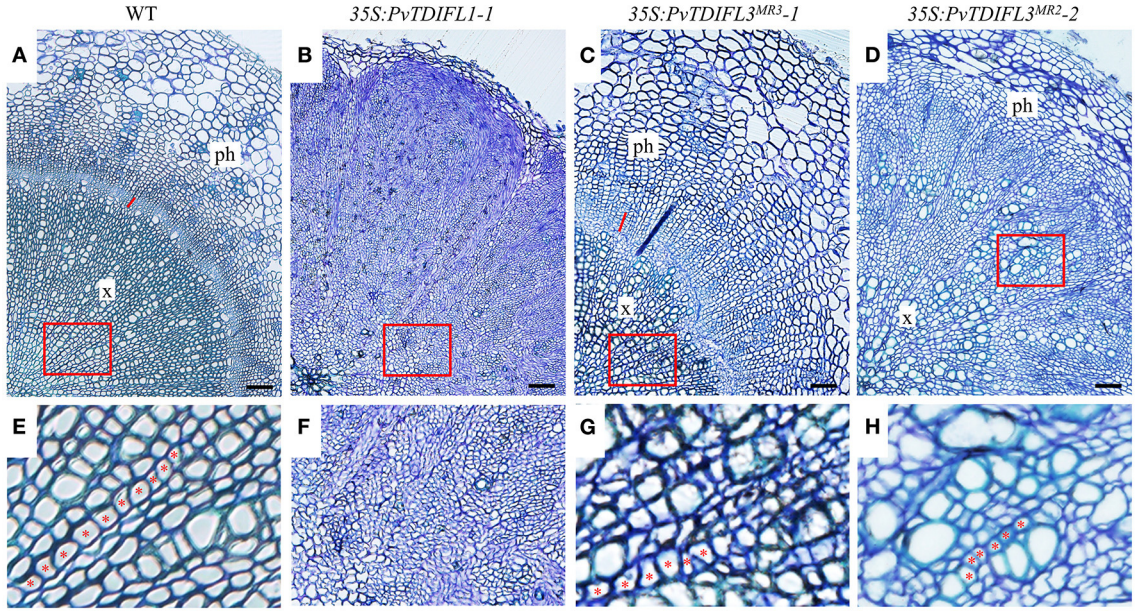

FIGURE 7 | Histology of 6-week-old *Arabidopsis* lines expressing *PvTDIFL* transgenes. **(A–D)** Histological observation of hypocotyls from WT **(A)** and transgenic seedlings harboring *35S:PvTDIFL1-1* **(B)**, *35S:PvTDIFL3^{MR3}-1* **(C)**, and *35S:PvTDIFL3^{MR2}-2* **(D)** transgenes. Transverse sections that were 2.5 μm thick were stained with 0.05% (w/v) aqueous toluidine blue. Bar = 50 μm. × and ph indicate xylem and phloem, respectively. The red line indicates cambium in **(A)** and **(C)**. **(E–H)** High magnification images from the areas in red boxes from **(A–D)**, respectively. Red asterisks show examples of organized files of cells.

the motif sequences of PvTDIFL peptides are not the same as the endogenous TDIF/TDIFL peptides of *Arabidopsis*. Therefore, the affinity of the PXY/TDR receptor in *Arabidopsis* for the PvTDIFL peptides is difficult to predict and requires more experimentation to understand. Thirdly, although the typical sequence of the TDIF peptide is HEVPSGPNPISN (Ito et al., 2006), the conserved sequences flanking the TDIFL motifs from PvTDIFL3^{MR3} and 3^{MR2} provide evidence that possible variants of the mature motifs are encoded by these two genes. Finally, the experiments in this study have multiple variables, therefore it is hard to know whether all the TDIFL motifs from PvTDIFL3^{MR3} and 3^{MR2} have been successfully processed. The proteomics analysis of small proteins based on liquid chromatography with tandem mass spectrometry (LC-MS/MS) technique (Wang et al., 2020) can be applied to the analysis of transgenic lines harboring the transgenes that encode multiple PvTDIFL motifs with various alanine substitutions. This may help to analyze the processing of multiple PvTDIFL motifs.

The PvTDIFL3^{MR3} contains a 47-amino acids insertion between the amino acid residues 77 and 123. This insertion introduces an extra TDIFL motif in PvTDIFL3^{MR3} relative to PvTDIFL3^{MR2} (**Figure 2C**). The extra TDIFL motif is corresponding to PvTDIFL_4p (**Figure 4H**). A moderate TDIF-overexpression phenotype was apparent in the hypocotyl sections of the 6-week-old *35S:PvTDIFL3^{MR2}* plants, which provides evidence that at least one of the PvTDIFL peptides (motif 1 and motif 3) was successfully processed. On the contrary, although vascular development in *35S:PvTDIFL3^{MR3}* plants was reduced, the vascular organization of the hypocotyl was well maintained. These data suggest a processing of motif 2 from PvTDIFL3^{MR3} and indicate that PvTDIFL_4P may serve as an antagonist of PvTDIFL_2P (PvTDIFL3^{MR3}_motif 1), PvTDIFL_3P (PvTDIFL3^{MR3}_motif 3), and the endogenous TDIF peptide. The inhibitory effect derived from motif 2 of PvTDIFL3^{MR3} in the *PvTDIFL3^{MR3}* heterologous expression experiments is consistent with the inhibition of stele development by PvTDIFL_4p that was observed during the exogenous peptide treatments in 10-day-old *Arabidopsis* seedlings (**Figures 4F,G**).

Previous reports showed that although TDIF has no inhibitory effect on root elongation in *Arabidopsis* (Ito et al., 2006; Whitford et al., 2008), TDIF mildly inhibits root elongation in rice and pine (Kinoshita et al., 2007; Strabala et al., 2014). In this study, heterologous expression of *PvTDIFLs* significantly shortened the roots of *Arabidopsis*, especially in the *35S:PvTDIFL1* lines (**Figures 6A–G**). These data are consistent with the diversification of *TDIF/TDIFL* gene function in different species. However, little is known about the mechanism responsible for these differences in peptide activity.

Tissue-Specific Expression of *TDIF* to Increase Biomass in Plant

As a PBC, *P. virgatum* is a commonly used material to study the synthesis of biomass. In this study, heterologous expression of *PvTDIFLs* in *Arabidopsis* caused dwarf seedlings and a disordered vasculature, indicating that constitutive heterologous expression of *PvTDIFLs* reduced biomass. It is consistent with the previous studies on overexpression of the endogenous *TDIF* genes in *Arabidopsis* (Hirakawa et al., 2008; Whitford et al., 2008; Etchells

and Turner, 2010). However, the phloem-specific expression of *PttCLE41* leads to increased woody biomass in *Populus* and thus, demonstrates that it is possible to increase the biomass by manipulating the TDIF–PXY/TDR signaling module in plants (Etchells et al., 2015). In hybrid poplar, the *PttWOX4* genes act downstream of PXY/TDR to control cell division activity in the vascular cambium and hence, to increase stem girth (Kucukoglu et al., 2017). Overexpression of the *WOX* gene *STF* (*STENOFOLIA*) improves biomass yields in grasses (Wang et al., 2017). In this study, five *TDIF/TDIFL* genes in *P. virgatum* were identified. Three of these genes in *Arabidopsis* were cloned and heterologous expressed. Overexpression technologies and exogenous peptide treatment experiments gave a better understanding of the functions and activities of various TDIFL peptides, including PvTDIFL peptides, and also provide clues that will drive future applied research on biomass improvement by manipulating the TDIF–PXY/TDR–WOX4 signaling pathway in plants.

CONCLUSION

In this study, 93 genes that are homologous to *CLE* were identified in *P. virgatum* and were divided into 6 groups based on a phylogenetic analysis. A total of five PvCLE members were assigned to the fourth group that consisted of the H-type CLEs. The five genes that were most similar to *Arabidopsis TDIF* were named *PvTDIFL1*, *PvTDIFL2*, *PvTDIFL3*^{MR3}, *PvTDIFL3*^{MR2}, and *PvTDIFL4*. PvTDIFL3^{MR3} and 3^{MR2} contain three and two TDIFL peptide motifs, respectively. Expression analysis showed that *PvTDIFL* genes were highly expressed in the rachis, which is rich in vascular tissue. Experiments with exogenous polypeptides demonstrated that, apart from PvTDIFL_4p, the ability to influence the development of the stele in the hypocotyl is conserved in both PvTDIFL and *Arabidopsis* TDIF peptides. The heterologous expression of *PvTDIFL1*, *3*^{MR3}, and *3*^{MR2} all affected the growth of *Arabidopsis* plants and the development of the vascular tissue in the hypocotyl to varying degrees. The *Arabidopsis* plants that stably expressed *PvTDIFL3*^{MR3} and *3*^{MR2} did not develop elevated levels of CLE peptide activity that might be expected from the multiple CLE motifs contained in the proteins encoded by these genes. At present, there are few studies on the processing and activity of plant CLEs containing multiple motifs. This study will shape future work that aims to increase biomass by modifying the TDIF signaling pathway.

DATA AVAILABILITY STATEMENT

The datasets presented in this study can be found in online repositories. The names of the repository/repositories and accession number(s) can be found in the article/**Supplementary Material**.

AUTHOR CONTRIBUTIONS

BZ and XS conceived and designed the experiments. XS, ZZ, and LL identified the *PvCLE* genes. LL, KD, JT, and DT performed the experiments and analyzed the corresponding results. DT drafted the manuscript. RL, BZ, and XS revised this manuscript. All authors contributed to the article and approved the submitted version.

FUNDING

This work was supported by the Fundamental Research Funds for the Central Universities (2662020YLPY026, 2662018PY071), and the National Natural Science Foundation of China (31770639, 31370673).

SUPPLEMENTARY MATERIAL

The Supplementary Material for this article can be found online at: https://www.frontiersin.org/articles/10.3389/fpls.2021.737219/full#supplementary-material

Supplementary Figure 1 | Nucleotide sequences of *PvTDIFL3*^{MR3} and *PvTDIFL3*^{MR2}. The nucleotide sequences were obtained by clones. Green, blue, and pink font represent 5′-UTR, CDS, and 3′-UTR, respectively. The sequences corresponding to the TDIFL motifs are underlined.

Supplementary Figure 2 | Weblogo images of CLE motifs from six groups in *Arabidopsis* and switchgrass. Weblogo images were created by using the Weblogo online tool with the amino acid sequences from the predicted CLE motifs.

Supplementary Table 1 | Amino acid sequences from TDIF/TDIFL used for chemical synthesis.

Supplementary Table 2 | Primers used in this study.

Supplementary Table 3 | Information of PvCLE proteins identified in this study.

REFERENCES

Bjellqvist, B., Hughes, G. J., Pasquali, C., Paquet, N., Ravier, F., Sanchez, J. C., et al. (1993). The focusing positions of polypeptides in immobilized pH gradients can be predicted from their amino-acid-sequences. *Electrophoresis* 14, 1023–1031. doi: 10.1002/elps.11501401163

Chen, Q., and Song, G. Q. (2019). Protocol for agrobacterium-mediated transformation and transgenic plant production of switchgrass. *Methods Mol. Biol.* 1864, 105–115. doi: 10.1007/978-1-4939-8778-8_8

Clifton-Brown, J., Harfouche, A., Casler, M. D., Jones, H. D., Macalpine, W. J., Murphy-Bokern, D., et al. (2019). Breeding progress and preparedness for mass-scale deployment of perennial lignocellulosic biomass crops switchgrass, miscanthus, willow and poplar. *GCB Bioenergy* 11, 118–151. doi: 10.1111/gcbb.12566

Clough, S. J., and Bent, A. F. (1998). Floral dip: a simplified method for *Agrobacterium*-mediated transformation of *Arabidopsis thaliana*. *Plant J.* 16, 735–743. doi: 10.1046/j.1365-313x.1998.00343.x

Cock, J. M., and McCormick, S. (2001). A large family of genes that share homology with *CLAVATA3*. *Plant Physiol.* 126, 939–942. doi: 10.1104/pp.126.3.939

Crooks, G. E., Hon, G., Chandonia, J. M., and Brenner, S. E. (2004). WebLogo: a sequence logo generator. *Genome Res.* 14, 1188–1190. doi: 10.1101/gr.849004

Etchells, J. P., Mishra, L. S., Kumar, M., Campbell, L., and Turner, S. R. (2015). Wood formation in trees is increased by manipulating PXY-regulated cell division. *Curr. Biol.* 25, 1050–1055. doi: 10.1016/j.cub.2015.02.023

Etchells, J. P., Provost, C. M., Mishra, L., and Turner, S. R. (2013). *WOX4* and *WOX14* act downstream of the PXY receptor kinase to regulate plant vascular proliferation independently of any role in vascular organisation. *Development* 140, 2224–2234. doi: 10.1242/dev.091314

Etchells, J. P., Smit, M. E., Gaudinier, A., Williams, C. J., and Brady, S. M. (2016). A brief history of the TDIF-PXY signalling module: balancing meristem identity and differentiation during vascular development. *New Phytol.* 209, 474–484. doi: 10.1111/nph.13642

Etchells, J. P., and Turner, S. R. (2010). The PXY-CLE41 receptor ligand pair defines a multifunctional pathway that controls the rate and orientation of vascular cell division. *Development* 137, 767–774. doi: 10.1242/dev.044941

Fiers, M., Golemiec, E., Xu, J., van der Geest, L., Heidstra, R., Stiekema, W., et al. (2005). The 14-amino acid CLV3, CLE19, and CLE40 peptides trigger consumption of the root meristem in *Arabidopsis* through a CLAVATA2-dependent pathway. *Plant Cell* 17, 2542–2553. doi: 10.1105/tpc.105.034009

Fiers, M., Ku, K. L., and Liu, C. M. (2007). CLE peptide ligands and their roles in establishing meristems. *Curr. Opin. Plant Biol.* 10, 39–43. doi: 10.1016/j.pbi.2006.11.003

Fisher, K., and Turner, S. (2007). PXY, a receptor-like kinase essential for maintaining polarity during plant vascular-tissue development. *Curr. Biol.* 17, 1061–1066. doi: 10.1016/j.cub.2007.05.049

Fletcher, L. C., Brand, U., Running, M. P., Simon, R., and Meyerowitz, E. M. (1999). Signaling of cell fate decisions by CLAVATA3 in *Arabidopsis* shoot meristems. *Science* 283, 1911–1914. doi: 10.1126/science.283.5409.1911

Gimeno, J., Eattock, N., Van Deynze, A., and Blumwald, E. (2014). Selection and validation of reference genes for gene expression analysis in switchgrass (*Panicum virgatum*) using quantitative real-time RT-PCR. *PLoS ONE* 9:e91474. doi: 10.1371/journal.pone.0091474

Goad, D. M., Zhu, C., and Kellogg, E. A. (2017). Comprehensive identification and clustering of *CLV3/ESR-related* (*CLE*) genes in plants finds groups with potentially shared function. *New Phytol.* 216, 605–616. doi: 10.1111/nph.14348

Goodstein, D. M., Shu, S., Howson, R., Neupane, R., Hayes, R. D., Fazo, J., et al. (2012). Phytozome: a comparative platform for green plant genomics. *Nucleic Acids Res.* 40, D1178–1186. doi: 10.1093/nar/gkr944

Hall, B. G. (2013). Building phylogenetic trees from molecular data with MEGA. *Mol. Biol. Evol.* 30, 1229–1235. doi: 10.1093/molbev/mst012

Han, H., Zhang, G., Wu, M., and Wang, G. (2016). Identification and characterization of the *Populus trichocarpa* CLE family. *BMC Genomics* 17:174. doi: 10.1186/s12864-016-2504-x

Hirakawa, Y., Kondo, Y., and Fukuda, H. (2010a). Regulation of vascular development by CLE peptide-receptor systems. *J. Integr. Plant Biol.* 52, 8–16. doi: 10.1111/j.1744-7909.2010.00904.x

Hirakawa, Y., Kondo, Y., and Fukuda, H. (2010b). TDIF peptide signaling regulates vascular stem cell proliferation via the *WOX4* homeobox gene in *Arabidopsis*. *Plant Cell* 22, 2618–2629. doi: 10.1105/tpc.110.076083

Hirakawa, Y., Shinohara, H., Kondo, Y., Inoue, A., Nakanomyo, I., Ogawa, M., et al. (2008). Non-cell-autonomous control of vascular stem cell fate by a CLE peptide/receptor system. *Proc. Natl. Acad. Sci. U.S.A.* 105, 15208–15213. doi: 10.1073/pnas.0808444105

Hu, B., Jin, J., Guo, A. Y., Zhang, H., Luo, J., and Gao, G. (2015). GSDS 2.0: an upgraded gene feature visualization server. *Bioinformatics* 31, 1296–1297. doi: 10.1093/bioinformatics/btu817

Ito, Y., Nakanomyo, I., Motose, H., Iwamoto, K., Sawa, S., Dohmae, N., et al. (2006). Dodeca-CLE peptides as suppressors of plant stem cell differentiation. *Science* 313, 842–845. doi: 10.1126/science.1128436

Karimi, M., Inze, D., and Depicker, A. (2002). GATEWAY((TM)) vectors for *Agrobacterium*-mediated plant transformation. *Trends Plant Sci.* 7, 193–195. doi: 10.1016/S1360-1385(02)02251-3

Keshwani, D. R., and Cheng, J. J. (2009). Switchgrass for bioethanol and other value-added applications: a review. *Bioresource Technol.* 100, 1515–1523. doi: 10.1016/j.biortech.2008.09.035

Kinoshita, A., Nakamura, Y., Sasaki, E., Kyozuka, J., Fukuda, H., and Sawa, S. (2007). Gain-of-function phenotypes of chemically synthetic CLAVATA3/ESR-related (CLE) peptides in *Arabidopsis thaliana* and *Oryza sativa*. *Plant Cell Physiol.* 48, 1821–1825. doi: 10.1093/pcp/pcm154

Kondo, T., Sawa, S., Kinoshita, A., Mizuno, S., Kakimoto, T., Fukuda, H., et al. (2006). A plant peptide encoded by *CLV3* identified by *in situ* MALDI-TOF MS analysis. *Science* 313, 845–848. doi: 10.1126/science.1128439

Kondo, Y., and Fukuda, H. (2015). The TDIF signaling network. *Curr. Opin. Plant Biol.* 28, 106–110. doi: 10.1016/j.pbi.2015.10.002

Kucukoglu, M. (2020). A novel NAC domain transcription factor *XVP* controls the balance of xylem formation and cambial cell divisions. *New Phytol.* 226, 5–7. doi: 10.1111/nph.16400

Kucukoglu, M., Nilsson, J., Zheng, B., Chaabouni, S., and Nilsson, O. (2017). *WUSCHEL-RELATED HOMEOBOX4* (*WOX4*)*-like* genes regulate cambial cell division activity and secondary growth in *Populus* trees. *New Phytol.* 215, 642–657. doi: 10.1111/nph.14631

Letunic, I., and Bork, P. (2018). 20 years of the SMART protein domain annotation resource. *Nucleic Acids Res.* 46, D493–D496. doi: 10.1093/nar/gkx922

Li, X., Yang, H., Wang, C., Yang, S., and Wang, J. (2018). Distinct transgenic effects of poplar *TDIF* genes on vascular development in *Arabidopsis*. *Plant Cell Rep.* 37, 799–808. doi: 10.1007/s00299-018-2268-7

Li, Z., Liu, G., Zhang, J., Zhang, J., and Bao, M. (2008). Extraction of high-quality tissue-specific RNA from London plane trees (*Platanus acerifolia*), permitting the construction of a female inflorescence cDNA library. *Funct. Plant Biol.* 35, 159–165. doi: 10.1071/FP07212

McLaughlin, S. B., and Adams Kszos, L. (2005). Development of switchgrass (*Panicum virgatum*) as a bioenergy feedstock in the United States. *Biomass Bioenergy* 28, 515–535. doi: 10.1016/j.biombioe.2004.05.006

Meng, L., Buchanan, B. B., Feldman, L. J., and Luan, S. (2012). CLE-like (CLEL) peptides control the pattern of root growth and lateral root development in *Arabidopsis*. *Proc. Natl. Acad. Sci. U.S.A.* 109, 1760–1765. doi: 10.1073/pnas.1119864109

Oelkers, K., Goffard, N., Weiller, G. F., Gresshoff, P. M., Mathesius, U., and Frickey, T. (2008). Bioinformatic analysis of the CLE signaling peptide family. *BMC Plant Biol.* 8:1. doi: 10.1186/1471-2229-8-1

Ogawa-Ohnishi, M., Matsushita, W., and Matsubayashi, Y. (2013). Identification of three hydroxyproline O-arabinosyltransferases in *Arabidopsis thaliana*. *Nat. Chem. Biol.* 9, 726–730. doi: 10.1038/nchembio.1351

Ohyama, K., Ogawa, M., and Matsubayashi, Y. (2008). Identification of a biologically active, small, secreted peptide in *Arabidopsis* by *in silico* gene screening, followed by LC-MS-based structure analysis. *Plant J.* 55, 152–160. doi: 10.1111/j.1365-313X.2008.03464.x

Ohyama, K., Shinohara, H., Ogawa-Ohnishi, M., and Matsubayashi, Y. (2009). A glycopeptide regulating stem cell fate in *Arabidopsis thaliana*. *Nat. Chem. Biol.* 5, 578–580. doi: 10.1038/nchembio.182

Ondzighi-Assoume, C. A., Willis, J. D., Ouma, W. K., Allen, S. M., King, Z., Parrott, W. A., et al. (2019). Embryogenic cell suspensions for high-capacity genetic transformation and regeneration of switchgrass (*Panicum virgatum* L.). *Biotechnol Biofuels* 12:290. doi: 10.1186/s13068-019-1632-3

Parrish, D. J., and Fike, J. H. (2005). The biology and agronomy of switchgrass for biofuels. *Crit. Rev. Plant Sci.* 24, 423–459. doi: 10.1080/07352680500316433

Pfaffl, M. W. (2001). A new mathematical model for relative quantification in real-time RT-PCR. *Nucleic Acids Res.* 29:e45. doi: 10.1093/nar/29.9.e45

Ragni, L., and Hardtke, C. S. (2014). Small but thick enough–the *Arabidopsis* hypocotyl as a model to study secondary growth. *Physiol. Plantarum* 151, 164–171. doi: 10.1111/ppl.12118

Sanderson, M. A., Adler, P. R., Boateng, A. A., Casler, M. D., and Sarath, G. (2006). Switchgrass as a biofuels feedstock in the USA. *Can. J. Plant Sci.* 86, 1315–1325. doi: 10.4141/P06-136

Sanderson, M. A., Reed, R. L., McLaughlin, S. B., Wullschleger, S. D., Conger, B. V., Parrish, D. J., et al. (1996). Switchgrass as a sustainable bioenergy crop. *Bioresource Technol.* 56, 83–93. doi: 10.1016/0960-8524(95)00176-X

Sawa, S., Kinoshita, A., Betsuyaku, S., and Fukuda, H. (2008). A large family of genes that share homology with CLE domain in Arabidopsis and rice. *Plant Signal. Behav.* 3, 337–339. doi: 10.4161/psb.3.5.5344

Schoof, H., Lenhard, M., Haecker, A., Mayer, K. F. X., Jurgens, G., and Laux, T. (2000). The stem cell population of *Arabidopsis* shoot meristems is maintained by a regulatory loop between the *CLAVATA* and *WUSCHEL* genes. *Cell* 100, 635–644. doi: 10.1016/S0092-8674(00)80700-X

Solovyev, V., Kosarev, P., Seledsov, I., and Vorobyev, D. (2006). Automatic annotation of eukaryotic genes, pseudogenes and promoters. *Genome Biol.* 7:(Suppl. 1):S10.1–12. doi: 10.1186/gb-2006-7-s1-s10

Stahl, Y., Wink, R. H., Ingram, G. C., and Simon, R. (2009). A signaling module controlling the stem cell niche in *Arabidopsis* root meristems. *Curr. Biol.* 19, 909–914. doi: 10.1016/j.cub.2009.03.060

Strabala, T. J., O'Donnell, P., J., Smit, A. M., Ampomah-Dwamena, C., Martin, E. J., et al. (2006). Gain-of-function phenotypes of many *CLAVATA3*/*ESR* genes, including four new family members, correlate with tandem variations in the conserved CLAVATA3/ESR domain. *Plant Physiol.* 140, 1331–1344. doi: 10.1104/pp.105.075515

Strabala, T. J., Phillips, L., West, M., and Stanbra, L. (2014). Bioinformatic and phylogenetic analysis of the *CLAVATA3*/*EMBRYO-SURROUNDING REGION* (*CLE*) and the *CLE-LIKE* signal peptide genes in the *Pinophyta*. *BMC Plant Biol.* 14:47. doi: 10.1186/1471-2229-14-47

Ursache, R., Nieminen, K., and Helariutta, Y. (2013). Genetic and hormonal regulation of cambial development. *Physiol. Plantarum* 147, 36–45. doi: 10.1111/j.1399-3054.2012.01627.x

Wang, H., Niu, L., Fu, C., Meng, Y., Sang, D., Yin, P., et al. (2017). Overexpression of the *WOX* gene *STENOFOLIA* improves biomass yield and sugar release in transgenic grasses and display altered cytokinin homeostasis. *PLoS Genet.* 13:e1006649. doi: 10.1371/journal.pgen.1006649

Wang, J., Kucukoglu, M., Zhang, L., Chen, P., Decker, D., Nilsson, O., et al. (2013). The *Arabidopsis* LRR-RLK, PXC1, is a regulator of secondary wall formation correlated with the TDIF-PXY/TDR-WOX4 signaling pathway. *BMC Plant Biol.* 13:94. doi: 10.1186/1471-2229-13-94

Wang, P., Wang, Y., and Ren, F. (2019). Genome-wide identification of the CLAVATA3/EMBRYO SURROUNDING REGION (CLE) family in grape (*Vitis vinifera* L.). *BMC Genomics* 20:553. doi: 10.1186/s12864-019-5944-2

Wang, S., Tian, L., Liu, H., Li, X., Zhang, J., Chen, X., et al. (2020). Large-scale discovery of non-conventional peptides in Maize and Arabidopsis through an integrated peptidogenomic pipeline. *Mol. Plant* 13, 1078–1093. doi: 10.1016/j.molp.2020.05.012

Whitford, R., Fernandez, A., De Groodt, R., Ortega, E., and Hilson, P. (2008). Plant CLE peptides from two distinct functional classes synergistically induce division of vascular cells. *Proc. Natl. Acad. Sci. U.S.A.* 105, 18625–18630. doi: 10.1073/pnas.0809395105

Xi, Y., Ge, Y., and Wang, Z. Y. (2009). Genetic transformation of switchgrass. *Methods Mol. Biol.* 581, 53–59. doi: 10.1007/978-1-60761-214-8_4

Yang, J. H., Lee, K.-H., Du, Q., Yang, S., Yuan, B., Qi, L., et al. (2020). A membrane-associated NAC domain transcription factor *XVP* interacts with TDIF co-receptor and regulates vascular meristem activity. *New Phytol.* 226, 59–74. doi: 10.1111/nph.16289

Zhang, H., Lin, X., Han, Z., Wang, J., Qu, L. J., and Chai, J. (2016). SERK family receptor-like kinases function as co-receptors with PXY for plant vascular development. *Mol. Plant* 9, 1406–1414. doi: 10.1016/j.molp.2016.07.004

Zhang, J., Elo, A., and Helariutta, Y. (2011). Arabidopsis as a model for wood formation. *Curr. Opin. Biotechnol.* 22, 293–299. doi: 10.1016/j.copbio.2010.11.008

Zhang, Z., Liu, L., Kucukoglu, M., Tian, D., Larkin, R. M., Shi, X., et al. (2020). Predicting and clustering plant *CLE* genes with a new method developed specifically for short amino acid sequences. *BMC Genomics* 21:709. doi: 10.1186/s12864-020-07231-4

Conflict of Interest: The authors declare that the research was conducted in the absence of any commercial or financial relationships that could be construed as a potential conflict of interest.

Publisher's Note: All claims expressed in this article are solely those of the authors and do not necessarily represent those of their affiliated organizations, or those of the publisher, the editors and the reviewers. Any product that may be evaluated in this article, or claim that may be made by its manufacturer, is not guaranteed or endorsed by the publisher.

frontiers in Plant Science

ORIGINAL RESEARCH
published: 11 January 2022
doi: 10.3389/fpls.2021.706633

The Phloem Intercalated With Xylem-Correlated 3 Receptor-Like Kinase Constitutively Interacts With Brassinosteroid Insensitive 1-Associated Receptor Kinase 1 and Is Involved in Vascular Development in *Arabidopsis*

Ke Xu[1,2], Joris Jourquin[1,2], Maria Fransiska Njo[1,2], Long Nguyen[3,4], Tom Beeckman[1,2†] and Ana Ibis Fernandez[1,2†]*

[1] Department of Plant Biotechnology and Bioinformatics, Ghent University, Ghent, Belgium, [2] VIB Center for Plant Systems Biology, Ghent, Belgium, [3] Screening Core, VIB, Ghent, Belgium, [4] Centre for Bioassay Development and Screening (C-BIOS), Ghent University, Ghent, Belgium

Leucine-rich repeat receptor-like kinases (LRR-RLKs) play fundamental roles in cell-to-cell and plant-environment communication. LRR-RLKs can function as receptors perceiving endogenous or external ligands, or as coreceptors, which stabilize the complex, and enhance transduction of the intracellular signal. The LRR-RLK BAK1 is a coreceptor for different developmental and immunity pathways. In this article, we identified PXY-CORRELATED 3 (PXC3) as a BAK1-interacting LRR-RLK, which was previously reported to be transcribed in vascular tissues co-expressed with PHLOEM INTERCALATED WITH XYLEM (PXY), the receptor of the TDIF/CLE41 peptide. Characterization of *pxc3* loss-of-function mutants revealed reduced hypocotyl stele width and vascular cells compared to wild type, indicating that PXC3 plays a role in the vascular development in *Arabidopsis*. Furthermore, our data suggest that PXC3 might function as a positive regulator of the CLE41/TDIF–TDR/PXY signaling pathway.

Keywords: LRR-RLK, BAK1, PXC3, CLE41, PXY, vascular development

OPEN ACCESS

Edited by:
Reidunn Birgitta Aalen, University of Oslo, Norway

Reviewed by:
Yokoyama Ryusuke, Tohoku University, Japan
Jie Le, Key Laboratory of Plant Molecular Physiology, Institute of Botany (CAS), China

***Correspondence:**
Tom Beeckman
Tom.Beeckman@psb.ugent.be

† These authors have contributed equally to this work

Specialty section:
This article was submitted to Plant Physiology, a section of the journal Frontiers in Plant Science

Received: *07 May 2021*
Accepted: *13 December 2021*
Published: *11 January 2022*

Citation:
Xu K, Jourquin J, Njo MF, Nguyen L, Beeckman T and Fernandez AI (2022) The Phloem Intercalated With Xylem-Correlated 3 Receptor-Like Kinase Constitutively Interacts With Brassinosteroid Insensitive 1-Associated Receptor Kinase 1 and Is Involved in Vascular Development in Arabidopsis. Front. Plant Sci. 12:706633. doi: 10.3389/fpls.2021.706633

INTRODUCTION

Plants are sessile multicellular organisms and to perceive developmental cues and environmental stimuli, they rely on numerous sensory proteins on their cell surfaces. Receptor-like kinases (RLKs), one of the most important sensory protein groups in plants, play fundamental roles in cell-to-cell and plant–environment communication (van der Burgh and Joosten, 2019; Xi et al., 2019; Ou et al., 2021). The largest group of RLKs in plants have an extracellular leucine-rich repeat (LRR) domain and are therefore called LRR-RLKs. The *Arabidopsis* genome encodes more than 200 LRR-RLKs, which can be further grouped into 13 subfamilies (Shiu and Bleecker, 2001, 2003). Many of these LRR-RLKs function as receptors for phytohormones, endogenous peptides,

and pathogen-derived molecules, regulating plant growth and defense responses (De Smet et al., 2009; Couto and Zipfel, 2016; He et al., 2018). LRR-RLKs sensing ligand signals in plants include BRASSINOSTEROID INSENSITIVE 1 (BRI1) for the phytohormone brassinosteroid (Li and Chory, 1997), PHYTOSULFOKINE RECEPTOR (PSKR) for endogenous PHYTOSULFOKINE peptides (Matsubayashi et al., 2002), FLAGELLIN SENSING 2 (FLS2) for the pathogen-derived flagellin (Gomez-Gomez and Boller, 2000; Chinchilla et al., 2006), and many more.

Somatic embryogenesis receptor kinases (SERKs), belonging to LRR-RLK subfamily II, have been extensively shown to serve as coreceptors for various LRR-RLK signaling pathways, in both plant growth and immunity pathways (Ma et al., 2016; He et al., 2018). SERK3, also called BRI1-ASSOCIATED RECEPTOR KINASE 1 (BAK1), is the best-studied ones among the five SERK family members in *Arabidopsis*. BAK1 was initially found to be involved in brassinosteroid perception (Li et al., 2002), but recent studies have shown diverse functions for BAK1 in the regulation of plant growth and immune responses by forming ligand-induced complexes with different LRR-RLKs. For example, BAK1 dimerizes with RGF1 INSENSITIVE receptors to regulate root development (Ou et al., 2016; Song et al., 2016), with HAESA and HAESA-LIKE 2 to control cell separation during floral organ abscission (Meng et al., 2016; Santiago et al., 2016), with ERECTA and ERECTA-LIKE 1 to regulate stomatal development (Meng et al., 2015), and with PSKR1 to regulate cell proliferation and elongation (Ladwig et al., 2015; Wang et al., 2015). Furthermore, BAK1 participates in plant immune responses by interacting with receptors, like FLS2 (Chinchilla et al., 2007), ELONGATION FACTOR-TU RECEPTOR (Roux et al., 2011), and PEP1 RECEPTOR 1 (PEPR1) (Tang et al., 2015). In many cases, although not all, dimerization of the ligand-binding receptor with SERK coreceptors is induced by the ligand. In addition to the ligand-induced receptor–coreceptor interactions, recent studies revealed the occurrence of ligand-free constitutive interactions between different LRR-RLKs (Smakowska-Luzan et al., 2018). The BAK1-INTERACTING RECEPTOR-LIKE KINASE 2 (BIR2) and BIR3 have been shown to constitutively interact with BAK1 and act as negative regulators of FLS2-BAK1 and/or BRI1–BAK1 complex formation (Halter et al., 2014; Imkampe et al., 2017). Also, the NUCLEAR SHUTTLE PROTEIN-INTERACTING KINASE 1 (NIK1) (Li et al., 2019), FLS2-INTERACTING RECEPTOR (FIR) (Smakowska-Luzan et al., 2018), and IMPAIRED OOMYCETE SUSCEPTIBILITY 1 (IOS1) (Yeh et al., 2016) constitutively interact with BAK1 or the ligand-sensing receptor. These ligand-free interactions have been shown often to regulate receptor–coreceptor complex formation.

BAK1, as well as SERK1 and 2, were also shown to be involved in vascular development by serving as coreceptors for TDIF RECEPTOR (TDR)/PHLOEM INTERCALATED WITH XYLEM (PXY), which senses the TRACHEARY ELEMENT DIFFERENTIATION FACTOR (TDIF) peptide (Fisher and Turner, 2007; Hirakawa et al., 2008), encoded by both the *CLE41* and *CLE44* genes (Ito et al., 2006). The SERK1-3 and PXY ectodomains were shown to interact in the presence of TDIF and, accordingly, the triple loss-of-function (*lof*) mutant *serk1-1serk2-1bak1-5* is insensitive to TDIF peptide treatments and shows defects in procambial cell organization (Zhang et al., 2016). Activation of the TDIF–TDR/PXY pathway results in upregulation of two *WUSCHEL RELATED HOMEOBOX (WOX)* genes, *WOX4*, and *WOX14* (Etchells and Turner, 2010; Hirakawa et al., 2010; Etchells et al., 2013). WOX14 induces the expression of another transcription factor, *TARGET OF MONOPTEROS 6 (TMO6)*. WOX14 and TMO6 in turn, stimulate the expression of *LATERAL ORGAN BOUNDARIES DOMAIN 4 (LBD4)* at the procambium–phloem boundary to control vascular stem cell proliferation (Smit et al., 2020).

In a previous study, three LRR-RLKs were identified and related to TDR/PXY *via in silico* co-expression and functional clustering analyses. These RLKs were named *PXY-CORRELATED (PXC) 1* to *3*, and PXC1 was indeed found to regulate vascular development by controlling secondary cell wall formation (Wang et al., 2013). Recent reports have shed light on the function of PXC2 (Goff and Van Norman, 2021). However, the function of *PXC3* remains unknown. In this article, we identified PXC3 as a BAK1 interactor and revealed that it functions in vascular development in a similar manner as TDR/PXY.

MATERIALS AND METHODS

Growing Conditions and Plant Material

Arabidopsis thaliana (Col 0) seedlings were sown on solid half MS medium (Duchefa Biochemie B.V.) supplemented with 1% sucrose (VWR), 0.1 g l^{-1} Myo-inositol (Sigma–Aldrich), 0.5 g l^{-1} 2-(*N*-morpholino)ethanesulfonic acid (MES) (Duchefa Biochemie B.V.), and 0.8% Plant Tissue Culture Agar (Lab M, MC029). The plates were stratified for 2 days at 4°C and grown at 21°C under continuous light conditions.

Entry clones carrying the LRR-RLKs in pDONR/zeo (Invitrogen) were ordered from the Arabidopsis Biological Resource Center (ABRC): N4G33430ZEF (BAK1), N5G48380ZEF (BIR1), N3G28450ZEF (BIR2), N1G27190ZEF (BIR3), N2G41820ZEF (PXC3), N4G08850ZEF (MIK2), and N3G14840ZEF (LIK1). Receptor entry clones were combined with the pEN-L4-4-R1 (Karimi et al., 2007), carrying the cauliflower mosaic virus (*CaMV*) *35S* promoter, and pEN-R2-n/cGFP-L3 (Boruc et al., 2010), containing the N- or C-terminal half of the GFP, into the pB7m34GW destination vector by Gateway LR recombination reaction, to generate the corresponding *35Spro:LRR-RLK-n/cGFP* expression clones that were used for infiltration of *Nicotiana benthamiana* leaves. BAK1 was fused similarly with a 3× HA tag (pEN-R2-3 × HA-L3) (Van Leene et al., 2007). The S2G41820HGF clone containing the *PXC3* coding sequence with a C-terminal GFP fusion driven by the *CaMV 35S* promoter was also ordered from ABRC.

The *pxc3-1* (SALK_121365) and *pxc3-2* (SALK_092805) mutants were requested from the Nottingham Arabidopsis Stock Centre (NASC). The *pxc2-1* (SALK_055351C) and *pxc2-2* (SALK_018730C) mutants (also called *canar-1* and *canar-2*, respectively) were described previously (Hajny et al., 2020) and were kindly donated by Jiří Friml. The *pxy* mutant has been reported (Etchells and Turner, 2010) and was kindly donated by

Eliana Mor and Bert De Rybel. The *pxypxc3-2* double mutant was obtained by crossing. The *BAK1pro:BAK1-GFP/bak1-4* has been reported (Ntoukakis et al., 2011) and was kindly donated by Ciryl Zipfel.

Microsomal Extraction From *Arabidopsis thaliana* Seedlings

Microsomal extraction was performed according to Abas and Luschnig (2010) with modifications. *BAK1pro:BAK1-GFP/bak1-4/iGLV6* homozygous seedlings were germinated in a 2,000 ml Erlenmeyer containing 600 ml of liquid half MS medium. Five days after germination (DAG), mock or estradiol (2 μM) was added to the medium and incubated for 24 h. Then the growing medium was discarded and plant tissue was cross-linked on ice-cold 1% formaldehyde in PBS pH 7.4 for 30 min, then quenched with 300 mM glycine in cold PBS for 30 min and washed three times for 10 min with cold PBS. Four grams of tissue were weighed and frozen in liquid N_2. Tissue was ground with a mortar and 1.5 ml of 1.4× extraction buffer [EB: 50 mM Tris pH 7.5, 25% D-Sorbitol, 10 mM Ethylenediaminetetraacetic acid (EDTA), 10 mM Ethylene glycol-bis (2-aminoethylether)-*N,N,N',N'*-tetraacetic acid (EGTA), 50 mM sodium fluoride, 40 mM β-glycerol phosphate, 1mM sodium molybdate, 1 mM dithiothreitol (DTT), 1 mM phenylmethylsulfonyl fluoride (PMSF), and 1× cOmplete ULTRA Tablets (5892791001; Roche)] per gram of tissue was added. The samples were transferred to a 50 ml falcon tube, vortexed, then transferred to another tube containing high molecular weight insoluble polyvinylpolypyrrolidone (PVPP, 50 mg per gram of tissue) that had been previously equilibrated with EB, vortexed, and spun down. After transfer to the PVPP pellet, samples were vortexed, incubated on ice for 5 min, then centrifuged at 600 *g* for 5 min at 4°C. The supernatant was transferred to another tube and the pellet was extracted again twice with half and one-third of the initial EB volume. All supernatants were pooled. Finally, the pellet was centrifuged at 2,000 *g* for 5 min, the supernatant was added to the previous supernatant pool and the pellet was discarded. Pooled supernatants were vortexed and centrifuged at 6,000 *g* for 5 min then filtered through a mesh (Miracloth) to eliminate the remaining debris. Then an equal volume of water was added and samples were vortexed and centrifuged at 100,000 *g* for 2 h in a Beckman Coulter ultracentrifuge (Beckman Coulter L8-70). The microsomal pellet was washed with 10 mM Tris pH 7.3 and resuspended by pipetting in 1 ml of resuspension buffer [10 mM Tris pH 7.3, 150 mM NaCl, 1 mM EDTA, 10% glycerol, 1% Triton X-100, 1 mM PMSF, 20 mM NaF and 1× cOmplete ULTRA Tablets (Roche)]. The sample was transferred to a 2 ml eppendorf and centrifuged on a bench centrifuge at 21,000 *g* for 30 min at 4°C (Eppendorf Centrifuge 5427 R). The supernatant was transferred to a new tube and total protein was quantified with the Bradford assay.

Affinity Purification and Sample Preparation

Two milligrams of total protein from microsomal extractions were incubated with 50 μl of anti-GFP μMACS MicroBeads (Miltenyi Biotec) for 1 h at 4°C. Beads were captured into μMACS columns (Miltenyi Biotec) according to the manufacturer's instructions and washed four times with microsomal resuspension buffer. Then rinsed twice with 500 μl ABC Buffer [50 mM NH_4HCO_3 in H_2O] to remove all the detergent. The column was removed from the magnet and immediately placed into a 0.5 mL low-bind eppendorf tube. Fifty microliters of ABC Buffer pre-heated at 95°C was added to the column to elute the beads.

For MS analysis, on-bead digestion, and sample preparation were performed as previously described (Wendrich et al., 2017), with the exception that the initial DTT and iodoacetamide treatments were performed for 1 h instead of 2 h.

Mass Spectrometry and Data Analysis

The obtained peptide mixtures were introduced into an LC-MS/MS system, the Ultimate 3000 RSLC nano (Dionex, Amsterdam, Netherlands) in-line connected to an LTQ Orbitrap Velos (Thermo Fisher Scientific, Bremen, Germany). The sample mixture was loaded on a trapping column (made in-house, 100 μm internal diameter (I.D.) × 20 mm (length), 5 μm C18 Reprosil-HD beads (Dr. Maisch GmbH, Ammerbuch-Entringen, Germany). After back-flushing from the trapping column, the sample was loaded on a reverse-phase column (made in-house, 75 μm I.D. x 150 mm, 5 μm C18 Reprosil-HD beads, Dr. Maisch). Peptides were loaded with solvent A (0.1% trifluoroacetic acid, 2% acetonitrile), and separated with a linear gradient from 2% solvent A' (0.1% formic acid) to 50% solvent B' (0.1% formic acid and 80% acetonitrile) at a flow rate of 300 nl/min, followed by a wash step reaching 100% solvent B'.

The mass spectrometer was operated in data-dependent mode, automatically switching between MS and MS/MS acquisition for the 10 most abundant peaks in a given MS spectrum. In the LTQ-Orbitrap Velos, full scan MS spectra were acquired in the Orbitrap at a target value of 1E6 with a resolution of 60,000. The 10 most intense ions were then isolated for fragmentation in the linear ion trap, with a dynamic exclusion of 20 s. Peptides were fragmented after filling the ion trap at a target value of 1E4 ion counts.

The raw files were processed using the MaxQuant software (version 1.5.1.2) using standard settings as described in Wendrich et al. (2017).

Nicotiana benthamiana Leaf Infiltration

The constructs for bimolecular fluorescence complementation (BIFC) and Co-IP were transformed into *A. tumefaciens* strain C58C1 by electroporation. *A. tumefaciens* cultures carrying receptor fusions to tags or the P19 suppressor (Scholthof, 2006), were diluted with infiltration buffer (10 mM $MgCl_2$, 10 mM MES pH 5.7, and 100 μM acetosyringone) to obtain OD_{600} = 1. Then equal amounts of each culture were mixed and used for infiltration. Three days after infiltration, *N. benthamiana* leaves were imaged for BIFC or harvested in liquid N_2 for Co-IP. Receptor interactions were compared only when they were infiltrated in the same leaves.

Bimolecular Fluorescence Complementation

For BIFC assays, five leaves were infiltrated each time and five images were taken and averaged for each receptor pair combination per leaf with a Zeiss LSM 710 confocal microscope. GFP was excited at 488 nm and acquired at 493–542 nm. Quantification of the GFP signal in each image was performed with ImageJ using the mean gray value function.

Protein Extraction and Western Blot

For Co-IP, frozen tobacco leaves were ground in liquid N_2 and the extraction buffer [50 mM Tris pH 7.5, 150 mM NaCl, 1 mM EDTA, 10% (v/v) glycerol, 1% (v/v) Triton X-100, 1 mM PMSF, and 1× complete ULTRA Tablets (5892791001, Roche)] was added at the ratio of 2 μl per mg tissue (1:2 w:v). Samples were vortexed and centrifuged at 10,000 *g* for 15 min. The supernatant was collected and then filtered through a mesh (Miracloth) to eliminate the remaining debris. Protein concentration was quantified using the Qubit protein assay kit (Thermo Fischer Scientific). Approximately, 200 mg protein was used for Co-IP with GFP-trap magnetic agarose beads (gtma, Chromotek) for 1 h at 4°C with gentle shaking. The beads were collected and washed three times with washing buffer (10 mM Tris pH 7.5, 150 mM NaCl, 0.05% NP-40, and 0.5 mM EDTA). Bound proteins were eluted by boiling in Laemli sample buffer. Proteins were loaded on the gel and analyzed by Western blot with anti-HA antibody (1/2,000, 26183, Thermo Fisher Scientific), followed by secondary horseradish peroxidase (HRP)-conjugated anti-mouse antibody (1/10,000, NA931, Amersham Biosciences). Membranes were stripped with stripping buffer [1:1 (v:v) 100 mM Glycine-HCl pH 2.5 and 10% SDS buffer], and reblotted with anti-GFP antibody (1/5,000, ab290, Abcam), followed by secondary HRP-conjugated anti-rabbit antibody (1/10,000, NA934V, GE Healthcare).

For BAK1 protein level analysis in *Arabidopsis*, 30 seedlings at 5 DAG were harvested, and protein extraction and quantification were done as described above using the extraction buffer [50 mM Tris pH 7.5, 100 mM NaCl, 10% glycerol, 0.5% Triton X-100, 1 mM PMSF, 1 mM EDTA and 1× cOmplete ULTRA Tablets (5892791001; Roche)]. Samples were centrifuged for 30 min at 13,000 *g*, and 20 μg of total protein from the supernatant was loaded on the gel and blotted with anti-BAK1 antibody (1/5,000, AS12, Agrisera). Membranes were stripped with stripping buffer and reblotted with anti-tubulin antibody (1/2,000, T6199, Sigma). BAK1 signal in blots was quantified with ImageLab (Bio-Rad) 6.0 using the relative quantity function.

Hypocotyl Stele Width Measurement

Three DAG seedlings of wild type, *pxy*, *pxc2-1*, *pxc2-2*, *pxc3-1*, *pxc3-2,* and *pxypxc3-2* were transferred from solid to liquid half MS medium with or without 5 μM of synthetic TDIF peptide (His-Glu-Val-Hyp-Ser-Gly-Hyp-Asn-Pro-Ile-Ser-Asn) (GenScript) and grown with gentle shaking for 4 days. Samples were then harvested and fixed with 4% (w/v) paraformaldehyde for 1 h under vacuum, washed twice with PBS, and then transferred into ClearSee solution [10% (w/v) xylitol, 15% (w/v) sodium deoxycholate, and 25% (w/v) urea] (Kurihara et al., 2015). After 3 days, cell walls were stained with 100 μg/ml calcofluor white in ClearSee solution for 1 h under vacuum and washed with ClearSee solution for 30 min. The stele width was measured in images obtained with a Zeiss LSM 710 confocal microscope. Calcofluor white was excited at 405 nm and acquired at 410–524 nm.

Cross-Sections

For anatomical analysis of hypocotyl vascular development in *Arabidopsis* seedlings, cross-sections were made as described (Beeckman and Viane, 2000; De Smet et al., 2004). Briefly, 7 DAG seedlings were harvested and fixed by FAA solution (4% formaldehyde, 5% glacial acetic acid, and 50% ethanol) for 2 days and washed twice with phosphate buffer. Dehydration was performed using 30, 50, 70, 85, and 96% ethanol. Resin infiltration was performed using 30, 50, 70, and 100% Technovit 7100 (VWR, HKUL64709003). Two-step embedding was used and 5μm sections were cut with a microtome (Reichert Jung 2040). Sections stained with toluidine blue and images were taken with an Olympus BX53 DIC microscope using 500× magnification.

qPCR Analysis

PXC3 expression levels in *pxc3* mutants were determined in 7 DAG seedlings of wild type, *pxc3-1*, and *pxc3-2*. To test the *WOX4* and *WOX14* expression, 3 DAG seedlings of wild type, *pxy*, *pxc2-1*, *pxc2-2*, *pxc3-1*, *pxc3-2,* and *pxypxc3-2* were transferred from solid half MS medium to liquid half MS medium for 4 days with shaking. A 5 μM of TDIF peptide or mock was added to the samples for 8 h. Samples were harvested and frozen. RNA was extracted with the ReliaPrep RNA Miniprep System (Promega). First-strand cDNA was synthesized using the qScript cDNA Supermix (Quantabio). qPCR was performed using SyberGreen (Roche) and LightCycler real-time thermocycler (Roche). *ACT2* and *TUA4* were used as reference transcripts. Primers are listed in **Supplementary Table 2**.

Statistical Analysis

To compare the mean fluorescence intensity from BIFC analysis and the hypocotyl stele width, a one-way ANOVA with multiple comparison analysis followed by Tukey's test was performed using Graphpad Prism 8. For comparison of the TDIF treatment effect on the stele width of wild type and mutants, a linear model was fitted to the data using the genotype, the treatment and their interaction as explanatory variables. A two-way ANOVA was performed, followed by post hoc comparison of contrasts between the wild type and each mutant genotype using a Dunnett's correction. The analysis was performed in R-4.0.3 using the "Car" and "Emmeans" packages. To compare the effect of TDIF peptide treatment on *WOX4* and *WOX14* expression between the different genotypes, peptide/mock transcript fold change was calculated and converted to Log2. Statistical differences between genotypes were then determined with one-way ANOVA followed by a post hoc comparison Tukey's test using Graphpad Prism 8. For comparison of the

relative BAK1 protein level, a one-way ANOVA with multiple comparison analysis followed by Tukey's test was performed in Graphpad Prism 8.

RESULTS

Phloem Intercalated With Xylem-Correlated 3 Constitutively Interacts With Brassinosteroid Insensitive 1-Associated Receptor Kinase 1

We have previously identified GLV6, a signaling peptide from the GOLVEN/Root meristem Growth Factor/CLE-like family, as a regulator of lateral root development (Fernandez et al., 2015). Considering that the *bak1-4* mutant partially suppressed the GLV6 phenotype and could be a coreceptor for the GLV pathway during lateral root development (data not shown) we designed an experiment to identify BAK1 interactors upon induction of the pathway. For this, we crossed an estradiol-inducible *GLV6* overexpression line (*iGLV6*) (Fernandez et al., 2020) with a reported *BAK1pro:BAK1-GFP/bak1-4* line (Ntoukakis et al., 2011) and performed affinity purification mass spectrometry (AP-MS) experiments in microsomal-enriched fractions using anti-GFP beads after estradiol induction or mock. Unfortunately, statistical analysis of estradiol-treated *vs.* mock seedlings did not reveal significant differences, which could be because BAK1 is a coreceptor for different pathways resulting in diluted output (**Supplementary Table 1**). We remarked that regardless of the treatment, known BAK1 interactors were pulled down, as would be expected. These included peptides from the LRR-RLKs BIR1, BIR2, and BIR3, which have been shown to constitutively interact with BAK1 and negatively regulate its complex formation with ligand-binding receptors (Gao et al., 2009; Halter et al., 2014; Imkampe et al., 2017). In addition, several peptides for three other LRR-RLKs; PXC3, MALE DISCOVERER 1 (MDIS1)/INTERACTING RECEPTOR LIKE KINASE2 (MIK2), and LYSM RLK1-INTERACTING KINASE 1 (LIK1) were recovered (**Supplementary Table 1**). Interestingly, in a similar experiment where a SERK1-CFP fusion was used as a bait, five of these receptors coeluted with SERK1, and four of them (BIR2, BIR3, LIK1, and PXC3) were significantly enriched compared to the control (Smaczniak et al., 2012).

Because known, as well as, unknown LRR-RLKs BAK1 interactors coeluted in all samples, we hypothesized that these are constitutive BAK1 interactors. To test this, we fused BAK1 to the C-terminal half (cGFP) and the six identified LRR-RLKs to the N-terminal half (nGFP) of the GFP protein, and performed BIFC analysis after transient expression in *N. benthamiana* leaves. As a negative control we used PEPR1, whose ectodomain has been shown to interact with BAK1 only upon addition of the AtPEP1 peptide ligand (Tang et al., 2015). BIFC assays revealed GFP signal for all tested combinations, which was associated to the plasma membrane, indicating that when fused to the GFP halves and combined, the tested pair of receptors still localized to the plasma membrane (**Figure 1A**). Quantification of the mean fluorescence intensity revealed a weak and patchy signal in the PEPR1-nGFP/BAK1-cGFP pair. This could be due to some PEPR1–BAK1 pre-complex formation without the ligand, basal expression of the PEP1 ligand in *N. benthamiana* leaves and/or some spontaneous association of the two GFP halves. Thus, we considered the PEPR1-nGFP/BAK1-cGFP as background and regarded as true interactions only those for which the measured signal was significantly higher than this value. In agreement with previous results, all three BIR1, BIR2, and BIR3 showed interaction with BAK1 by BIFC. Both, MIK2 and LIK1 receptors, showed weak GFP signal similar to the negative control. In contrast, PXC3 showed strong BIFC signal that could be indicative of true interaction with BAK1 (**Figure 1B**), which has not been previously reported.

To further validate the PXC3–BAK1 interaction, co-immunoprecipitation (Co-IP) assays were performed by co-infiltrating PXC3-GFP and BAK1-HA fusion proteins in tobacco leaves. Pull down with anti-GFP beads and western blot analyses showed that the BAK1-HA protein co-IPed with PXC3-GFP (**Figure 1C**). This confirms that PXC3 constitutively interacts with BAK1.

Phloem Intercalated With Xylem-Correlated 3 Mutants Show Defects in Hypocotyl Vascular Development

PXC3 was previously shown to be co-expressed with TDR/PXY. In agreement with this, a *PXC3* transcriptional reporter (*PXC3pro::GUS*) displayed a signal in vascular strands of hypocotyl and roots in young seedlings (Wang et al., 2013). Nevertheless, no further studies were performed on PXC3 function. To gain insights into the PXC3 function we obtained two *lof* mutants, *pxc3-1* (SALK_121365) and *pxc3-2* (SALK_092805), both containing a T-DNA insertion in the coding sequence (**Figure 2A**). Expression analysis by qPCR showed that the *PXC3* mRNA levels were significantly reduced in both mutants compared to wild type (**Figure 2B**). We then analyzed longitudinal confocal sections of 7 DAG wild type and *pxc3* hypocotyls. The *pxy* mutant was also added as a control. The results show that the stele width in *pxy* is significantly reduced compared to wild type, in agreement with previous reports (**Figures 2C,D**; Hirakawa et al., 2010). Furthermore, similar defects were observed in both *pxc3* mutants (**Figures 2C,D**). The analysis of *pxc3* mutants suggests that PXC3 is involved in vascular development.

To further study the vascular defects in *pxc3* mutants, we performed hypocotyl cross-sections. As previously shown, the number of procambium cells in *pxy* mutants was reduced and the xylem and phloem were sometimes found in contact with each other (Fisher and Turner, 2007). Similarly, in the *pxc3-1* mutant, the number of procambium cells separating the xylem and the phloem poles was found to be reduced (**Figure 2E**). In summary, the defects observed in *pxc3* mutants are similar but milder than those in the *pxy* mutant.

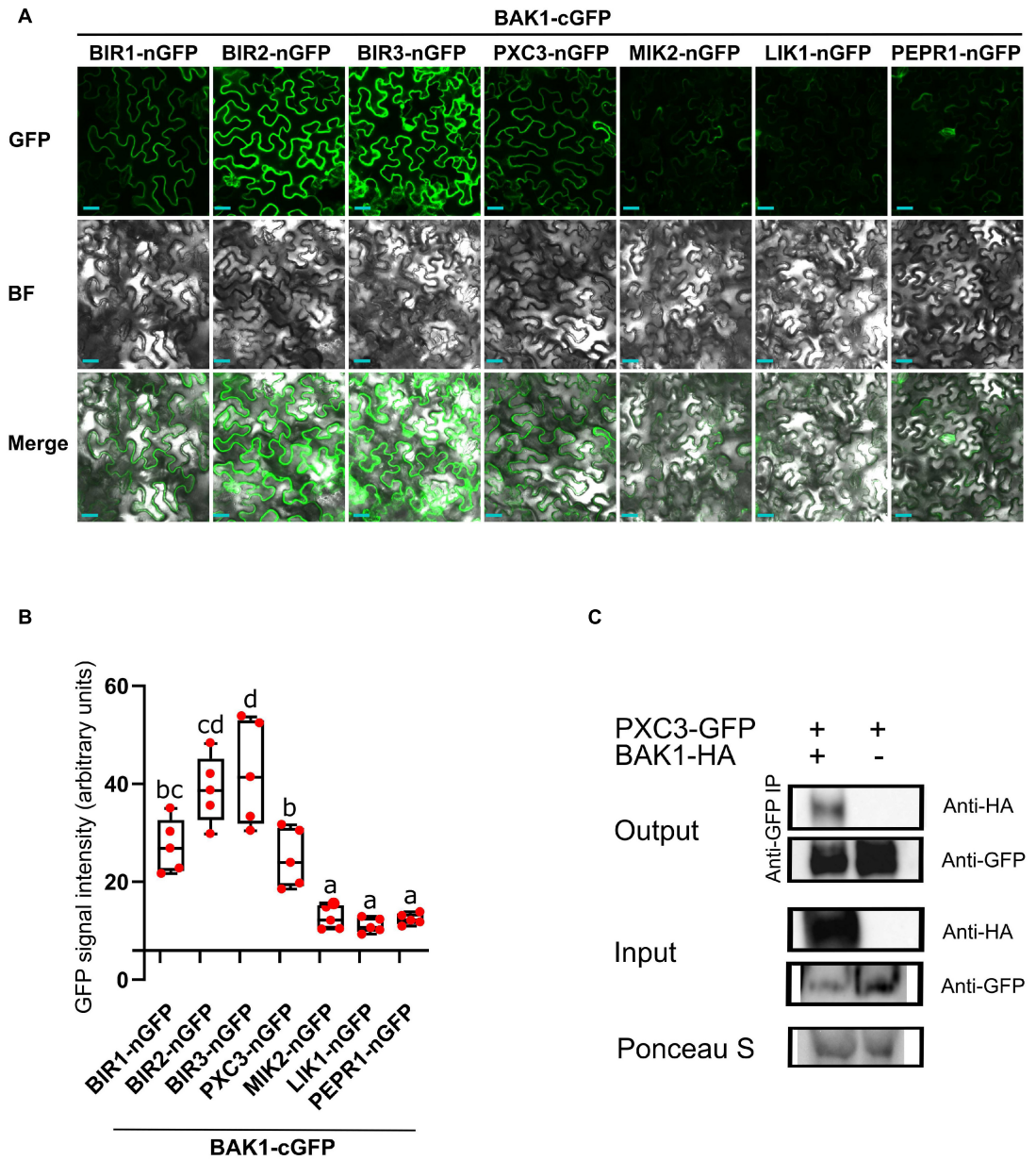

FIGURE 1 | BAK1 interaction with identified LRR-RLKs. **(A)** BIFC experiments after transient expression in tobacco leaves of BAK1 and other receptors fused to the C-term or N-term halves of GFP, respectively. Scale bars represent 20 μm. This experiment was done three times with similar results. BF, bright field. **(B)** Quantification of the mean GFP signal in BIFC experiments. Individual data points represent values for different leaves (average of 5 images per interaction per leaf). A one-way ANOVA analysis was performed followed by Tukey's test and the lowercase letters indicate statistical differences ($P < 0.05$). **(C)** Co-immunoprecipitation assay between BAK1 and PXC3 proteins. Protein extracts obtained from tobacco leaves infiltrated with Agrobacterium harboring *35Spro:BAK1-HA* and *35Spro:PXC3-GFP* were analyzed by western blot using anti-GFP and anti-HA antibodies.

Phloem Intercalated With Xylem-Correlated 3 Positively Regulates the CLE41/TDIF–TDR/PXY Signaling Pathway During Vascular Development

pxc3 lof mutants showed a reduction in stele width and procambial cell number, similar to *pxy* mutant. In addition, we found that PXC3 interacts with BAK1 (**Figures 1A–C**). Since procambial proliferation is controlled by the CLE41/TDIF–TDR/PXY signaling, for which BAK1 is a coreceptor, we decided to investigate whether PXC3 is also part of this pathway. *CLE41* overexpression or synthetic TDIF peptide treatment leads to ectopic vascular cell proliferation and radial enlargement of the stele (Whitford et al., 2008; Etchells and Turner, 2010; Hirakawa et al., 2010). To determine whether PXC3 is involved in the CLE41/TDIF–TDR/PXY signaling pathway, we analyzed the stele

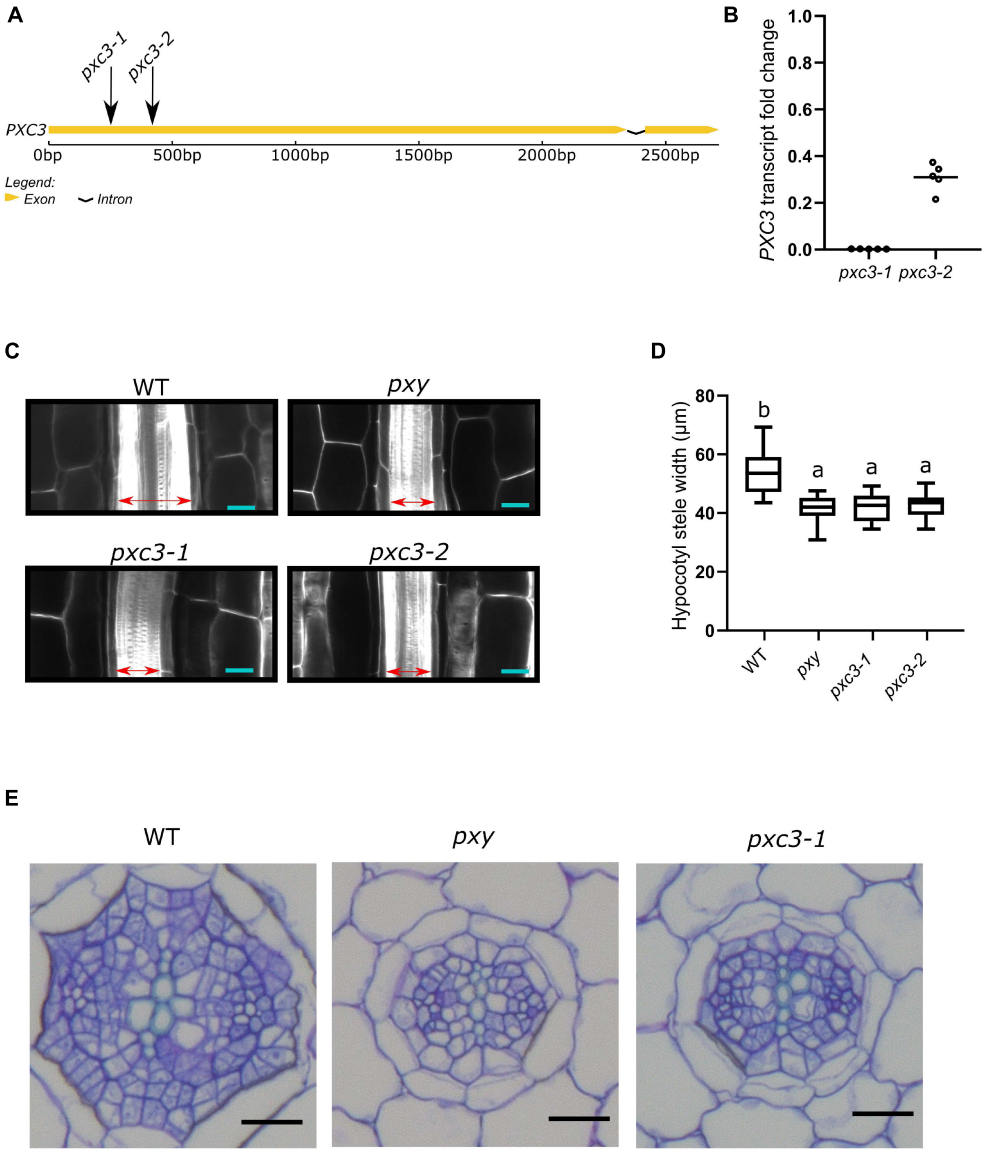

FIGURE 2 | *pxc3* mutants have reduced stele in the hypocotyl of *Arabidopsis* seedlings. **(A)** Structure of *PXC3* gene. The arrows indicated the approximate position of the T-DNA insertion in *pxc3* mutants. **(B)** *PXC3* expression levels in *pxc3-1* and *pxc3-2* mutants compared to wild type determined by qPCR in 5 independent biological replicates (individual data points). Transcript fold change relative to wild type is shown. **(C)** Longitudinal confocal sections of wild type and mutant hypocotyls (7 DAG seedlings). The double-sided arrow indicates the stele width. Scale bars represent 20 μm. This experiment was done three times with similar results. **(D)** Quantification of the stele width in wild type and mutant hypocotyls ($n \geq 15$). One-way ANOVA followed by Tukey's test was performed, and the lowercase letters indicate statistical differences ($P < 0.05$). **(E)** Cross-section of wild type and mutant hypocotyls (7 DAG seedlings). Scale bars represent 20 μm.

width in hypocotyls of wild type, *pxy*, and the two *pxc3* mutants treated or not with the TDIF peptide. The result showed that, after the TDIF peptide treatment, the stele width was significantly enlarged in wild type while such an enlargement was not observed in the *pxy* mutant as previously reported (Hirakawa et al., 2010). In the two *pxc3* mutants, radial expansion of the stele was also observed upon TDIF peptide treatment, but the enlargement was significantly smaller than in the wild type in two out of three replicates, suggesting that *pxc3* mutants are less sensitive to TDIF peptide treatment (**Figures 3A,B**).

The CLE41/TDIF–TDR/PXY signaling pathway regulates procambial cell proliferation, through upregulation of *WOX4* and *WOX14* expression (Hirakawa et al., 2010; Etchells et al., 2013). To further confirm that PXC3 is involved in this signaling pathway, we analyzed the expression levels of *WOX4* and *WOX14* in wild type, *pxy*, and the *pxc3* mutants after TDIF peptide treatment for 8 h. As expected, TDIF peptide treatment triggered upregulation of *WOX4* and *WOX14* expression in wild-type seedlings while this effect was largely suppressed in *pxy* mutants (**Figure 3C**). Furthermore, the TDIF-induced increase

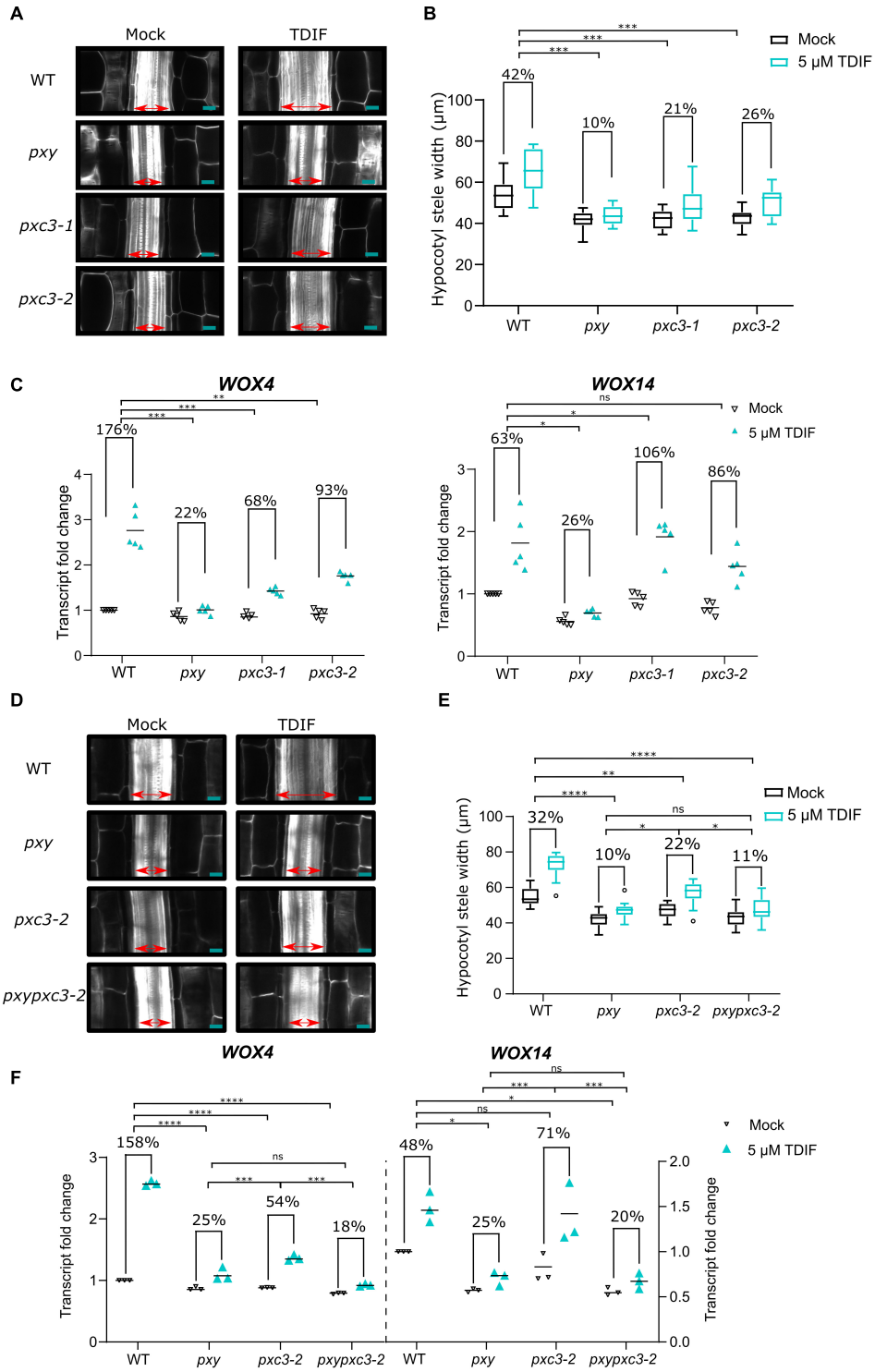

FIGURE 3 | *pxc3* mutants have reduced sensitivity to TDIF peptide treatment. **(A)** Longitudinal confocal sections of wild type and mutant hypocotyls (7 DAG seedlings) treated or not with the TDIF (5 μM) peptide for 4 days as indicated. The double-sided arrow indicates the stele width. Scale bars represent 20 μm. **(B)** Quantification of the stele width ($n \geq 15$). This experiment was done three times. In two out of three replicates, a significant interaction between treatment and genotype was found for *pxc3* mutants compared to wild type. Numbers indicate fold change in the mean stele width relative to the untreated sample for each genotype. A two-way ANOVA followed by a Dunnett's test was performed and the asterisks indicate a significant genotype and treatment interaction compared to wild type (***$P < 0.001$). **(C)** *WOX4* and *WOX14* transcript levels after 8 h TDIF treatment of wild-type and mutant seedlings. Fold change relative to wild type (mock) is shown. Numbers indicate fold change in the mean value (line) relative to the untreated sample for each genotype ($n = 5$ independent replicates). A one-way

(Continued)

FIGURE 3 | ANOVA followed by a Tukey's test was performed on Log2-transformed peptide/mock gene expression ratio, and the asterisks indicate a significant genotype and treatment interaction compared to wild type (*$P < 0.05$, ** $P < 0.01$, and ***$P < 0.001$, and ns indicates that no significant difference was found). **(D)** Longitudinal confocal sections of wild type and mutant hypocotyls (7 DAG seedlings) treated or not with the TDIF (5 μM) peptide for 4 days as indicated. The double-sided arrow indicates the stele width. Scale bars represent 20 μm. **(E)** Quantification of the stele width ($n \geq 15$). This experiment was done two times. Numbers indicate fold change in the mean stele width relative to the untreated sample for each genotype. A two-way ANOVA followed by a Dunnett's test was performed and the asterisks indicate a significant genotype and treatment interaction (*$P < 0.05$, **$P < 0.01$, and ****$P < 0.0001$, and ns indicates that no significant difference was found). **(F)** *WOX4* and *WOX14* transcript levels after 8 h TDIF treatment of wild-type and mutant seedlings. Fold change relative to wild type (mock) is shown. Numbers indicate fold change in the mean value (line) relative to the untreated sample for each genotype ($n = 3$ independent replicates). A one-way ANOVA followed by a Tukey's test was performed on Log2-transformed peptide/mock gene expression ratio, and the asterisks indicate a significant genotype and treatment interaction (*$P < 0.05$, *** $P < 0.001$, and ***$P < 0.001$, and ns indicates that no significant difference was found).

in *WOX4* transcription was also partially suppressed in both the *pxc3* mutants, again confirming that the mutants are partially resistant to TDIF peptide treatment. However, opposite to *pxy*, *pxc3-1* and *pxc3-2* mutants did not suppress the induction of *WOX14* transcript by TDIF treatment. A slightly higher *WOX14* transcript induction was observed in *pxc3* mutants compared to the wild type (**Figure 3C**).

To determine whether PXY and PXC3 are part of the same or parallel pathway(s), we generated a *pxypxc3-2* double mutant and monitored hypocotyl width and *WOX4* and *WOX14* transcription in response to the TDIF peptide. The defects observed in *pxy* and *pxc3-2* mutants were not additive both, under mock conditions or peptide treatment, and the double mutant was indistinguishable from *pxy*, indicating that these two LRR-RLKs act most likely in the same genetic pathway (**Figures 3D–F**).

Wang et al. (2013) previously identified PXC1 to 3 to be co-expressed with PXY, which could indicate that not only PXC3 but also PXC1 and 2 are associated with the TIDIF–PXY pathway. Therefore, we finally investigated whether mutants in other *PXC* genes responded differently than wild type to the TDIF peptide. We could not recover mutants for *PXC1*, but we obtained two independent mutants for *PXC2* (also recently called Canalization-related Receptor-like kinase, CANAR) (Hajny et al., 2020). Interestingly, both *pxc2* mutants showed reduced response to TDIF, although in contrast to *pxc3* mutants, they did not show decreased stele width under mock conditions (**Supplementary Figure 1**).

Phloem Intercalated With Xylem-Correlated 3 Loss-of-Function Does Not Affect Brassinosteroid Insensitive 1-Associated Receptor Kinase 1 Levels

Our data showed that PXC3 constitutively interacts with BAK1 and seems to be involved in CLE41/TDIF–TDR/PXY signaling during vascular development. It could be that PXC3 positively regulates the CLE41/TDIF–TDR/PXY pathway by stabilizing BAK1. In addition to exerting a negative regulation on BRI1–BAK1 dimerization, BIR3 was reported to constitutively interact with and stabilize BAK1 in a ligand-independent manner. Accordingly, BAK1 levels are significantly reduced in *bir3* mutants compared to wild type (Imkampe et al., 2017). To test whether PXC3–BAK1 interaction results in BAK1 stabilization, we monitored BAK1 protein levels using anti-BAK1 antibodies in wild type and *pxc3* seedlings but no significant changes in BAK1 levels between *pxc3* mutants and wild type were detected (**Figures 4A,B**). Thus, the defects observed in *pxc3* mutants cannot be explained by decreased in BAK1 stability.

DISCUSSION

In this work, we found six LRR-RLKs that co-eluted with BAK1 in AP-MS experiments. Since three of these were recognized BAK1 interactors while the other three were not at the time we performed the experiment, we decided to verify the interaction with BAK1 by independent methods. Using BIFC, as well as Co-IP, we confirmed that PXC3 constitutively interacts with BAK1. Although we also detected some GFP signals in the BIFC experiment using MIK2 and LIK1, comparison to the PEPR1–BAK1 interaction did not reveal significant differences. However, PEPR1 and BAK1 may still weakly dimerize in tobacco leaves and if so, comparing to this stringent control will underestimate other positive BAK1 interactions. In agreement with PEPR1–BAK1 preassembly, we detected also PEPR1 peptides in our AP-MS experiment in *Arabidopsis* seedlings (**Supplementary Table 1**).

MIK2 belongs to subgroup XII of the LRR-RLKs and has been associated with different developmental processes in plants including plant reproduction, response to cell wall damage, salt stress, and pathogen-triggered immunity (PTI) (Julkowska et al., 2016; Wang et al., 2016; Van der Does et al., 2017; Coleman et al., 2021). A recent publication showed a weak association of MIK2 and BAK1 by co-IP and this interaction was enhanced by the addition of a *Fusarium* PTI-eliciting extract (Coleman et al., 2021). Furthermore, MIK2 was shown to perceive the phytocytokine SERINE RICH ENDOGENOUS PEPTIDE 12 (SCOOP12), and likely other peptides of the same family present in *Arabidopsis* and *Fusarium*, which also induces heterodimerization of MIK2 and BAK1 (Rhodes et al., 2021). It is thus likely, that the low MIK2–BAK1 association detected here represents pre-complexes that form but are not very abundant. The same may be true for LIK1. LIK1 associates to the LysM receptor-like kinase (LysM-RLK1/CERK1) involved in chitin perception and was proposed to negatively regulate chitin-induced innate immunity (Le et al., 2014). *lik1* mutants showed enhanced sensitivity not only to chitin but also to the bacterial-derived peptide flg22. Since BAK1 association to pattern recognition receptors such as FLS2 (the plant receptor sensing flg22) is necessary for PTI responses, LIK1 could act as a negative regulator of bacterial and fungal immunity by

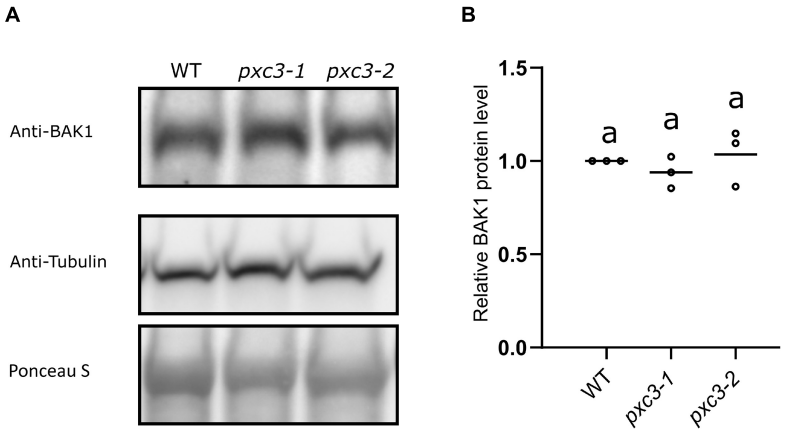

FIGURE 4 | BAK1 protein levels in wild type and *pxc3* mutants. **(A)** Western blot analysis of BAK1 protein levels as detected by anti-BAK1 antibodies in wild type and *pxc3* mutant seedlings. Blots were reblotted with anti-tubulin in two out of three performed experiments, all showing similar results. **(B)** Quantification of BAK1 protein levels in wild type and *pxc3* mutants. For each experiment, BAK1 signal in the mutants was normalized by that in wild type. Individual data points for each experiment are shown. One-way ANOVA analysis was performed followed by Tukey's test, and the lowercase letters indicate statistical differences ($P < 0.05$).

sequestering the coreceptor BAK1, as it has been shown for BIR proteins. However, this hypothesis, as well as the LIK1–BAK1 interaction, still has to be confirmed by independent approaches.

In higher plants, the vasculature is essential for the movement of resources, like water and sugars, throughout the plant body. CLE41/TDIF–TDR/PXY signaling controls vascular development by regulating vascular cell division, bundle organization, and xylem differentiation (Fisher and Turner, 2007; Etchells and Turner, 2010; Fukuda and Hardtke, 2020). This pathway also uses BAK1 as coreceptor (Zhang et al., 2016). Here, we found PXC3 to interact with BAK1 and *pxc3* mutants show reduced stele width compared to wild type, corresponding to a decreased number of procambial cells. Besides, *pxc3* mutants are less sensitive to TDIF peptide treatments, as monitored by the TDIF-induced stele enlargement and *WOX4* upregulation. Altogether, our data suggest that PXC3 controls procambial division as part of the CLE41/TDIF–TDR/PXY signaling pathway.

We could see two possible scenarios for PXC3 function. First, PXC3 could positively regulate the PXY and BAK1 interaction as it has been previously shown for other ligand-free LRR-RLK interactions. For example, the LRR-RLK FIR, as well as IOS1, interact with FLS2 and BAK1 constitutively and promotes FLS2–BAK1 complex formation in the presence of the flg22 ligand (Yeh et al., 2016; Smakowska-Luzan et al., 2018). Another possibility is that PXC3 binds and senses the TDIF peptide in parallel to PXY to regulate cell division. PXC3 belongs to subgroup XI of LRR-RLKs and its ectodomain contains 18 LRRs, thus, it could function as a ligand-sensing receptor. An alternative receptor for the TDIF peptide has been proposed since the *pxywox4*, but not *pxywox14*, double mutant show enhanced division defects compared to the *pxy* mutant alone (Hirakawa et al., 2010; Etchells et al., 2013). Because the vascular expansion caused by overexpressing *CLE41* is to a large extent suppressed in *pxy*, this alternative receptor signaling would only have a minor contribution to vascular cell division (Etchells and Turner, 2010; Etchells et al., 2013). In agreement with this model, we observed a decrease in TDIF-induced *WOX4* but not *WOX14* transcript in *pxc3* mutants compared to wild type, indicating that PXY and PXC3 redundantly regulate TDIF-induced *WOX4*, but not *WOX14* levels. A similar reduction in stele width and procambial cell number of *pxy* and *pxc3* mutants (although reductions in *pxc3* are milder) also correlates with this proposition. The mild increase in *WOX14* transcription in *pxc3* mutants could be part of a feedback/compensatory mechanism. Nevertheless, the constitutive PXC3–BAK1 interaction argues against this hypothesis, since receptor–coreceptor interactions are most often induced by the ligand (Hohmann et al., 2017). The generation of a double *pxypxc3-2* mutant further confirmed that PXC3 and PXY are likely part of the same genetic pathway and it is most probable that PXC3 has a regulatory function (i.e., in PXY–BAK1 complex formation) as has been shown for other BAK1-dependent receptor complexes (Yeh et al., 2016; Smakowska-Luzan et al., 2018).

The reported *PXC3* expression (Wang et al., 2013) comprises vascular tissues in both roots and shoots, which can be confirmed from public microarray compendia[1]. Based on this, it is possible that PXC3 has a similar function in procambial cell proliferation in the root as in the hypocotyl. However, since the TDIF–PXY/TDR pathway has been mostly characterized in shoot tissues, the function of PXC3 in root vascular development should be investigated in future studies. In addition, the *PXC3* expression in shoot tissues expands to non-vascular cells (Wang et al., 2013). However, we have to point out that we did not observe any other obvious developmental defects at the vegetative or reproductive stage, nor did we find a defect in other hypocotyl cell layers in transversal sections (i.e., epidermis or cortex cell number/size). Nevertheless, we cannot rule out a less significant function of PXC3 in other shoot cells/tissues or

[1]http://bar.utoronto.ca/eplant/

under certain conditions (i.e., stress). Thus, targeted investigation of other cells or plant processes not considered in this study may reveal additional functions of the PXC3-BAK1 interaction in future studies.

In the original report where PXC3 was identified by co-expression analysis, two other LRR-RLKs, PXC1, and PXC2 were identified as well, although their involvement in the CLE41/TDIF–TDR/PXY pathway was not further investigated (Wang et al., 2013). Analysis of *pxc1* mutants revealed reduced lignin content in inflorescence stems, and thus, PXC1 was associated with secondary wall deposition in fiber cells (Wang et al., 2013). Recently, PXC2/CANAR was associated with the regeneration of vascular strands after wounding (Hajny et al., 2020). A preprint article also shows that *pxc2* mutants enhanced the defects in *irk4*, a mutant of another LRR-RLK, in the root apical meristem, which results in ectopic anticlinal divisions in endodermal and stele cells. The *pxc2irk4* double mutants display even more enlarged stele than single *irk4* mutants, suggesting a function for PXC2 in restricting anticlinal divisions in endodermis and stele cells in the root (Goff and Van Norman, 2021). Here we showed that *pxc2* mutants also responded less to the TDIF peptide, indicating that the originally identified *PXC* genes are potential regulators of the CLE41/TDIF–TDR/PXY pathway. Multiple interactions and interplay between different LRR-RLKs have in the last years revealed to be highly complex (Smakowska-Luzan et al., 2018). Thus, the function of PXC1 to 3 in the CLE41/TDIF–TDR/PXY, as well as, other pathways needs to be fully characterized in the future.

DATA AVAILABILITY STATEMENT

The original contributions presented in the study are publicly available. This data can be found here: ProteomeXchange *via* the PRIDE database with accession number: PXD026487.

AUTHOR CONTRIBUTIONS

AF performed AP-MS experiments. KX, AF, and LN confirmed receptor interactions. KX, JJ, and MN performed and analyzed hypocotyl cross-sections. KX analyzed the stele width and performed qPCR experiments. KX and JJ performed the statistical analysis. KX, AF, and TB wrote the manuscript with input from all other authors. AF and TB provided supervision on the experiments and the analysis of the results. All authors contributed to the article and approved the submitted version.

FUNDING

This research was supported by the FWO postdoctoral and project grants (Nos. 1293817N and G020918N to AF) as well as an FWO doctoral fellowship (Grant No. 1168218N to JJ), and a China Scholarship Council grant (No. 201606350134 to KX).

SUPPLEMENTARY MATERIAL

The Supplementary Material for this article can be found online at: https://www.frontiersin.org/articles/10.3389/fpls.2021.706633/full#supplementary-material

Supplementary Figure 1 | *pxc2* Mutants have reduced sensitivity to TDIF peptide treatment. **(A)** Longitudinal confocal sections of wild type and mutant hypocotyls (7 DAG seedlings) treated or not with the TDIF (5 μM) peptide for 4 days as indicated. The double-sided arrow indicates the stele width. Scale bars represent 20 μm. **(B)** Quantification of the stele width ($n \geq 15$). This experiment was done two times. Numbers indicate fold change in the mean stele width relative to the untreated sample for each genotype. A two-way ANOVA followed by a Dunnett's test was performed and the asterisks indicate a significant genotype and treatment interaction compared to wild type (***$P < 0.001$ and ****$P < 0.0001$). **(C)** *WOX4* and *WOX14* transcript levels after 8 h TDIF treatment of wild type and mutant seedlings. Fold change relative to wild type (mock) is shown. Numbers indicate fold change in the mean value (line) relative to the untreated sample for each genotype ($n = 3$ independent replicates). A one-way ANOVA followed by a Tukey's test was performed on Log2-transformed peptide/mock gene expression ratio, and the asterisks indicate a significant genotype and treatment interaction compared to wild type (*$P < 0.05$, ***$P < 0.001$, and ****$P < 0.0001$, and ns indicates that no significant difference was found).

Supplementary Table 1 | Protein groups obtained after MaxQuant analysis of mock and estradiol-treated *BAK1pro:BAK1-GFP/bak1-4/iGLV6.* Protein groups are ordered by the intensity-based absolute quantification (iBAQ) values.

Supplementary Table 2 | Primers used to monitor transcript levels by qPCR of *PXC3*, *WOX4*, and *WOX14*.

REFERENCES

Abas, L., and Luschnig, C. (2010). Maximum yields of microsomal-type membranes from small amounts of plant material without requiring ultracentrifugation. *Anal. Biochem.* 401, 217–227. doi: 10.1016/j.ab.2010.02.030

Beeckman, T., and Viane, R. (2000). Embedding thin plant specimens for oriented sectioning. *Biotech. Histochem.* 75, 23–26. doi: 10.3109/10520290009047981

Boruc, J., Van den Daele, H., Hollunder, J., Rombauts, S., Mylle, E., Hilson, P., et al. (2010). Functional modules in the *Arabidopsis* core cell cycle binary protein-protein interaction network. *Plant Cell* 22, 1264–1280. doi: 10.1105/tpc.109.073635

Chinchilla, D., Bauer, Z., Regenass, M., Boller, T., and Felix, G. (2006). The Arabidopsis receptor kinase FLS2 binds flg22 and determines the specificity of flagellin perception. *Plant Cell* 18, 465–476. doi: 10.1105/tpc.105.036574

Chinchilla, D., Zipfel, C., Robatzek, S., Kemmerling, B., Nurnberger, T., Jones, J. D., et al. (2007). A flagellin-induced complex of the receptor FLS2 and BAK1 initiates plant defence. *Nature* 448, 497–500. doi: 10.1038/nature05999

Coleman, A. D., Maroschek, J., Raasch, L., Takken, F. L. W., Ranf, S., and Huckelhoven, R. (2021). The Arabidopsis leucine-rich repeat receptor-like kinase MIK2 is a crucial component of early immune responses to a fungal-derived elicitor. *New Phytol.* 229, 3453–3466.

Couto, D., and Zipfel, C. (2016). Regulation of pattern recognition receptor signalling in plants. *Nat. Rev. Immunol.* 16, 537–552. doi: 10.1038/nri.2016.77

De Smet, I., Chaerle, P., Vanneste, S., De Rycke, R., Inze, D., and Beeckman, T. (2004). An easy and versatile embedding method for transverse sections. *J. Microsc.* 213, 76–80. doi: 10.1111/j.1365-2818.2004.01269.x

De Smet, I., Voss, U., Jurgens, G., and Beeckman, T. (2009). Receptor-like kinases shape the plant. *Nat. Cell Biol.* 11, 1166–1173. doi: 10.1038/ncb1009-1166

Etchells, J. P., and Turner, S. R. (2010). The PXY-CLE41 receptor ligand pair defines a multifunctional pathway that controls the rate and orientation of vascular cell division. *Development* 137, 767–774. doi: 10.1242/dev.044941

Etchells, J. P., Provost, C. M., Mishra, L., and Turner, S. R. (2013). WOX4 and WOX14 act downstream of the PXY receptor kinase to regulate plant vascular

proliferation independently of any role in vascular organisation. *Development* 140, 2224–2234. doi: 10.1242/dev.091314

Fernandez, A. I., Vangheluwe, N., Xu, K., Jourquin, J., Claus, L. A. N., Morales-Herrera, S., et al. (2020). GOLVEN peptide signalling through RGI receptors and MPK6 restricts asymmetric cell division during lateral root initiation. *Nat. Plants* 6, 533–543. doi: 10.1038/s41477-020-0645-z

Fernandez, A., Drozdzecki, A., Hoogewijs, K., Vassileva, V., Madder, A., Beeckman, T., et al. (2015). The GLV6/RGF8/CLEL2 peptide regulates early pericycle divisions during lateral root initiation. *J. Exp. Bot.* 66, 5245–5256. doi: 10.1093/jxb/erv329

Fisher, K., and Turner, S. (2007). PXY, a receptor-like kinase essential for maintaining polarity during plant vascular-tissue development. *Curr. Biol.* 17, 1061–1066. doi: 10.1016/j.cub.2007.05.049

Fukuda, H., and Hardtke, C. S. (2020). Peptide signaling pathways in vascular differentiation([OPEN]). *Plant Physiol.* 182, 1636–1644. doi: 10.1104/pp.19.01259

Gao, M., Wang, X., Wang, D., Xu, F., Ding, X., Zhang, Z., et al. (2009). Regulation of cell death and innate immunity by two receptor-like kinases in Arabidopsis. *Cell Host Microbe* 6, 34–44. doi: 10.1016/j.chom.2009.05.019

Goff, J., and Van Norman, J. M. (2021). *Polarly Localized Receptor-Like Kinases PXC2 and IRK Act Redundantly During Arabidopsis Root Development In The Radial Axis. biorxiv [Preprint]*. Available online at: https://www.biorxiv.org/content/10.1101/2021.02.11.429611v1 [Accessed Februrary 21, 2021].

Gomez-Gomez, L., and Boller, T. (2000). FLS2: an LRR receptor-like kinase involved in the perception of the bacterial elicitor flagellin in *Arabidopsis*. *Mol. Cell* 5, 1003–1011. doi: 10.1016/s1097-2765(00)80265-8

Hajny, J., Prat, T., Rydza, N., Rodriguez, L., Tan, S., Verstraeten, I., et al. (2020). Receptor kinase module targets PIN-dependent auxin transport during canalization. *Science* 370, 550–557. doi: 10.1126/science.aba3178

Halter, T., Imkampe, J., Mazzotta, S., Wierzba, M., Postel, S., Bucherl, C., et al. (2014). The leucine-rich repeat receptor kinase BIR2 Is a negative regulator of BAK1 in plant immunity. *Curr. Biol.* 24, 134–143. doi: 10.1016/j.cub.2013.11.047

He, Y., Zhou, J., Shan, L., and Meng, X. (2018). Plant cell surface receptor-mediated signaling – a common theme amid diversity. *J. Cell Sci.* 131:jcs209353. doi: 10.1242/jcs.209353

Hirakawa, Y., Kondo, Y., and Fukuda, H. (2010). TDIF peptide signaling regulates vascular stem cell proliferation *via* the WOX4 homeobox gene in *Arabidopsis*. *Plant Cell* 22, 2618–2629. doi: 10.1105/tpc.110.076083

Hirakawa, Y., Shinohara, H., Kondo, Y., Inoue, A., Nakanomyo, I., Ogawa, M., et al. (2008). Non-cell-autonomous control of vascular stem cell fate by a CLE peptide/receptor system. *Proc. Natl. Acad. Sci. U.S.A.* 105, 15208–15213. doi: 10.1073/pnas.0808444105

Hohmann, U., Lau, K., and Hothorn, M. (2017). The structural basis of ligand perception and signal activation by receptor kinases. *Annu. Rev. Plant Biol.* 68, 109–137. doi: 10.1146/annurev-arplant-042916-040957

Imkampe, J., Halter, T., Huang, S., Schulze, S., Mazzotta, S., Schmidt, N., et al. (2017). The *Arabidopsis* leucine-rich repeat receptor kinase BIR3 negatively regulates BAK1 receptor complex formation and stabilizes BAK1. *Plant Cell* 29, 2285–2303. doi: 10.1105/tpc.17.00376

Ito, Y., Nakanomyo, I., Motose, H., Iwamoto, K., Sawa, S., Dohmae, N., et al. (2006). Dodeca-CLE peptides as suppressors of plant stem cell differentiation. *Science* 313, 842–845. doi: 10.1126/science.1128436

Julkowska, M. M., Klei, K., Fokkens, L., Haring, M. A., Schranz, M. E., and Testerink, C. (2016). Natural variation in rosette size under salt stress conditions corresponds to developmental differences between *Arabidopsis* accessions and allelic variation in the LRR-KISS gene. *J. Exp. Bot.* 67, 2127–2138. doi: 10.1093/jxb/erw015

Karimi, M., Bleys, A., Vanderhaeghen, R., and Hilson, P. (2007). Building blocks for plant gene assembly. *Plant Physiol.* 145, 1183–1191. doi: 10.1104/pp.107.110411

Kurihara, D., Mizuta, Y., Sato, Y., and Higashiyama, T. (2015). ClearSee: a rapid optical clearing reagent for whole-plant fluorescence imaging. *Development* 142, 4168–4179. doi: 10.1242/dev.127613

Ladwig, F., Dahlke, R. I., Stuhrwohldt, N., Hartmann, J., Harter, K., and Sauter, M. (2015). Phytosulfokine regulates growth in *Arabidopsis* through a response module at the plasma membrane that includes CYCLIC NUCLEOTIDE-GATED CHANNEL17, H+-ATPase, and BAK1. *Plant Cell* 27, 1718–1729. doi: 10.1105/tpc.15.00306

Le, M. H., Cao, Y., Zhang, X. C., and Stacey, G. (2014). LIK1, a CERK1-interacting kinase, regulates plant immune responses in *Arabidopsis*. *PLoS One* 9:e102245. doi: 10.1371/journal.pone.0102245

Li, B., Ferreira, M. A., Huang, M., Camargos, L. F., Yu, X., Teixeira, R. M., et al. (2019). The receptor-like kinase NIK1 targets FLS2/BAK1 immune complex and inversely modulates antiviral and antibacterial immunity. *Nat. Commun.* 10:4996. doi: 10.1038/s41467-019-12847-6

Li, J., and Chory, J. (1997). A putative leucine-rich repeat receptor kinase involved in brassinosteroid signal transduction. *Cell* 90, 929–938. doi: 10.1016/s0092-8674(00)80357-8

Li, J., Wen, J., Lease, K. A., Doke, J. T., Tax, F. E., and Walker, J. C. (2002). BAK1, an Arabidopsis LRR receptor-like protein kinase, interacts with BRI1 and modulates brassinosteroid signaling. *Cell* 110, 213–222. doi: 10.1016/s0092-8674(02)00812-7

Ma, X., Xu, G., He, P., and Shan, L. (2016). SERKing coreceptors for receptors. *Trends Plant Sci.* 21, 1017–1033. doi: 10.1016/j.tplants.2016.08.014

Matsubayashi, Y., Ogawa, M., Morita, A., and Sakagami, Y. (2002). An LRR receptor kinase involved in perception of a peptide plant hormone, phytosulfokine. *Science* 296, 1470–1472. doi: 10.1126/science.1069607

Meng, X., Chen, X., Mang, H., Liu, C., Yu, X., Gao, X., et al. (2015). Differential function of *Arabidopsis* SERK family receptor-like kinases in stomatal patterning. *Curr. Biol.* 25, 2361–2372. doi: 10.1016/j.cub.2015.07.068

Meng, X., Zhou, J., Tang, J., Li, B., de Oliveira, M. V. V., Chai, J., et al. (2016). Ligand-induced receptor-like kinase complex regulates floral organ abscission in *Arabidopsis*. *Cell Rep.* 14, 1330–1338. doi: 10.1016/j.celrep.2016.01.023

Ntoukakis, V., Schwessinger, B., Segonzac, C., and Zipfel, C. (2011). Cautionary notes on the use of C-terminal BAK1 fusion proteins for functional studies. *Plant Cell* 23, 3871–3878. doi: 10.1105/tpc.111.090779

Ou, Y., Kui, H., and Li, J. (2021). Receptor-like kinases in root development: current progress and future directions. *Mol. Plant* 14, 166–185. doi: 10.1016/j.molp.2020.12.004

Ou, Y., Lu, X., Zi, Q., Xun, Q., Zhang, J., Wu, Y., et al. (2016). RGF1 INSENSITIVE 1 to 5, a group of LRR receptor-like kinases, are essential for the perception of root meristem growth factor 1 in *Arabidopsis thaliana*. *Cell Res.* 26, 686–698. doi: 10.1038/cr.2016.63

Rhodes, J., Yang, H., Moussu, S., Boutrot, F., Santiago, J., and Zipfel, C. (2021). Perception of a divergent family of phytocytokines by the *Arabidopsis* receptor kinase MIK2. *Nat. Commun.* 12:705. doi: 10.1038/s41467-021-20932-y

Roux, M., Schwessinger, B., Albrecht, C., Chinchilla, D., Jones, A., Holton, N., et al. (2011). The *Arabidopsis* leucine-rich repeat receptor-like kinases BAK1/SERK3 and BKK1/SERK4 are required for innate immunity to hemibiotrophic and biotrophic pathogens. *Plant Cell* 23, 2440–2455. doi: 10.1105/tpc.111.084301

Santiago, J., Brandt, B., Wildhagen, M., Hohmann, U., Hothorn, L. A., Butenko, M. A., et al. (2016). Mechanistic insight into a peptide hormone signaling complex mediating floral organ abscission. *Elife* 5:e15075. doi: 10.7554/eLife.15075

Scholthof, H. B. (2006). Timeline – the tombusvirus-encoded P19: from irrelevance to elegance. *Nat. Rev. Microbiol.* 4, 405–411. doi: 10.1038/nrmicro1395

Shiu, S. H., and Bleecker, A. B. (2001). Receptor-like kinases from *Arabidopsis* form a monophyletic gene family related to animal receptor kinases. *Proc. Natl. Acad. Sci. U.S.A.* 98, 10763–10768. doi: 10.1073/pnas.181141598

Shiu, S. H., and Bleecker, A. B. (2003). Expansion of the receptor-like kinase/Pelle gene family and receptor-like proteins in *Arabidopsis*. *Plant Physiol.* 132, 530–543. doi: 10.1104/pp.103.021964

Smaczniak, C., Li, N., Boeren, S., America, T., van Dongen, W., Goerdayal, S. S., et al. (2012). Proteomics-based identification of low-abundance signaling and regulatory protein complexes in native plant tissues. *Nat. Protoc.* 7:2144–2158. doi: 10.1038/nprot.2012.129

Smakowska-Luzan, E., Mott, G. A., Parys, K., Stegmann, M., Howton, T. C., Layeghifard, M., et al. (2018). An extracellular network of *Arabidopsis* leucine-rich repeat receptor kinases. *Nature* 553, 342–346. doi: 10.1038/nature25184

Smit, M. E., McGregor, S. R., Sun, H., Gough, C., Bagman, A. M., Soyars, C. L., et al. (2020). A PXY-mediated transcriptional network integrates signaling mechanisms to control vascular development in *Arabidopsis*. *Plant Cell* 32, 319–335. doi: 10.1105/tpc.19.00562

Song, W., Liu, L., Wang, J., Wu, Z., Zhang, H., Tang, J., et al. (2016). Signature motif-guided identification of receptors for peptide hormones essential for root meristem growth. *Cell Res.* 26, 674–685. doi: 10.1038/cr.2016.62

Tang, J., Han, Z., Sun, Y., Zhang, H., Gong, X., and Chai, J. (2015). Structural basis for recognition of an endogenous peptide by the plant receptor kinase PEPR1. *Cell Res.* 25, 110–120. doi: 10.1038/cr.2014.161

van der Burgh, A. M., and Joosten, M. (2019). Plant immunity: thinking outside and inside the box. *Trends Plant Sci.* 24, 587–601. doi: 10.1016/j.tplants.2019.04.009

Van der Does, D., Boutrot, F., Engelsdorf, T., Rhodes, J., McKenna, J. F., Vernhettes, S., et al. (2017). The Arabidopsis leucine-rich repeat receptor kinase MIK2/LRR-KISS connects cell wall integrity sensing, root growth and response to abiotic and biotic stresses. *PLoS Genet.* 13:e1006832. doi: 10.1371/journal.pgen.1006832

Van Leene, J., Stals, H., Eeckhout, D., Persiau, G., Van De Slijke, E., Van Isterdael, G., et al. (2007). A tandem affinity purification-based technology platform to study the cell cycle interactome in *Arabidopsis thaliana*. *Mol. Cell Proteomics* 6, 1226–1238. doi: 10.1074/mcp.M700078-MCP200

Wang, J., Kucukoglu, M., Zhang, L., Chen, P., Decker, D., Nilsson, O., et al. (2013). The Arabidopsis LRR-RLK, PXC1, is a regulator of secondary wall formation correlated with the TDIF-PXY/TDR-WOX4 signaling pathway. *BMC Plant Biol.* 13:94. doi: 10.1186/1471-2229-13-94

Wang, J., Li, H., Han, Z., Zhang, H., Wang, T., Lin, G., et al. (2015). Allosteric receptor activation by the plant peptide hormone phytosulfokine. *Nature* 525, 265–268. doi: 10.1038/nature14858

Wang, T., Liang, L., Xue, Y., Jia, P. F., Chen, W., Zhang, M. X., et al. (2016). A receptor heteromer mediates the male perception of female attractants in plants. *Nature* 531, 241–244. doi: 10.1038/nature16975

Wendrich, J. R., Boeren, S., Moller, B. K., Weijers, D., and De Rybel, B. (2017). In vivo identification of plant protein complexes using IP-MS/MS. *Methods Mol. Biol.* 1497, 147–158. doi: 10.1007/978-1-4939-6469-7_14

Whitford, R., Fernandez, A., De Groodt, R., Ortega, E., and Hilson, P. (2008). Plant CLE peptides from two distinct functional classes synergistically induce division of vascular cells. *Proc. Natl. Acad. Sci. U.S. A.* 105, 18625–18630. doi: 10.1073/pnas.0809395105

Xi, L., Wu, X. N., Gilbert, M., and Schulze, W. X. (2019). Classification and interactions of LRR receptors and Co-receptors within the *Arabidopsis* plasma membrane – an overview. *Front. Plant Sci.* 10:472. doi: 10.3389/fpls.2019.00472

Yeh, Y. H., Panzeri, D., Kadota, Y., Huang, Y. C., Huang, P. Y., Tao, C. N., et al. (2016). The *Arabidopsis* malectin-Like/LRR-RLK IOS1 is critical for BAK1-dependent and BAK1-independent pattern-triggered immunity. *Plant Cell* 28, 1701–1721. doi: 10.1105/tpc.16.00313

Zhang, H. Q., Lin, X. Y., Han, Z. F., Wang, J. Z., Qu, L. J., and Chai, J. J. (2016). SERK family receptor-like kinases function as co-receptors with PXY for plant vascular development. *Mol. Plant* 9, 1406–1414.

Conflict of Interest: The authors declare that the research was conducted in the absence of any commercial or financial relationships that could be construed as a potential conflict of interest.

Publisher's Note: All claims expressed in this article are solely those of the authors and do not necessarily represent those of their affiliated organizations, or those of the publisher, the editors and the reviewers. Any product that may be evaluated in this article, or claim that may be made by its manufacturer, is not guaranteed or endorsed by the publisher.

Advantages of publishing in Frontiers

OPEN ACCESS
Articles are free to read for greatest visibility and readership

FAST PUBLICATION
Around 90 days from submission to decision

HIGH QUALITY PEER-REVIEW
Rigorous, collaborative, and constructive peer-review

TRANSPARENT PEER-REVIEW
Editors and reviewers acknowledged by name on published articles

Frontiers
Avenue du Tribunal-Fédéral 34
1005 Lausanne | Switzerland

Visit us: www.frontiersin.org
Contact us: frontiersin.org/about/contact

REPRODUCIBILITY OF RESEARCH
Support open data and methods to enhance research reproducibility

DIGITAL PUBLISHING
Articles designed for optimal readership across devices

FOLLOW US
@frontiersin

IMPACT METRICS
Advanced article metrics track visibility across digital media

EXTENSIVE PROMOTION
Marketing and promotion of impactful research

LOOP RESEARCH NETWORK
Our network increases your article's readership